

**A HETEROGENEOUS SENSOR SUITE FOR REDUCING THE  
COGNITIVE BURDEN OF UPPER LIMB ROBOTIC CONTROL**

**MARCUS JIAN LI GARDNER**  
*(PhD, NUS)*

**A THESIS SUBMITTED  
FOR THE DEGREE OF DOCTOR OF PHILOSOPHY  
DEPARTMENT OF MECHANICAL ENGINEERING  
NATIONAL UNIVERSITY OF SINGAPORE**

2017

**Supervisors:**

Dr. Ravi Vaidyanathan, Imperial College London, Main Supervisor  
Professor Boo Cheong Khoo, Co-Supervisor  
Professor Etienne Burdet, Imperial College London, Co-Supervisor

**Examiners:**

Professor Geok Soon Hong  
Professor Yiannis Demiris, Imperial College London  
Professor Christopher James, University of Warwick

## DECLARATION

I hereby declare that the thesis is my original work and it has been written by me in its entirety. I have duly acknowledged all the sources of information which have been used in the thesis.

This thesis has also not been submitted for any degree in any university previously.



---

Marcus Jian Li Gardner  
28 February 2017

---

## Acknowledgements

I would first like to express my utmost gratitude to my supervisor Dr Ravi Vaidyanathan for providing me with the opportunity to pursue this research. Thank you for your support, encouragement and enthusiasm throughout. Your limitless energy and drive has helped guide me in the completion of this PhD, and has kept me motivated in times of need.

Without the collaborative support of Professor Boo Cheong Khoo, this research would not have been possible. I am very grateful for your support and guidance throughout my 20 month stay in Singapore; it was an incredible experience, and I wish that I could have stayed there for longer. I would also like to thank Professor Heow Pueh Lee for helping me settle down at NUS, and providing me support throughout my visit.

To Professor Etienne Burdet, who gave me a space in the Human Robotics Group for the first 15 months of my PhD, your advice and help throughout all stages of my PhD, in the UK and in Singapore, were invaluable. The opportunities that you provided not only benefited my research, but also had a large impact on my personal life, and for that I am truly thankful.

I would like to thank my friends in the Human Robotics Group where I spent my first 15 months: Ale, Alex, Alfredo, Andrew, Asif, Atsushi, Carlo, Consuelo, Daniel, Elisa, Flavia, Francesco, Ildar, Luca, Matjaz, Nat, Sharah, Siva, Tong and Wayne. Working alongside you has given me some of the best times of my life, and I don't know what it would have been like without the numerous coffee breaks, Chop Chop dinners, pranks, late nights out and the gym, squash and sauna sessions. You have all made a massive impact on me, personally and socially, and I am incredibly happy to have made some amazing friends and a loving partner.

To the past and current members of the Biomechatronics group: Ash, Enrico, James, Lewis, Marcel, Matt, Mike, Paolo, Richard and Sam; a big thank you for all the enjoyable times you have provided; it has made my final year a fantastic one. To Sam in particular, the work you have put into the NU IMU has benefited me tremendously, and I am very grateful for all the time you have spent improving it.

I would also like to express my gratitude to all the participants involved in this research.

---

Without your time, effort and feedback, this work wouldn't have been possible. A big thank you to Imperial College London and the National University of Singapore for providing the opportunity for a fantastic joint program and their financial support.

Finally, I would like to thank my parents Jeremy and Soon Mui, and brother Jeremy, for their financial help and emotional support throughout my PhD journey, I could not have done it without you. I would also like to express my gratitude to the entire Lee family, for helping me feel at home during my stay in Singapore and making the experience worth remembering.

# Contents

<b>Contents</b>	<b>iii</b>
<b>Summary</b>	<b>ix</b>
<b>List of Tables</b>	<b>xi</b>
<b>List of Figures</b>	<b>xiii</b>
<b>Nomenclature</b>	<b>xxxiii</b>
<b>1 Introduction</b>	<b>1</b>
1.1 Motivation and Thesis Focus . . . . .	2
1.2 Summary of Contributions . . . . .	4
1.3 List of Publications . . . . .	5
1.4 Structure of Thesis . . . . .	5
<b>2 Background</b>	<b>7</b>
2.1 The Importance of Assistive Technologies . . . . .	7
2.2 Description of Interfacing Technologies . . . . .	9
2.2.1 Physiological motion Systems . . . . .	10
2.2.2 Gaze Tracking Systems . . . . .	14
2.2.2.i Eye Tracking . . . . .	15
2.2.2.ii Gaze Estimation . . . . .	17
2.2.2.iii Electrooculography (EOG) . . . . .	18
2.2.3 Oral Communication Interfaces . . . . .	18

---

2.2.4	Biofeedback Devices . . . . .	21
2.2.4.i	Non-pattern recognition strategies . . . . .	24
2.2.4.ii	Pattern recognition strategies . . . . .	25
2.2.5	Bioacoustic . . . . .	27
2.3	Intelligent Prosthetics . . . . .	28
2.4	Chapter Summary . . . . .	37
<b>3</b>	<b>Conceptual Design of a Low-cost Heterogeneous Sensor Suite</b>	<b>39</b>
3.1	Control System Architecture . . . . .	39
3.1.1	Muscle Activation Subsystem (MASS) . . . . .	42
3.1.2	Computer Vision Subsystem (CVSS) . . . . .	43
3.1.3	Grasp Prediction Subsystem (GPSS) . . . . .	44
3.2	Local Control System: The Bebionic V2 Hand . . . . .	45
3.2.1	System Control . . . . .	45
3.2.2	Grasp Patterns . . . . .	46
3.2.3	Limitations . . . . .	48
3.2.3.i	Grasp Availability . . . . .	49
3.2.3.ii	Manually Opposed Thumb . . . . .	49
3.2.3.iii	Grasp Localisation . . . . .	49
3.2.4	Design Considerations . . . . .	50
3.3	Myoelectric hand adapter design . . . . .	51
3.4	Chapter Summary . . . . .	54
<b>4</b>	<b>Mechanomyography and Environmental Vision</b>	<b>55</b>
4.1	Mechanomyogram Acoustic Sensing . . . . .	55
4.1.1	Sensor Design . . . . .	56
4.1.2	Signal processing . . . . .	57
4.2	Computer Vision . . . . .	60
4.2.1	Algorithm Considerations . . . . .	60
4.2.2	Object Recognition . . . . .	62

---

4.2.2.i	Image Processing . . . . .	62
4.2.2.ii	Blob Filtering . . . . .	64
4.2.2.iii	Object Properties . . . . .	65
4.3	MMG and Computer Vision for Hand Prosthesis Control . . . . .	66
4.3.1	Control System Architecture . . . . .	67
4.3.1.i	MMG Sensor Pair . . . . .	68
4.3.1.ii	Computer Vision System . . . . .	69
4.3.2	Grasp Selection . . . . .	70
4.4	Experimental Testing . . . . .	71
4.5	Results . . . . .	73
4.6	Discussion . . . . .	75
4.7	Chapter Summary . . . . .	77
<b>5</b>	<b>Decoding Physiological Activity</b>	<b>79</b>
5.1	Data Collection . . . . .	80
5.1.1	Participants . . . . .	81
5.1.2	Software Test Environment . . . . .	82
5.1.3	Experimental Protocol . . . . .	83
5.2	Measuring Motion . . . . .	89
5.2.1	Background: Describing Orientation . . . . .	89
5.2.1.i	Rotation Matrices . . . . .	89
5.2.1.ii	Euler Angles . . . . .	90
5.2.1.iii	Quaternions . . . . .	91
5.2.2	Background: Calculating Orientation . . . . .	92
5.2.3	Signal Processing . . . . .	95
5.3	Feature Extraction . . . . .	97
5.3.0.i	Displacement Features . . . . .	98
5.3.0.ii	Velocity Features . . . . .	98
5.3.0.iii	Acceleration Features . . . . .	99
5.3.1	Object: Bottle . . . . .	100

---

5.3.1.i	Displacement: Healthy . . . . .	102
5.3.1.ii	Displacement: Amputee . . . . .	104
5.3.1.iii	Velocity: Healthy . . . . .	105
5.3.1.iv	Velocity: Amputee . . . . .	107
5.3.1.v	Acceleration: Healthy . . . . .	108
5.3.1.vi	Acceleration: Amputee . . . . .	110
5.3.2	Object: Lid . . . . .	111
5.3.2.i	Displacement: Healthy . . . . .	113
5.3.2.ii	Displacement: Amputee . . . . .	115
5.3.2.iii	Velocity: Healthy . . . . .	116
5.3.2.iv	Velocity: Amputee . . . . .	118
5.3.2.v	Acceleration: Healthy . . . . .	119
5.3.2.vi	Acceleration: Amputee . . . . .	120
5.3.3	Object: Box . . . . .	121
5.3.3.i	Displacement: Healthy . . . . .	122
5.3.3.ii	Displacement: Amputee . . . . .	124
5.3.3.iii	Velocity: Healthy . . . . .	126
5.3.3.iv	Velocity: Amputee . . . . .	128
5.3.3.v	Acceleration: Healthy . . . . .	129
5.3.3.vi	Acceleration: Amputee . . . . .	131
5.4	Feature Selection . . . . .	132
5.5	Grasp Classification . . . . .	136
5.5.1	Background: Classifiers . . . . .	137
5.5.1.i	K-Nearest Neighbours (KNN) . . . . .	137
5.5.1.ii	Discriminant Analysis . . . . .	137
5.5.1.iii	Decision Trees . . . . .	138
5.5.1.iv	Support Vector Machine . . . . .	139
5.5.2	Classifier Comparison . . . . .	140
5.6	Discussion . . . . .	142



---

5.6.1	Subject-specific physiological motion . . . . .	144
5.6.2	Anthropomorphic Correlation . . . . .	147
5.6.3	Influence of displacement, velocity and acceleration . . . . .	148
5.7	Chapter Summary . . . . .	149

## **6 A Low-Cost Heterogeneous Sensor Suite for Automated Grasp Switching of a Myoelectric Hand Prosthesis 153**

6.1	Sensor Suite . . . . .	154
6.1.1	Sensors . . . . .	154
6.1.1.i	Setup . . . . .	155
6.1.2	Control Flow . . . . .	156
6.1.3	Software Environment . . . . .	159
6.1.3.i	Bebalance+ . . . . .	159
6.1.3.ii	Sensor Control Interface . . . . .	159
6.2	Participants . . . . .	161
6.3	Pre-assessment Training . . . . .	162
6.4	Classification Performance Assessment . . . . .	165
6.4.1	Experimental Protocol . . . . .	165
6.4.2	Results . . . . .	166
6.4.2.i	Computer Vision . . . . .	166
6.4.2.ii	Grasp Prediction . . . . .	167
6.4.3	Discussion . . . . .	171
6.4.3.i	Computer Vision . . . . .	171
6.4.3.ii	Muscle Activation with MMG Sensing . . . . .	173
6.4.3.iii	Grasp Prediction . . . . .	175
6.5	Task Performance Assessment . . . . .	177
6.5.1	Experimental Protocol . . . . .	178
6.5.2	Results . . . . .	180
6.5.3	Discussion . . . . .	182
6.5.4	HMI Comparison . . . . .	185

---

6.6	Chapter Summary . . . . .	186
<b>7</b>	<b>Conclusions and Future Work</b>	<b>189</b>
7.1	Thesis Summary . . . . .	189
7.2	Conclusions . . . . .	190
7.2.1	Summary of Contributions . . . . .	191
7.2.2	Suggested Future Directions . . . . .	192
7.2.2.i	Correctional Feedback . . . . .	193
7.2.2.ii	Sensor Design . . . . .	194
7.2.2.iii	Further Studies . . . . .	195
7.2.2.iv	Applications in Rehabilitation . . . . .	195
7.3	Final Comments . . . . .	196
	<b>References</b>	<b>197</b>
	<b>Appendices</b>	<b>219</b>
<b>A</b>	<b>Preliminary validation of motion-based grasp prediction</b>	<b>221</b>
A.1	Experimental Procedure . . . . .	221
A.2	Data Processing . . . . .	222
A.3	Results . . . . .	224
A.4	Discussion and Conclusion . . . . .	225
<b>B</b>	<b>Inter-subject Kruskal-Wallis p-values for individual features</b>	<b>229</b>
<b>C</b>	<b>Inter-population Kruskal-Wallis p-values for individual features</b>	<b>233</b>
<b>D</b>	<b>Correlation between anthropomorphic and physiological features</b>	<b>237</b>

# Summary

A Human machine interface (HMI) acts like a bridge between motor function and the brain. Bypassing these natural pathways allows disabled individuals to perform actions that might otherwise be too difficult or impossible. The loss or impairment of voluntary muscle control can have a detrimental effect on an individual's quality of life. By utilising natural physiological motion with sensor fusion techniques, grasp intention can be predicted, leading to an assistive HMI concept that can reduce the cognitive load that traditional HMIs impose on the user.

This thesis investigates a novel design concept for a heterogeneous sensor suite, by fusing mechanomyogram (MMG) sensors for muscle activation, computer vision for object recognition, and inertial measurement sensors for predicting grasp intention. The developed architecture focuses on the prediction of intentional grasp activity of 1 amputee and 10 healthy subjects, using the natural physiological motion of the arm when reaching to grasp 3 objects with up to 3 different grasp patterns. 84 motion features are extracted and used as a classification tool for predicting intention, yielding an average grasp classification accuracy of 100%, 82.5% and 88.9% for bottle, lid and box objects across all subjects.

The novel heterogeneous sensor suite is applied to automate the grasp control of a myoelectric hand prosthesis. Real-time task-based experiments evaluated the performance of the proposed system, comparing it against conventional control using MMG sensors, yielding an 8.5% average faster completion time, as well as a reduction in overall cognitive and physical burden. The results of this research provide excellent potential for the use of natural motion to replace discrete muscle input as a selection and intention prediction tool, where the emphasis is on reducing the cognitive load imposed by assistive technologies.



# List of Tables

5.1	Participant information for physiological data collection experiment consisting of 10 healthy subjects, and 1 amputee subject. It must be noted that the majority of subjects have an engineering background. . . . .	81
5.2	Summary of the average p-values yielded across all features for each object and grasp from a Kruskal-Wallis test. Each grasp for each object class rejects the null hypothesis that each set of subject samples come from the same distribution at a $< 1\%$ significance level. . . . .	144
5.3	Summary of the average p-values yielded across all features for each object and grasp from a Kruskal-Wallis test. The Kruskal-Wallis test rejects the null hypothesis that healthy and amputee population feature values come from the same distribution at the $< 5\%$ significance level on average. It must be noted that only a single amputee subject took part in the study. . . .	146
6.1	Participant information for physiological data collection experiment consisting of 10 healthy subjects, and 1 amputee subject. . . . .	162
6.2	Table displaying the median timings for each subject carrying out the task performance assessment experiment for sensor suite, MMG and natural control strategies. The sensor suite provided a faster medium to carry out the task, with an 8.53% time improvement over conventional control. . . .	182
B.1	Individual displacement feature p-values returned by a Kruskal-Wallis test for each object and grasp across all subjects grasping at table height and ascending elevation, with the null hypothesis that each set of subject samples	

---

	comes from the same distribution. . . . .	229
B.2	Individual velocity feature p-values returned by a Kruskal-Wallis test for each object and grasp across all subjects grasping at table height and ascending elevation, with the null hypothesis that each set of subject samples comes from the same distribution. . . . .	230
B.3	Individual acceleration feature p-values returned by a Kruskal-Wallis test for each object and grasp across all subjects grasping at table height and ascending elevation, with the null hypothesis that each set of subject samples comes from the same distribution. . . . .	231
C.1	Individual displacement feature p-values returned by a Kruskal-Wallis test for each object and grasp across all subjects grasping at table height and ascending elevation, with the null hypothesis that healthy and amputee populations come from the same distribution. . . . .	233
C.2	Individual velocity feature p-values returned by a Kruskal-Wallis test for each object and grasp across all subjects grasping at table height and ascending elevation, with the null hypothesis that healthy and amputee populations come from the same distribution. . . . .	234
C.3	Individual acceleration feature p-values returned by a Kruskal-Wallis test for each object and grasp across all subjects grasping at table height and ascending elevation, with the null hypothesis that healthy and amputee populations come from the same distribution. . . . .	235
D.1	Individual physiological feature Pearson's coefficients and p-values for a statistically significant correlation with the hand span of healthy subjects across all object locations. . . . .	238
D.2	Individual physiological feature Pearson's coefficients and p-values for a statistically significant correlation with the arm span of healthy subjects across all object locations. . . . .	239

# List of Figures

1.1	The human machine interface (HMI) concept. A HMI translates an action such as muscle movement, resulting from a decision made by the brain, to either interact with the environment directly, or to provide the brain with more information to plan its next task. . . . .	2
2.1	Examples of research-based head tracking input systems. (a) A head-operated joystick that uses infrared to determine head position (reproduced from [1]). (b) The HeadJoystick utilises inertial measurement to track head position as a pointing device (reproduced from [2]). . . . .	11
2.2	Examples of research-based assistive exoskeletons. (a) The Power-Assist Glove assists grasping force by using angle sensors to predict grasp intention (reproduced from [3]). (b) The Grip Aid System uses bending force sensors to assist grip if the finger's bend angle passes an angle threshold (reproduced from [4]). . . . .	12
2.3	(a) Research-based IMU and MMG HMI uses arm gestures to select grasp patterns on a prosthetic hand (reproduced from [5]). (b) The commercial-based Symbiotic Leg Prosthesis by Össur (reproduced from [6]). . . . .	13
2.4	Examples of research-based gaze tracking systems. (a) A low-cost gaze estimation system for control of a volumetric cursor (reproduced from [7]). (b) EOG integrated goggles for gesture-based interaction (reproduced from [8]). . . . .	15
2.5	The research-based Tongue Drive System for controlling a wheel chair (re-	

---

produced from [9]). . . . .	21
2.6 (a) The commercial-based I-limb Quantum myoelectric hand prosthesis by Touch Bionics (reproduced from [10]). (b) An 8 channel EMG interface used to distinguish between 7 different finger movements (reproduced from [11]). . . . .	25
2.7 Sound waves recorded as a result of supramaximal twitches from (a) an air coupled microphone, (b) piezoelectric contact sensor, and (c) accelerometer (reproduced from [12]). . . . .	28
2.8 The cognitive vision system developed by S. Došen <i>et al.</i> attached to a CyberHand fitted to an orthopaedic splint, using EMG electrodes for myoelectric control (reproduced from [13]). . . . .	32
2.9 System architecture of the stereo AR system developed by M. Marković, comprising of (1) a semi-autonomous controller, (2) AR glasses with integrated stereo cameras, (3) a dual channel myoelectric interface and (4) a dexterous prosthetic hand (reproduced from [14]). When the myoelectric interface receives a trigger command, the stereo vision system calculates the size and geometric shape of the target object, selecting the prosthesis aperture size and grasp pattern, and projects an image overlay on to the AR displays. . . . .	33
2.10 System architecture of the CASP system developed by M. Marković, comprising of (1) a dual channel myoelectric interface, (2) a RGB-D computer vision sensor, (3) a processing unit, (4) a dexterous prosthetic hand, and (5) an IMU sensor (reproduced from [15]). When the myoelectric interface receives a trigger command, the processing unit determines the prosthesis aperture, grasp pattern, orientation and depth of the target object from the computer vision sensor, providing autonomous hand preshaping and wrist rotation. The IMU tracks prosthesis orientation, adjusting wrist rotation when required. . . . .	35
3.1 Overview of system flow from the heterogeneous sensor suite to the control	



---

of a robotic end-effector for interaction. The system flow can be separated into a *Local Control System (LCS)*, responsible for internal motor feedback control for the robotic end-effector, and the *Sensor Control System (SCS)*, which receives sensory feedback from the operator and the environment. . . . 40

3.2 The system flow diagram for the proposed heterogeneous sensor suite. The *Muscle Activation Subsystem* consists of a single-site MMG sensor. It monitors the operator’s acoustic muscle response, filtering it in real-time. The IMU sensors provide motion feedback to reduce the number of misclassifications due to arm movement. Once the activation threshold has been reached, and the motion conditions have been met, the hand will either open, if the hand is in the closed state, or initiate the grasp selection pipeline. The first stage is the *Computer Vision Subsystem*, which uses a low-cost web camera positioned in an eye-to-hand configuration to take a single snapshot of the operator’s point of view. This image goes through a series of processing filters to detect the edges of objects within the scene. These are separated into blobs, whereby the one of largest interest is classified against a set of image templates using the blob’s properties. The detected object specifies a set of possible grasp patterns unique to that object, which is then used by the *Grasp Prediction Subsystem* to determine the most suitable grasp. A pair of IMUs are used to record the motion of the arm during the reaching phase of grasp. The recorded motion measures the X, Y and Z quaternion components of the forearm and upper arm. The resulting motion profile is filtered, and its features extracted. Specific features are used to classify against a template unique to the individual to select the most suitable grasp pattern. The current grasp selection on the *LCS* is then checked against the desired grasp, to determine whether a *grasp change* command needs to be sent before sending a *close* command. Once this has been determined, the appropriate commands are then sent to the *LCS*. . . . . 41

3.3 The MMG sensor directly linked to the upper arm IMU to utilise gyroscopic

---

feedback in order to reduce unintentional muscle activation due to arm motion.	43
3.4 A tree diagram of all available grasp patterns for the Bebionic hand in terms of availability and thumb position. . . . .	47
3.5 Exploded SolidWorks model of the myoelectric hand adapter, consisting of 5 different 3-D printed components: the <i>housing</i> , <i>cover</i> , <i>connector lock</i> , <i>clip</i> and <i>EQD housing</i> . . . . .	52
3.6 The 3-D printed hand adapter showing (a) the complete assembly, (b) adapter <i>key</i> and forearm prosthesis lock, (c) EQD connector fastened with the <i>connector lock</i> , (d) microcontroller, high-current voltage regulator and LiPo battery, and (e) the Bebionic hand held inside the <i>EQD housing</i> using the <i>clips</i> . . . . .	53
4.1 The MMG sensor design reproduced from work by R. Woodward <i>et al.</i> (reproduced from [16]). The design utilises a single microphone sensor, which measures the pressure change within a conical chamber enclosed by a Mylar membrane. . . . .	56
4.2 The manufactured MMG sensor reproduced from work by R. Woodward <i>et al.</i> [16]. The sensor is sewn into wearable clothing using several through-holes in the Clip. . . . .	57
4.3 The processed MMG signal, taken from the author, during isometric contractions of the forearm during single and double contractions. A single contraction increases the MMG response briefly above the threshold, and is used to open or close the hand. A double contraction extends the duration of the response above the threshold, and is used to activate a <i>soft</i> grasp switch.	59
4.4 The cumulative effect of image processing steps on original image (a) consisting of (b) contrast correction, (c) grayscale conversion, (d) Sobel edge detection, (e) Canny edge detection, (f) 5x5 Gaussian smoothing and (g) binary thresholding. . . . .	63
4.5 Flow diagram of the blob filtering process to find the object of interest. Blobs are removed if they fall outside the threshold boundaries of various	

---

properties. $A_{min}$ and $A_{max}$ represents the minimum and maximum blob area cutoff respectively. $H_{cam}$ and $W_{cam}$ represent the height and width of the camera resolution, and $E_{Dist}$ and $E_{cen}$ denote the euclidean distance from the blob's centre of gravity from the center of the camera, and the cutoff threshold respectively. . . . .	65
4.6 Complete blob processing for (a) bottle, (b) lid, (c) box and (d) timer objects, with original image displayed on top, and processed image on bottom.	67
4.7 Conceptual design of the preliminary control system architecture for MMG and computer vision sensor fusion. The control architecture is split into 4 subsystems: 1) a pair of MMG sensors, 2) the computer vision system, which estimates object parameters, translating them into a suitable grasp pattern using a set of rules, 3) a serial communication interface to translate processed sensor outputs into usable signals for the Bebionic V2 hand; and 4) the Bebionic V2 hand controller that contains the pre-programmed grasp patterns. The computer vision system processes an image taken from the web camera, filtering out any redundant blobs and classifying the grasp based on the object's size, while the MMG sensor pair are used to detect alternating muscle activation. The open and close commands sent by the MMG sensors, and grasp change commands sent from the computer vision system are passed on to the serial communication interface, which converts the sensor outputs into voltage commands to be sent to the Bebionic Hand. .	68
4.8 MMG sensor pair positioned on the flexor and extensor digitorum of the non-grasping arm using a tubular bandage. . . . .	69
4.9 Flow diagram of the preliminary computer vision system used to select grasp patterns. . . . .	70
4.10 The Grasp Selection Decision Tree. If the blob's area is greater than a threshold of 75000 pixels, a <i>Power</i> grasp is selected. If the area is below the threshold, then a <i>Pinch</i> grasp is selected. . . . .	71
4.11 The preliminary eye-in-hand prosthesis testing two objects: a squash ball	

---

	for a <i>pinch</i> grasp and a deodorant bottle for a <i>power</i> grasp. . . . .	72
4.12	A series of images taken during the experiment from rows 1) to 3), where a) shows an observer's perspective at the different time intervals. The resulting computer vision output of b) raw grayscaling, c) convolution, d) noise removal and blob labelling, and e) binary thresholding and blob filtering. . .	73
4.13	Classification success rate for the grasping task on pairs of small and large handheld objects. The objects were paired as follows: squash ball and deodorant, paint pot and battery, and pink glass and USB pen. . . . .	74
5.1	The amputee participant's forearm prosthesis connected to the Bebionic Hand using a custom 3-D printed adapter. The forearm prosthesis was designed for use with a mechanical hook, however the adapter enabled its use with the myoelectric hand. . . . .	82
5.2	The software interface developed to collect grasp trajectory data from subjects. The software consisted of separate tabs for object template collection, grasp data collection and real-time control. . . . .	83
5.3	The settings dialogue box allowed individual experiment selection and grasp randomisation after initialising the grasp experiment. . . . .	83
5.4	The sensor sleeve used for collecting physiological data fitted on a healthy subject. The attached MMG sensor is not used during this study. . . . .	84
5.5	A tree diagram depicting the different grasps used for each object. The bottle was grasped with <i>power</i> and <i>lateral</i> grasps, the box with <i>power</i> , <i>lateral</i> and <i>precision</i> grasps, and the lid with <i>lateral</i> and <i>precision</i> grasps. . . . .	85
5.6	The <i>rest</i> position while (a) sitting has the subject's dominant hand placed along its bottom edge, with the centre of the palm approximately 10 cm from the edge of the table, and (b) standing has subject's dominant arm pointed downwards by their side, approximately in line with the centre of the seated <i>rest</i> position. . . . .	86
5.7	Object locations during data collection showing locations at $-45^\circ$ , $0^\circ$ and $45^\circ$ with depths of 20 cm and 30 cm. These object locations are also used at	

---

three elevation levels: <i>ascending</i> , <i>descending</i> and <i>table height</i> . Each object is tested consecutively at these 9 possible position variations. . . . .	86
5.8 The amputee subject carrying out a <i>power</i> grasp on a bottle at an <i>ascending</i> elevation in the study. . . . .	87
5.9 Left to right: Grasps being made with an elevation at ascent, table height and descent by a healthy subject. . . . .	87
5.10 Steps taken when carrying out a single experimental trial, where the subject (a) starts in the <i>rest</i> position, (b) reaches towards the object when prompted, (c) grasps the object in the designated grasp pattern, (d) returns the hand to the <i>rest</i> position. . . . .	88
5.11 Block diagram representation of the complete orientation estimation algorithm for a magnetic angular rate and gravity (MARG) implementation including magnetic distortion compensation (reproduced from [17]) . . . . .	95
5.12 Quaternion vector (a) displacement, (b) velocity and (c) acceleration profiles of <i>lateral</i> and <i>power</i> grasps made on a bottle at a depth of 30 cm and angle of 0° at table height from a single healthy subject. The grasp profiles have been extracted from the 3 second trials, and have been aligned using cross-correlation. <i>Lateral</i> and <i>power</i> grasps have very different reach trajectories, especially in forearm orientation, emphasised by the large difference in FAz. . . . .	100
5.13 Quaternion vector (a) displacement, (b) velocity and (c) acceleration profiles of <i>lateral</i> and <i>power</i> grasps made on a bottle at a depth of 30 cm and angle of 0° at table height from a single amputee subject. The grasp profiles have been extracted from the 3 second trials, and have been aligned using cross-correlation. <i>Power</i> grasps made have very little overall displacement, with UAz providing most of the motion during grasp. <i>Lateral</i> grasps have a much greater range of motion, mostly provided by forearm vector components FAx and FAz. . . . .	101
5.14 Example data from a single healthy subject comparing Max(+) displace-	

---

ment features across all elevation, depth and angular positions for *lateral* and *power* grasps made on a bottle. The forearm and upper arm X, Y and Z components are represented by the terms F<sub>Ax</sub>, F<sub>Ay</sub>, F<sub>Az</sub>, U<sub>Ax</sub>, U<sub>Ay</sub> and U<sub>Az</sub> respectively. Substantial discrimination is evident between the two grasps at Max(+):F<sub>Az</sub> displacement at table height and ascending elevation, however at descending, the *power* grasp reduces to zero. F<sub>Ax</sub> shows positive Max(+):F<sub>Ax</sub> displacement only at a descending elevation. A change in depth doesn't cause much variation in Max(+), however a change of angular position from negative to positive shows a small increase in Max(+):F<sub>Ax</sub> displacement from zero, as well as a decrease in Max(+):F<sub>Ay</sub> towards zero. Upper arm Max(+) features have lower separation across all elevation locations, but have much lower variance. . . . . 103

5.15 Example data from a single amputee subject comparing Max(+) displacement features across all depth and angular positions at table height and ascending for *lateral* and *power* grasps made on a bottle. The forearm and upper arm X, Y and Z components are represented by the terms F<sub>Ax</sub>, F<sub>Ay</sub>, F<sub>Az</sub>, U<sub>Ax</sub>, U<sub>Ay</sub> and U<sub>Az</sub> respectively. Max(+) displacement show very high discrimination between the two grasps for F<sub>Az</sub>, and F<sub>Ax</sub> components respectively, with the large separation providing plenty of room for any variance between object locations. Other components have much less discriminatory power. . . . . 105

5.16 Example data from a single healthy subject comparing Max(+) velocity features across all elevation, depth and angular positions for *lateral* and *power* grasps made on a bottle. The forearm and upper arm X,Y and Z components are represented by the terms F<sub>Ax</sub>, F<sub>Ay</sub>, F<sub>Az</sub>, U<sub>Ax</sub>, U<sub>Ay</sub> and U<sub>Az</sub> respectively. Max(+):F<sub>Az</sub> velocity has the greatest discrimination between the two grasps compared to the other vector components, showing reasonable invariance across all object locations with the exception of those made at a descent, which has a much lower magnitude. Max(+):F<sub>Ax</sub> and Max(+):F<sub>Ay</sub>

---

have relatively poor separation across all object locations. Max(+) upper arm components show reasonably good discrimination between the two grasps, and are also quite invariant across all object locations, including those made at descending. . . . .	106
5.17 Example data from a single amputee subject comparing Max(+) velocity features across all elevation, depth and angular positions for <i>lateral</i> and <i>power</i> grasps made on a bottle. The forearm and upper arm X,Y and Z components are represented by the terms FAx, FAy, FAz, UAx, UAy and UAz respectively. Max(+) velocity show high discrimination between grasps in FAz and FAx respectively, with other vector components having much lower separability in comparison. Max(+) upper arm components UAx and UAz show some discrimination between the two grasps, however are subject to variance due to changes in angular position. . . . .	108
5.18 Example data from a single healthy subject comparing Max(+) acceleration features across all elevation, depth and angular positions for <i>lateral</i> and <i>power</i> grasps made on a bottle. The forearm and upper arm X,Y and Z components are represented by the terms FAx, FAy, FAz, UAx, UAy and UAz respectively. Max(+) forearm acceleration shows overall strong discrimination between the two grasps with Max(+):FAx and Max(+):FAz being the most invariant to changes in object location with the exception of those made at a descent, which shows a reduction in magnitude across all features. Max(+) has the poorest discrimination of the Max(+) forearm features and increases in variance due to changes in angular location. Max(+) upper arm acceleration shows lower discrimination in comparison with the exception of Max(+):UAz which shows good overall discrimination with low variance. . . . .	109
5.19 Example data from a single amputee subject comparing Max(+) acceleration features across all elevation, depth and angular positions for <i>lateral</i> and <i>power</i> grasps made on a bottle. The forearm and upper arm X,Y and	

---

Z components are represented by the terms FAX, FAY, FAZ, UAX, UAY and UAZ respectively. Max(+) acceleration features display good discrimination between the two grasps, with overall greater separation at table height compared to ascending. Max(+):FAX and Max(+):FAZ show stronger discrimination with the least variance. Upper arm components show greater variance and lower discriminatory power compared to the forearm vector components. . . . .	111
5.20 Quaternion vector (a) displacement, (b) velocity and (c) acceleration over time of <i>lateral</i> and <i>precision</i> grasps made on a lid at a depth of 30 cm and angle of 0° at table height from a single healthy subject. The grasp profiles have been extracted from the 3 second trials, and have been aligned using cross-correlation. The trajectories of these two grasps are much more similar, with only minor visible differences. Velocity and acceleration profiles show greater differences, however, the similarities in the two grasps leaves much less room for variance due to changes in object location. . . . .	112
5.21 Quaternion vector (a) displacement, (b) velocity and (c) acceleration over time of <i>lateral</i> and <i>precision</i> grasps made on a lid at a depth of 30 cm and angle of 0° at table height from a single amputee subject. The grasp profiles have been extracted from the 3 second trials, and have been aligned using cross-correlation. The two grasps have much more similar motion, with the highest displacement coming from FAX and FAZ. The upper arm looks to have a larger role in determining grasp trajectory, especially UAY. . . . .	113
5.22 Example data from a single healthy subject comparing Max(-) displacement features across all elevation, depth and angular positions for <i>lateral</i> and <i>precision</i> grasps made on a lid. The forearm and upper arm X,Y and Z components are represented by the terms FAX, FAY, FAZ, UAX, UAY and UAZ respectively. Max(-):FAX shows strong discrimination between grasps and invariance in displacement at table height and ascending elevation, with a decrease in negative displacement at descending, however still shows strong	



---

	discrimination between grasps. The remaining forearm and upper arm components have overall poor separation, with Max(-):FAz, Max(-):UAX and Max(-):UAY approximated to zero across all object locations. . . . .	114
5.23	Example data from a single amputee subject comparing Max(-) displacement features across all elevation, depth and angular positions for <i>lateral</i> and <i>precision</i> grasps made on a lid. The forearm and upper arm X,Y and Z components are represented by the terms FAX, FAY, FAZ, UAX, UAY and UAZ respectively. Max(-) features has higher consistency of discrimination between grasps from components FAX and UAY, both being fairly invariant to changes in object location. All other Max(-) vector features show negligible discrimination between the two grasps. . . . .	115
5.24	Example data from a single healthy subject comparing RMS velocity features across all elevation, depth and angular positions for <i>lateral</i> and <i>precision</i> grasps made on a Lid. The forearm and upper arm X,Y and Z components are represented by the terms FAX, FAY, FAZ, UAX, UAY and UAZ respectively. RMS:FAX shows relatively good discrimination and invariance in comparison to the other forearm components across all object locations, with the exception of those at descending elevation. Upper arm RMS velocity features have stronger invariance but lower discriminatory power, with RMS:UAX being the most prominent. . . . .	117
5.25	Example data from a single amputee subject comparing RMS velocity features across all elevation, depth and angular positions for <i>lateral</i> and <i>precision</i> grasps made on a lid. The forearm and upper arm X,Y and Z components are represented by the terms FAX, FAY, FAZ, UAX, UAY and UAZ respectively. RMS velocity shows fairly weak separation between grasps, with upper arm features performing better overall. Discrimination appears to be stronger at table height. . . . .	118
5.26	Example data from a single healthy subject comparing RMS acceleration features across all elevation, depth and angular positions for <i>lateral</i> and	

---

	<i>precision</i> grasps made on a lid. The forearm and upper arm X,Y and Z components are represented by the terms FAX, FAY, FAZ, UAX, UAY and UAZ respectively. RMS forearm acceleration features have overall poor discrimination and high variance. RMS:FAX has stronger discriminatory power however is subject to variance due to changes in depth location. RMS upper arm features show higher discrimination in comparison, with RMS:UAX and RMS:UAZ being more invariant to changes in object location. Grasps made at a descent show a reduction in magnitude and discriminatory power.	120
5.27	Example data from a single amputee subject comparing RMS acceleration features across all elevation, depth and angular positions for <i>lateral</i> and <i>precision</i> grasps made on a lid. The forearm and upper arm X,Y and Z components are represented by the terms FAX, FAY, FAZ, UAX, UAY and UAZ respectively. RMS acceleration features show very little separation between grasps and high variance across all object locations. . . . .	121
5.28	Quaternion vector (a) displacement, (b) velocity and (c) acceleration over time of <i>lateral</i> , <i>power</i> and <i>precision</i> grasps made on a box at a depth of 30 cm and angle of 0° at table height from a single healthy subject. The grasp profiles have been extracted from the 3 second trials, and have been aligned using cross-correlation. All three grasps have very similar reach trajectories, making it more difficult to differentiate between them. . . . .	122
5.29	Quaternion vector (a) displacement, (b) velocity and (c) acceleration over time of <i>lateral</i> , <i>power</i> and <i>precision</i> grasps made on a box at a depth of 30 cm and angle of 0° at table height from a single amputee subject. The grasp profiles have been extracted from the 3 second trials, and have been aligned using cross-correlation. All three grasps have very similar reach trajectories, with FAX and FAZ providing the largest change in motion. <i>Precision</i> grasps show slightly greater displacement in the negative direction, but upper arm motion looks to be very similar across all grasps. . . . .	123
5.30	Example data from a single healthy subject comparing PoG displacement	

features across all elevation, depth and angular positions for <i>lateral</i> , <i>power</i> and <i>precision</i> grasps made on a box. The forearm and upper arm X,Y and Z components are represented by the terms FAx, FAy, FAz, UAx, UAy and UAz respectively. The main discrimination emphasis between the <i>lateral</i> and <i>precision</i> grasps are from forearm IMU components PoG:FAx and PoG:FAz, with PoG:FAy also showing reasonable discrimination across object locations. A reduction in object depth shows a reduction in the distinction between the grasps. Forearm features show greater separation between the three grasps at both depth positions in comparison to the upper arm features. Grasps made at a descending elevation shows greatly reduced displacement. . . . .	124
5.31 Example data from a single amputee subject comparing PoG displacement features across all elevation, depth and angular positions for <i>lateral</i> , <i>power</i> and <i>precision</i> grasps made on a box. The forearm and upper arm X,Y and Z components are represented by the terms FAx, FAy, FAz, UAx, UAy and UAz respectively. PoG:FAx shows good discrimination between <i>precision</i> and the other two grasps, having stronger individual discrimination at ascent in comparison to table height. Despite having low separation, the upper arm components do show some consistency between the three grasps. . . . .	125
5.32 Example data from a single healthy subject comparing Max(-) velocity features across all elevation, depth and angular positions for <i>lateral</i> , <i>power</i> and <i>precision</i> grasps made on a box. The forearm and upper arm X,Y and Z components are represented by the terms FAx, FAy, FAz, UAx, UAy and UAz respectively. Max(-):FAy provides the largest discrimination and the least variance between the 3 grasps of the forearm components, with the separation of <i>precision</i> grasp being the most prominent. Max(-):FAy has higher variation from -45° to +45°, whereas Max(-):FAz shows overall very poor discrimination. Upper arm components show lower discrimination between the grasps, but show stronger separation between the <i>power</i> grasp	

---

	and the other two, with Max(-):UAY being the strongest component. . . . .	126
5.33	Example data from a single amputee subject comparing Max(-) velocity features across all elevation, depth and angular positions for <i>lateral</i> , <i>power</i> and <i>precision</i> grasps made on a box. The forearm and upper arm X,Y and Z components are represented by the terms FAX, FAY, FAZ, UAX, UAY and UAZ respectively. Max(-) upper arm vector features have poor separability, and forearm features Max(-):FAY has high variance across changes in depth and angular position, while Max(-):FAZ remains at approximately zero throughout. . . . .	128
5.34	Example data from a single healthy subject comparing P2P acceleration features across all elevation, depth and angular positions for <i>lateral</i> , <i>power</i> and <i>precision</i> grasps made on a box. The forearm and upper arm X,Y and Z components are represented by the terms FAX, FAY, FAZ, UAX, UAY and UAZ respectively. P2P:FAX shows overall better discrimination between all three grasps than the other features, with the separation of <i>precision</i> grasps being the most prominent, however is subjected to higher variance with changes in object depth. P2P upper arm features show better separation of <i>power</i> grasps, however the overall grasp discrimination is still fairly low, not giving much room for variance due to changes in object location. Grasps made at a descent show overall better separation between <i>precision</i> grasps, however show overall lower discriminatory power. . . . .	130
5.35	Example data from a single amputee subject comparing P2P acceleration features across all elevation, depth and angular positions for <i>lateral</i> , <i>power</i> and <i>precision</i> grasps made on a box. The forearm and upper arm X,Y and Z components are represented by the terms FAX, FAY, FAZ, UAX, UAY and UAZ respectively. P2P acceleration features show poor discrimination between grasps and high variance across all object locations. . . . .	131
5.36	Cumulative feature scores of all subjects for grasping a (a) bottle with <i>lateral</i> and <i>power</i> grasps, where Max(+) velocity features performed the best	

---

	across all forearm and upper arm vector components, however Max(-):FAx Velocity had the highest score overall; (b) lid with <i>lateral</i> and <i>precision</i> grasps, where forearm and upper arm vector components are spread more evenly, with the strongest performing feature being PoG:Uay displacement, closely followed by Max(-):Uay displacement; and (c) box with <i>lateral</i> , <i>power</i> and <i>precision</i> grasps across all object locations, where the displacement profile had the strongest scores all round, with PoG:FAx being the strongest, while velocity profile features show overall poor performance, and acceleration profile features scored zero across all feature sets. . . . .	133
5.37	Feature scores of a single amputee subject for grasping a (a) bottle with <i>lateral</i> and <i>power</i> grasps, where discrimination was so strong that it only required a single displacement feature, PoG:FAx, to distinguish between the two grasp patterns; (b) lid with <i>lateral</i> and <i>precision</i> grasps, where upper arm velocity features appeared to provide the strongest separation; and (c) box with <i>lateral</i> , <i>power</i> and <i>precision</i> grasps across all object locations, where displacement features were the best performing, with PoG:FAx providing the best discrimination. . . . .	134
5.38	Cumulative feature scores of all healthy subjects at table height and ascending elevation for grasping a (a) bottle with <i>lateral</i> and <i>power</i> grasps, where PoG displacement providing the largest discrimination between the two; (b) lid with <i>lateral</i> and <i>precision</i> grasps, where displacement features show stronger discrimination, with velocity features still playing an important role in classification; and (c) box with <i>lateral</i> , <i>power</i> and <i>precision</i> grasps, where displacement features are the most prominent, with velocity features also playing a large role in grasp discrimination. . . . .	135
5.39	Example decision tree for an amputee subject when grasping a lid, where x1 and x2 represent different features. Triangular nodes represent a <i>branch</i> , and a circular node represents a <i>leaf</i> . . . . .	139
5.40	Comparison of mean misclassification rates for 10 healthy subjects for bot-	

---

tle, lid and box objects across (a) all object locations and (b) all object locations at ascending and table height only. The KNN classifier performed the best across all objects, with a mean misclassification rate of 3.83%, 23.03% and 13.59% at all object locations, and 0%, 18.35% and 11.51% at just table height and ascending elevations for the bottle, lid and box respectively, while SVM performed the worst. . . . .	141
5.41 Comparison of misclassification rates for a single amputee subject for bottle, lid and box objects for grasps made at all object locations at ascending and table height. The KNN classifier performed the best across all objects, with a mean misclassification rate of 0%, 3.36% and 4.47%, while SVM performed the worst. . . . .	142
5.42 Comparison of individual subject POG:FAx displacement distributions for <i>lateral</i> grasps made on a bottle at table height and ascending elevation. The median and variance of the feature is considerably varied between subjects, provides evidence to suggest that the features are subject-specific. . . . .	145
5.43 Comparison of healthy and amputee POG:FAx displacement distributions for <i>lateral</i> grasps made on a bottle at table height and ascending elevation. The Kruskal-Wallis test rejected the null hypothesis that POG:FAx displacement from both subject populations come from the same distribution. This suggests that subjects can be grouped according to these two demographics, however it must be noted that only a single amputee subject took part in the study. . . . .	146
5.44 Correlation across healthy subjects of (a) height and arm span, showing a strong positive correlation, whereby taller subjects have a wider arm span; and (b) arm span and hand span, showing a weak positive correlation, indicating that taller subjects tend to have slightly larger hands. . . . .	147
5.45 Displacement, velocity and acceleration feature score distribution across forearm and upper arm for (a) healthy subjects for all object locations, (b) healthy subjects for all objects locations at table height and ascending, and	

---

(c) amputee subjects for all object locations at table height and ascending. Displacement features provided the greatest discrimination between grasps, with velocity features also showing strong importance. Acceleration features on the other hand have very low discriminatory power. Both forearm and upper arm motion shows a relatively even distribution between scoring features, with forearm features performing slightly better. This suggests that upper arm motion is just as important as forearm motion when determining grasp. . . . .	149
6.1 Various sensors built into the sensor suite, including: (a) the MMG sensor sewn into the compression sleeve, (b) the forearm IMU sewn into the wrist split over the Bebionic hand and adapter, (c) the computer vision system consisting of a pair of safety goggles, web camera and fish eye lens, and (d) the audio headset used to prompt user actions. . . . .	154
6.2 Healthy subject fitted with the sensor suite and Bebionic V2 Hand. . . . .	156
6.3 Complete sensor suite control architecture for controlling a Bebionic V2 hand. When a user intends to interact with an object, he or she turns their head towards it, centering its position in the camera's image. The user activates the extensor digitorum in the forearm, and the muscular response is measured with a MMG sensor. If the muscle response goes beyond a certain threshold, and arm motion is not detected by the IMU gyroscopes, then the response is considered an intentional muscle activation. If the hand is already in a closed position, then a <i>grasp open</i> command is sent, opening the hand. If the hand is in the open position, then the system proceeds to predict whether a grasp change is required before closing the hand. The camera is used to take a snapshot of the user's point of view, where the image follows a series of image processing and blob filtering steps to classify the target object of interest. Once classified, arm motion is recorded for 3 seconds as the user reaches towards the object. Grasp features are then extracted and compared against a user-specific grasp template for that object	

---

	class, predicting the desired grasp pattern according to a KNN classifier. The classified grasp pattern is then selected using a <i>grasp change</i> command if required, followed by a <i>grasp close</i> command, closing the hand around the object. . . . .	158
6.4	Bebalance+ software to adjust the configuration of the Bebionic hand, how it is controlled and the selection of pre-installed grasp patterns. . . . .	160
6.5	The sensor control interface output when carrying out a grasp task using the sensor suite. The interface displays the live video input to the cam- era, orientation of the IMU sensors, and processed MMG signal, as well as calibration and manual control options. . . . .	160
6.6	A healthy subject collecting partial template data using the sensor sleeve and Bebionic V2 hand. . . . .	164
6.7	Classification performance assessment workspace. The object is located in the center of the left cordon, and is transported towards the right cordon using a specific grasp pattern, and vice versa. The hand starts and ends at the <i>rest</i> position. . . . .	165
6.8	A healthy subject carrying out the classification performance experiment on a bottle using a <i>power</i> grasp, starting with the hand in the (a) <i>rest</i> position, (b) grasping the bottle in the left cordon, (c) transporting the bottle towards the right cordon, and (d) returning to the <i>rest</i> position. . . . .	167
6.9	An amputee subject carrying out the classification performance assessment on a bottle using a <i>power</i> grasp. . . . .	168
6.10	Confusion matrix for the average classification performance of the CVSS across both healthy and amputee participants. . . . .	168
6.11	Confusion matrix for the overall classification performance of the system for (a) bottle, (b) lid and (c) box for all healthy subjects, and (d) bottle, (e) lid and (f) box for amputee subjects. . . . .	169
6.12	3-Class confusion matrices for individual grasp classification performance across correctly identified objects for (a) bottle, (b) lid and (c) box for all	



---

healthy subjects, and (d) bottle, (e) lid and (f) box for the amputee subject. .	170
6.13 Pie charts displaying the average classification outcomes for each object across both healthy and amputee subjects. . . . .	172
6.14 Task assessment workspace. 1) The timer is started using a <i>finger point</i> grasp. 2) The bottle is transported from the left cordon into the box in the centre cordon using a <i>power</i> grasp. 3) The lid is transported from the right cordon into the box in the centre cordon using a <i>precision</i> grasp. 4) The box is transported from the centre cordon to the right cordon using a <i>lateral</i> grasp. 5) The timer is stopped using a <i>finger point</i> grasp. The hand starts at the <i>rest</i> position whenever a grasp is initiated. . . . .	179
6.15 Flow diagram highlighting the change in grasp during the task, where D and A represent the default and alternate grasp patterns respectively. A dashed line represents a grasp made with the thumb in the opposed position, and a solid line represents a grasp made with the thumb in the non-opposed position.	180
6.16 A subject carrying out the task performance experiment. Starting with the hand in the (a) <i>rest</i> position, the subject uses the sensor suite to (b) press the triangle with a <i>finger point</i> grasp to start the timer, (c) return the hand to the <i>rest</i> position, (d) manually change the thumb position, (e) pick up the bottle using a <i>power</i> grasp, (f) place the bottle in the box, (g) return the hand to the <i>rest</i> position, (h) pick up the lid using a <i>precision</i> grasp, (i) place the lid into the box, (j) return the hand to the <i>rest</i> position, (k) manually change the thumb position, (l) use a <i>lateral</i> grasp on the box, (m) move the box to the right cordon, (n) return the hand to the <i>rest</i> position, and (o) touch the triangle using a <i>finger point</i> grasp to stop the timer. . . . .	181
6.17 Timing results of the task performance assessment showing (a) raw results, and (b) boxplots for each subject performing five trials for each of the three control strategies. The sensor suite provided a faster medium to carry out the task, with an 8.53% time improvement over conventional control. . . .	183
A.1 1: Very Small (VS) object class grasped using a) <i>power</i> , b) <i>pinch</i> and c)	

---

	<i>open palm</i> grasp; 2: Small (S) object class grasped using a) <i>power</i> , b) <i>pinch</i> , and c) <i>tripod</i> grasp; 3: Cup (C) object class grasped using a) <i>power</i> and b) <i>tripod</i> grasp. . . . .	222
A.2	A pair of x-IMU sensors fitted on the forearm and upper arm using a velcro strap. A wrist strap was used to prevent wrist flexion and extension during grasp. . . . .	223
A.3	Subject Forearm IMU (top) and Upper arm IMU (bottom) quaternion vectors over time for the very small object class . . . . .	225
A.4	Subject Forearm IMU (top) and Upper arm IMU (bottom) quaternion vectors over time for the small object class . . . . .	226
A.5	Subject Forearm IMU (top) and Upper arm IMU (bottom) quaternion vectors over time for the cup object class . . . . .	227
A.6	Grasp class clusters using the top 3 most identifiable features for each subject for the very small object class . . . . .	227
A.7	Grasp class clusters using the top 3 most identifiable features for each subject for the small object class . . . . .	228
A.8	Grasp class clusters using the top 3 most identifiable features for each subject for the cup object class . . . . .	228

# Nomenclature

ACC	Acceleration
ADL	Activities of daily living
ALS	Amyotrophic lateral sclerosis
ANS	Automatic nervous system
AR	Augmented reality
AT	Assistive technologies
BT	Bluetooth
CNS	Central nervous system
CPA	Classification performance assessment
CVS	Cognitive vision system
CVSS	Computer vision subsystem
DISP	Displacement
DOF	Degrees of freedom
DT	Decision Trees
ECOC	Error correcting output coding
EKF	Extended Kalman filter

---

EMG	Electromyography / electromyogram
EOG	Electrooculography
FA <sub>x</sub>	Forearm X-direction vector
FA <sub>y</sub>	Forearm Y-direction vector
FA <sub>z</sub>	Forearm Z-direction vector
FES	Functional electric stimulation
FSR	Force sensitive resistor
GPSS	Grasp prediction subsystem
HD	High definition
HMI	Human machine interface
IMU	Inertial measurement unit
IR	Infrared
KNN	K-nearest neighbours
LCS	Local control system
LDA	Linear discriminant analysis
LIS	Locked-in syndrome
MARG	Magnetic angular rate and gravity
MASS	Muscle activation subsystem
Max(+)	Maximum in the positive direction
Max(-)	Maximum in the negative direction
MEMS	Micro electro-mechanical systems

---

MMG	Mechanomyography / mechanomyogram
MS	Multiple sclerosis
MSE	Mean-squared error
NPR	Non-pattern recognition
P2P	Peak to peak difference
PCB	Printed circuit board
PK-Dist	Peak to peak distance
PK-RMS	Peak to root-mean-squared
PNS	Peripheral nervous system
PoG	Point of Grasp
PPS	Post-polio syndrome
PR	Pattern recognition
QDA	Quadratic discriminant analysis
RF	Radio frequency
RGB	Red green blue
RGB-D	Red green blue - depth
RMS	Root-mean-squared
SCI	Spinal Cord Injury
SCS	Sensor control system
SLA	Stereolithography
SNR	Signal-to-noise ratio

---

SNS	Somatic nervous system
STD	Standard deviation
SVM	Support vector machines
TPA	Task performance assessment
UAx	Upper arm X-direction vector
UAy	Upper arm Y-direction vector
UAz	Upper arm Z-direction vector
USB	Universal serial bus
VEL	Velocity

# Chapter 1

## Introduction

Recent development in wearable sensors and technology enable a wide variety of biological and physiological activity to be monitored during daily life, thus having a large impact in the growth of portable medical and rehabilitative devices. Their adoption by the biomedical field has enabled advanced care to patients for a wide variety of neurological disorders and physical disabilities, providing rapid response indicators, monitoring of daily activities for mobility assessment, enhancing the function of devices to aid patients in motor tasks and providing artificial limb solutions for those that need them. Having previously been restricted to a clinical setting, the advancement of wearable sensor technology has provided vast improvements to home assessment, rehabilitation and prosthesis control, providing more meaningful quantitative data to continue to increase the effectiveness of care and the quality of lives. The growing variety of sensors available can form a bridge between body activity and interactive technology, or a human machine interface (HMI). Figure 1.1 illustrates this concept, whereby an action such as muscle movement, voluntary or involuntary, following a decision made by the brain, can be used as an input to a HMI to either interact with the environment directly, or to provide the brain with more information to plan its next task. The high versatility of this concept facilitates an infinite number of applications not just limited to the biomedical field, but also in automotive, aerospace, military, manufacturing and entertainment industries. As gains in technological advancement drive the world forward into the future, wearable technology will become a part of our daily lives.

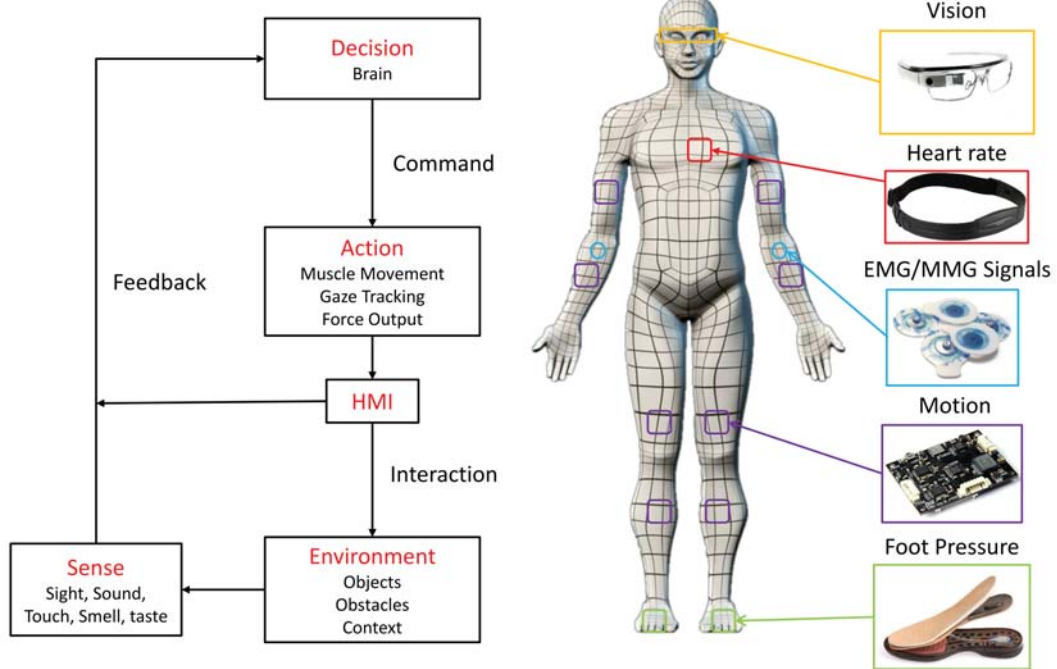


Figure 1.1: The human machine interface (HMI) concept. A HMI translates an action such as muscle movement, resulting from a decision made by the brain, to either interact with the environment directly, or to provide the brain with more information to plan its next task.

## 1.1 Motivation and Thesis Focus

The human hand is a complicated but versatile end-effector involving at least 24 degrees of freedom. It is capable of performing complex object manipulation with speed and accuracy. The design and development of robotic hands with multiple degrees of freedom has advanced significantly in recent years; a comparison of anthropomorphic devices, both commercially available and research-based, bench marked against performance is given in [18]. Despite vast work of significant impact, appropriate and relevant control strategies are still lacking ([19]; see [20], [21] for recent surveys). Current prosthetic hand control strategies can be broadly categorized by two main features [22]. The first being the method by which the hand states are generated from physiological signals: proportionally controlled or based on the classification of features extracted from biosignals. The second is the proximity of the sensor to the nervous system with either the electrodes positioned non-invasively or invasively within the individual. Today, virtually every system in regular patient use relies



---

on proportional control and non-invasive electrodes; however, the control is still severely limited by the simplicity offered by such interfaces. Higher levels of control are potentially available through more sophisticated sensor development, placement, and processing that have been demonstrated in many laboratory experiments (assessed in [20], [22]), but most systems entail a significant cognitive burden on the user. The convention is that the user does almost everything, e.g. directly controls all active degrees of freedom (DOF) with significant cognitive load, or only provides open/close movements and is forced to use a free hand to switch operational modes, severely inhibiting utility. Offloading this cognitive load from the user to the prosthesis has the potential to immediately improve systems in use today.

Hand prostheses in clinical use are typically controlled using electromyographic (EMG) signals from the remaining muscle in the forearm, enabling the prosthetic hand to open and close. Different grasp patterns are used to perform various hand gestures and functions, which often have to be selected manually with the use of a push button, cycling through a small selection of pre-programmed patterns or by assigning different gestures for each grasp e.g. 2 quick EMG pulses selects a *power* grasp and a 2 second co-contraction selects a *tripod* grasp. A trade-off is made between greater control and simplicity, thus physically burdening the user by often requiring the use of a second hand or multiple muscle contractions, and mentally through selection of an appropriate grasp depending on the object and desired function, as well as memorising and reproducing the associated EMG gesture, all while making adjustments to the hand's orientation and positioning based only on visual feedback. Being able to use the prosthesis without the physical and cognitive burden of controlling it may have a large impact on prosthesis use and the lives of amputees.

This work focuses on the development of a sensor fusion control system that will allow effective translation of data obtained from wearable technology into useful machine commands. The system integrates a camera for object recognition, a motion tracker for grasp selection and mechanomyogram sensors for muscle activation. The main focus is the decoding of user intention through the extraction of meaningful physiological signals from various predefined grasp patterns. The extracted features are analysed using various pattern

---

recognition strategies for grasp prediction including linear discriminant analysis (LDA), quadratic discriminant analysis (QDA), k-nearest neighbours (KNN), decision trees (DT) and support vector machines (SVM). Computer vision is used to provide object recognition of the target object of interest, resulting in an unobtrusive vision system to reduce the cognitive burden of hand prosthesis control.

The decoded physiological signals will be used in parallel with the vision system for object recognition and mechanomyogram sensors for muscle activation to create a sensor fusion control system for smart prosthesis control. The comparison and assessment of numerous physiological features and multiple pattern recognition strategies provides a trained classifier for improving the accuracy and reliability of the sensor fusion system for real-time control. By conducting timed, activity-based experiments with a prosthetic hand, the potential of using natural motion as a novel HMI will be evaluated.

## **1.2 Summary of Contributions**

### **1. Decoding Grasp Intention**

- Analysis of displacement, velocity and acceleration features inherent in arm motion during grasp established a novel method for predicting grasp intention when grasping different objects with various grasp patterns.

### **2. Human-machine Interfaces**

- Development of an unobtrusive eye-in-hand vision system for automated grasp pattern selection in modern hand prosthesis to grasp different sized objects.
- Development of a wearable heterogeneous sensor fusion control system combining mechanomyogram sensors, computer vision and inertial motion for upper limb robotic control.
- Real-time implementation of the proposed heterogeneous sensor suite to provide improved natural control over myoelectric hand prosthesis.

---

### 1.3 List of Publications

- M. Gardner, R. Vaidyanathan, E. Burdet, and B. C. Khoo, "Motion-based grasp selection: Improving traditional control strategies of myoelectric hand prosthesis," IEEE International Conference on Rehabilitation Robotics (ICORR), pp. 307–312, Singapore, Aug. 11-14, 2015 (*Attended and presented*)
- M. Gardner, R. Woodward, R. Vaidyanathan, E. Burdet, and B. C. Khoo, "An unobtrusive vision system to reduce the cognitive burden of hand prosthesis control," 13th International Conference on Control Automation Robotics Vision (ICARCV), pp. 1279–1284, Dec. 10-12, 2014 (*Attended and presented*)
- R. Woodward, M. Gardner, P. Angeles, S. Shefelbine, and R. Vaidyanathan, "A Novel Acoustic Interface for Bionic Hand Control," Towards Autonomous Robotic Systems (TAROS), pp. 296–297, Oxford, UK, Aug. 28-30, 2013 (*Attended and presented*)

### 1.4 Structure of Thesis

This thesis has been organised into seven chapters with a synopsis of the remaining six chapters given as follows.

**Chapter 2** provides a literature survey of HMI technology currently available. Various HMI technologies are described and grouped according to the source of the commanding signal, with a focus on their application as an assistive technology. HMI fusion specifically applied for robotic arm control termed *intelligent prosthetics* will be studied in more detail, assessing their effectiveness and usability as assistive technology, especially in the control of prosthetic devices.

**Chapter 3** describes the conceptual design of a heterogeneous sensor suite its respective control architecture are described in detail. The HMI is developed for integration with a Bebionic V2 hand [23] for prosthesis control. The limitations of the hardware and how they are accounted for in terms of system integration is discussed.

- 
- Chapter 4** specifically looks at the design and utilisation of MMG sensors for muscle activation, and computer vision for object recognition. Early work on an unobtrusive vision system is described, which fuses MMG sensors with computer vision for real-time image processing and grasp selection of the Bebionic V2 hand based on object size.
- Chapter 5** focuses on the detection, extraction and decoding of useful features from physiological movement during reach when grasping various objects with various grasp patterns. Analytic tools are used to extract the most useful features from the data in order to discriminate between the different grasp patterns.
- Chapter 6** evaluates the proposed sensor suite, which utilises both object recognition and motion tracking for grasp prediction and MMG signals for sensing muscle contractions. Real-time implementation of the sensor suite with the Bebionic V2 hand is presented. Interactive experiments are conducted that focus on grasp prediction and selection for grasping tasks within a controlled environment.
- Chapter 7** gives an overview of the PhD thesis, with a general discussion of conclusions and potential future work.

## Chapter 2

# Background

As discussed in Chapter 1, an assistive HMI is a communication interfacing technology that acts like a bridge between motor function and the brain, allowing disabled individuals to perform actions that might otherwise be too difficult or impossible. The loss or impairment of voluntary muscle control can have a detrimental effect on an individual's quality of life. The development of assistive technologies aims to restore loss of motor function or provide a means of communication, greatly improving their lives. The high diversity of the level of disability has led to a wide range of research in this area, and will form the core of this literature survey. Due to the vast number of HMI technologies available, these will be categorised according to input method, and will feature examples of some of the latest work within these areas. A further survey will focus more specifically on HMI fusion for improved robotic hand control, termed *intelligent prosthetics*.

### 2.1 The Importance of Assistive Technologies

There is such a wide plethora of disabilities that affect so many people worldwide, and with an ageing population, there is an ever growing need to reduce the effects of impairment for suffering individuals. These debilitating disabilities come about in many forms, such as congenital defects from birth, acutely due to accidents or illness, and even as degenerative diseases, causing deterioration of bodily functions over time. A relatively recent study surveying 59 countries in 2011 reports an estimated 2.2% of the population are affected

---

with a significant disability, within both higher and lower income countries [24].

1-2% of new-born babies are affected by congenital anomalies, 10% of which affect the upper extremities, and can be classified according to failure of formation, failure of differentiation, duplication and overgrowth [25] of the associated bone, tendons, ligaments, muscle and structure. Congenital anomalies can either occur in isolation or as a result of systemic conditions, and can lead to the amputation of the impaired limb if severe enough. The main cause of limb loss however, is the result of vascular disease (54%) and trauma (45%), with a 65% and 35% split between amputation involving the lower and upper extremities respectively [26].

Varying levels of spinal cord injury (SCI) can result in impairment or loss of motor and sensory function in the pelvic, trunk and legs (paraplegia), and including the arms (tetraplegia or quadriplegia) [27]. SCI is a major cause of loss in motor function, accounting for 23% of paralysis in the US [28], with the main cause due to neurological disorders, where 29% and a further 17% of paralysis is attributed to Stroke and multiple sclerosis (MS) respectively. The same study suggests that almost 1 in 50 people in the US are living with some form of paralysis. Stroke, being the main cause of loss in motor control is the result of either a blood clot, which stops the flow of blood and oxygen into the brain (ischaemic), or from a burst blood vessel within the skull (haemorrhagic). Up to 80% of all stroke survivors experience some form of motor impairment, typically affecting movement of the face, arm and leg of one side of the body [29]. MS on the other hand is a degenerative disorder which can result in stiffness, spasms, fatigue and tremor to name just a few of the physical symptoms, and is caused by damage to the myelin and axons of the spinal cord, which are essential to a correctly functioning nervous system [30]. Motor impairment can also be the result of a number of motor neuron diseases, such as Amyotrophic lateral sclerosis (ALS), progressive muscular atrophy and post-polio syndrome (PPS). Extreme cases of motor impairment involving complete immobility except for blinking and vertical eye movements is termed locked-in syndrome (LIS), whereby cognitive function is still preserved [31].

With an extraordinarily high proportion of the general population suffering from such

---

a multitude of motor conditions, the development of assistive technologies (AT) is essential to bypass motor impairment to restore some degree of mobility and communication. Central to the usability of these devices is an assistive HMI, which is used as the medium to communicate between the individual and the AT. In order to provide the most benefit to the individual, interfaces must be able to bypass the dysfunction in an unobtrusive, intuitive, and relevant manner. HMIs must be functional, simple and easy to use for extended periods of time, without imposing a high cognitive load or physical burden on the individual. Perhaps one of the oldest and well known HMI is the computer mouse, alongside keyboards, joysticks, remote controllers and digital pens. These have been around for decades, and are still commonly in use today [32]. These conventional interfaces offer manipulation of graphics, text and other devices in a simple and very intuitive manner, however, all of them require the use of an upper extremity for control. For impaired individuals who have limited, or no use of their upper extremities, this can be tremendously debilitating, and has an immensely negative impact on their daily lives. With such a high demographic living with severe physical disabilities and motor impairments, and with no current treatment available to restore normal motor function, there is a necessity for the continual development of HMI technologies to help improve the quality of life of affected individuals so that they can regain independence and lead normal lives.

## **2.2 Description of Interfacing Technologies**

This literature review offers a more general overview of the state of modern interfacing technologies and the wide range of assistive applications of which they can be utilised. The author introduces a wide range of assistive HMI technologies that have been categorised according to the method of user input. Physiological motion systems refer to those that utilise the physical displacement of parts of the body as an input control method. Gaze tracking extracts information from the eyes to infer intention and input selection. Oral communication interfaces involve the use of the vocal tract, nasal passage and oral cavity for interaction. Biofeedback interfaces use the underlying internal processes behind physiological motion, namely, the electromyogram (EMG). While biofeedback interfaces generally

---

involve the measurement of internal electrical processes, bioacoustic interfaces measure the internal mechanical response of the body, such as muscle and bone vibrations.

### **2.2.1 Physiological motion Systems**

Physiological motion systems can be thought of as input devices which rely on the physical movement of joints and body parts for direct or passive control. Conventional HMIs such as the computer mouse or keyboard, can be considered physiological input devices, as they rely on direct, physical displacement of the device by the user to obtain a resulting action, however, as mentioned previously, these require the use of an upper extremity to operate. For those with motor impairment or amputation of the upper limb, these conventional interfaces can be very difficult to manipulate, if at all.

Those suffering from tetraplegia as a result of SCI have no upper-limb motor function, but usually still have the ability to move their head, as SCI usually doesn't affect the spinal accessory nerve, which is responsible for head motion. As a result, a variety of control interfaces have used the head as a tracking device by measuring the rotation or physical displacement of the neck. These can come in the form of a physical controller, such as a chin-operated joystick [33] for wheel chair control, however this type of device however can be tiring and strenuous to use, requiring constant bodily movement, as well as causing irritation and discomfort due to continuous skin contact. Emitting sensing technologies have been used as trackers, such as infrared (IR) light emitting diodes and photodetectors, which can be mounted adjacently on a computer and on the user's head [1] (figure 2.1 (a)), or by wearing reflective markers [34]. Mounted ultrasound [35] and tilt sensors [36] have also been used to track head position. IR approaches are generally the most widely used for head tracking, with the main drawback being the requirement for the user to wear a mounted sensor array, or a reflective target, however this is only a minor concern. Wireless inertial sensors can also be worn to measure multi-directional head movement [2] (figure 2.1 (b)), having the added benefit of not using a receiver that requires being in line of sight.

The use of computer vision has become a popular method of recording head motion by using cameras that track certain facial features such as the upper lip, or tip of the nose



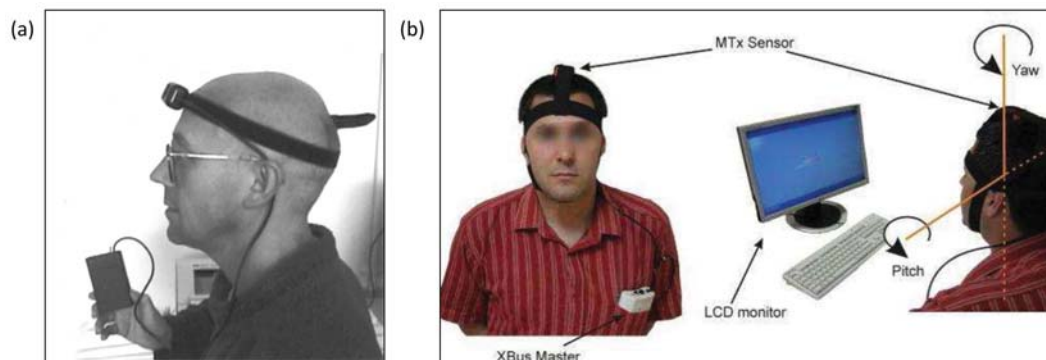


Figure 2.1: Examples of research-based head tracking input systems. (a) A head-operated joystick that uses infrared to determine head position (reproduced from [1]). (b) The Head-Joystick utilises inertial measurement to track head position as a pointing device (reproduced from [2]).

[37, 38]. These have the advantage of not requiring the user to wear any kind of headgear, however can be subject to tracking accuracy issues due to fast, sudden movements, and can also have a high sensitivity to changes in environmental conditions such as lighting and shadows. These systems can also be quite processor hungry, and may require a large mobile power source.

Although a lot of vision based research has focused on utilising head motion as a pointing device, work has also been conducted using head gestures to provide multiple control inputs, and can be carried out using face detection [39], or by using a point of reference such as the lips [40] to provide hands-free wheelchair control. Hand gesture control has become popular with able bodied users recently due its simplicity and intuitive nature, but can also be applied in the AT space, mainly targeted at individuals who still have the use of an upper extremity but are not very mobile. One example is the use of a wearable pendant that can use hand gestures to control household appliances such as room lighting and entertainment equipment [41]. The use of hand gestures as a communication tool for deaf individuals to enable communication without requiring an interpreter has also been explored using datagloves to measure movement of the hand and fingers directly [42, 43, 44] or cameras either externally [45] or as a wearable device [46].

Individuals who may have suffered a stroke or other brain injury may still retain some degree of motor control in the upper extremities, however they require extensive periods of

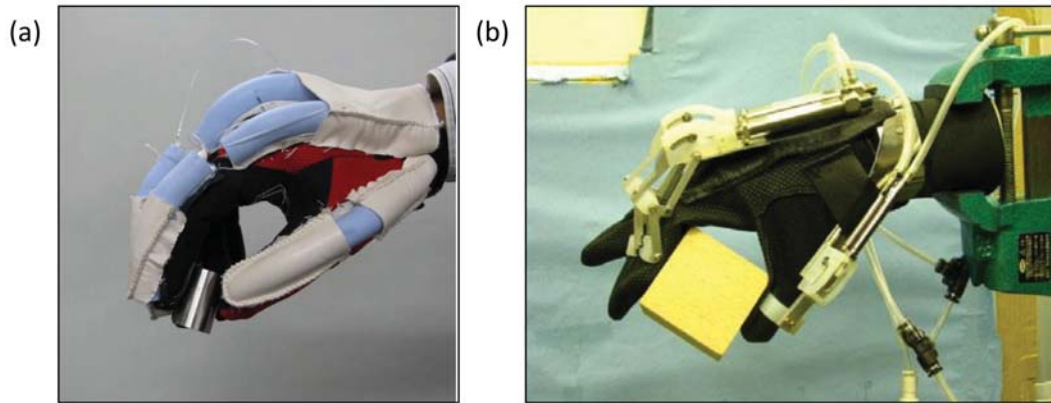


Figure 2.2: Examples of research-based assistive exoskeletons. (a) The Power-Assist Glove assists grasping force by using angle sensors to predict grasp intention (reproduced from [3]). (b) The Grip Aid System uses bending force sensors to assist grip if the finger's bend angle passes an angle threshold (reproduced from [4]).

rehabilitation and physiotherapy. Conventionally this can be a very time consuming, labour intensive and expensive process. With stroke being such a prevalent and major cause of upper arm motor impairment, there has been a lot of research into robotic rehabilitation to replace manual physiotherapy. It has been shown that repetitive movement training can be a more effective treatment [47]. Despite intensive rehabilitation, some stroke patients may suffer from permanent loss or weakened hand functionality. Only 5-8% of stroke patients show complete functional recovery [48]. Individuals who still suffer from some form of motor impairment are able to use assistive exoskeletons to aid in making certain grasping motions such as pinching. Linkage structures are usually used on each of the joints, whereby the centre of rotation of the structure coincides with that of the finger joint. The links are generally controlled using a tendon driven cable system, however power transmission can also be carried out using belts, linkages or by direct actuation. These systems can be actuated by various methods such as electrical motors and pneumatic pistons. Exoskeletons have been developed using a wide range of interfacing technologies, but in terms of body input methods, these can be provided by motion, by measuring the bending angle of the finger [49, 3] (figure 2.2 (a)), or also used to measure the resulting force applied as a product of motion [4, 50, 51, 52] (figure 2.2 (b)). Although these devices are more widely used in a clinical setting, their application as a mobile assisted device is very limited, as they can

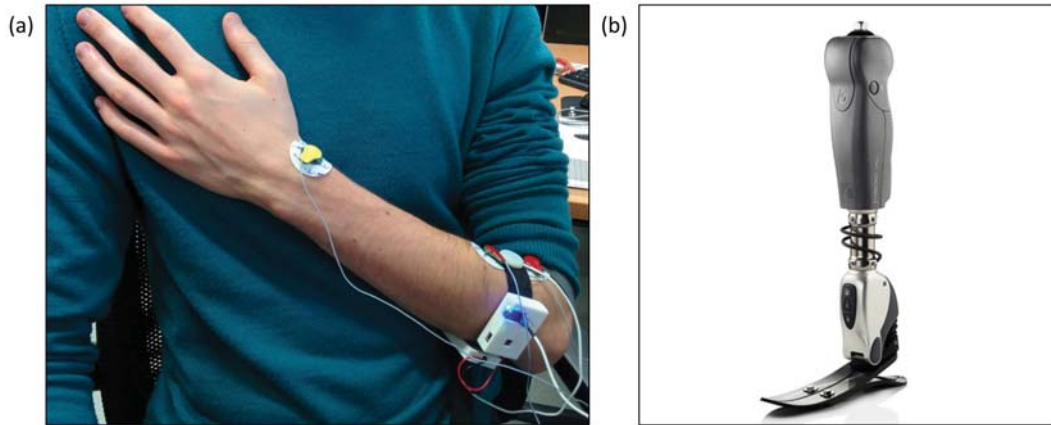


Figure 2.3: (a) Research-based IMU and MMG HMI uses arm gestures to select grasp patterns on a prosthetic hand (reproduced from [5]). (b) The commercial-based Symbiotic Leg Prosthesis by Össur (reproduced from [6]).

be bulky, obtrusive and expensive, and don't provide enough benefits to warrant the high inconvenience of use.

Inertial motion sensing has been utilised in lower limb orthosis to provide real-time gait analysis for detecting drop foot, which can occur after stroke. The IMU is used detect the different gait phases, and use the information to trigger foot stimulation using functional electrical stimulation (FES) [53, 54]. Upper body positioning can also be evaluated using IMUs located on the forearm and upper arm with respect to a given reference, enabling vibration feedback to be given in order to correct poor posture.

Physiological motion has not been typically used directly for prosthesis control, however relatively recent research has led to its implementation in lower limb prosthesis for powered knee joints [55] and ankle joints [56] as a gait measurement tool to determine whether the amputee is walking, standing, sitting or walking up or down inclines and stairs. This information is used to apply the required level of assistance or impedance of the powered joint to assist in carrying out smooth leg swings and stances. IMUs are currently used in many commercial powered lower limb prosthetic devices for improved gait control such as the Symbiotic Leg 3 (figure 2.3 (b)) by Össur [6].

Arm gestures have also been used for interactive grasp switching of myoelectric hands in combination with EMG and MMG for muscle activation [5] (figure 2.3 (a)). An IMU located on the forearm is used to recognise when the XYZ orientation is within a specified

---

region to enable a grasp switch upon sending a muscle activation signal, alternating between two different grasp patterns. The commercial I-limb Quantum by Touch Bionics uses motion gestures to select grasps by moving the hand in one of four directions [10]. With IMU technology becoming more prevalent in lower limb and upper limb powered prosthesis, it is evident that this technology is very suitable for the measurement of physiological motion. Having the advantages of being small, lightweight, accurate and having low power consumption, makes it ideal for use in mobile assistive devices.

### 2.2.2 Gaze Tracking Systems

Somewhat related to tracking physiological motion, gaze tracking is based entirely on estimating the direction of gaze using eye movements when fixating on objects in a scene. Gaze tracking is generally split into three main methods: Eye tracking, gaze estimation and Electrooculography (EOG). Eye tracking focuses on the detection and tracking of the eye itself, and interpreting its position across video frames, normally using the pupil as the point of reference. Gaze estimation on the other hand, focuses on the estimation and projection of the 3D line of sight within an environment [57]. Both methods usually just require a good view of the eye, which can be obtained using a camera, however sometimes an IR light source or filter is used to improve eye detection. EOG is much different from the other two methods, as it tracks gaze intention using electrical signals rather than studying the movement of the eye itself.

Gaze tracking has many useful applications in AT, especially for those who suffer from severe motor impairment such as ALS or tetraplegia as a result of SCI. Gaze estimation systems have been used to replace head tracking solutions as a control method for pointers [58, 59, 60, 61], and for wheel chair control using eye tracking [62, 63, 64] and EOG [65, 66, 67, 68]. Eye and gaze tracking can hold many benefits over head tracking solutions such as faster selection speeds, very low fatigue, and does not necessarily require cumbersome sensors to be worn. However can be sensitive to unintentional movements due to the *Midas touch* problem. With any interface that relies on cameras, changes in the environment such as lighting conditions or occlusions can have a large effect on usability [69].

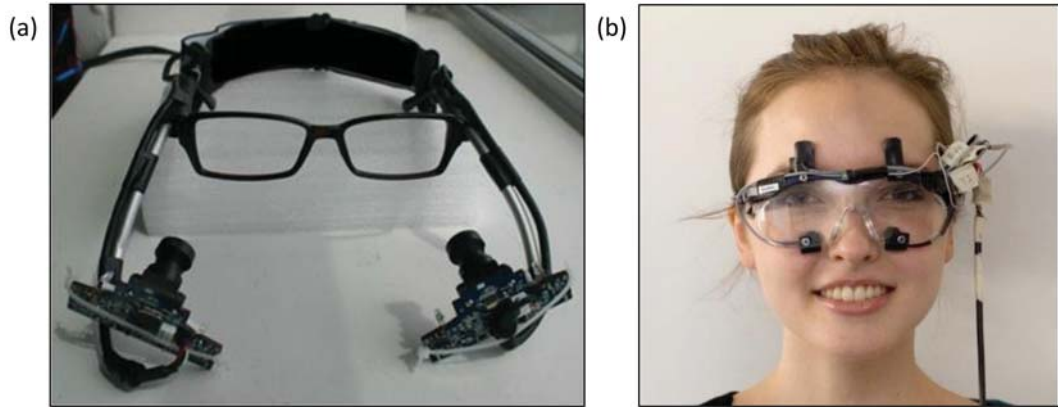


Figure 2.4: Examples of research-based gaze tracking systems. (a) A low-cost gaze estimation system for control of a volumetric cursor (reproduced from [7]). (b) EOG integrated goggles for gesture-based interaction (reproduced from [8]).

Generally, gaze tracking systems can be very expensive, however there have been recent efforts to develop low-cost, mobile solutions with cameras [7] (figure 2.4 (a)) and EOG [8] (figure 2.4 (b)).

### 2.2.2.i Eye Tracking

Despite a lot of research being done in this area, eye tracking is still considered a very complex task due to the high number of factors that can affect the eyes appearance. The appearance of eye regions can differ drastically as a result of environmental factors, such as illumination, viewing angle and environment reflection, as well as physiological factors such the level of openness of the eye, occlusion due to the eye lid and variability in size, reflectivity, eye colour, eye texture, head pose and the position of the iris within the eye socket. Eye detection techniques can usually be separated into four categories: *shape-based*, *feature-based*, *appearance-based* and *hybrid* [57].

Shape-based methods usually use a geometrical model of eye and a similarity measure, whereby the model's parameters are used to define the extent of template deformations. Methods tend to be based on point or contour features such as the pupil or limbus, and are generally subdivided into being either *fixed shape* or *deformable shape* depending on whether the prior model is elliptical or more complex in nature. Fixed shape, or simple elliptical methods normally rely on either a *voting-based* method, whereby features are

---

selected according to a voting process for a given hypothesis [70, 71, 72], or a *model fitting* method for fitting selected features to an elliptical model [73, 74, 75]. Deformable shape methods are much more complex, but can provide a much more detailed eye shape model [76, 77, 78] showing greater accuracy than fixed shape methods. However they can be computationally demanding, have to be initialised close to the eye for localisation and are generally quite sensitive to eye occlusions and changes in head pose [57].

Feature-based methods use human eye characteristics to recognise distinguishing features around the eyes. Some common features include the corneal limbus, pupil (bright/dark images) and corneal reflections. The eye can be split into different regions based on grey-level differences of a monochrome image of the eye [79, 80]. This method tries to identify local features that are less prone to changes in light and viewpoint. Different filters can be used to enhance desirable eye characteristics, and suppress others [81, 82]. This can be used to split the eye into regions for eye detection. With a close-up view of the eye, a common and often reliable eye feature that can be used for eye detection is the pupil itself. The contrast between the pupil and iris and their surroundings make it easy to use thresholds to obtain useful information [83, 84]. These methods show good robustness, but tend to be more reliable for indoor applications, as the pupil's intensities are sensitive to changes in light, and show a reduction in size in bright environments [57].

Appearance-based methods involve the direct detection and tracking of the eye based on appearance, characterised by colour distribution or filter responses. Appearance-based methods are those used for objects in general and are not specific to the eye, and are usually either image template-based, or holistic in approach. Image template-based methods [85, 86] use the pixel and intensity information of the object, and templates are usually unique to the individual, and can be subjected to scaling and rotational changes, as well as be affected by changes in head pose and relative eye position. Holistic approaches [87, 88] look at the object as a whole by performing statistical-based analysis on the intensity distribution. Generally, these methods require the acquisition of a large amount of training data of different subjects, head poses, face orientations and illumination conditions in order to construct the classifier or regression model.



---

Hybrid methods combine different eye models to reduce the disadvantages that using a single approach may have. Examples of shape and appearance-based models include [89] and [90], however these methods tend to still rely on being initialised close to the eye, meaning they can be subject to problems occurring as a result of large head movements.

### **2.2.2.ii Gaze Estimation**

Gaze estimation is the process of projecting an individual's gaze into 3D space. Eye movements can generally be classed as either from *saccades*, which are very fast eye rotations between two points of interest, *fixations*, which occur when the gaze rests on a point of interest for between 80-100 ms, or *pursuits*, which are smooth movements of the eye that occur when following a point of interest that is moving; these movements can infer an individual's intention. Gaze direction can be estimated by using the reflection of light on the cornea, which produces a series of reflections called *Purkinje images* [91], with the first reflection being referred to as the *glint*. Both head tracking and eye tracking are necessary to estimate gaze with a certain degree of accuracy, as the direction of gaze can be affected by both changes in head pose and eyeball orientation. Head pose is often estimated implicitly by the mapping function in the case regression-based methods, or using the *Purkinje images* in 3D model-based approaches.

The most popular gaze estimation methods are based on the detection of local features, such as contours, eye corners and reflections using the pupil and glints. These are usually regression-based [92], which map the image features to gaze coordinates according to a parametric [93] or non-parametric model [94], or 3D model-based [95, 96], where eye features are used to directly estimate the gaze based on a geometric model of the eye so that the point of gaze intersects the object being focused.

The main issue with gaze estimation is the triggering of unintentional actions just through normal observations, known as the *Midas Touch* problem [97]. Due to the continuous use of the eyes in every aspect of daily living, this can be a substantial problem, and has led to a lot of research being conducted to try to solve it. Some methods include fixating on a button to initiate an intentional gaze sequence [98], using voice commands

---

[99], manually by hand [100], using intentional winks [7] and also tooth-clicking [101].

### **2.2.2.iii Electrooculography (EOG)**

Electrooculography (EOG) is the measure of the potential across the cornea and retina due to eye movements [102]. This is due to the concentration of electrically active nerves in the retina compared to the front of the eye [103]. A pair of surface electrodes are positioned opposite each other on the eye socket over each eye, as well as a reference electrode placed on the forehead. When the eyes move from the centre position, the difference in potential is measured as a result of the change in dipole orientation causing changes in the electric potential field [104].

Eye motion can be considered one of the most frequent human motions [105], and the EOG can be used as an effective communication device for disabled individuals who are still able to control their eyes. EOG has the benefit of being non-invasive, low-cost and easy to use [106]. The EOG has an easily detectable waveform with relatively high amplitude, and forms a linear relationship with eye movements [103]. However, the signal is affected by head and muscle movement, signal drift and cross talk [107, 61]. Performance changes are also affected by physiological defects, changes in position of an individual relative to a reference point, head tilt, and perception of gaze location [106]. Like many types of eye-based HMI, EOG can be affected by the Midas Touch problem, whereby EOG signals are being picked up all the time, which can lead to undesirable activation of commands [68].

### **2.2.3 Oral Communication Interfaces**

Oral communication can be generated from a variety of methods located within the oral cavity, vocal tract and nasal passageway. This includes the use of tongue motion and tooth clicks as orally generated signals. Oral communication interfaces have had a lot of use in AT, with early devices utilising a *sip and puff* approach to either produce analogue signals from varying the air pressure within the device, or digital signals according to commands generated by either sips or puffs [108]. This simple, but reliable approach has been in consumer use for a long time, and has the advantages of being low-cost and easy to use.



---

However only a small number of direct commands are available, and its use does require relatively good control of airflow and the diaphragm which may not always be possible depending on the extent of the user's condition [109]. The sip and puff interface has been used by those suffering from tetraplegia and other severe motor impairment conditions to control wheelchairs [108] and to control input on a computer [110].

Research in speech recognition has spanned over six decades, and has grown tremendously, from isolated digit recognition in 1952 to the recognition of complete sentences in a variety of different languages, dialects and accents today [111]. Speech recognition has been integrated into a diverse range of applications, utilising voice commands for various inputs devices, such as wheel chair control [112, 113, 114] and prosthesis control [115]. Voice commands can also be used to carry out a number of different discrete computer interactions, however sometimes there is a desire for better control of a pointer, such as when drawing or playing games. Although there are alternatives such as tongue control, gaze tracking, and head tracking for example, voice control doesn't require any complex hardware or restriction of movement. Harada *et al.* proposed a vocal joystick, that could control a pointer by altering vocal characteristics such as pitch, amplitude and vowel quality. Vowel quality is classified according to a 4-way or 8-way 2D vowel space to control the cursor's movement direction, while the sound amplitude varied the cursor speed. Discrete sounds can also be made to control mouse clicks [116]. A similar method involves the use of non-verbal features such as utterance duration, pitch and discrete sound frequency to control interface methods such as scrolling, while using discrete commands to control direction of movement [117]. Humming and whistles can also be used to discriminate between gestures varied by pitch to move a cursor in 4 directions [118]. The main disadvantage of using voice for input is that it can be subject to a lot of noise interference when used outdoors, providing unintentional classifications as a result of external noise. Distinguishing between normal conversation and intentional voice commands for control can be difficult, so using sounds that don't normally occur should be used to reduce misinterpretations.

Severe cases of motor impairment or conditions which can effect speech, such as stroke, voice control may not be an option. Tongue control on the other hand is connected

---

to the brain via the hypoglossal cranial nerve, and generally escapes injury and disease. The tongue is capable of providing complex movements with very little fatigue, enabling continuous use over extensive periods of time [109]. The movement of the tongue is not perturbed within the mouth cavity by movement of the head or any other part of the body. This allows freer movement without the risk of signal misclassifications due to external motion artefacts. Control of the tongue is also less prone to involuntary movements, and can be manipulated in a natural and cognitive-free manner. These devices generally require the insertion of a mouthpiece, and can employ a variety of different control strategies. Nutt *et al.* [119] used a 16x16 piezoelectric ceramic strip as a tongue touch screen to control a mouse pointer on a screen, whereas Salem *et al.* [120] used a mouth piece embedded with a pressure sensitive miniature isometric joystick. The tongue drive system developed by Ghovanloo *et al.* [109, 9] (figure 2.5), interprets tongue motions as a method of input using an array of magnetic sensors in the mouth attached to the teeth as an orthodontic brace, or attached to the outside of the mouth on an external headset. The system measures the disturbance of a magnetic field using a permanent magnet fixed to the tongue via a tissue adhesive, piercing or clipping. Specific tongue motions can send commands to interface with a computer or control a wheelchair.

Devices located within the mouth can be very obtrusive, and can impair speech and obstruct breathing and eating, however relatively recent research has found solutions in using the propagation of bone vibrations resulting from tongue movements as a useful input strategy. Although somewhat related to bioacoustic interfaces, the tongue control strategy developed by Mace *et al.* [121] successfully classified tongue flicks on the left, right, top and under sides of the teeth using a microphone embedded earpiece, while also rejecting interference caused by coughs, speech, swallowing and muscular artefacts. This input strategy can be used as a general HMI for impaired individuals, but has also demonstrated success in the control of a myoelectric hand [22]. An alternate strategy involving the measurement of vibrations on an accelerometer-based earpiece as a result of tooth clicks was used to interface with a computer using simple input commands [122]. Another method by Mohamed *et al.* [123] used a throat microphone on the cheek to measure the vibration of teeth

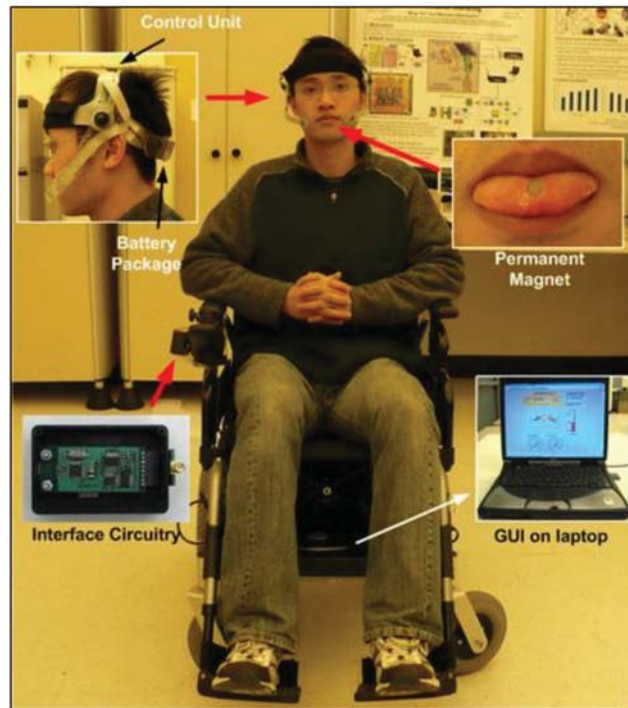


Figure 2.5: The research-based Tongue Drive System for controlling a wheel chair (reproduced from [9]).

clicks to interface with a computer. The use of tooth clicks however can be potentially more physically demanding compared to the tongue due to extensive use of the jaw.

Individuals suffering from LIS are completely paralysed, and are not even able to provide the required motor input for these types of interfaces. Studies have shown that voluntary control of sniffing is still available to those with severe levels of motor impairment [124]. A sniffing controller was developed which measures changes in pressure within the nasal canal as a function of soft-palate positioning. A low-flow stream of air is passed into the nasal mask, whereby closing and opening the soft palate can control the pressure of airflow, generating a signal independent of breathing. The sniffing controller was used by LIS sufferers to control a wheelchair, as well as typing on a screen [124].

#### 2.2.4 Biofeedback Devices

Biofeedback systems typically relate to the underlying processes involved within the nervous system which result in physiological motion. These processes are moderated by the peripheral nervous system (PNS) which connects all the organs and limbs to the central ner-

---

vous system (CNS), and can be further subdivided into the *automatic nervous system (ANS)* and the *somatic nervous system (SNS)*. The ANS provides a passive, reflective response to external stimuli, affecting changes such as heart rate, respiration rate and perspiration rate, whereas the SNS enables intentional, voluntary control of muscles and sensory organs, such as providing movement of the limbs or eyes [125]. Biofeedback HMIs typically involve extracting information from the response of the SNS to infer intentional use of motor functions. The most well-known biofeedback response is the electromyogram (EMG).

Electromyography is the measurement of electrical current as a result of electrical activity generated from motor neurons when muscle fibres are activated during contraction [126]. Furthermore, EMG signals can also pick up isometric muscle activity which doesn't cause movement; this allows the classification of motionless gestures for subtle control over applications [106]. The measurement of EMG is usually done from the surface of the skin using electrodes.

Electrode placement is very important as it determines the amplitude of EMG signals and the amount of crosstalk from adjacent muscles. Placement should be relative to the individual's body dimensions, and should be referenced to anthropometric landmarks in order to determine correct positions. The electrodes should generally be positioned on the bulk of the muscle, parallel to the muscle fibres. The electrode size and inter-electrode distance depends on their application and the muscles involved. For lower crosstalk and interference from electrocardiogram signals or for use with smaller muscles, smaller electrodes with narrower spacing are required. Narrowly spaced electrodes must be positioned so that they do not meet when the muscle shortens, as it can cause interference problems. For larger muscles where larger amplitude or greater global information is required, larger electrodes with a wider spacing can be used. The most common surface electrode contact area is 50 mm<sup>2</sup> with an inter-electrode distance of between 4 and 5 cm as it provides a good compromise in terms of selectivity, representativity and signal amplitude for medium to large muscles. The skin surface may need to be prepared before applying the EMG electrode by cleansing and possible shaving depending on the type of electrode used. A conductive gel is sometimes used to improve the sensitivity of the electrode to improve the amplitude and

---

quality of the signal [127]. Dry EMG sensors have been developed, however due to the lower signal-to-noise ratio (SNR), only basic information can be gathered. Dry sensors are used for the control of prosthetic hands due to greater convenience, and are operated using simple threshold strategies for the control of basic open and close hand functions such as extending and flexing the fingers and thumb. A reference electrode is normally positioned far away from the measurement electrodes on an electrically neutral tissue such as over a bony prominence and used as an input to a differential amplifier to improve detection and to reduce noise.

EMG has the advantage of being non-invasive (although invasive electrodes can provide a much clearer response), which is a key requirement in obtaining neural signals safely for long term day-to-day use. Surface electrodes produce a high signal-to-noise ratio (SNR), making it easier for the classification of gestures. These characteristics make EMG a very convenient method for obtaining neural signals as a HMI for various applications. Despite this, EMG does come with its drawbacks, such as its susceptibility to sensing background noise, which can be caused by numerous sources such as electromagnetic radiation, integral equipment noise, motion artefacts, and crosstalk. Crosstalk is the observed muscle activity from near-by muscles of the measurement site, which creates a significant problem if the muscle contraction is relatively weak, as it makes it difficult to separate specific muscle signals and distinguish them from background noise [128]. Due to the electrical nature of the EMG, the surface resistance of the skin can be a problem, as the signal can be distorted due to changes in the resistance of the skin due to stretching or perspiration. The costs of EMG electrodes are relatively high, and the more commonly used ones are single-use. Electrode repositioning also has a negative effect on signal reproduction, and may require recalibrating whenever the HMI is donned. The lengthening and shortening of muscle fibres show a similar effect on signal reproduction [129].

Although EMG-based applications in the medical field tend to be used mainly as assessment tools during rehabilitation of conditions such as stroke and muscular injuries, they can offer AT solutions for wheelchair control using the muscle in the neck [130, 131], however their main applications revolve around the control of orthotic and prosthetic devices.

---

In terms of orthotics, EMG interfaces have been used to reproduce and correct movements for those with muscle impairment in both upper limb [132, 133] and lower limb [134]. Due to the large extent of EMG implementation within these two main application categories, this survey will focus more on prosthetic devices, specifically towards the control of a myoelectric hand.

EMG signal processing strategies can generally be categorised as either being pattern recognition (PR) based, which uses the extraction of features to distinguish between different muscle movements or gestures, or non-pattern recognition based (NPR), which relies more on simple strategies such as proportional control using analogue-based input, or discrete control using thresholds. Almost all commercial orthotic and prosthetic systems use NPR strategies for the HMI. As this work focuses heavily on the application towards prosthetic hand control, it seems appropriate to go into greater detail on the two different types of strategies.

#### **2.2.4.i Non-pattern recognition strategies**

NPR strategies form the industry standard for hand prosthesis control, and are applied to perform both proportional and discrete control based on an individual's preference. The latest prosthetic hands use a selection of pre-shaped grasp patterns with open/close functions such as *power*, *pinch*, *precision* and *lateral* grasps. The large selection of patterns available allow the amputee to complete a wide variety of activities. EMG is used for opening and closing the hand, while the different grasp patterns are selected manually, using a push button with the Bebionic V3 hand [23], EMG gestures such as a 2-second co-contraction on a Michelangelo hand [135] or most recently, physiological gestures using IMUs with the I-limb Quantum [10] (figure 2.6 (a)). Using multiple sites, control can be gained over not only the opening and closing of the fingers of the hand, but also the rotation of artificial wrist joints, also available commercially, where each electrode site would control a single DOF, either proportionally or discretely. Only two sites are required for open and close control of a myoelectric hand, and are typically located on the flexor and extensor digitorum on the forearm.

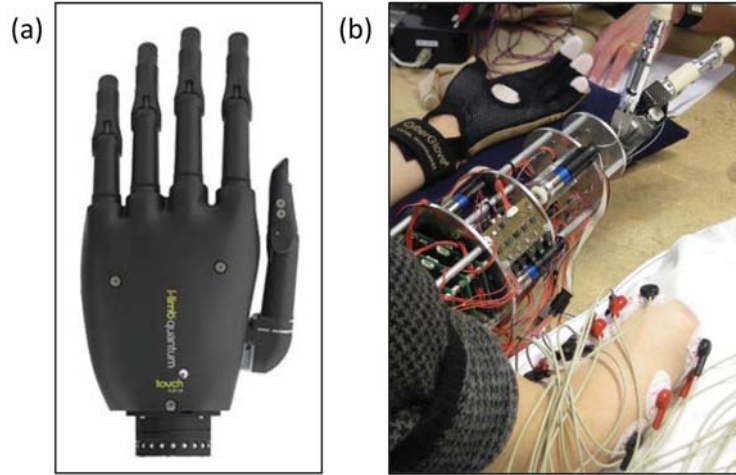


Figure 2.6: (a) The commercial-based I-limb Quantum myoelectric hand prosthesis by Touch Bionics (reproduced from [10]). (b) An 8 channel EMG interface used to distinguish between 7 different finger movements (reproduced from [11]).

NPR strategies can be considered quite simplistic in nature, as they are only able to control a single DOF, and can only really carry very simple functions such as activating grasp selection functions or opening and closing prepared motor configurations. Generally, these strategies are inflexible and do not provide the user with much control. As a result, the user adapts their arm motion to the requirements of the hand's pre-shaped grasp, leading to awkward and unnatural movements. Despite these drawbacks, these strategies are fairly intuitive, are much more reliable than PR methods, and impose a much lower cognitive load on the user; only a few simple major muscle contractions are required for control.

#### 2.2.4.ii Pattern recognition strategies

Research into the transient burst of myoelectric signals found useful information during the onset of contraction, which could be used to extract a number of different features [136]. These can be found in the time-domain such as waveform length, slope sign changes and mean absolute value slope, as well as in the time-frequency domain, such as calculation of the wavelet transform [137]. After a number of features have been extracted, and a feature selection process has identified the most discriminatory features, a classifier is used to distinguish between different gestures.

PR strategies are unique to the individual, and may require large quantities of data to



---

be able to distinguish between EMG gestures with a relatively high accuracy. As mentioned previously, the EMG can be sensitive to changes in the electrical impedance of the skin, and with the finer measurement of different gestures, the effect can have a much greater impact than for NPR methods. Machine learning is required to adjust the classifier accordingly to reduce the number of classifications such as the methods proposed in [138, 139]. As with many similar signals such as EOG or MMG, the stochastic nature can lead to parameter measurement errors that cause issues with intentional control. These strategies tend to require a number of different gestures to be effective, and not all amputee patients are able to reproduce them to the degree of accuracy required. The extent of which the amputee can reproduce these signals reliably depends a lot on the individual, and their control over the remaining muscle in the stump. Although this is also true for NPR methods, but to a much lesser extent, as they would only typically require contractions of the major muscle groups, and not the finer control associated with individual gestures.

A greater number of classes can be discriminated between with a larger number of EMG channels. Tenore *et al.* successfully distinguished between 12 individual flexion and extension movements of the fingers using 32 channel EMG on an able bodied subject with an accuracy of 98% [140] and between 10 classes for a transradial amputee [141] with an accuracy of 90%. Accuracies of 79% and 89% were obtained from 5 transradial amputees and 5 able bodied subjects respectively using an 8 channel EMG interface to categorise between 7 different classes [11] (figure 2.6 (b)). Using a high number of electrodes can be very inconvenient for the amputee, and be impractical in mobile use, however there has been some success reported with a 2 channel system to separate 9 classes with an accuracy of 93%, although tests were conducted with only able bodied subjects [142]. Despite having a greater number of DOF potentially available with PR control, its implementation for active prosthesis is still a long way away. Although technical developments have improved greatly over the past few years, especially in the miniaturisation of mechanical and electronic components, a prosthetic hand with too many active DOF will be far too heavy and bulky to use, and will also require a much larger power source.



---

### 2.2.5 Bioacoustic

As mentioned previously, using teeth clicks [123] or flicks with the tongue [22] can cause acoustic vibrations in the bone, which can be recorded using a microphone. Although originating within the oral cavity, then can be also considered as oral communication devices, however they represent acoustic behaviour within the body. Bioacoustic interfaces can be described as low frequency mechanical waves that permeate through the body. Due to the propagation properties inherent in acoustic signals, these are usually recorded using microphones [123] or accelerometers [122] either placed directly on the skin or close to it, providing a completely non-invasive interface.

The most commonly measured bioacoustic signal is known as the mechanomyogram (MMG), which records *muscle sound*. It was found that this sound was associated with muscle activity, and its properties related to muscle contractions [12]. These acoustic signals are recorded from vibrations on the surface of the skin using accelerometers, microphones and piezoelectric contact sensors at an optimal frequency of between 2 and 50 hz [143, 12, 144]. Accelerometers required a minimal strapping force to avoid any relative motion with respect to the muscle's surface. A strap with a high rigidity would apply too much pressure on the sensor during strong muscle contractions. The use of a microphone enclosed in a shell avoided this issue, however it was found that there were signal distortions as a result of oscillations from a skin diaphragm formation, which transmitted transverse mechanical activity. Signal shape and characteristics varied a lot between sensor types, which may have also been related to its fixture to the skin's surface. The signal shape between that of the microphone and piezoelectric sensor was much more similar than to that of the accelerometer. The recorded signal comes in discrete bursts during muscle contractions instead of a continuous sound. Some suggest that the sound is a result of shock waves generated by the sudden change in thickness of active muscle fibres [143], or from muscle fibres sliding over one another [145]. The MMG signal was found to have good propagation properties, as well as influenced by muscle length, with a peak-to-peak sound amplitude and length relationship during muscle twitches similar to that of a length-tension relationship. The peak-to-peak sound amplitude is also heavily influenced by temperature, whereby a reduction in temper-

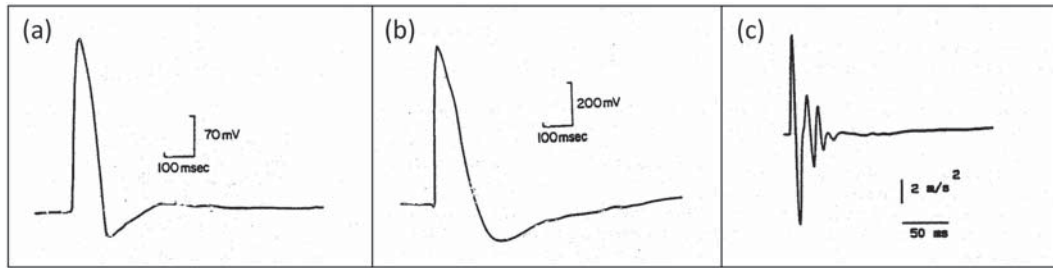


Figure 2.7: Sound waves recorded as a result of supramaximal twitches from (a) an air coupled microphone, (b) piezoelectric contact sensor, and (c) accelerometer (reproduced from [12]).

ature see a reduction in sound amplitude. The muscle's vibration is also strongly influenced by the intensity of effort, showing a reduction in amplitude during increased fatigue [12].

Although MMG has typically been used in the study of muscle fatigue [146] and muscle stretching [147, 148], it has been used for the assessment of neurological disorders such as Parkinson's disease [149] and stroke [150]. MMG sensors could be used as a replacement for EMG in the control of AT systems such as control of orthotic [151] and prosthetic devices [152, 5]. Islam *et al.* [153] gives a good overview of MMG signals for use in the study of muscle, signal processing, sensor development, diagnosis of neurological disorders, and applications in rehabilitation and prosthesis control. MMG sensors are not only significantly less expensive, but are also unaffected by changes in skin impedance e.g. sweat. The propagation properties of the signal allow imprecise sensor placement [12, 152]. MMG sensors do not require the use of conductive gel or the shaving of placement area, making it a much more convenient method of gathering data from the muscles. The main disadvantage is the high signal interference as a result of external perturbation of the skin, such as tapping on the skin surface, and the presence of motion artefacts due to arm motion. Care must be taken to reduce these effects during signal processing to reduce the number of misinterpreted muscle signals.

## 2.3 Intelligent Prosthetics

A study in 2007 by Biddiss *et al.* [154] on adult and paediatric upper limb prosthesis users found that the rate of rejection of electric hands was 41%, with body-powered hands

---

at 65%, body-powered hooks at 51% and passive hands at 47%. The internet study on amputees consisted of 16% with limb absence at or distal to the wrist, 54% transradial, 21% trans-humeral and 7% at shoulder level or higher. Although there was greater interest in use of electric prosthesis for non-users, the rate of rejection is still very high for those that have used them before. A more recent, separate study in Norway [155] reported prosthesis rejection and discontinuation rates to be just 17.9%, with above elbow amputees 12.8 times more likely to reject usage compared to below elbow amputees.

It was found that overall weight, and weight distribution was a major priority for all upper limb prosthesis users, especially for those with electric prosthesis. Wear temperature was also a key concern, with lack of breathability combined with the heat generated by the electric motors making them very uncomfortable to use for extended or even short period of time. The ease of donning and doffing the prosthesis was another frequent complaint, which was found by many to be frustrating and time consuming. Adult users prioritised functionality over other concerns, such as a reduction in unplanned movements, increased reliability, and dexterity. Above elbow amputees required better shoulder and elbow control, with prosthesis without a shoulder reach function being more of a hindrance than a help. Sensory feedback, wrist control, and improved control over individual joints such as fingers, wrist, elbow and shoulder were also desired. Other concerns involved glove durability, moisture and dirt resistance, life-like functionality and appearance and a reduction in overall cost. Body-powered prosthesis users had some similar concerns, however most emphasised the importance of comfort, with complaints of physical exhaustion after extended periods of use, as well as sores and pain due to harness discomfort and perspiration. Greater control of grasping force was also desired. Overall, amputees had a negative view on the usefulness of prosthesis use, with many finding that they did not provide any extra functional benefit over using the residual limb to carry out activities of daily living [154].

It is evident that prosthesis rejection is a big problem, as many amputees just are not finding them useful enough compared to the amount of discomfort they can cause. With functionality reported to be a major issue for prosthesis users, it is important that some of the issues are addressed in the future direction of upper limb prosthesis control. With individual

---

motor control still far from commercial implementation, current myoelectric devices using proportional and discrete control with various grasp patterns will continue to be the state of the art available to consumers. As these devices will continue to be in consumer use for the foreseeable future, it is important that efforts are not just focused on new hardware developments such as additional motor control and weight reduction, but also on the control of the system itself, which currently imposes a high cognitive load on the user. Improving current systems at the control level can help to reduce the cognitive and physical load on the user by making control more intuitive and less mentally and physically demanding. Thus there have been some recent technological developments in *intelligent prosthetics*, which focuses on improving control methodologies in order to reduce the cognitive burden of prosthesis use.

Related work has focused mainly on the use of computer vision to aid in grasp selection. Although research into vision systems for robotic manipulators and grippers is a very mature field, there has been limited work in adapting this technology for hand prosthesis control. The vast improvements in imaging systems over the past decade has made it possible to use cost-effective, miniature high resolution cameras and real-time signal processing for prosthetic devices. Where there has been a large move towards autonomous operations in industry such as pick-and-place robots, spot welding robotic arms and building robots, there has been a desire to develop systems with accurate visual feedback that can provide detailed information of the working environment. *Visual prosthetics*, an adaptation of visual servoing, can be defined as the utilisation of vision systems to aid in servo planning and control of prosthetic limbs, and can be considered a subset of *intelligent prosthetics*. Visual prosthetics is a complex problem that has the potential to vastly improve the accuracy of grasping applications. Visual servoing and visual prosthetics systems can generally be categorised into two classes, where the camera or vision system is said either to be *eye-in-hand* or *eye-to-hand*.

Eye-in-hand cameras are mounted on to the end-effector, which gives it the manoeuvrability to explore the scene. The close proximity of the camera to the end-effector results in improved target recognition and inspection by increasing the effective resolution of the

---

image. Eye-in-hand cameras solve the problem of occlusion, and minimises parallax error. On the other hand, an eye-in-hand camera isn't able to interact with its entire work space [156], [157].

Eye-to-hand cameras are fixed, and observe the robot from within its workspace, allowing it to gather global information so that it can adapt to modifications to the environment [157]. However, this configuration is limited to workspaces where the manipulator is not obscured from the cameras, and can be subjected to numerous errors such as mechanical backlash, modelling and parallax errors. To obtain precise estimates of manipulator position, the system must be well calibrated at all times.

While visual prosthetics is a new area of research, some recent work has shown significant promise for eventual clinical impact. S. Došen *et al.* [13, 158] proposed an autonomous controller empowered by computer vision and rule-based reasoning to control a multi-fingered prosthetic hand through the estimation of the target objects intrinsic properties (size, shape). The system consisted of a CyberHand prototype [159] and a cognitive vision system (CVS) composed of a low-cost web camera, ultrasound sensor and laser pointer mounted on to the hand as shown in figure 2.8. The objects size is estimated from its distance away from the ultrasound sensor, the focal length of the camera, and the pixel length of the objects axes. A rule-based algorithm is then used to select between 9 different grasp modes: *palmer* (small, medium and large), *lateral* (small, medium and large), 2-finger and 3-finger *pinch* (small and medium). A *palmer* grasp is used for large, wide objects, *lateral* for large, thin objects, with 3 and 2-finger *pinch* grasps used for small and tiny objects, respectively.

In the experiment, the hand is initialized in a neutral posture, and when the subject decides on an object to grasp, the laser is pointed towards it. The subject activates his/her finger extensors to start the CVS algorithm. Once the object size has been calculated, and grasp has been selected (2-3 seconds), commands are sent to the hand to pre-shape the grasp to an open position. The subject then positions the hand around the object, and closes the grasp by activating his/her finger flexors. The object is held until the subject contracts his/her finger extensors again. This opens the hand and releases the object. After a 3 second

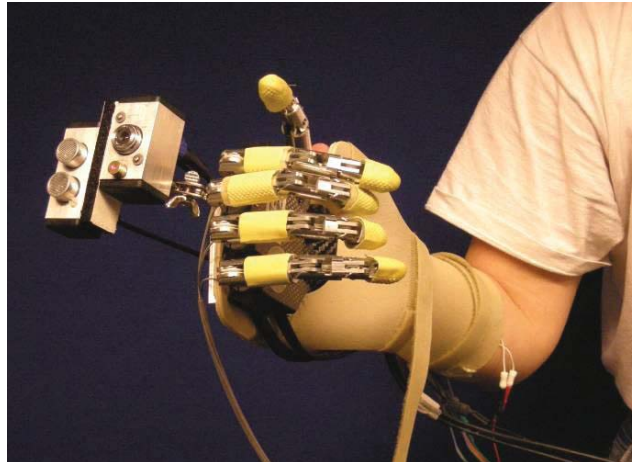


Figure 2.8: The cognitive vision system developed by S. Došen *et al.* attached to a CyberHand fitted to an orthopaedic splint, using EMG electrodes for myoelectric control (reproduced from [13]).

delay, the hand returns to a neutral posture. The CVS was 84% accurate in grasp type and size estimation. An additional 6% of cases ended in a successful task, despite wrong grasp or size selection.

The practicality of the CVS is limited by the hardware used, and its resulting control method. The system bases its control on 4 basic grasp patterns for different size configurations. Although useful for pick and place tasks, it is limited in terms of versatility for more specialized tasks (e.g. clicking a mouse), as the system limits the number of grasps per object to a single pattern. The CVS can only be used by the CyberHand, which is unavailable for patient use, but can potentially be used for other hands with higher degrees of freedom. The system is also bulky and obtrusive; reducing its practicality in real-world environments.

This research was extended by M. Marković [14], which utilised stereo vision for grasp selection and augmented reality (AR) to provide proprioceptive feedback. The system architecture is described in figure 2.9, comprising of AR glasses with stereoscopic display and embedded stereo cameras, a dual channel EMG sensor interface and a SmartHand prosthesis [160] mounted on a custom-made splint. The user directs his/her head towards an object, initiating the stereo vision system to begin object recognition. After an object is recognised, the size and geometrical shape will be calculated using a state of the art computer vision processing pipeline comprising of depth estimation, object segmentation, 3D

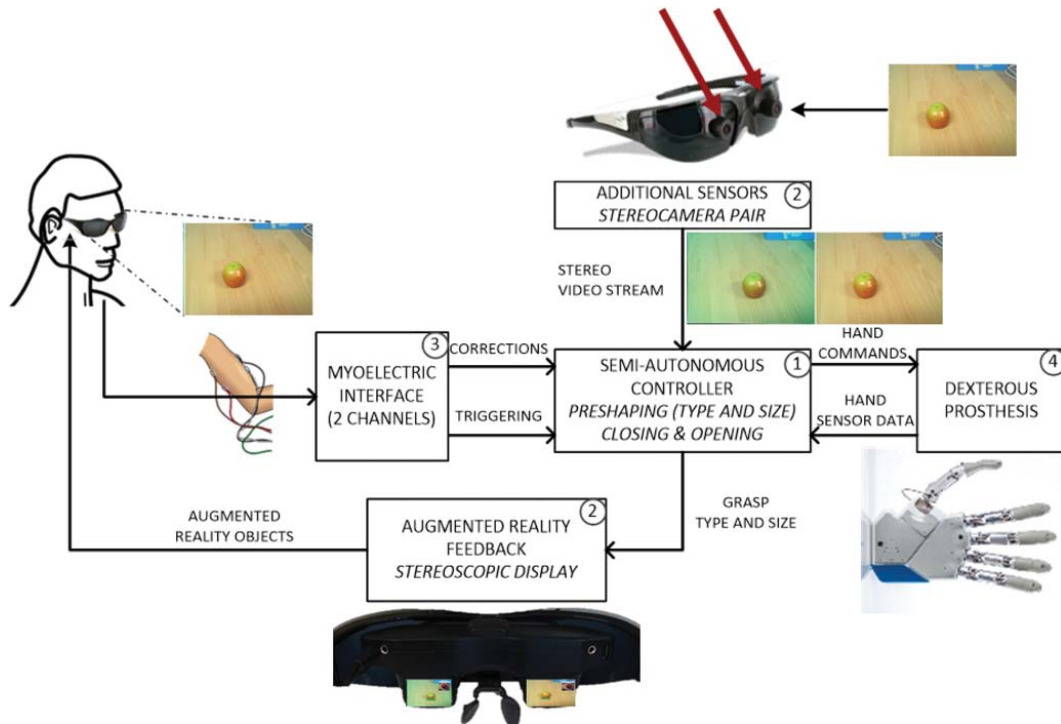


Figure 2.9: System architecture of the stereo AR system developed by M. Marković, comprising of (1) a semi-autonomous controller, (2) AR glasses with integrated stereo cameras, (3) a dual channel myoelectric interface and (4) a dexterous prosthetic hand (reproduced from [14]). When the myoelectric interface receives a trigger command, the stereo vision system calculates the size and geometric shape of the target object, selecting the prosthesis aperture size and grasp pattern, and projects an image overlay on to the AR displays.

point cloud generation, geometric model fitting, virtual object creation and projection on to the AR screens, creating an overlay across the object on the AR glasses. The grasp type and aperture size is selected based on the object's properties using a series of IF-THEN rules, displaying an image of them on the AR displays. Grasps and aperture sizes and their selection are identical to those described by s. Došen et al. in [13]. The user is able to restart the grasp selection process if he/she is not happy with the estimated grasp by sending a specific EMG command. Once happy, the user can then direct the prosthesis to the object, and issue another EMG command to close the grasp around the object. Once the desired object manipulation has been completed, another EMG command is sent to open the prosthesis and to restart the grasp selection process.

Thirteen able-bodied subjects took part in a pick-and-place experiment grasping 20 different randomly presented objects using the system as described. The prosthesis was



---

positioned out of sight of the stereo cameras while looking at the target object to avoid misclassification. Subjects were given 10 minutes to familiarise themselves with the system beforehand. The hand was placed back to the starting position after each trial. Four different control strategies were tested, with 5-10 minutes' rest between each: *AUTO-AR*, where subjects are unable to correct the grasp, *SEMI-AR*, where corrections to the grasp are allowed, *SEMI-AR-RE*, which introduces random errors to *SEMI-AR* after the grasp type was determined, forcing the subject to make corrections, and *SEMI-VIS-RE*, which introduces random errors to *SEMI-AR* with the AR feedback disabled.

Experimental results for *AUTO-AR* produced a 73% success rate, with the failure rate having a split of 10% grasp control failure and 17% myoelectric or prosthesis control failure. The addition of AR correction (*SEMI-AR*) increased the success rate to 81% with a failure rate split of 3% and 16%. *SEMI-AR-RE* showed a slight improvement with a success rate of 84% with a 2% and 14% failure rate split, and *SEMI-VIS-RE* produced a 78% success rate with a 2% and 19% failure rate split. The results suggest that given the opportunity to correct the grasp after automated selection reduces the grasp control failure rate, and that AR feedback is a viable medium to provide the user with information for correcting mistakes made by the automated controller.

M. Marković showed how intentional grasp correction can be used to reduce the grasp control failure rate, where AR feedback can help reduce user correction error, however myoelectric prosthesis control failure is still a large issue. Although the grasp control success rate is high, the system is restricted to only grasping an object for pick-and-place applications, limiting overall versatility for practical use.

Further research presented by M. Marković in [15] involved using a RGB-D vision system combined with position sensors embedded in the Michelangelo prosthetic hand [135] to provide hand aperture size and wrist rotation, as well as an inertial sensor for tracking arm orientation relative to an external co-ordinate system (figure 2.10). The semi-automatic controller will automatically select a grasp type and change the aperture size if the user decides to pick up the object from a different angle. The user provides manual control using the EMG sensors for correctional grasp adjustment and positioning.



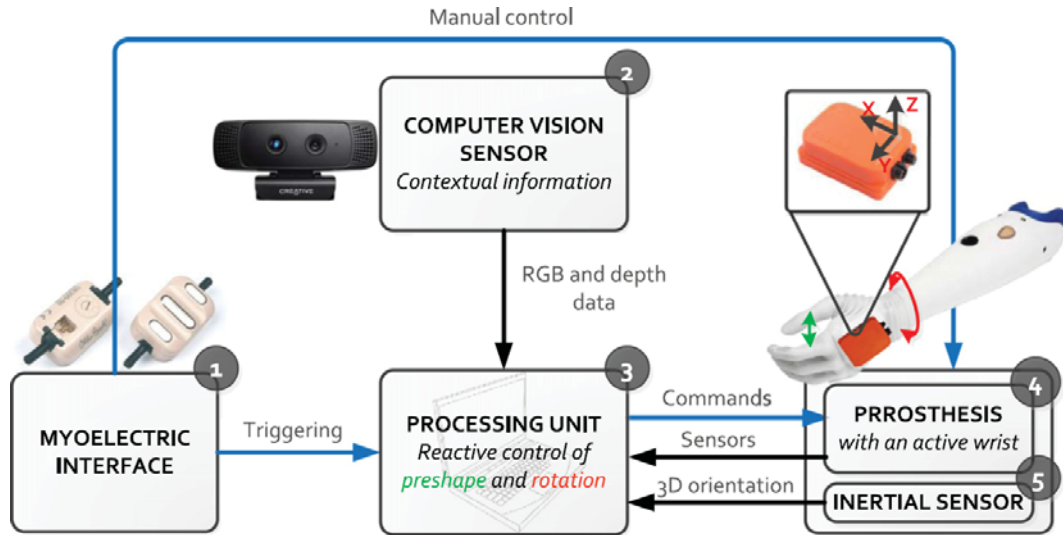


Figure 2.10: System architecture of the CASP system developed by M. Marković, comprising of (1) a dual channel myoelectric interface, (2) a RGB-D computer vision sensor, (3) a processing unit, (4) a dexterous prosthetic hand, and (5) an IMU sensor (reproduced from [15]). When the myoelectric interface receives a trigger command, the processing unit determines the prosthesis aperture, grasp pattern, orientation and depth of the target object from the computer vision sensor, providing autonomous hand preshaping and wrist rotation. The IMU tracks prosthesis orientation, adjusting wrist rotation when required.

From a resting position, the user faces towards the target object, and activates the system by contracting the extensors, which rotates the prosthesis according to the arm's location, and pre-shapes the hand according to grasp pattern and aperture size based on the target object. The user now assumes manual control using the EMG sensors to either correct the decisions made by the controller, or to open/close the hand with proportional or discrete control, switching between the two methods by co-contracting. If the user started pronating the prosthesis, then the system would automatically rotate the hand till the palm is horizontal. A manual override can be sent with the EMG sensors to stop automated rotations if required. The flexors are used to close the hand on the object. When contact is detected, the automatic control is turned off, and when the object is released the system is reset to carry out another operation.

10 healthy subjects and a single amputee subject took part in a pick-and-place experiment that involved using the system with four different control conditions. *MAN1* consisting of proportional control using a power grasp with the wrist fixed in the neutral position; *MAN2* with added co-contraction controlled grasp selection between power and

---

lateral grasps; *MAN3* added user control of wrist rotation, using co-contraction to cycle through power, lateral grasps and wrist rotation; *CASP* with the control system described in figure 2.10. The experiment was conducted over two sessions on consecutive days for training and evaluation respectively, both consisting of the same protocol of using each of the control strategies to grasp, lift, transport and release a selection of daily objects for 17 trials each. A single object was presented at a time, and released into a container using the prosthesis.

The experiment reported an error rate of less than 1% for the *CASP* control strategy, however, if a gross error had occurred, described by an incorrect grasp type or wrong orientation, then the trial was repeated. The time taken to grasp an object was slightly longer than *MAN1* and *MAN2* strategies, but much less than *MAN3*. No difficulty was reported in using the pair of dry EMG sensors in the detection of muscle activation. It was noted that the automated wrist-hand adjustments improved the ease of grasp, for the amputee subject, whom had prior experience with conventional myoelectric prosthesis control. It was evident from the results that automated grasp adjustment was beneficial in terms of reducing the cognitive load on the user, allowing them to focus on carrying out the task rather than manoeuvring the prosthesis. The *CASP* system only took slightly longer on average than conventional control strategies, with the exception of *MAN3*, to carry out the pick-and-place task, but had the added benefit of requiring less shoulder rotation and abduction movement, reducing overall fatigue.

It is clear that providing automation in terms of grasp selection can improve the ease of myoelectric hand control, however, grasp selection isn't just based on an object's size, shape and orientation, but it is based on the intention of the user. The use of an object recognition system is important for not just for inferring the shape, but also inferring the intention. The *CASP* system does an excellent job in identifying the object's geometrical properties in order to form the most suitable grasp pattern and aperture size, but appears to be only suitable for pick-and-place applications. Many objects can be interacted with in a number of different ways depending on the intended purpose. There is a need to infer this intention in order to provide the user with a wider range of interactive options when using a

---

myoelectric hand.

## 2.4 Chapter Summary

The main focus of this chapter was to give an overview of the current state of the art in assistive human machine interfaces, with the motivation highlighted by the wide variety of disabilities and the sheer size of this demographic. These interfaces can provide a method of communication and mobility for individuals suffering from severe motor impairment or limb loss where there are no restorative procedures yet available. The various types of interfaces were categorised according to their input method, including physiological motion, gaze tracking, oral communication, biofeedback and bioacoustic sensing. This literature survey aimed to review as many of the different varieties of HMIs and their application in AT as possible, but due to the sheer extent of research within each of these disciplines, only a small portion of the literature has been covered.

A more detailed survey of the most relevant work to this thesis in *intelligent prosthetics* has been studied. Although only limited work has been conducted in this area, the importance of this research has been highlighted. While the majority of the literature relies on computer vision systems to assist in grasp selection based on the target object, there is still a need to infer the intention of the grasp itself.



## **Chapter 3**

# **Conceptual Design of a Low-cost Heterogeneous Sensor Suite**

Following the discussion of the current state of the art in human machine interfaces in Chapter 2, a novel design concept for a heterogeneous sensor suite is proposed. The proposed sensor fusion interface aims to solve some of the current limitations of conventional myoelectric prosthesis control systems. The system intends to improve existing systems by automating grasp selection based on the grasp intention of the user. Although some research has been conducted in automated grasp selection for modern prosthesis control, the field of research is far from mature. Most systems involve the estimation of grasp based on the size and shape of the object, however, humans are capable of interacting with objects in numerous ways depending on the task and application. Unscrewing the lid of a bottle requires a different grasp than when drinking from it. The grasp doesn't just depend on the object, but also on the purpose of interaction. This chapter attempts to address this key limitation of existing control systems, by describing a novel control architecture used in conjunction with the proposed sensor suite to automate grasp selection by determining grasp intention.

### **3.1 Control System Architecture**

Looking at the bigger picture of control system flow, it can be seen from figure 3.1 that the overall system structure mimics the hierarchical neurological structure of human motor

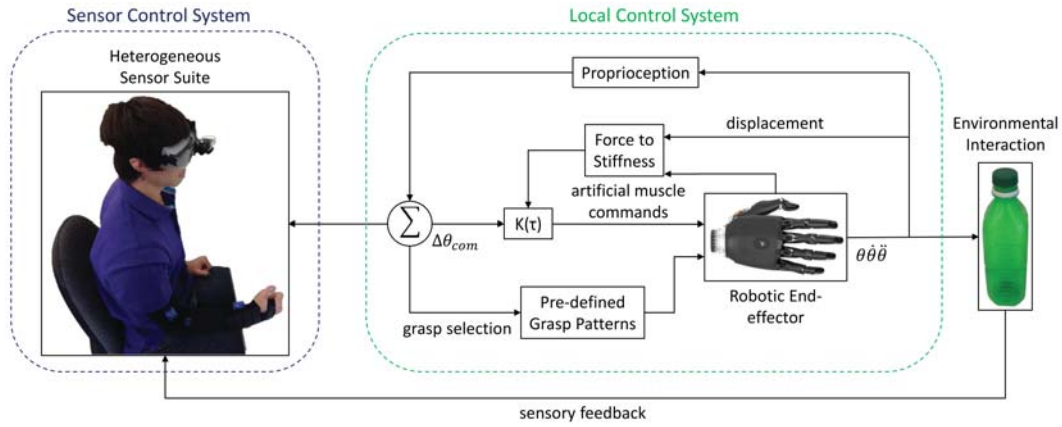


Figure 3.1: Overview of system flow from the heterogeneous sensor suite to the control of a robotic end-effector for interaction. The system flow can be separated into a *Local Control System (LCS)*, responsible for internal motor feedback control for the robotic end-effector, and the *Sensor Control System (SCS)*, which receives sensory feedback from the operator and the environment.

systems. The robotic end-effector is used to represent the human hand with the purpose of interacting with the environment. The system flow diagram presented isn't restricted for use with only prosthetic hands, but is used to represent a wider range of robotic arms and end-effectors that can be applied to a large range of AT applications. Other than the possibilities in upper limb prosthetics, the system control architecture can be used to represent tele-operative control of compliant robotic arms in a range of different fields, for example, conducting remote experiments, bomb disposal or carrying out essential maintenance in space exploration. Although sensory feedback in this specific implementation is not within the scope of this thesis, it is important to note that the use of additional sensors enabling complete feedback in terms of touch, pressure, texture, and force to name but a few, can be used to enhance the operator's situational and environmental awareness, further improving control. The overall system flow can be separated into a *Local Control System (LCS)*, responsible for internal motor feedback control for the robotic end-effector, and the *Sensor Control System (SCS)*. The SCS provides operational control over the LCS by sending it suitable commands based on the operator's intention and visual feedback from the environment.

A detailed flow diagram of the SCS is given in figure 3.2, which describes the system flow of the proposed heterogeneous sensor suite. The control architecture shown has been

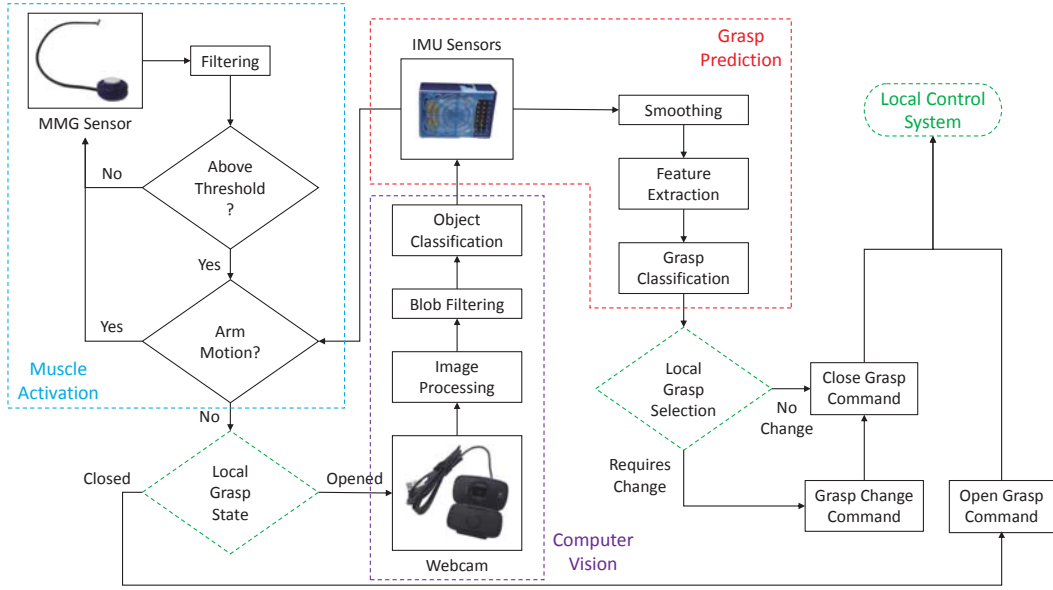


Figure 3.2: The system flow diagram for the proposed heterogeneous sensor suite. The *Muscle Activation Subsystem* consists of a single-site MMG sensor. It monitors the operator’s acoustic muscle response, filtering it in real-time. The IMU sensors provide motion feedback to reduce the number of misclassifications due to arm movement. Once the activation threshold has been reached, and the motion conditions have been met, the hand will either open, if the hand is in the closed state, or initiate the grasp selection pipeline. The first stage is the *Computer Vision Subsystem*, which uses a low-cost web camera positioned in an eye-to-hand configuration to take a single snapshot of the operator’s point of view. This image goes through a series of processing filters to detect the edges of objects within the scene. These are separated into blobs, whereby the one of largest interest is classified against a set of image templates using the blob’s properties. The detected object specifies a set of possible grasp patterns unique to that object, which is then used by the *Grasp Prediction Subsystem* to determine the most suitable grasp. A pair of IMUs are used to record the motion of the arm during the reaching phase of grasp. The recorded motion measures the X, Y and Z quaternion components of the forearm and upper arm. The resulting motion profile is filtered, and its features extracted. Specific features are used to classify against a template unique to the individual to select the most suitable grasp pattern. The current grasp selection on the *LCS* is then checked against the desired grasp, to determine whether a *grasp change* command needs to be sent before sending a *close* command. Once this has been determined, the appropriate commands are then sent to the *LCS*.

through some design iterations following preliminary work in the development of the individual subsystems. The design concept can be separated into three subsystems, designated the: *Muscle Activation Subsystem (MASS)*, *Computer Vision Subsystem (CVSS)* and *Grasp Prediction Subsystem (GPSS)*, the output of which is sent to the *LCS*. The system utilises the combination of outputs from each subsystem to send either an *open* or *close* with or

---

without a *grasp change* command to the LCS. The *open* and *close* grasp commands depend on the current open/close state of the LCS, in this case, a myoelectric hand. The *grasp change* command depends on the current grasp selection, however, this will vary according to the end-effector and its internal LCS. To summarise, if the hand is in a closed state, an *open* command will be sent, if the hand is in an open state and a change in grasp is not required, a *close* command will be sent, and if the hand is in an open state and a change in grasp is required, a *grasp change* followed by a *close* command will be sent to the LCS.

### 3.1.1 Muscle Activation Subsystem (MASS)

The MASS consists of using a single MMG sensor for single site input. Preliminary work used dual site muscle activation inputs for individual open and close control, which is generally used in the control of consumer grade myoelectric hand prosthesis, however, this is dependent on the type and severity of the amputation, and the control of the remaining muscle in the residual limb; some amputees may not be capable of multi-site control. In order to accommodate for the large differences in remaining muscle in the residual limb among amputees, the system was simplified to require just a single-site muscle activation input.

As discussed in Chapter 2, MMG sensors measure the mechanical response of the muscle, in comparison to the electrical response recorded by EMG sensors. Both of which can be used for the detection of muscle activation for discrete control of the opening and closing of a myoelectric hand using a threshold that can be adjusted to the operator. Due to the presence of motion artefacts affecting the MMG signal due to arm motion, the sensor receives gyroscopic feedback from the IMUs. The MMG sensor is directly connected to the upper arm IMU as shown in figure 3.3, however the motion in both IMUs are programmatically utilised so that complete arm motion is taken into account when muscle activation occurs. The aim of this is to reduce unintentional muscle activation input due to arm motion. If the MASS detects an activation input that meets the required criteria to activate a grasp, the grasp state of the LCS is checked to decide on a suitable system flow direction. If the hand is in the closed state, the system immediately sends an *open* grasp command to the LCS. If the hand is in an open state, the CVSS is initialised, and the MASS prevents MMG input



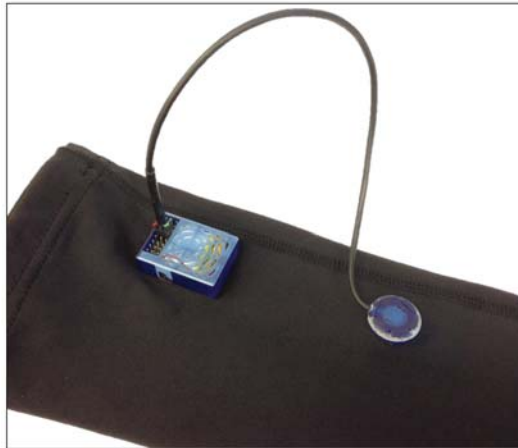


Figure 3.3: The MMG sensor directly linked to the upper arm IMU to utilise gyroscopic feedback in order to reduce unintentional muscle activation due to arm motion.

until the resulting command to the LCS has been executed. The MMG sensor is only used to detect muscle activation as part of the MASS to trigger the start of the grasp prediction pipeline or to close the hand.

### 3.1.2 Computer Vision Subsystem (CVSS)

The CVSS uses a single low-cost web camera in an eye-to-hand configuration to capture environmental information, providing the SCS with situational awareness. The camera provides an interface for determining the operator's target for interaction. Preliminary work took an eye-in-hand approach to computer vision, which will be discussed in greater detail in Chapter 4. The preliminary research conducted prompted a change to an eye-to-hand approach and a change in the conceptual control architecture of the SCS to the one illustrated in figure 3.2.

Once the MASS has prompted the initiation of the CVSS by meeting the required activation criteria, the subsystem begins by taking a snapshot of operator's point of view. The image taken goes through series of filters for edge detection and removes any detected blobs of little interest. The intrinsic properties of the remaining blob, or region of interest are calculated. The blob's properties are classified against a set of templates, containing multiple images of different objects in a variety of perspectives. Each object in this template has been designated a set of grasp patterns that are commonly used for interaction. A

---

large number of different grasp patterns are available, each having their own functions and applications. The CVSS is used to narrow this selection down to a few key grasp patterns that are best suited to interacting with that particular object. This set of grasp patterns is then sent to the GPSS, which selects the grasp based on user intention.

### **3.1.3 Grasp Prediction Subsystem (GPSS)**

The GPSS uses a pair of IMUs to record the motion of the arm during the reaching phase before interaction with an object. After the object of interest has been classified by the CVSS, the resulting set of object-specific grasp patterns for interaction are presented to the GPSS. The system initiates the recording of inertial motion from the pair of IMUs, positioned on the forearm on the wrist, and on the upper arm across the bicep. The two sensors estimate the change in orientation of the forearm and upper arm over time. Once recording begins, the operator reaches towards the object of interest stopping at the point of contact for their desired interaction. The system stops recording, and attempts to predict grasp intention by classifying inherent physiological features during reach with those stored in a pre-existing template that has been calibrated to the operator's unique arm motion. After a grasp pattern has been classified, an output command is sent to the LCS to change to the selected grasp if required and to close the end-effector.

A preliminary study was conducted to validate the use of arm motion for predicting grasp, which can be found in Appendix A. The study demonstrated relatively successful grasp classification rates of 90.8%, 69.2% and 88.1% for three generic object classes: *Very Small*, *Small* and *Cup* respectively, using the most commonly used grasp patterns for those objects at a single location. The study concluded that although the grasp classification rates were relatively high, object classes are deemed too generic, and the grasp patterns should be more object specific in order to infer intention. A greater analysis of upper limb motion features was required to be able to classify grasps with high accuracy across a variety of locations in 3-dimensional space with additional improvements to be made on classification algorithms. A follow up in-depth study on the effect that variation in object position has on upper limb motion during grasp on more task-specific and unique object classes was

---

conducted, with the analysis consolidated in Chapter 5.

## **3.2 Local Control System: The Bebionic V2 Hand**

Although the design of the sensor suite can be applied to a wider range of applications, its utilisation in upper limb prosthetics is an obvious choice for the purpose of validating the system for practical applications. Through early collaboration with RSL Steeper, a Bebionic V2 Large myoelectric hand was obtained for conducting research studies, and as a result, has been utilised throughout the development of this thesis as the end-effector for the LCS. Despite the system being easily adaptable to any consumer grade myoelectric hand, it is important to note that not all myoelectric hands have the same control architecture. As a result, it is important to understand how the Bebionic V2 hand functions, so that the output from the SCS can be adapted to control it.

### **3.2.1 System Control**

Although the Bebionic V2 hand is the predecessor to the newer Bebionic V3 and its respective medium and small size iterations, the control architecture remains the same. Like other consumer grade myoelectric hands, the Bebionic V2 hand utilises either one or two EMG sensors to provide single or dual site control of hand open and close DOF with options for either proportional or discrete control. Combined with a selection of predefined grasp patterns, the hand can carry a wide variety of tasks. The hand can also be attached to a motorised wrist which can provide clockwise and anticlockwise rotation, however requires greater control of remaining muscle in the residual limb and additional EMG sensors to record at multiple sites for more DOF. For the purpose of simplicity and availability, the focus will be on single/dual site control of the hand itself.

The hand contains five motors located in the palm, providing flexion and extension of individual finger and thumb digits. Each motor is assigned its own control board for constant tracking in order to provide precise control and synchronisation between digits. Each individual motor rotates a lead screw that extends and retracts a link that connects the proximal, middle and distal phalanges, enabling a single motor to uniformly close and open

---

the entire digit. Although the thumb has its own motor for digit flexion and extension, it is opposed manually. The thumb can either be set in the opposed or non-opposed position, and uses a reed switch to identify its position for grasp selection.

Grasp patterns are selected, or cycled through, using two switching mechanisms. A *hard* switch, which is a physical button located on the back of the hand, and a *soft* switch, which is made by sending a pair of consecutive *open* commands to the hand using the EMG sensors. Using this method, up to 4 grasp patterns can be selected for each thumb position. The *soft* switch is used to cycle between the default and alternate grasp patterns. The *hard* switch swaps between a primary and secondary set of grasp patterns, which can be cycled through using the *soft* switch.

### 3.2.2 Grasp Patterns

The Bebionic hand is pre-programmed with 14 reliable grasp patterns and hand positions, however only 8 are available on the hand at a single time, 4 for each thumb position. The most desirable and frequently used patterns must be selected and pre-programmed into the hand. These can be changed using RSL Steeper's Bebalance+ software, which is also capable of setting the number of EMG sensors used and tuning the thresholds for the user, as well as selecting between proportional and discrete grasp control. When the hand is switched on, the hand fully opens and calibrates before use, setting the current grasp pattern to the default selection of the primary set. An additional 3 grasp positions are achieved as a part of other patterns, namely, *hook*, *adduction* and *open palm*. Mechanical adjustment of the thumb position is required to enable certain patterns, for example, adjusting the thumb position for the thumb to contact with just the index finger for *pinch* and *precision* grasps, or having it contact both middle and index fingers for a *tripod* grasp. A tree graph depicting the availability of each grasp pattern is given in figure 3.4, with each pattern described as follows [161]:

#### ***Tripod***

Grips objects between the thumb and the index and middle fingers, useful for interacting with a variety of everyday objects such as car keys, coins, jar lids and pens.

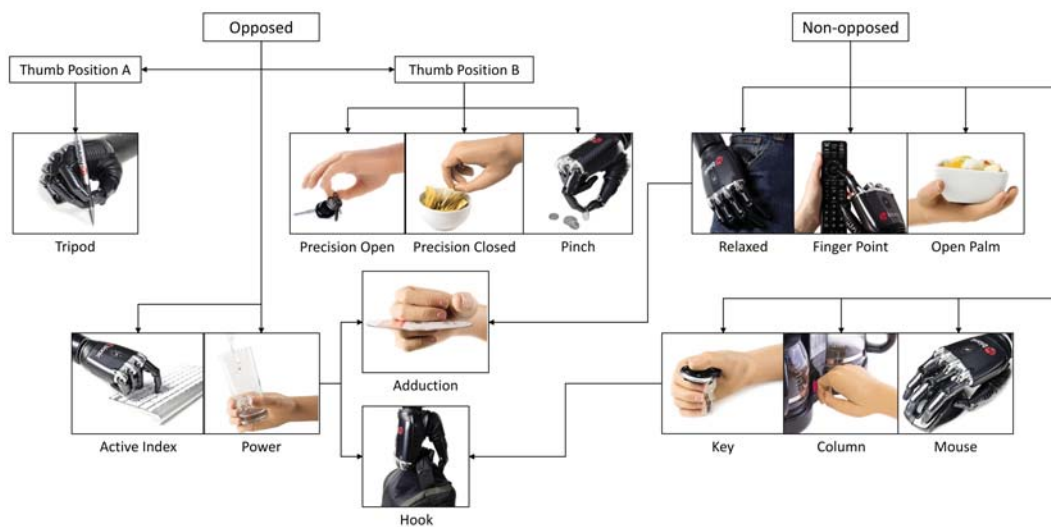


Figure 3.4: A tree diagram of all available grasp patterns for the Bebionic hand in terms of availability and thumb position.

***Pinch*** Similar to that of a *tripod* grasp, everyday objects are gripped between the thumb and index finger.

***Power*** All 4 fingers and thumb are used to wrap the hand around larger objects such as fruit, bottles, tools and utensils.

***Active Index*** Used to grip the handle of an object similar to that of a *power* grasp, but with the index finger positioned over the level of the device, such as a spray bottle. The index finger can be independently controlled to activate the object's lever. This grip also works well for typing on a keyboard.

***Key*** Also known as a *lateral* grasp, this grip is ideal for interacting with thin flat objects such as papers, credit cards, or turning a key in a lock.

***Finger Point*** The index finger is left pointed out with the rest of the fingers retracted, and is normally used for typing on an input pad, pressing a doorbell, pushing buttons or as a gesture.

***Column*** The index and middle fingers rest on top of the thumb, and can be used to press larger switches, or to interact with a car gear stick.

---

<b><i>Mouse</i></b>	Used to grip the sides of the mouse with the thumb and little fingers, with the middle and ring fingers used for stabilisation. The index finger can be independently controlled for clicking the mouse button.
<b><i>Precision Open</i></b>	Uses the index and thumb to grip objects with greater precision, by pausing the thumb midway for positional adjustment. The remaining fingers are extended to provide more room for the grasp.
<b><i>Precision Closed</i></b>	Identical to the <i>precision open</i> grasp, with the exception that the remaining fingers are closed.
<b><i>Hook</i></b>	With the hand set to proportional control, the <i>power</i> grasp can be paused midway to create a hook shape, which can be useful for carrying a shopping bag or briefcase.
<b><i>Adduction</i></b>	As the Bebionic hand closes, the fingers naturally adduct closer together, enabling the grasping of thin objects such as cutlery or a toothbrush. This grasp is considered to be the most functional when used with a <i>power</i> grasp, however it can also be used with the hand in <i>tripod</i> or <i>key</i> grasps.
<b><i>Open Palm</i></b>	Can be made with the hand fully open with the thumb non-opposed, and can be used for carrying flat objects such as a bowl or plate.
<b><i>Relaxed Hand</i></b>	This grasp pattern with the thumb non-opposed, provides a more natural looking posture when not actively using other hand functions. Applying a further signal can drive the fingers to form a non-opposed <i>hook</i> grasp.

### 3.2.3 Limitations

Despite the Bebionic Hand being one of the most advanced myoelectric hand prosthesis available commercially, there are still a number of key limitations, which restrict the hand in terms of usability and versatility.

---

### 3.2.3.i Grasp Availability

Although the Bebionic technical manual [161] boasts 14 different grasp patterns, not all of them are available simultaneously. Only a maximum of 8 programmed patterns are available at a single time, with three additional patterns being formed as part of the other grasps. The requirement of using the physical button on the back of the hand, allowing access to only 4 of the patterns digitally, greatly reduces usability for a bilateral amputee. As shown in figure 3.4, due to the thumb requiring tooled manual adjustment, the user must choose between having access to the *tripod* grasp or *precision open*, *precision closed* and *pinch* grasps. Proportional control of the hand is desired to provide better start and stop precision of the motors to enable partial grasp patterns such as the *hook* grasp.

### 3.2.3.ii Manually Opposed Thumb

Perhaps the largest physical restriction is the manually opposed thumb. This restriction greatly reduces the versatility of the system in terms of digital control. In order to switch between thumb positions, the operator must use their opposite hand or part of the environment to adjust the thumb manually. Competitor myoelectric hands such as the Michelangelo hand [135] or i-Limb [10] have a motorised opposable thumb, allowing access to different grasp patterns without needing physical intervention.

### 3.2.3.iii Grasp Localisation

Another major drawback is the lack of a pattern localisation system, making it difficult to identify what grasp pattern the hand is currently set. The system provides no digital indication on the grasp, with the only identifier being visual while the grasp is being made, or having the order of the patterns thoroughly embedded in the operator's memory. Without knowing the exact pattern the hand is in, it is easy to make incorrect grasps, and forms a large aspect of the cognitive load involved when using a myoelectric hand.

---

### 3.2.4 Design Considerations

Having studied the major limitations of the Bebionic V2 hand that will be used, it is important to consider them in terms of the system's implementation. Although the control system architecture will remain the same, the implementation for real-time application is dependent on the LCS. This means that the control architecture can be used for many different systems, not just restricted to the myoelectric prosthesis, however will require an implementation strategy tailored to fit the LCS of the end-effector used. For the purpose of system implementation with the Bebionic Hand, a specific design strategy is designed to rectify, to a certain extent, some of the limitations imposed by the LCS.

With the hand requiring tool adjustment, to access certain grasp patterns, the number of available grasps are limited. The *precision* and *pinch* patterns were chosen over the *tripod* pattern because of the finer control those grasps can provide when picking up small objects, making them ideal for testing purposes, however in general, the *tripod* grasp may be better for multipurpose use, as the larger grip is capable of interaction with slightly larger objects as well as items such as a pen or pencil.

It must be noted that with manual control required to switch between sets of grasp patterns, only 4 grasps patterns can be used at any one time, two per thumb position. With physical interaction required in order to change the thumb position, only two patterns can be selected digitally, which is definitely not ideal for the purpose of this system. When the thumb position is changed, the default grasp for that position is set, giving digital control only over switching between the default and alternate patterns for each thumb position. The lack of digital selection of grasp patterns is the largest caveat of system implementation with the Bebionic Hand. As a result, the assumption must be made that motorised thumb access is available, and should be manually switched prior to initialising the grasp prediction algorithm, as it can also be assumed that the operator knows which grasps they want to make. In order to make this assumption, the location of the thumb position must be known at all times in order to select the grasp pattern correctly, however the hand itself doesn't provide any form of digital feedback as to which thumb position the hand is in. Without the addition of external sensors, the location of the thumb position can be tracked programmatically



---

depending on the grasp pattern used in the grasp. For example, if the operator intends to use a *lateral* grasp, with the assumption that the thumb position has been physically changed before initiating the grasp, the system can assume that the thumb is in the non-opposed position. Although knowledge of the thumb position is not required for predicting the grasp itself, it is required when sending the correct output to the hand to tell it whether to use a *soft* grasp switch or not if that grasp is set as the default. Keeping track of the thumb position allows active tracking of the current grasp, provided that the object has been correctly identified. If the object classification is incorrect, the wrong grasp parameters will be used in classifying the correct grasp, which will usually result in a misclassification. The open/close state of the hand can be easily tracked by monitoring the *open* and *close* commands sent to the hand. The usage of this method can be seen as the final part of the sensor suite control system architecture provided in figure 3.2.

### 3.3 Myoelectric hand adapter design

The fixture for the Bebionic Hand is designed specifically for use with a myoelectric forearm prosthesis, however, the amputee participant only had access to a molded forearm prosthesis designed for use with a mechanical hook. An adapter was designed and 3-D printed in order to fix the two together. The adapter also acted as a battery housing for a mobile power supply, as well as containing a micro controller to receive output commands from the sensor suite via Bluetooth (BT), to control the hand. The SolidWorks model shown in figure 3.5 is made up of 8 components: the *housing*, *cover*, *connector lock*, and  $4 \times$  *clips*, and are 3-D printed out of a black resin using a Form 1+ stereolithography (SLA) printer by FormLabs.

The 3-D printed adapter is given in figure 3.6 (a). The *housing* forms the main structure of the adapter, providing cover on one side with 3 longitudinal bars used for support. A circular extrusion is located between two of the supporting bars, which is used to hold a circular flip switch for powering on and off the device. At both ends of the *housing* are two end plates, the bottom of which, has a slotted *key* that locks into the forearm prosthesis. The bottom plate has 4 holes, 3 of which are used to fit around matching spherical features on

the end of the forearm. The fourth hole is used to lock the orientation of the adapter to the forearm using a lever, preventing the *key* from unlocking (see figure 3.6 (b)). At the top end of the *housing*, the EQD connector, which provides the hand with power, ground and open/close output signals from the micro controller, is threaded through the opening, with the *connector lock* fitted behind it, holding it in place (see figure 3.6 (c)). Wires from the EQD connector are connected to the micro controller and a 1300mAh 3S 11.1v 25C Lipo Battery by Overlander, which goes through a high-current voltage regulator, as shown in (d). A high-current voltage regulator is required to start up the motors in the myoelectric hand on initialisation. The LiPo battery can provide the hand with power for approximately 5 hours. The *EQD housing* fits on top of the *housing* around the EQD connector. A pair of countersunk screws are fed through the *EQD housing*, *housing* and *connector lock*, using a washer and nut to secure them together. The 4 channels in the *EQD housing* enable the hand to fit in 4 different orientations. The *clips* are used to fit over the lip of the Bebionic hand as shown in (e), preventing any potential loosening of the power connector while under use. The *clips* are secured in place with tape. A *cover* is used to enclose the battery and circuitry within the *housing*, using small slats on either side for alignment. Tape is used around the top and bottom of the *cover* and *housing*, keeping the enclosure shut.

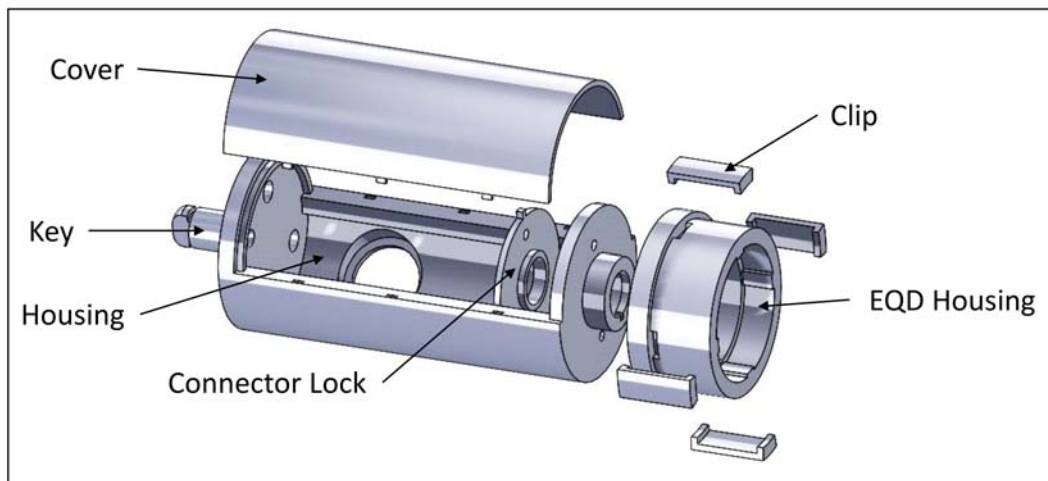


Figure 3.5: Exploded SolidWorks model of the myoelectric hand adapter, consisting of 5 different 3-D printed components: the *housing*, *cover*, *connector lock*, *clip* and *EQD housing*.

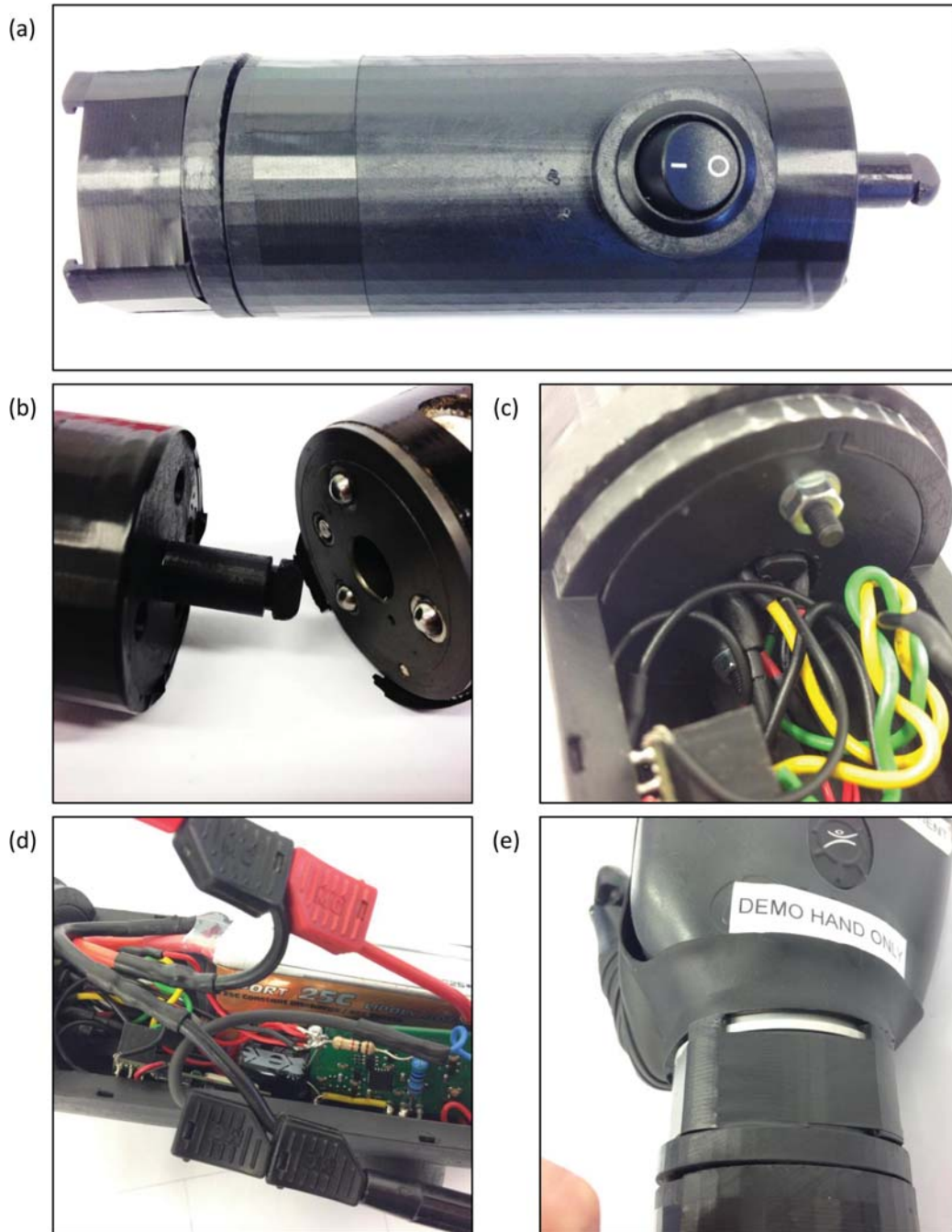


Figure 3.6: The 3-D printed hand adapter showing (a) the complete assembly, (b) adapter key and forearm prosthesis lock, (c) EQD connector fastened with the *connector lock*, (d) microcontroller, high-current voltage regulator and LiPo battery, and (e) the Bebionic hand held inside the *EQD housing* using the *clips*.

---

### 3.4 Chapter Summary

This chapter described the novel design concept for a heterogeneous sensor suite, which aims to reduce the cognitive load imposed by myoelectric hand control. The system aims to not just base grasp selection on the object's intrinsic properties using object recognition, but select it according to user intention. The main idea being that each object can be interacted with in a variety of ways for different purposes. The complete system flow is described in detail, from the SCS to the LCS, which carries out the intended interaction. Intentional muscle activation is detected using an MMG sensor, which either sends an *open* command to the LCS if the hand is closed, or initiates the grasp selection process when the hand is open. The computer vision system takes a snapshot of the operator's point of view, classifying the object according to various intrinsic properties. Once the object is classified, the IMUs start recording motion as the operator reaches for the object. Features are extracted during reach to classify the grasp based on the operator's intention, sending an appropriate *grasp change* command to the LCS, followed by a *close* command.

The control strategy of the Bebionic V2 hand is explained due to its application as the LCS. The limitations of the device are discussed in full, as well as the design considerations required to monitor and control it. Although there are a few commercially available myoelectric hands that would be much better suited for integration with the described control architecture, the current hardware limitations are considered and bypassed and best as possible. The design of a myoelectric hand adapter was described, which is used to connect a myoelectric hand on to a hook-based forearm prosthesis. The adapter contains the necessary circuitry and power supply to control the hand using BT. The adapter was used to fit the Bebionic hand to the amputee's forearm prosthesis, and was also hand held by healthy subjects to carry out real-time experimentation.

## **Chapter 4**

# **Mechanomyography and Environmental Vision**

The sensor suite described in Chapter 3 integrates three main sensing technologies, mechanomyography, computer vision and inertial measurement, each of which can be individually developed, tested and integrated into the main system. Although MMG sensing and computer vision are not considered novel aspects of the sensor suite concept, their integration with the novel inertial-based interface for grasp prediction, actively contributes to the system's overall successful implementation. This chapter aims to describe the design and implementation of the MMG and computer vision systems within the scope of this research, as well as discussing preliminary work fusing the two systems together for active grasp control of the Bebionic V2 hand.

### **4.1 Mechanomyogram Acoustic Sensing**

As described in Chapter 2, there has been a vested interest in MMG sensors for a number of years due to its potential advantages over EMG. Although this research doesn't focus on further development of the design of MMG sensors, it is important to go into detail on the design and characterisation of the sensor used, as it forms an integral part of the overall system.

---

#### 4.1.1 Sensor Design

The specific type of MMG sensor used was recreated from the design by R. Woodward *et al.* [16], which was based on that developed by Posatskiy *et al.* [162, 163]. The acoustic MMG signal is captured with a Knowles SPU1410 microphone that measures the pressure change in an encapsulated chamber by the perturbation of an aluminised 4  $\mu\text{m}$  Mylar membrane by Homefly [164]. When positioned on the skin above the muscle of interest, the sound produced during muscle contraction propagates through the skin, and perturbs the Mylar membrane, causing a pressure difference within the chamber. The recorded signal is a low frequency vibration between 25Hz and 50Hz [165, 144, 12, 166].

The design shown in figure 4.1 by R. Woodward *et al.* uses the ideal pressure chamber dimensions reported by Posatskiy *et al.* [162, 163], having a conical shape with height and diameter of 5 mm and 7 mm respectively, which is said to produce the maximum signal gain, while reducing the frequency-response fluctuation and high-frequency distortions. The clip and Housing were manufactured by 3DSystems out of Visijet M3 Navy plastic using 3D printing technology. The microphone PCB boards were manufactured by Elecrow, with the surface mount microphone positioned by hand and soldered using a reflow oven. After testing for short circuits, positive, ground and signal multi-core wires are soldered by hand.

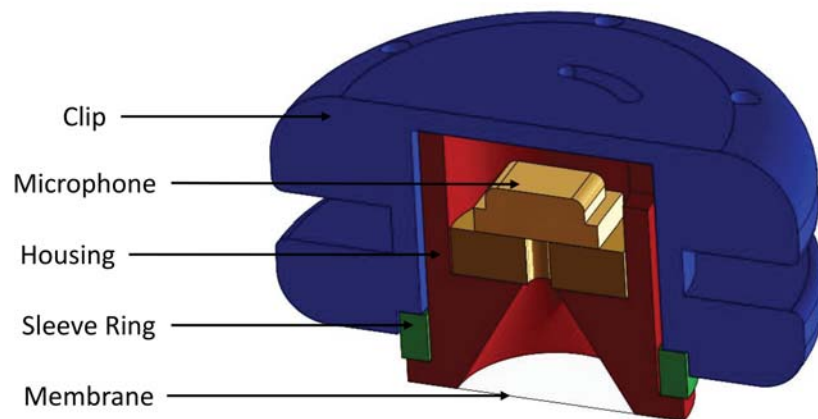


Figure 4.1: The MMG sensor design reproduced from work by R. Woodward *et al.* (reproduced from [16]). The design utilises a single microphone sensor, which measures the pressure change within a conical chamber enclosed by a Mylar membrane.



Figure 4.2: The manufactured MMG sensor reproduced from work by R. Woodward *et al.* [16]. The sensor is sewn into wearable clothing using several through-holes in the Clip.

The PCB is fitted into the Housing, making sure that it is flush with the exit to the conical chamber so that the hole to the microphone and the chamber are aligned. Silicone is inserted on top of the microphone to reduce back propagation of sound to improve containment, as well as keeping it in place. The silicone is required to be left for 24 hours to set. The Mylar membrane is pulled taut over the chamber's entrance and tightened using the Sleeve ring for fastening, where any excess membrane is removed. The wires are subsequently pulled through the Clip, and the Housing pushed all the way inside. The wires are crimped and fastened to female housings where they can interact with the header pins available on the NU IMU developed by S. Wilson. The completed MMG sensor is displayed in figure 4.2.

#### 4.1.2 Signal processing

The raw acoustic signal is first filtered using a second order digital band-pass Butterworth filter and rectified to obtain a signal between 10 Hz and 100 Hz, reproduced according to [16] in equation 4.1 in s-plane notation.

$$F(s) = \frac{s^2 - 1}{s^2 - 1.518s + 0.550} \quad (4.1)$$

Further improvements were made following research conducted by S. Wilson, consisting of using the resulting signal and passing it through the Hilbert transform function given by



---

equation 4.2, where  $PV$  is the *Cauchy principal value*.

$$H(t) = \frac{1}{\pi} PV \int_{-\infty}^{\infty} \frac{f(x)dx}{x - t} \quad (4.2)$$

The absolute value is taken and used for thresholding according to equation 4.3 to detect intentional muscle activation according to a user specific threshold,  $OC_{Thres}$ .

$$G(t) = |H(t)| \quad (4.3)$$

A function is used to track local minima to avoid fluctuations in the raw signal from misinterpreting multiple instances of the threshold being crossed. The most recent local minima  $f(a)$  is tracked according to an interval designated by the length of the semi-minor axis of an ellipse, denoted  $c_w$ . The value  $f(x)$  becomes the local minima if equation 4.4 is satisfied. This provides better differentiation between intentional muscle activation and detected motion artefacts. The sampling rate is actually reduced to lower the chance of unintentional activations as a result from these artefacts.

$$f(x) = f(a), \text{ where } \begin{cases} f(a) - c_h \geq f(x) \geq f(a) + c_h \\ \text{interval : } x \rightarrow x + c_w \end{cases} \quad (4.4)$$

The complete processed signal is displayed in figure 4.3, showing mechanomyogram recordings during isometric contraction of the forearm. The threshold itself depends on the position of the sensor above the muscle as well as the average acoustic amplitude resulting from flexion. The size of this threshold can vary according to the individual and can be easily changed if required. Muscle fatigue does have an effect on the amplitude of the signal, so over time, the average threshold may decrease, however this can be adapted accordingly by changing the threshold. Machine learning would be of benefit when using the MMG over extended periods of time to provide adaptive control based on muscle fatigue, however, this was found not to be an issue. From figure 4.3, it can be seen that a secondary peak is produced after the contraction as a result of signal rectification; this is taken into account to avoid muscle activation misclassification.



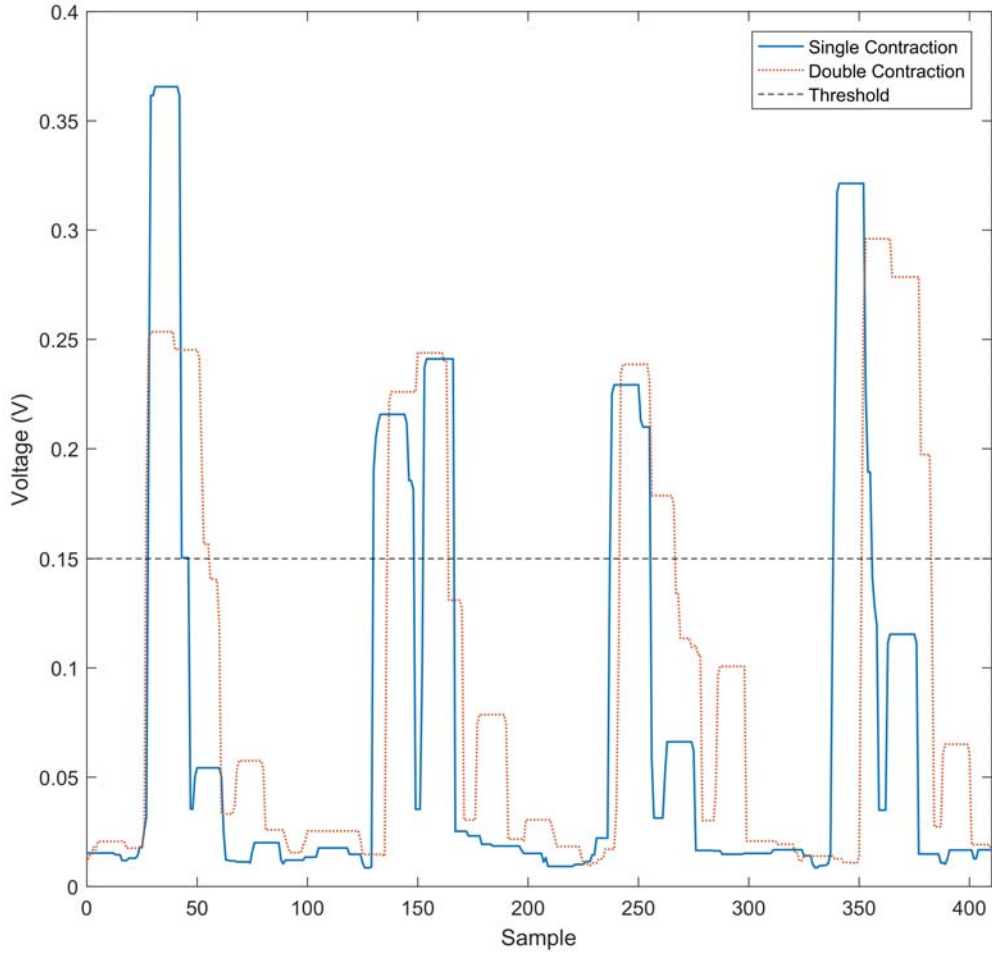


Figure 4.3: The processed MMG signal, taken from the author, during isometric contractions of the forearm during single and double contractions. A single contraction increases the MMG response briefly above the threshold, and is used to open or close the hand. A double contraction extends the duration of the response above the threshold, and is used to activate a *soft* grasp switch.

By contracting the muscle in the forearm, the signal increases past the set threshold value. However, it is only when the signal crosses the threshold on its way back down that intentional muscle activation is recorded. The reason for this is to be able to take into account the secondary peak caused by rectifying the signal. If the recorded signal remains above the threshold for too short a period of time, it is ignored, preventing additional unintentional activation output.

As described in Section 3.2, EMG control of the Bebionic V2 hand uses a double *Open* signal while the hand is open in order to activate the *soft* switch to cycle between the default

---

and alternate grasp patterns. The same mechanism can be reproduced by the MMG signal, as a double contraction of the muscle produces a response that has a prolonged duration above the threshold, as shown in figure 4.3. By setting a response length based on the sampling rate, a double response can be used to activate the *soft* switch in the same way that the Bebionic hand does with EMG.

## 4.2 Computer Vision

Computer vision serves a major function within the design of the complete sensor suite, serving to reduce the numerous available grasps to those specific to that of an object class, which in turn, enhances the grasp prediction capability of the inertial system by limiting the selection of grasp patterns to the most relevant. As discussed in Chapter 2, the majority of research towards *intelligent prosthetics* has relied on object recognition and computer vision. Although the development of a novel image processing algorithm for this system is not within the scope of this thesis, it is important to discuss the methods used. The object recognition algorithm presented utilises numerous image processing techniques to create a template of intrinsic object properties, which can be used to classify objects in real-time.

For use in conjunction with the inertial-based grasp prediction system, it is important that the object recognition classification rate is extremely high, as it will affect the template chosen for predicting grasp. Although current state of the art object recognition algorithms can be very effective, it is important to take into account the application involved, and the potential considerations in regards to the algorithm used.

### 4.2.1 Algorithm Considerations

For the majority of applications, making the system highly accurate with a fast processing speed will always be ideal, however, normally the more accurate (and complex) the algorithm is, the greater the processing power required. With a prosthetic hand, the system will be restricted to battery powered processors with an emphasis on mobility. With the battery aiming to power the prosthesis, sensors and data transmission via BT, the effectiveness of processor-hungry algorithms can be limited. Larger batteries can aid in reducing this lim-

---

itation, however they can be heavy and cumbersome to carry, and can put excess strain on the operator's arm and shoulder.

Real-time implementation of the system requires object recognition processing to be as fast as possible, ideally at near instantaneous speeds. The faster the object is classified, the faster the grasp prediction algorithm can be initiated, allowing the operator to interact with objects in the environment without interruption, improving the natural flow of movement. With this in mind, simpler object recognition techniques can be considered more applicable, however, can suffer from higher misclassification rates.

One of the major problems in object recognition is distinguishing the object of interest from its background as well as nearby objects in cluttered every day environments. Rapid improvements in camera technology has led to the development of RGB-D cameras, which can measure the distance between the camera and objects in the image. Using depth, the image can be split into foreground and background, which can greatly improve usage in everyday settings. A pair of cameras for stereoscopic vision can also be used to calculate the depth properties in an image. Despite the obvious advantages of utilising depth in object recognition, current affordable technology is bulky and obtrusive. The nature of the mobile sensor suite would consider the obtrusiveness of the system an important factor in terms of usability. Further hardware development in affordable consumer products will be able to address this problem in the future.

Overall, it is important to make a balance between mobility, accuracy and speed when considering computer vision for this application. With the scope of this research mainly focused towards inertial-based grasp prediction and the design and validation of the integrated sensor suite, a relatively simplistic approach was taken towards the design of the CVSS for use in a controlled environment. Given additional time and resources, a more complex approach would be taken to improve overall flexibility and robustness for use in cluttered everyday environments.

---

## 4.2.2 Object Recognition

The object recognition algorithm uses a series of image processing filters to detect edges in the environment, separating groups of adjacent pixels into different regions or blobs. These blobs then undergo a filtering process to remove any insignificant regions in order to find the object of interest within the image. After obtaining a single region with the object of interest, the region's properties are calculated and saved to a template to create the object classifier.

### 4.2.2.i Image Processing

The input image from the camera first undergoes contrast correction, increasing the RGB values of bright pixels, and decreasing the RGB values of dark pixels in order to enhance the difference between colours in the image. The contrasted image is then converted into a grayscale image. Increasing the contrast of the image beforehand, increases the difference in grayscale values, which improves the detection of edges. Edge detection is then performed by applying the Sobel edge operator, which uses two 3x3 kernels,  $G_x$  (Eq. 4.5) and  $G_y$  (Eq. 4.6) that are convolved with the image to find approximations for the horizontal and vertical derivatives respectively, where the output image is calculated by equation 4.7.

$$G_x = \begin{bmatrix} -1 & 0 & +1 \\ -2 & 0 & +2 \\ -1 & 0 & +1 \end{bmatrix} \quad (4.5)$$

$$G_y = \begin{bmatrix} +1 & +2 & +1 \\ 0 & 0 & 0 \\ -1 & -2 & -1 \end{bmatrix} \quad (4.6)$$

$$|G| = |G_x| + |G_y| \quad (4.7)$$

The Canny edge detection algorithm is then applied, which uses Gaussian smoothing

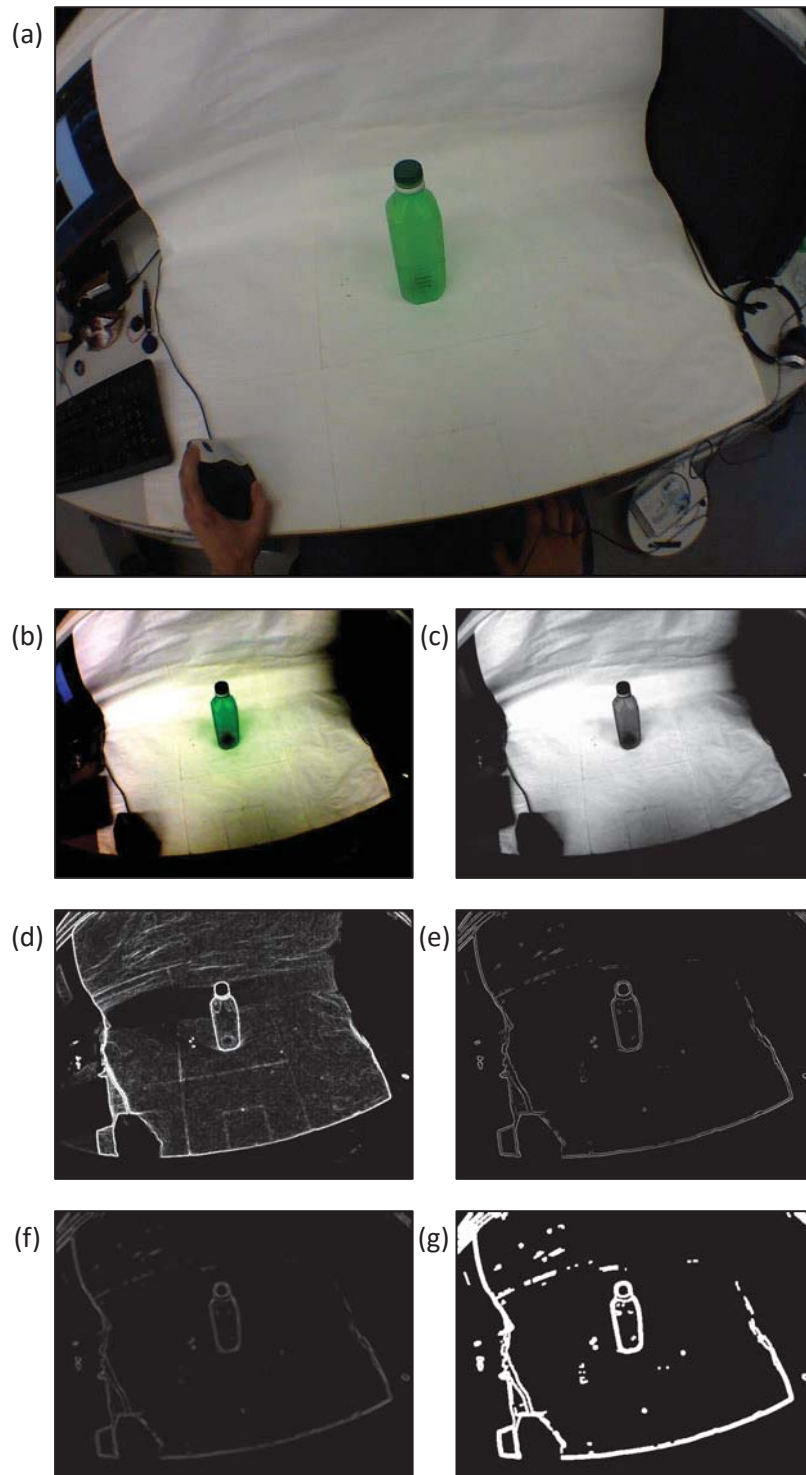


Figure 4.4: The cumulative effect of image processing steps on original image (a) consisting of (b) contrast correction, (c) grayscale conversion, (d) Sobel edge detection, (e) Canny edge detection, (f) 5x5 Gaussian smoothing and (g) binary thresholding.

---

followed by non-local maxima suppression and hysteresis thresholding [167] to enhance the major edges, and remove the minor edges found by the Sobel operator. Smoothing is then applied using a 5x5 Gaussian filter with  $\sigma = 3$  to merge nearby pixels to enclose regions, given by equation 4.8.

$$G(x, y) = \frac{1}{2\pi\sigma^2} e^{-\frac{x^2+y^2}{2\sigma^2}} \quad (4.8)$$

A binary filter is finally applied to enhance the detected edges according to the threshold,  $B_{Thres} = 10$  in the range of 0 – 255, given by equation 4.9. The cumulative effect of the image processing steps is shown in figure 4.4.

$$I_m = \begin{cases} 1, & G \geq B_{Thres} \\ 0, & G \leq B_{Thres} \end{cases} \quad (4.9)$$

#### 4.2.2.ii Blob Filtering

Following the completion of the image processing step, the resulting output image highlights a large number of pixel regions, also known as blobs. The blobs are separated by the amount of neighbouring pixels, some of which can be very small, caused by a bit of dirt, pencil mark or even a crease in the paper. A single image can contain more than a hundred different sized blobs, and only one of which contains the object of interest. In order to find this object, all other blobs must be filtered out. This is done in a series of steps (see figure 4.5), whereby the blobs are removed based on various properties.

Firstly, all blobs with a pixel density below  $A_{min} = 10$  and above  $A_{max} = 5000$  are removed. Blobs that are too small or too large are not likely to be a graspable object. Any blobs that have a height or width greater or equal to that of the image are also removed ( $H_{cam} = 480$  and  $W_{cam} = 640$ ), as they are most likely from part of the background environment. The Euclidean distance of each blob's centre of gravity from the centre of the image is then calculated and compared to a distance threshold ( $E_{cen} = 125$ ). It can be assumed that within the scope of this study, the subject's gaze is fixed in a straight line, approximately represented by the centre of the image. The object of interest is therefore assumed to be located in the centre of the subject's line of sight. Adjustment is made by

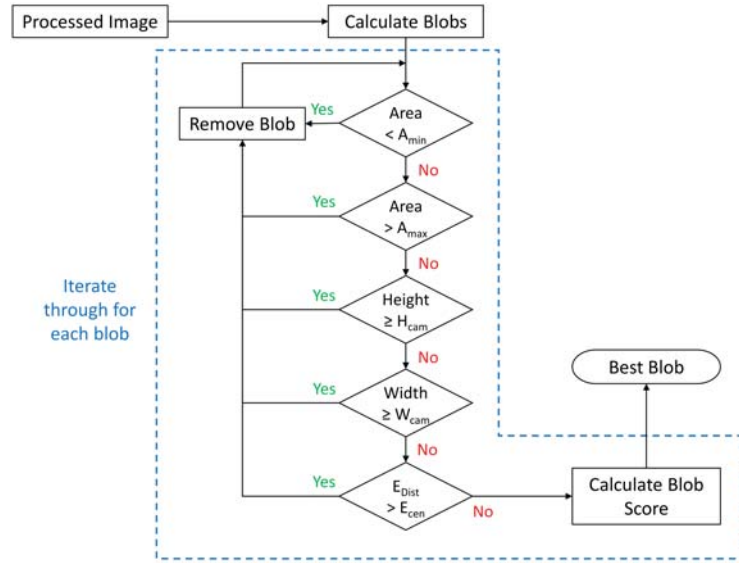


Figure 4.5: Flow diagram of the blob filtering process to find the object of interest. Blobs are removed if they fall outside the threshold boundaries of various properties.  $A_{min}$  and  $A_{max}$  represents the minimum and maximum blob area cutoff respectively.  $H_{cam}$  and  $W_{cam}$  represent the height and width of the camera resolution, and  $E_{Dist}$  and  $E_{cen}$  denote the euclidean distance from the blob's centre of gravity from the center of the camera, and the cutoff threshold respectively.

tilting and turning the head towards the object of interest. Blobs with a centre of gravity too far away from the centre of the image are considered not within the subject's visual interest, and are therefore removed. Blobs that pass through the second stage of filtering are then given a score according to equation 4.10, where  $A$  is the blob's area, and  $E_{Dist}$  is the euclidean distance from the blob's centre of gravity from the centre of the image.

$$B_{Score} = \frac{A}{E_{Dist}} \quad (4.10)$$

#### 4.2.2.iii Object Properties

After the best blob has been found through the blob filtering step, additional properties are calculated to be used as features. Prior to calculating the features, the blob undergoes a pre-processing step which involves calculating and drawing the convex hull on top of the blob, given by equation 4.11, and then filling in the holes to form a filled shape, as shown

in figure 4.6.

$$\text{Conv}(S) = \left\{ \sum_{i=1}^{|S|} \alpha_i x_i \mid (\forall i : \alpha_i \geq 0) \wedge \sum_{i=1}^{|S|} \alpha_i = 1 \right\} \quad (4.11)$$

These features will be used to create a template for each object, using 20 images of the object from different viewpoints. Real-time object recognition will calculate the features from the taken image against those in the template using a KNN classifier. A total of six different property features are used, taken from the convex hull.

**Perimeter**                      The number of pixels around the edge of the blob.

**Area**                              The number of pixels within the entire blob.

**Major-Minor Ratio**      The ratio of the blob's major axis to its minor axis (Eq. 4.12).

**Eccentricity**                      A parameter denoting how non-circular the blob is (Eq. 4.13).

**Area-Axis Ratio**              Ratio of the blob's area to the bounding box (Eq. 4.14).

**Area-Ellipse Ratio**          Ratio of the blob's area to the bounding ellipse (Eq. 4.15).

$$\text{Major-Minor Ratio} = \frac{\text{Major Axis}}{\text{Minor Axis}} \quad (4.12)$$

$$\text{Eccentricity} = 2 \sqrt{\frac{\left(\frac{\text{Major Axis}}{2}\right)^2 - \left(\frac{\text{Minor Axis}}{2}\right)^2}{\text{Major Axis}}} \quad (4.13)$$

$$\text{Area-Axis Ratio} = \frac{\text{Area}}{\text{Major Axis} \times \text{Minor Axis}} \quad (4.14)$$

$$\text{Area-Ellipse Ratio} = \frac{\text{Area}}{\pi \left(\frac{\text{Major Axis}}{2}\right) \left(\frac{\text{Minor Axis}}{2}\right)} \quad (4.15)$$

### 4.3 MMG and Computer Vision for Hand Prosthesis Control

MMG sensing and computer vision were fused together to form the initial stage of the complete sensor suit. The preliminary work conducted resulted in improvements to overall conceptual design of the control system architecture, as well as the sensor locale from an



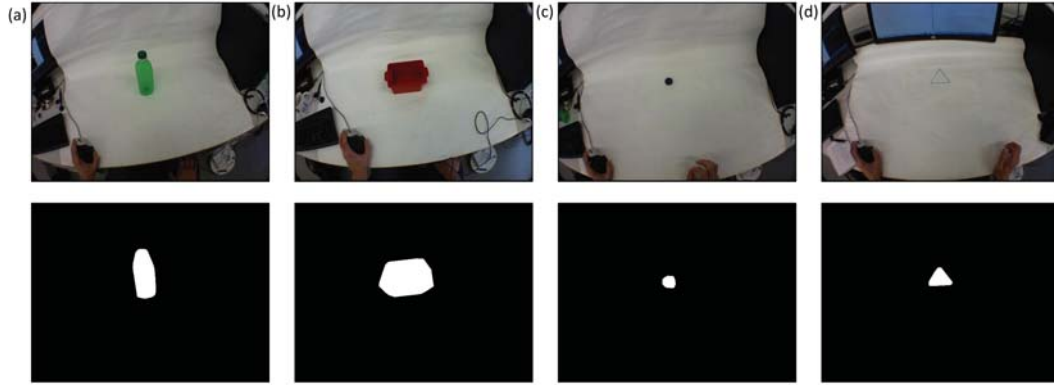


Figure 4.6: Complete blob processing for (a) bottle, (b) lid, (c) box and (d) timer objects, with original image displayed on top, and processed image on bottom.

eye-in-hand approach to an eye-to-hand approach. This section aims to present this peer-reviewed research as a preliminary stage towards the construction of the complete system.

The work presented introduces an inexpensive prosthetic hand control system designed to reduce the cognitive burden on amputees. It is designed around a real-time eye-in-hand object recognition system using a web camera that automates grasp selection and switching, and a mechanomyography (MMG) sensor for hand opening and closing. The vision system estimates object parameters in real-time which are then used to select from 2 different pre-set grasp patterns: Power and Pinch. A simple pick and place experiment was used to assess feasibility on which to base the complete system design. This work was peer-reviewed and published in [168].

#### 4.3.1 Control System Architecture

The preliminary sensor fusion system is split into 4 subsystems: 1) a pair of MMG sensors, 2) the computer vision system, which estimates object parameters, translating them into a suitable grasp pattern using a set of rules, 3) a serial communication interface to translate processed sensor outputs into usable signals for the Bebionic V2 hand; and 4) the Bebionic V2 hand controller that contains the pre-programmed grasp patterns. Data from the MMG sensors and the web camera are processed simultaneously in real-time. The computer vision system processes an image taken from the web camera, filtering out any redundant blobs and classifying the grasp based on the object's size, while the MMG sensor pair are used

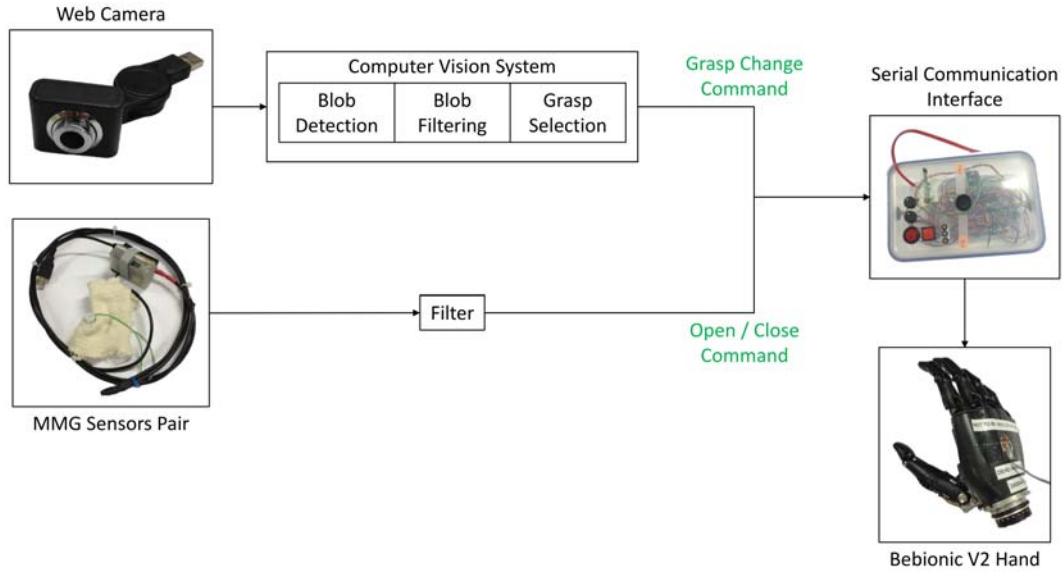


Figure 4.7: Conceptual design of the preliminary control system architecture for MMG and computer vision sensor fusion. The control architecture is split into 4 subsystems: 1) a pair of MMG sensors, 2) the computer vision system, which estimates object parameters, translating them into a suitable grasp pattern using a set of rules, 3) a serial communication interface to translate processed sensor outputs into usable signals for the Bebionic V2 hand; and 4) the Bebionic V2 hand controller that contains the pre-programmed grasp patterns. The computer vision system processes an image taken from the web camera, filtering out any redundant blobs and classifying the grasp based on the object's size, while the MMG sensor pair are used to detect alternating muscle activation. The open and close commands sent by the MMG sensors, and grasp change commands sent from the computer vision system are passed on to the serial communication interface, which converts the sensor outputs into voltage commands to be sent to the Bebionic Hand.

to detect alternating muscle activation. The open and close commands sent by the MMG sensors, and grasp change commands sent from the computer vision system are passed on to the serial communication interface, which converts the sensor outputs into voltage commands to be sent to the Bebionic Hand. The control system architecture is shown in figure 4.7.

#### 4.3.1.i MMG Sensor Pair

The system used a pair of microphone-based MMG sensors developed by R. Woodward *et al.* [16] to detect muscle activity in the forearm. The pair of sensors were sewn into a tubular bandage and positioned on the flexor and extensor digitorum, which flex and extend the fingers of the hand, as shown in figure 4.8. The sensors are connected to an inertial



Figure 4.8: MMG sensor pair positioned on the flexor and extensor digitorum of the non-grasping arm using a tubular bandage.

measurement unit acting as a signal filter and amplifier, and a small external sound card that transmits data directly to the laptop. The raw signal was filtered between 2Hz and 50Hz with a 2nd order band-pass Butterworth filter.

#### 4.3.1.ii Computer Vision System

A 640x480 miniature web camera (Logicam USB Webcam) with a focal length of 4.8 mm is fixed to the hand, overlooking the palm. When the webcam is running, images are taken as soon as the processing on the previous image has finished. A 2-dimensional low-pass 15x15 Gaussian filter is convolved with the kernel given by equation 4.16, which is used to smooth the image and for edge detection. The horizontal and vertical components are separated before convolution. The results are convolved with the image and recombined to form a new image with the edges highlighted, given by equation 4.17, where  $I_m$  is the resulting image,  $G$  the Gaussian filter,  $\sigma = 5$  the standard deviation and  $I$  the original image. Thresholding of  $I_m > 5.8$  is used to reduce unwanted noise in the image.

$$K = \begin{pmatrix} -1 & 0 & 1 \end{pmatrix} \quad (4.16)$$

$$I_m = \sqrt{(G(\sigma) \otimes K \otimes I)^2 + (G(\sigma) \otimes K^T \otimes I)^2} \quad (4.17)$$

Connected regions are selected and defined as blobs, which undergo a selection process in

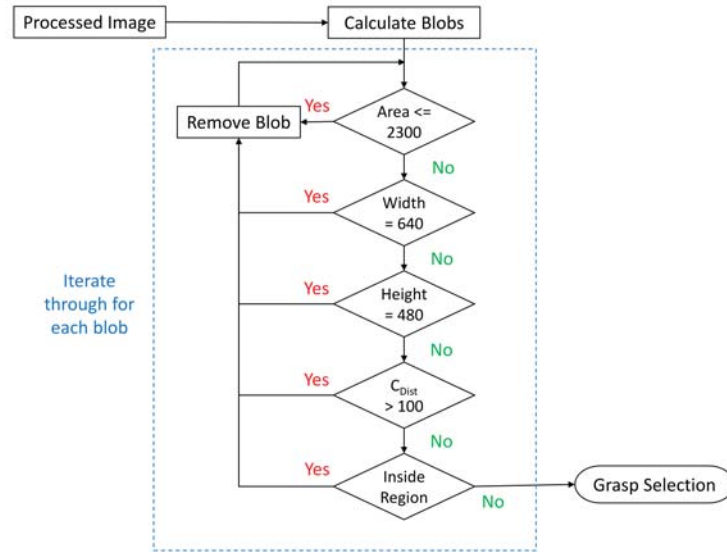


Figure 4.9: Flow diagram of the preliminary computer vision system used to select grasp patterns.

order to obtain a single blob (see figure 4.9). Firstly, all small regions are removed with an area of less than 2300 pixels. Many small regions tend to form in the image from patterns, shadows and noise. Noise in this case can be described as objects or parts of the background environment that are undesirable. Each frame taken by the camera produces an image with a border around its edges. This is removed along with any other objects that spill across the borders, as they can form a single blob. This is an image artefact from the type of web camera used during this preliminary study. A higher quality camera is used in the complete system. In working environments, there can be a lot of noise from distant objects and background scenery. To minimise this, only objects with a centre,  $C_{Dist}$ , within a distance of 100 pixels vertically and horizontally from the camera's centre will be processed further. Lastly, in order to take into account that many objects have patterns and labels, enveloped regions are removed. If no blobs meet the necessary requirements, then no grasp selection will occur.

### 4.3.2 Grasp Selection

Due to the mechanical limitations of the Bebionic hand, and also just being a validation study, only grasps with the thumb opposed were used to prevent the need to manually switch

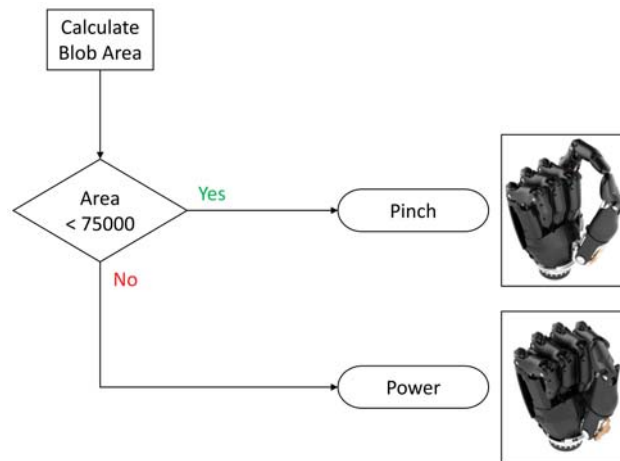


Figure 4.10: The Grasp Selection Decision Tree. If the blob's area is greater than a threshold of 75000 pixels, a *Power* grasp is selected. If the area is below the threshold, then a *Pinch* grasp is selected.

the thumb to select a different set of grasp patterns. Two patterns were chosen for 2 different sizes of objects: 1) *power* for large objects; and 2) *pinch* for small objects.

A rule-based algorithm was used to select between the two patterns depending on the intrinsic properties of the identified blob. Fig. 4.10 shows a decision tree used to determine the most suitable grasp pattern for the object's size. The blob is enclosed in an ellipse whose approximate area is compared to estimated pixel values based on the approximate distance between the web camera and the point of grasp. This distance was approximated using the difference in grasping location when grasping an object using *power* and *pinch*. When a large object is grasped, the object is enclosed around the palm, whereas a small object is picked up using the finger and thumb tips. Therefore, smaller objects will be positioned further away than larger objects when grasping occurs.

## 4.4 Experimental Testing

The aim of the experiment was test the accuracy and usefulness of the vision system as a method of improving control and reducing the cognitive burden of existing prosthetic hands. A simple pick-and-place experiment was conducted to evaluate the system before further development.

Six objects were selected in the initial experiment described here: three for each grasp.



Figure 4.11: The preliminary eye-in-hand prosthesis testing two objects: a squash ball for a *pinch* grasp and a deodorant bottle for a *power* grasp.

Two objects were assessed at a time. The objects were placed on an uncluttered table with a white background (see figure 4.11). The MMG sensors were placed on the non-grasping arm to control the open and close function of the myoelectric hand. The non-grasping arm was used to ease the control of the myoelectric hand when activating opposing muscle groups in the forearm. The myoelectric hand was held in the right hand by its sides to prevent interfering with the grasping of objects. The hand was positioned at the edge of the table, and was returned after every grasp task. The grasp task consisted of picking up the object, lifting it, and placing it back down on the table. The objects were alternated to activate the automated grasp switching function. Prior to proceeding with the experiment, the MMG sensors were calibrated to the subject. The choice of grasp pattern was validated for each object to determine the accuracy and repeatability of the system. 450 validations were made, 75 per object.

Fig. 4.12 shows the experiment on grasping a bottle of deodorant, and the object recognition output at each image processing stage during grasp. While grasping, the camera is able to process 3 images by the time the object is in grasping range, with the first image taken at (1) in the starting position, the second at the midpoint between the object, and the third at the point of grasp. At stage 1), the object is too far away to be classified, as the

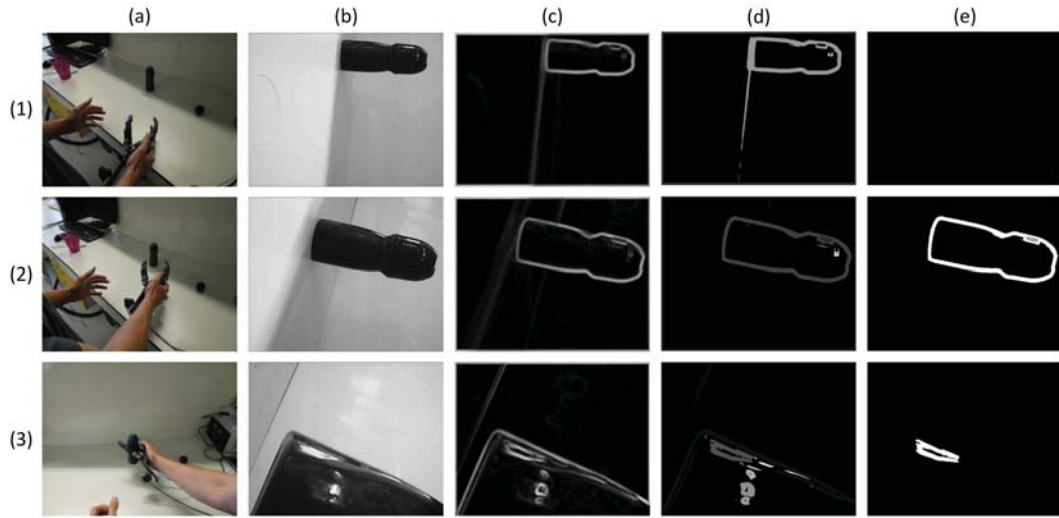


Figure 4.12: A series of images taken during the experiment from rows 1) to 3), where a) shows an observer's perspective at the different time intervals. The resulting computer vision output of b) raw grayscaling, c) convolution, d) noise removal and blob labelling, and e) binary thresholding and blob filtering.

object's location is not within the  $C_{Dist}$  range. During stage 2), the hand is at the ideal distance for object recognition to occur with this eye-in-hand setup. By stage 3, the subject would have closed the hand around the object. Once the hand is closed, any additional grasp selection is prevented. Column a) shows the grasp from a different point of view, whereas the remaining columns display the output of the computer vision system at different stages in the algorithm. Column b) shows the raw image taken after grayscaling, c) after convolution, d) after noise removal and blob labelling, and e) the final resulting image after binary thresholding and blob filtering.

## 4.5 Results

The success rates of various objects are shown in Fig. 4.13. The system showed similar results as S. Došen *et al* [13, 158] with an average success rate of 84.4%. The small objects had a higher success rate than that of the large ones, with a percentage difference of 13.3%. The pink glass, classified as a large object, had a much higher success rate than the other large objects, with a success rate of 93.3%. This is due to the simple shape and colour of the glass, making it easier to detect. The poorest performing object was the paint pot, which

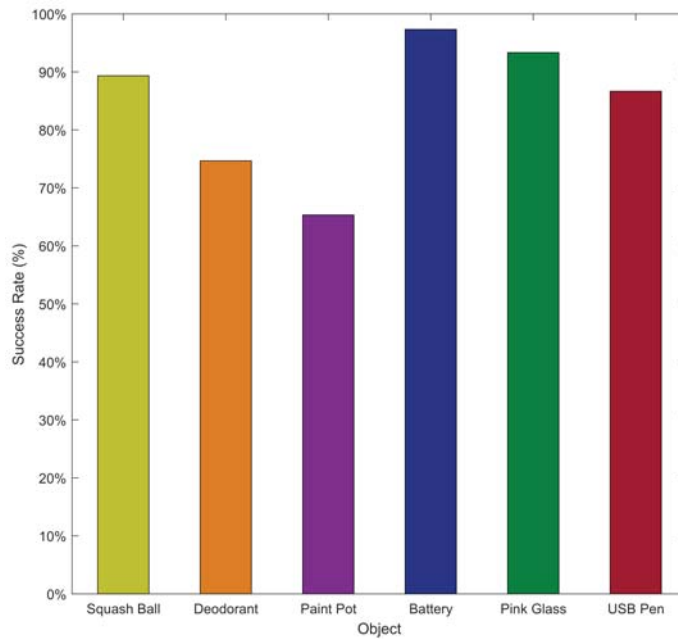


Figure 4.13: Classification success rate for the grasping task on pairs of small and large handheld objects. The objects were paired as follows: squash ball and deodorant, paint pot and battery, and pink glass and USB pen.

had a success rate of 60.33%, as the system found it more difficult to distinguish it from its background due to poor contrast as well as capturing the entire object in the image due to its size.

The results suggest that it is easier to detect smaller objects compared to large ones. This is due to the camera being unable to encapsulate larger objects at close range. The closer the object is to the camera, the larger the object appears. If the object is already large relative to the field of view of lens, then the camera will find it considerably harder to detect the object as it moves closer towards it, and instead pick up smaller artefacts on the object itself, wrongly classifying it as a small object. It was noticed that the success rate increased after a number of trials, suggesting that some degree of learning is involved. This may be due to the subject improving hand position and consistency over time, however the determination of the subject's learning capability is out of the scope of this study.



---

## 4.6 Discussion

The experiment shows that similar accuracy results can be obtained using a commercially available prosthetic hand to that of an experimental myoelectric hand. Despite our system appearing simpler than the one developed by S. Došen *et al.* (only switches between two different grasps), it can easily be further developed to include a whole range of different grasp patterns for a variety of different functions. This adaptability allows continuous system development through the classification of additional grasp patterns for specialized control in more complex object manipulation tasks. The relatively high success rates do show potential, however there are a number of disadvantages to this system.

Removing undesirable blobs using a simple rule-based algorithm and image thresholding worked well in a controlled testing environment, however transitioning this to real-world situations will produce problems. The number of blobs would increase dramatically, making depth measurement essential. Colour differences in objects and changes in lighting can greatly reduce the effectiveness of image thresholding algorithms. A more robust object recognition system is required for improved edge detection and object recognition. Taking into account a greater number of object features enables more effective classification of a greater number of object classes. With a greater number of classes and input features, a simple rule-based algorithm will not be sufficient. This resulted in improvements to the object recognition algorithm as described in section 4.2.

A disadvantage to the eye-in-hand approach was containing the object within the centre of the image, as well as fitting larger objects within the camera's field of view. This is difficult with an eye-in-hand approach, as the operator would have no concept of where the object is in relation to the camera unless looking at a screen with its output. The proximity of the object to the camera changes considerably during reach, and can result in misclassified grasps due to occlusion of the object when reaching towards it. This has resulted in the change from an eye-in-hand approach to an eye-to-hand approach in the complete system. This change increases the field of view considerably, and keeps the object's size and orientation relative to a set camera position. The object recognition algorithm relies on the

---

positioning of the object relative to the centre of the camera, which is relative to the position and angle it is on the hand. This produces an unnatural reaching trajectory in order to detect the object properly before grasping. The change to an eye-to-hand approach also solves this problem.

Determining an accurate estimation of the size of the object requires knowing the distance between the object and the camera. S. Došen *et al.* [169, 170] solved this by using an ultrasound sensor. Another method would be to use a miniature stereo camera module, which would also obtain a wider view of the target area, making it easier to classify large objects. Ultra-wide lenses can also be fitted to improve the field of view. RGB-D cameras have gained a lot of attention recently, however their current size makes them unsuitable for practical use in a portable application. Due to the simplicity of the monocular approach, the experiment was used to evaluate the application of vision in current prosthetic devices rather than comparing the results directly. Although no hardware-based actions were made to improve this area directly, the additional features described in section 4.2.2.iii make use of size ratios to improve the comparison of object properties. The use of size ratios also reduces the effect on their magnitude due to changes in distance between the user and the object.

In this preliminary study, only two grasps were used, however, the more advanced myoelectric hands, such as the I-Limb Quantum, can have up to 36 grasp patterns. More accurate object information, such as size and shape, obtainable through depth estimation using RGB-D cameras and advanced geometrical modelling, may be required in order to classify between the different grasp patterns using only computer vision. However, most real-world objects can be interacted with in a number of different ways, so a method of predicting the interaction between the amputee and the object is needed in order to determine the correct grasp pattern to use. As one of the main aims in this study is to restore natural and normal hand function to the amputee, ideally, the subject should be able to retain a natural reaching trajectory with the system being able to classify the intentional grasp correctly. Grasp prediction using inertial motion during reach was developed to classify different grasp patterns for a single object, enabling a greater variety of object interactions.

---

## 4.7 Chapter Summary

This chapter mainly focuses on just the MMG and computer vision aspects of the system. The MMG sensor design used was recreated from work conducted by R. Woodward *et al.* [16]. The details of the design and development process have been described to provide information about the type of sensor used. The MMG signal processing and threshold strategy were designed to emulate that of conventional discrete EMG prosthesis control. The computer vision system and the object recognition algorithm was discussed, taking mobility and processing constraints into consideration. Although the object recognition algorithm used is quite simplistic compared with the state of the art, this can easily be improved upon, given time and resources.

Preliminary work involving the integration of both MMG sensors and an eye-in-hand computer vision system was described, highlighting the potential of automated grasp selection using real-time vision. The preliminary control architecture described was adapted into the one used for the complete sensor suite. The work conducted allowed a number of changes to be made to the control strategy, in order to improve upon some of the issues found. This work was peer reviewed and published in [168].



## Chapter 5

# Decoding Physiological Activity

In order to predict user intention during reach when grasping different objects for various purposes, areas of intentional physiological activity need to be extracted from a continuous stream of random and non-interactive motion. Previous efforts in literature focus on predicting the grasp using mostly computer vision, however, this method does not infer the actual intention of the person for grasping the object. As part of the sensor suite, intention extraction is initialised through intentional muscle activation using an MMG sensor. Physiological data is streamed continuously from both IMU sensors, but the data is only recorded when the user activates the forearm muscles to initiate reach-to-grasp motion. It takes approximately between two and 3 seconds to reach towards an object of interest, depending on the type of grasp used, and the distance reached. By recording this window, data can be either saved for offline processing or used for real-time applications. This is possible due to the extraction process being user-initiated. This tells the system that the user already intends to grasp, enabling it to focus on predicting which grasp is desired, rather than filtering through unintentional arm movements. From the recorded data, areas of intentional activity need to be identified, thus requiring signal segmentation to find the start and end points of intentional reach-to-grasp motion. Once the segmented signal has been identified, useful features can be calculated.

The main challenge of assistive HMI applications is determining the user intention from sensory inputs. This intention is expressed through a selection of predefined actions.

---

For the application in hand prosthesis, these actions can be translated to different grasp patterns that have been designed for a variety of postures and environmental interactions. Once the intentional reach-to-grasp motion has been extracted, the decoding phase can begin. This focuses on applying pattern recognition techniques for feature extraction, selection and classification. Utilising the segmented data and applying the graphs of motion enable a selection of features to be extracted. The selected features are required to undergo dimensional reduction to identify the most useful features. These are then evaluated with a selection of pattern recognition methods for comparison in order to provide a strong classifier for predicting grasp intention. The culmination of this chapter is the implementation of a KNN classifier based on subject- and object-specific motion features from the analysis of displacement- velocity- and acceleration-time profiles. The classifier is used in the creation of subject-specific templates that are representative of the different grasps used to interact with different objects.

## **5.1 Data Collection**

Grasping an object can produce numerous reaching paths, that could potentially vary in forearm and upper arm orientation, velocity and acceleration. This provides a challenging problem which may not only depend on different anatomical features, but may also be heavily dependent on an individuals' neural control. To study this assumption, a unique data set is collected for each subject. The object's location in the subject's immediate workspace will provide a large variety of reaching paths for comparison. Thus, in order to see how object location affects reach trajectory, physiological data needs to be recorded in variable elevation/declination, angular and depth positions from the subject.

Inclusion criteria for participating in the experiments were that volunteers must be above 18 years of age, where healthy volunteers should have no motor or physical impairments, and amputee volunteers have a transradial amputation on their right arm (required to use a right-handed prosthesis). All experiments were approved by the Imperial College Research Ethics Committee (ICREC reference: 15IC3068), with participants giving their informed consent before taking part in the study.

Subject ID	Type	Sex	Age /yr	Height /m	Arm-span /m	Hand-span /m
A	Healthy	M	27	1.78	1.76	0.225
B	Healthy	M	33	1.69	1.70	0.219
C	Healthy	M	37	1.75	1.76	0.22
D	Healthy	M	23	1.85	1.89	0.245
E	Healthy	M	25	1.91	1.93	0.205
F	Healthy	M	29	1.75	1.73	0.225
G	Healthy	M	27	1.83	1.87	0.217
H	Healthy	F	24	1.72	1.73	0.204
I	Healthy	M	26	1.75	1.77	0.225
J	Healthy	M	22	1.74	1.72	0.18
K	Amputee	M	36	-	-	-

Table 5.1: Participant information for physiological data collection experiment consisting of 10 healthy subjects, and 1 amputee subject. It must be noted that the majority of subjects have an engineering background.

### 5.1.1 Participants

In total, 10 healthy subjects (9 males, and 1 female) participated in the collection of physiological data. Healthy subjects took part in two experiments, which took part on different days. The first experiment consisted of the collection of grasp data from all angular and elevation levels at a depth of 30 cm, and the second experiment at a depth of 20 cm away from the *rest* position. Before the experimental procedure commences, participant age, sex, height, arm-span and hand-span are recorded, and are summarised in table 5.1. All participants had a dominant right arm.

Only a single, male amputee subject participated in this research due to the difficulty of obtaining multiple amputee volunteers that matched the inclusion criteria. The subject is a quadruple amputee (lower limb: double transfemoral; upper limb: left-transhumeral and right-transradial), from the result of contracting Strep A, which manifested into Toxic Shock Syndrome, Septicaemia and Necrotising Fasciitis [171]. The experimental procedure for healthy subjects was modified for collecting physiological data with a hand prosthesis. The myoelectric hand was attached to his right forearm prosthesis (transradial) using a custom 3D printed adapter shown in figure 5.1. The details of the adapter design can be found in Chapter 3.



Figure 5.1: The amputee participant’s forearm prosthesis connected to the Bebionic Hand using a custom 3-D printed adapter. The forearm prosthesis was designed for use with a mechanical hook, however the adapter enabled its use with the myoelectric hand.

### 5.1.2 Software Test Environment

Data collection software was developed to record motion data during the trials, given in figure 5.2. The experiment information located at the bottom left of the interface details the object selected and the grasps being tested, as well as the elevation, depth and angular position represented by a number between 1-3. The elevation level is described by the ‘Experiment’ label, where the 3 elevation levels denoted by digits 1-3 represent grasp elevation at *table height*, *ascending* and *descending* respectively. The ‘Depth’ label represents the object’s distance between the *rest* position and the object, denoted by digits 1-2 for a distance of 30 cm and 20 cm respectively. The ‘Position’ label describes the angular position from the centre of the *rest* position, denoted by digits 1-3 for  $-45^\circ$ ,  $0^\circ$  and then to  $+45^\circ$  respectively. A randomisation option is also available to choose whether the grasp trials are randomised for healthy subjects, or kept consecutive for amputee subjects. These options are selected when initiating the experiment using the dialogue interface given in figure 5.3.

The software interface is used to visually prompt the participant to reach towards the object and return to the *rest* position. Data is recorded and saved to a database after each trial has been completed. Since the IMU data is sent via BT, after each trial, the size of the data is checked for packet loss. If the level of loss is too high, i.e. the input data rate is less than 80% of the sampling rate, then the trial is repeated. If this occurs consecutively for 5



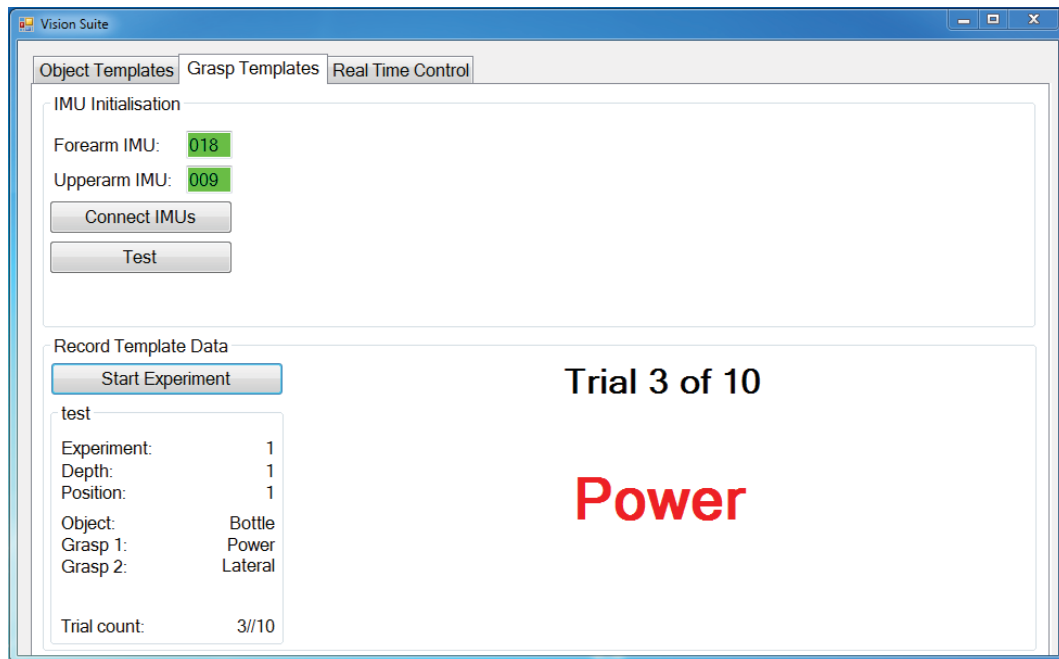


Figure 5.2: The software interface developed to collect grasp trajectory data from subjects. The software consisted of separate tabs for object template collection, grasp data collection and real-time control.

times, then the IMUs are reset. If excessive data loss still occurs after the reset, then a low battery event is diagnosed, and the IMU batteries are recharged.

### 5.1.3 Experimental Protocol

Experiments are conducted using a pair of non-invasive wearable IMU sensors fitted to a compression sleeve. The sensors are positioned on the forearm and upper arm to measure

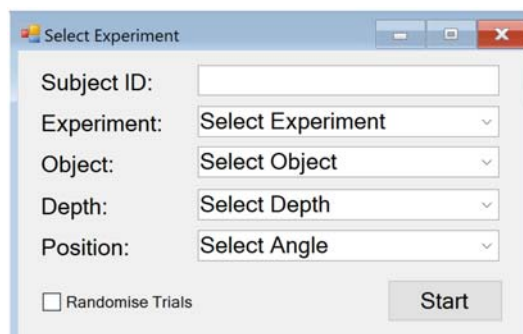


Figure 5.3: The settings dialogue box allowed individual experiment selection and grasp randomisation after initialising the grasp experiment.



Figure 5.4: The sensor sleeve used for collecting physiological data fitted on a healthy subject. The attached MMG sensor is not used during this study.

complete upper limb movement as in figure 5.4. Prior to experimentation, participants are required to give their informed consent, and have the opportunity to read through the participant information sheet, the details of which are explained before donning the sensor sleeve.

The collection of physiological data involves reaching to grasp different objects with a variety of grasp patterns. For the purpose of further experimental validation, a timed task-based experiment with the complete sensor suite using a prosthetic hand is described in Chapter 6. Three objects were chosen to carry out selected predefined grasps. The chosen grasps mimic those available to the prosthetic hand. The bottle is designated two grasp patterns: A *power* grasp for holding the bottle for drinking and transporting, and a *lateral* grasp for unscrewing the lid. The lid itself also has two grasp patterns: a *lateral* grasp for screwing on the lid, and a *precision open* for transporting. The final object is a container, which has been assigned three different grasps: A *power* grasp for grabbing the front of an empty container for transportation, a *lateral* grasp for transportation of a filled container by its side, and a *precision open* grasp for picking up small objects within the container. See 5.5 for the objects and grasp patterns used.

The subject is sat down, with their dominant hand (fitted with the sensor sleeve) located

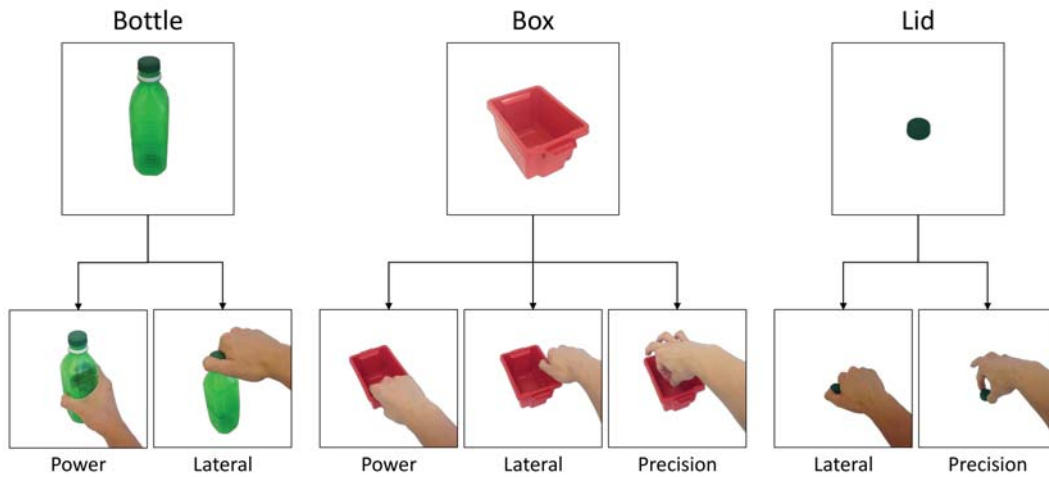


Figure 5.5: A tree diagram depicting the different grasps used for each object. The bottle was grasped with *power* and *lateral* grasps, the box with *power*, *lateral* and *precision* grasps, and the lid with *lateral* and *precision* grasps.

at the *rest* position, where the hand is placed along its bottom edge, with the centre of the palm approximately 10 cm from the edge of the table, as shown in figure 5.6 (a). The subject's chair is adjusted so that the elbow is approximately  $90^\circ$  when sitting up straight. When standing, the arm is pointed downwards by the subject's side, approximately in line with the centre of the *rest* position, shown in figure 5.6 (b). In the case of amputee subjects, the experimental procedure would differ depending on the subject's circumstances. The single amputee subject tested was a quadruple amputee, who was seated in his own wheel chair. The upper arm sensor sleeve was fitted further up the arm so that the residual limb had space to fit into the forearm prosthesis socket. The forearm prosthesis was fitted to the Bebionic V2 hand using the adapter, and the forearm sensor sleeve fitted over it with the metal support removed from the wrist splint.

Each object is tested consecutively at 9 possible position variations. Data recordings are made with the object's angular position at  $-45^\circ$ ,  $0^\circ$  and  $+45^\circ$ , and depth of 20 cm and 30 cm from the *rest* position (see figure 5.7), where the elevation is:

- at *table height* with the subject seated
- *ascending*, where the object is raised by 15cm with the subject seated
- *descending*, where the object is on the table with the subject standing.

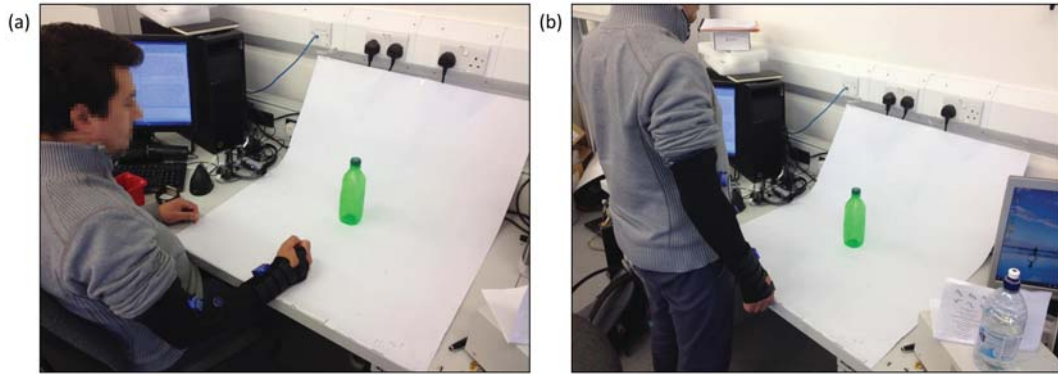


Figure 5.6: The *rest* position while (a) sitting has the subject's dominant hand placed along its bottom edge, with the centre of the palm approximately 10 cm from the edge of the table, and (b) standing has subject's dominant arm pointed downwards by their side, approximately in line with the centre of the seated *rest* position.

The amputee subject only took part in the data collection for objects with elevation at *table height* and *ascending*. The different grasp patterns are explained before each object is tested, and the subject is asked to make the grasp a few times to commit it to memory. For the amputee subject, the prosthetic hand's grasp pattern was manually changed to match the grasps for that object, and the grasp was closed and opened several times for the subject to

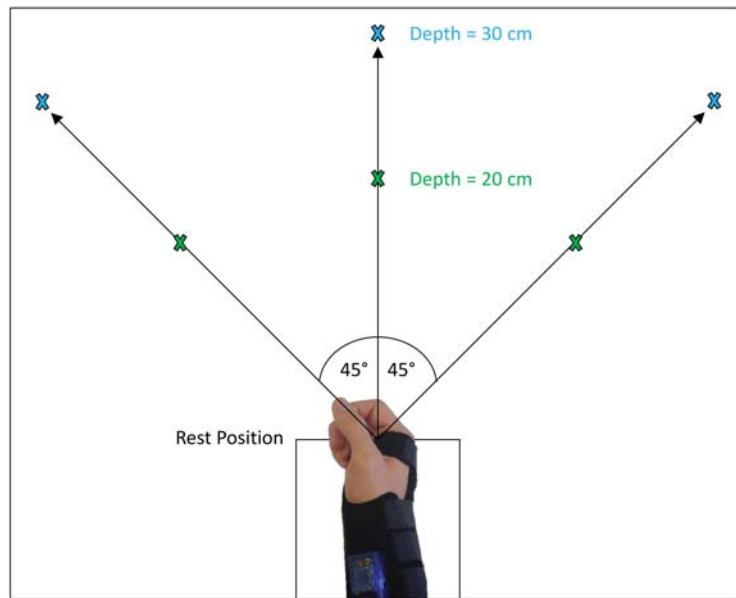


Figure 5.7: Object locations during data collection showing locations at  $-45^\circ$ ,  $0^\circ$  and  $45^\circ$  with depths of 20 cm and 30 cm. These object locations are also used at three elevation levels: *ascending*, *descending* and *table height*. Each object is tested consecutively at these 9 possible position variations.

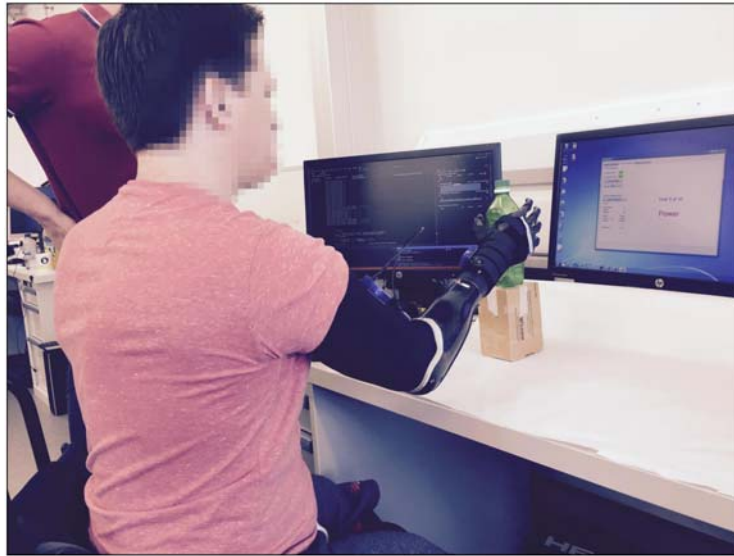


Figure 5.8: The amputee subject carrying out a *power* grasp on a bottle at an *ascending* elevation in the study.

find the most comfortable grasping point on the object. During experimentation, the amputee subject was not required to grasp the object with the prosthesis during the trials, but just to move and orientate it to the grasp point location previously found during practice, in order to reduce fatigue. The amputee had no prior experience using a myoelectric hand prosthesis. Figure 5.8 shows the amputee subject grasping a bottle with a *power* grasp at an *ascending* elevation. At each object location, 5 trials are made for each grasp pattern for that object. The grasp order is randomised for healthy subjects, and displayed on the software interface to prompt the subject to make the grasp. The order is not randomised

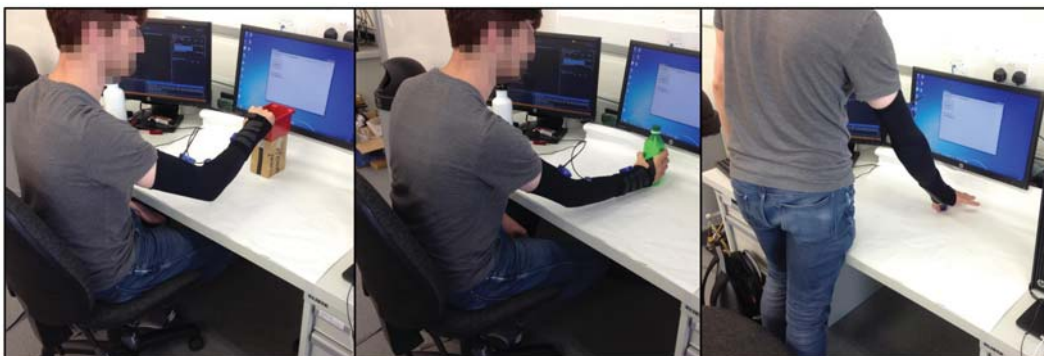


Figure 5.9: Left to right: Grasps being made with an elevation at ascent, table height and descent by a healthy subject.

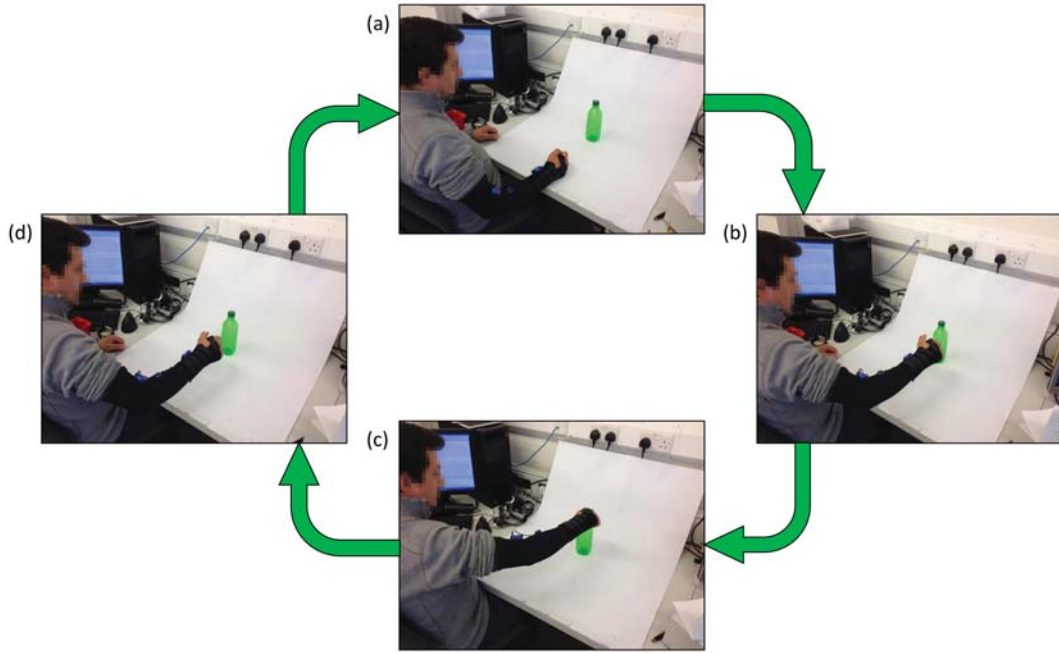


Figure 5.10: Steps taken when carrying out a single experimental trial, where the subject (a) starts in the *rest* position, (b) reaches towards the object when prompted, (c) grasps the object in the designated grasp pattern, (d) returns the hand to the *rest* position.

for the amputee subject, as a grasp switch may require manually changing the thumb opposition. When prompted by the software, the subject is given 3 seconds to reach his or her hand from the *rest* position to the object and make the grasp, without lifting it. The subject keeps his or her hand in the grasp position for the remainder of the 3 second interval until prompted to return back to the *rest* position. The subject has 2.5 seconds to return to the *rest* position, during which the data is pre-processed and saved to a database. This is repeated until all grasps have been made at that object location, moving from  $-45^\circ$ ,  $0^\circ$  and then to  $+45^\circ$ . The same procedure is conducted at each of the 3 elevation levels as shown in 5.9. The time taken for the experiment across all object locations at a single depth level takes approximately one hour. Healthy subjects returned to complete the same experiment at the second depth on a different day. The amputee subject completed all object locations at both depth levels (with the exception of those at *descent*) in a single session. Figure 5.10 shows each stage of a single grasp trial taken by a healthy subject, where the subject (a) starts in the *rest* position, (b) reaches towards the object when prompted, (c) grasps the object in the designated grasp pattern, (d) returns the hand to the *rest* position.



---

## 5.2 Measuring Motion

During experimentation, data is recorded using a pair of IMU devices developed in the Biomechatronics Lab. An inertial measurement unit (IMU) is a multi-sensor device that is capable of measuring changes in linear and angular acceleration and rotation using accelerometers, gyroscopes and magnetometers. The IMU used an LSM9DS0 module, which contains a 3-axis accelerometer, 3-axis gyroscope and 3-axis magnetometer, set at a scale of  $\pm 2$  g,  $\pm 500^\circ/\text{s}$  and  $\pm 2$  gauss respectively. Combining the sensors for optimal orientation estimation is essential in order to make corrections due to gravity and magnetic north, as well as to reduce drift.

**Accelerometer** Responsible for measuring linear acceleration and gravity, and can normally be represented as a damped mass on a string. In commercial devices however, they are most commonly built using a cantilever beam and a proof mass using Micro Electro-Mechanical Systems (MEMS) technology.

**Gyroscope** Measures its own angular velocity using the Coriolis Effect. Using MEMS technology, this is recorded using a high frequency oscillating mass with capacitive sense coms to pick up the signal.

**Magnetometer** Measures the magnetic field of its surroundings. A 3-axis magnetometer combined with an accelerometer is required to measure heading no matter which direction the device is facing. The magnetic field is usually measured from the deflection of current in a wire due to the Hall Effect.

### 5.2.1 Background: Describing Orientation

The orientation of a frame relative to a reference frame can be described using numerous methods; the most common being Rotation Matrices, Euler Angles and Quaternions.

#### 5.2.1.i Rotation Matrices

A rotation matrix is a matrix that will rotate a vector when multiplied, without altering its length. When considering two frames, A and B, which differ only by a rotation, we can

---

describe the rotation matrix  ${}^B\mathbf{R}_A$  as the transformation of A with respect to B, as shown in equation 5.1, where  ${}^B\mathbf{P}$  and  ${}^A\mathbf{P}$  are the coordinates of a point  $P$  relative to frames B and A respectively.

$${}^B\mathbf{P} = {}^B\mathbf{R}_A {}^A\mathbf{P} \quad (5.1)$$

Each rotation matrix makes a clockwise rotation in the direction of the designated X, Y or Z axis, given in equations 5.2, 5.3 and 5.4 respectively.

$$\text{ROT}(X, \theta) = \begin{bmatrix} 1 & 0 & 0 \\ 0 & \cos(\theta) & -\sin(\theta) \\ 0 & \sin(\theta) & \cos(\theta) \end{bmatrix} \quad (5.2)$$

$$\text{ROT}(Y, \alpha) = \begin{bmatrix} \cos(\alpha) & 0 & \sin(\alpha) \\ 0 & 1 & 0 \\ -\sin(\alpha) & 0 & \cos(\alpha) \end{bmatrix} \quad (5.3)$$

$$\text{ROT}(Z, \beta) = \begin{bmatrix} \cos(\beta) & -\sin(\beta) & 0 \\ \sin(\beta) & \cos(\beta) & 0 \\ 0 & 0 & 1 \end{bmatrix} \quad (5.4)$$

Multiple rotation matrices can be multiplied sequentially to find the complete transformation of a point in space (5.5). Transformations relative to the reference frame are pre-multiplied, and transformations relative to the current moving frame are post-multiplied.

$$\mathbf{R} = \text{ROT}(X, \theta)\text{ROT}(Y, \alpha)\text{ROT}(Z, \beta) \quad (5.5)$$

### 5.2.1.ii Euler Angles

Euler Angles refer to the three angles described by Euler's rotation theorem, whose sequential application is capable of describing the complete rotation of a frame (5.6).

$$\mathbf{R}_{123}(\phi\theta\psi) = \mathbf{R}_1(\phi)\mathbf{R}_2(\theta)\mathbf{R}_3(\psi) \quad (5.6)$$



---

The three angles are denoted  $\phi$  (roll),  $\theta$  (pitch) and  $\psi$  (yaw). In terms of rotation matrices, it is known that the resulting orientation is dependent on the sequence of the individual rotations. Most engineering applications generally use the (1,2,3) convention, which is known as an intrinsic rotation, whereby the rotations are made about the axis of the rotating frame, as opposed to an extrinsic rotation, where rotations are made about a fixed reference frame. Euler angles represented by a rotation matrix is given in equation 5.7, where  $c$  and  $s$  represent compact notation for  $\cos$  and  $\sin$  respectively. A complete catalogue of Euler Angle parameterisations can be found in [172].

$$\mathbf{R}_1(\phi)\mathbf{R}_2(\theta)\mathbf{R}_3(\psi) = \begin{bmatrix} c_\theta c_\psi & c_\theta s_\psi & -s_\theta \\ s_\phi s_\theta c_\psi - c_\phi s_\psi & s_\phi s_\theta s_\psi + c_\phi c_\psi & c_\theta s_\phi \\ c_\phi s_\theta c_\psi + s_\phi s_\psi & c_\phi s_\theta s_\psi - s_\phi c_\psi & c_\theta c_\phi \end{bmatrix} \quad (5.7)$$

The main limitation of using Euler angles to represent orientation, is that it suffers from a problem that is known as *gimbal lock*, which is the loss of one degree of freedom when two of the axes become parallel. The problem of gimbal lock makes the use of Euler angles unsuitable for certain applications.

### 5.2.1.iii Quaternions

The quaternion is a 4-tuple that can represent the rotation between two frames, originating from the equations drawn up by William Hamilton [173] given in equation 5.8.

$$i^2 = j^2 = k^2 = ijk = -1 \quad (5.8)$$

A quaternion defines an element in 4-dimensional space, with one real dimension, the scalar part  $q_0$ , and 3 imaginary dimensions, the vector part  $(q_1, q_2, q_3)$ , given in complex number notation by equation 5.9, where  $i, j$  and  $k$  represent imaginary numbers. Another common form of notation is representing the quaternion as a 4-dimensional vector, given by 5.10, where  $v = (x, y, z)$  is the vector part, and  $w$  is the scalar part.

$$q = q_0 + iq_1 + jq_2 + kq_3 \quad (5.9)$$

---


$$q = [w, v] = \begin{bmatrix} w \\ x \\ y \\ z \end{bmatrix} \quad (5.10)$$

Quaternions are known to be very difficult to visualise, however they can be represented in terms of axis-angle notation, where the quaternion can be given by equation 5.11, where  $\theta$  is the angle of rotation, and x, y and z represent axis of rotation.

$$q = \cos(\theta/2) + i(x * \sin(\theta/2)) + j(y * \sin(\theta/2)) + k(z * \sin(\theta/2)) \quad (5.11)$$

A rotation around the origin can be applied to a point, P using the quaternion conjugate  $q^{-1}$ , as in equation 5.12.

$$P_{new} = q * P * q^{-1} \quad (5.12)$$

Representing orientation through the use of quaternions may not be as computationally efficient as with Euler's angles, however has the advantage that it does not suffer from gimbal lock. This advantage has resulted in its usage across any applications involving the calculation of 3-dimensional rotation, particularly in 3-dimensional computer graphics [174, 175].

### 5.2.2 Background: Calculating Orientation

The Kalman Filter [176] is the most commonly used method that forms the basis of the majority of orientation algorithms. The Kalman filter is designed to be used as either a smoother, a filter or a predictor, and is used to remove noise, drift and other inaccuracies associated with fusing the individual sensor data in order to obtain an optimal estimation of orientation. The high accuracy and effectiveness of the Kalman filter in orientation estimation has resulted in its widespread use in many commercial products: Xsens [177], microstrain [178], VectorNav [179], and Intersense [180]. However, describing rotational kinematics in three dimensions requires large state vectors [17], usually resulting in the implementation of an Extended Kalman Filter (EKF), which aims to reduce the size of state

---

vectors and linearize non-linear state models to improve performance and accuracy. The use of the Kalman filter can provide an accurate estimation of orientation, however its high computational load can be a limiting factor. Further discussion of the usage of the EKF can be found in [181]. See [182, 183, 184, 185, 186] for implementations of an EKF for orientation estimation.

A novel gradient descent algorithm developed by S. Madgwick *et al.* [17] has achieved similar levels of accuracy to Kalman based algorithms;  $0.8^\circ$  static RMS error,  $< 1.6^\circ$  dynamic RMS error. The gradient descent algorithm is less computationally demanding, and can operate with lower sampling rates, enabling applications in low-cost, wearable IMU systems that are capable of running wirelessly over extended periods of time. S. Madgwick implemented the algorithm in the commercially available X-IMU [187].

The gradient descent algorithm estimates the orientation quaternion  ${}^S_E \hat{\mathbf{q}}$  that aligns a predefined reference direction of the magnetic field in the earth frame  ${}^E \hat{\mathbf{d}}$  with the measured field in the sensor frame  ${}^S \hat{\mathbf{s}}$ . Equation 5.13 describes the orientation for  $k$  iterations using an initial guess,  ${}^S_E \hat{\mathbf{q}}_0$ , with variable step size  $\mu$ , and equation 5.14 calculates the error direction based on the objective function  $\mathbf{f}$  and its Jacobian  $\mathbf{J}$ .

$${}^S_E \hat{\mathbf{q}}_{k+1} = {}^S_E \hat{\mathbf{q}}_k - \mu \frac{\nabla f({}^S_E \hat{\mathbf{q}}_k, {}^E \hat{\mathbf{d}}, {}^S \hat{\mathbf{s}})}{\left\| \nabla f({}^S_E \hat{\mathbf{q}}_k, {}^E \hat{\mathbf{d}}, {}^S \hat{\mathbf{s}}) \right\|}, k = 0, 1, 2 \dots n \quad (5.13)$$

$$\nabla f({}^S_E \hat{\mathbf{q}}_k, {}^E \hat{\mathbf{d}}, {}^S \hat{\mathbf{s}}) = \mathbf{J}^T({}^S_E \hat{\mathbf{q}}_k, {}^E \hat{\mathbf{d}}) \mathbf{f}({}^S_E \hat{\mathbf{q}}_k, {}^E \hat{\mathbf{d}}, {}^S \hat{\mathbf{s}}) \quad (5.14)$$

In terms of optimisation, if the convergence rate of the estimated orientation controlled by  $\mu_t$  is equal or greater than the rate of change of physical orientation, it is possible to just calculate the orientation using a single iteration of the algorithm at each time sample, given by equation 5.15. The objective function error  $\nabla \mathbf{f}$  can be calculated according to equation 5.16. To ensure this,  $\mu_t$  can be calculated by equation 5.17 where  $\Delta t$  represents the sampling period,  ${}^S_E \dot{\hat{\mathbf{q}}}_{\omega,t}$  is the rate of change of orientation described by the gyroscope, and  $\alpha$  is an augmentation of  $\mu$  to take into account sensor noise in the accelerometer and magnetometer. The subscript  $\nabla$  indicates that the quaternion has been calculated using

---

the gradient descent algorithm.

$${}^S_E \mathbf{q}_{\nabla,t} = {}^S_E \hat{\mathbf{q}}_{est,t-1} - \mu_t \frac{\nabla \mathbf{f}}{\|\nabla \mathbf{f}\|} \quad (5.15)$$

$$\nabla \mathbf{f} = \begin{cases} \mathbf{J}_g^T({}^S_E \hat{\mathbf{q}}_{est,t-1}) \mathbf{f}({}^S_E \hat{\mathbf{q}}_{est,t-1}, {}^S \hat{\mathbf{a}}_t) \\ \mathbf{J}_{g,b}^T({}^S_E \hat{\mathbf{q}}_{est,t-1}, {}^E \hat{\mathbf{b}}) \mathbf{f}_{g,b}({}^S_E \hat{\mathbf{q}}_{est,t-1}, {}^S \hat{\mathbf{a}}_t, {}^E \hat{\mathbf{b}}, {}^S \hat{\mathbf{m}}_t) \end{cases} \quad (5.16)$$

$$\mu_t = \alpha \| {}^S_E \dot{\mathbf{q}}_{\omega,t} \| \Delta t, \alpha > 1 \quad (5.17)$$

The sensor fusion algorithm described by equation 5.18 provides an estimation for orientation,  ${}^S_E \mathbf{q}_{\omega,t}$ , and is used to filter out high frequency errors and compensate for integral drift in  ${}^S_E \mathbf{q}_{\nabla,t}$  and  ${}^S_E \mathbf{q}_{\omega,t}$  respectively.  $\gamma_t$  and  $(1 - \gamma_t)$  are weights applied to each orientation calculation, and can be simplified to an approximation by equation 5.19, or assumed that  $\gamma_t \approx 0$  when optimal, where  $\beta$  represents the divergence rate of  ${}^S_E \mathbf{q}_{\omega}$ .

$${}^S_E \mathbf{q}_{est,t} = \gamma_t {}^S_E \mathbf{q}_{\nabla,t} + (1 - \gamma_t) {}^S_E \mathbf{q}_{\omega,t}, 0 \leq \gamma_t \leq 1 \quad (5.18)$$

$$\gamma_t \approx \frac{\beta \Delta t}{\mu_t} \quad (5.19)$$

Magnetic distortion due to electrical appliances and metal within furniture and building structures can be corrected by matching the measured direction of the earth's magnetic field in the earth frame at time  $t$ ,  ${}^E \hat{\mathbf{h}}_t$  (described by equation 5.20) with the algorithm's reference direction of the earth's magnetic field,  ${}^E \hat{\mathbf{b}}_t$ , given by equation 5.21.

$${}^E \hat{\mathbf{h}}_t = \begin{bmatrix} 0 & h_x & h_y & h_z \end{bmatrix} = {}^S_E \hat{\mathbf{q}}_{est,t-1} \otimes {}^S \hat{\mathbf{m}}_t \otimes {}^S_E \hat{\mathbf{q}}_{est,t-1}^* \quad (5.20)$$

$${}^E \hat{\mathbf{b}}_t = \begin{bmatrix} 0 & \sqrt{h_x^2 + h_y^2} & 0 & h_z \end{bmatrix} \quad (5.21)$$

The complete orientation estimation algorithm can be represented by the block diagram in figure 5.11. The gradient descent algorithm offers comparable accuracy to that of its

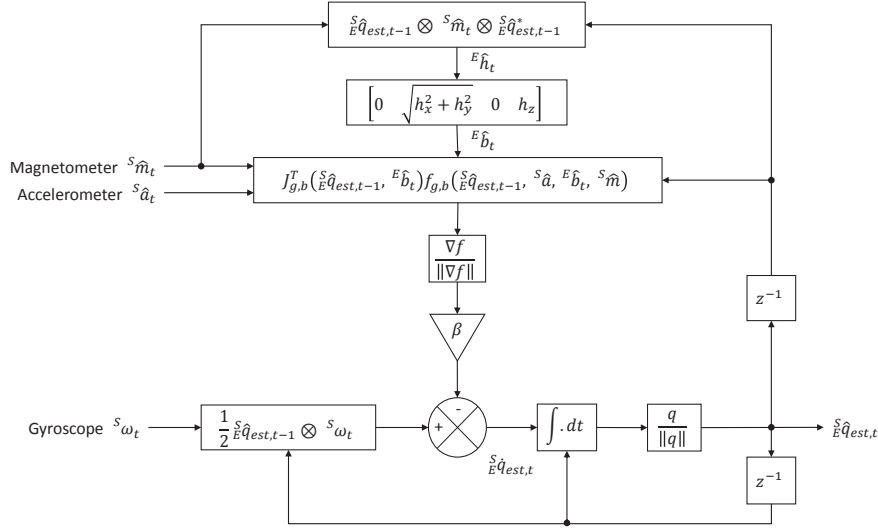


Figure 5.11: Block diagram representation of the complete orientation estimation algorithm for a magnetic angular rate and gravity (MARG) implementation including magnetic distortion compensation (reproduced from [17])

Kalman-based counter parts, while providing a significant reduction in computational load and eliminating the need for a predefined magnetic field direction, making it ideal for long term use for wearable, wireless applications [17].

### 5.2.3 Signal Processing

Using the gradient descent algorithm [17], the raw sensor data collected during each 3-second trial is converted into quaternions and saved in a database. Once all experimental data has been collected, the offline data processing phase begins. With both IMU sensors sending data at a rate of approximately 1 KHz (variable depending on the retrieval rate by BT), each 3-second trial collects just less than 3000 data points containing the X, Y and Z quaternion components for each IMU. Although a 1 KHz sampling rate may not be necessary for collecting quaternion data, a high sampling rate is useful for measuring MMG data, and the IMU firmware sent both at the same sampling rate. Newer versions of the hardware and firmware provide more flexibility regarding this, where the quaternion and analogue sampling rates can be individually adjusted to maximise the quality of data while prolonging battery life. Any major loss in data is due to unreceived data packets via BT.

---

Minor data loss is contributed to the real-time quaternion calculations taking place using the gradient descent algorithm during the trials, and is largely affected by processor speed.

Although quaternions represent the path between two points in 4 dimensional space, by considering the X, Y and Z quaternion components as an imaginary vector (the imaginary quaternion vector part) in 3-dimensional space with origin (0, 0, 0), the individual vector components can be used to represent the change in displacement of this point over time. Figure 5.12 (a) in section 5.3.1 displays the vector displacement over time of *lateral* and *power* grasps made by a single subject on a bottle at a depth of 30 cm and angle of 0° at table height while seated. The figure shows 5 trials taken per grasp during the experiment after being smoothed by a moving average filter (equation 5.22) with a span of  $N = 250$ . This helps smooth out any jittering caused by receiving and calculating quaternion data simultaneously from multiple IMUs, as well as any unintentional shaking from the subject during grasp, whilst minimising the distortion of the signal's shape. Y denotes the output signal, and X the input signal, where  $N$  is the window span.

$$Y_i = \frac{1}{N} \sum_{j=0}^{N-1} X_{i+j} \quad (5.22)$$

The high filter span smooths the vector displacement data enough to minimise the noise amplification effect when taking the derivative. By considering the X, Y and Z components as the displacement of an imaginary vector, differentiating will result in a velocity-time profile, which is then further smoothed with a second degree Savitzky-Golay filter, followed by the moving average filter given in equation 5.22, both with a span of 250, shown in 5.12 (b). The general equation for the Savitzky-Golay filter is given by equation 5.23, where Y denotes the output signal, X the input signal, where  $N$  is the window span,  $n$  is the number of data points in the signal, and  $C_j$  is a set of filter coefficients based on a polynomial of degree  $m$ .

$$Y_i = \sum_{j=-\frac{N-1}{2}}^{\frac{N-1}{2}} C_j X_{i+j} \quad (5.23)$$

The result is differentiated again to find the vector acceleration over time (5.12 (c)), which has been smoothed by the same moving average filter in equation 5.22. The time taken

---

during reach has a start and an end point, which are estimated from the processed data according to an initial and ending acceleration threshold of  $S_{acc} = 0.2 \times 10^{-6}$  (Eq. 5.24) and  $E_{acc} = 0.4 \times 10^{-6}$  (Eq. 5.25) respectively, where  $x$  is the time series of the trial data of length  $x_n$ .

$$\frac{d^2y}{dx^2} \geq S_{acc}, \quad x = 0, 1, \dots, x_n \quad (5.24)$$

$$\frac{d^2y}{dx^2} \geq E_{acc}, \quad x = x_n, x_n - 1, \dots, 0 \quad (5.25)$$

### 5.3 Feature Extraction

Feature extraction involves the analysis of existing measurable features from the processed data and generating new subspaces of features based on combinations or transformations of the original feature set [188] in order to extract the discriminatory power from the data. Useful methods exist which not only create more distinguishable features, but also help to reduce the higher dimensionality associated with it. The latent information existing within these features can be used to improve overall classifier performance. However, as the variability of the object's location within the workspace increases, so does the variation in physiological feature magnitudes.

Section 5.2.3 described the raw physiological signal output as the displacement of an imaginary vector point in the time domain, and how taking the first and second derivatives generates the associated velocity and acceleration profiles. This section intends to study the various features available within these profiles, to see how they are affected when making different grasps on different objects at different locations. This section is split by object where the individual features are qualitatively analysed in terms of (a) discrimination/separation; how well the grasps differentiate from each other, with greater discrimination being more desirable, and (b) variance/variability; how changes in object location affects the range of feature values, with lower variance being more desirable. Following qualitative observations of the data, a quantitative approach will be taken in the discussion. Before analysing the data, the features from each profile must first be defined.

---

### 5.3.0.i Displacement Features

Preliminary work detailed in Appendix A focused on using distribution features of the quaternion displacement trajectory during various grasp patterns, such as the mean, standard deviation, skewness and kurtosis. This proved to be a relatively successful approach, however, the tests were limited to the study of arm motion when grasping objects at table height, directly in line with the designated rest position. Varying the position of the object reduces the classifier accuracy considerably due to the high variability in the arms displacement, greatly reducing the separability between different grasps. Rather than looking just at distribution features of the whole displacement profile, single point features are also compared. The most desirable features are those that are invariable to changes in object location and the time taken to grasp. The displacement-time profile features that are considered are as follows:

- |               |  |
|---------------|--|
| <i>PoG</i>    | The final displacement of the arm at the point of grasp (PoG).   |
| <i>Max(+)</i> | The maximum displacement during grasp in the positive direction. |
| <i>Max(-)</i> | The maximum displacement during grasp in the negative direction. |

In many cases, *Max(+)* and *Max(-)* displacement would be approximately equivalent to the *PoG* displacement, however can potentially benefit from reducing the effect of drift that occurs after the grasp has been made, which can be seen on the upper arm IMU components on the lateral grasp motion in figure 5.12. They can also be used to visually control the differences between grasps for certain features, as maximum displacement features in one direction will have a value of zero in the negative direction. This may also be useful for different clustering algorithms, where a single feature set can have different clusters if there is a change of direction due to variations in object location.

### 5.3.0.ii Velocity Features

The velocity-time profile is represented by the derivation of the displacement-time profile, which effectively looks at the gradient change that occurs during vector displacement. The velocity-time profile of a grasping motion can provide an insight into how the velocity of



---

each IMU vector component changes over time, enabling observations of motion change in greater depth. During a grasp, theoretically, velocity starts at zero, and ends at zero, however, in practice, it can be seen from figure 5.12 (b) that this is not always the case. The slightest shaking of the arm can cause minor fluctuations in velocity, making it tough to find an initial and final velocity of zero. Drift can also have an effect, which can lead to irregular fluctuations in velocity. Descriptive features from the velocity-time profile can be used to separate the different grasp classes associated with each object. The velocity features selected across each vector component for both IMUs accumulated to a total of 30 different features. These include:

- Max(+)*     The maximum velocity along the positive vector axis.
- Max(-)*     The maximum velocity along the negative vector axis.
- RMS*         The root-mean-square velocity.
- PK-RMS*     The ratio of the largest absolute velocity value to the RMS value.
- Mean*         The mean average velocity.

RMS, PK-RMS and Mean velocity features rely on the distribution of velocity in the entire grasp, which can make it reliant on the accurate determination of the start and end of grasp motion, which tries to minimise the effect that stationary arm motion has on the feature values. Having said this, these features may be useful in reducing associated variance due to irregular changes in grasp velocity.

### **5.3.0.iii Acceleration Features**

The acceleration-time profile of a grasping motion can lead to the extraction of additional features from the velocity data. With every change in velocity, there is a change in acceleration and deceleration associated with it. Different grasps may provide differences in acceleration and deceleration for different vector components, and potentially find very minor changes, which could be used to improve the classification of grasps. The acceleration profile is generated through the second derivative of the displacement-time data, which produces the instantaneous acceleration at each point in time. Features include:

---

$Max(+)$	The maximum acceleration rate.
$Max(-)$	The maximum deceleration rate.
$RMS$	The root-mean-square acceleration.
$PK-RMS$	The ratio of the largest absolute acceleration value to the RMS value.
$P2P$	The maximum-to-minimum difference.
$PK-Dist$	The time distance between maximum and minimum peaks.

### 5.3.1 Object: Bottle

Figure 5.12 shows example healthy subject data during a 3 second trial when grasping a bottle with *lateral* and *power* grasps at a depth of 30 cm and angle  $0^\circ$  at table height of the (a) displacement profile, (b) velocity profile, and (c) acceleration profile. The trials are aligned visually by cross-correlating the first trial with subsequent trials for that grasp, where the

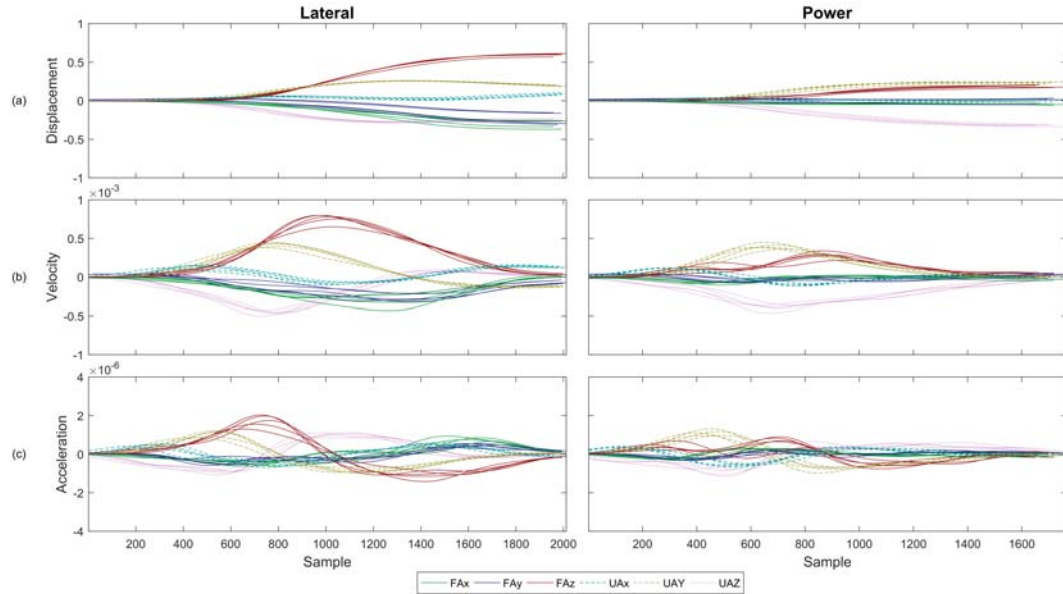


Figure 5.12: Quaternion vector (a) displacement, (b) velocity and (c) acceleration profiles of *lateral* and *power* grasps made on a bottle at a depth of 30 cm and angle of  $0^\circ$  at table height from a single healthy subject. The grasp profiles have been extracted from the 3 second trials, and have been aligned using cross-correlation. *Lateral* and *power* grasps have very different reach trajectories, especially in forearm orientation, emphasised by the large difference in  $FAz$ .

length of the trial has been shortened according to the start and end points calculations previously mentioned. The cross correlation function measures the similarity between the initial trial, and lagged copies of individual subsequent trials as a function of the lag. This function is not used for signal processing, but solely for visualisation purposes. It can be seen that both grasp patterns have very different trajectories due to the large difference in forearm orientation between the two grasps, which is emphasised by the difference in the average maximum magnitude of FAz (in red) of 0.411. The high difference in magnitude provides plenty of room for variance when the bottle's location is changed.

Similarly, amputee grasp profiles for the bottle, given in figure 5.13, show vast differences between the two grasps. *Power* grasps made have very little overall displacement, with UAz providing most of the motion during grasp. *Lateral* grasps have a much greater range of motion, similar to those of healthy subjects, with largest displacement coming from FAx and FAz with relatively little motion from the upper arm components compared

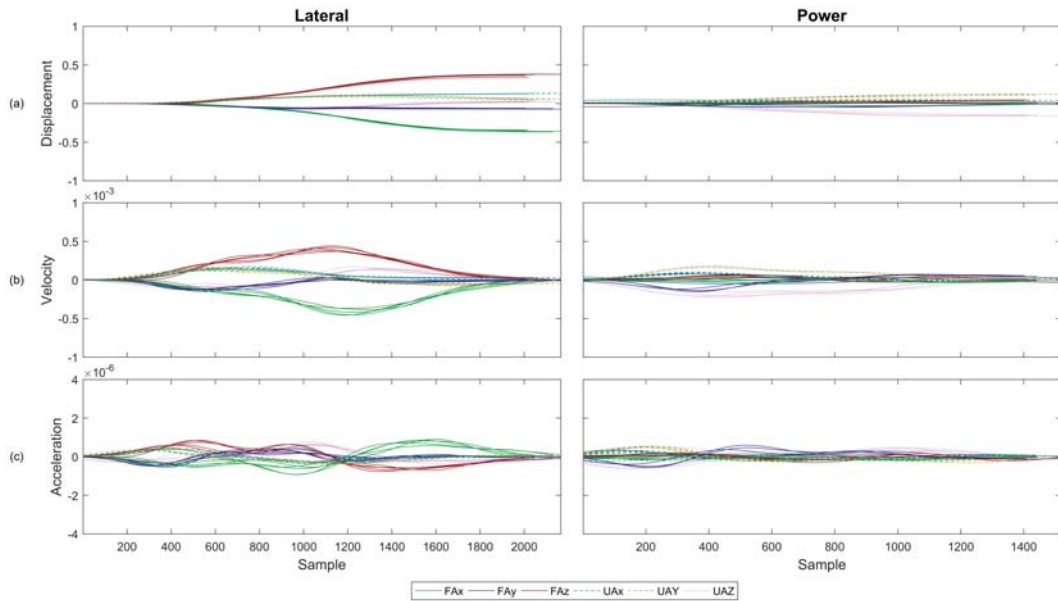


Figure 5.13: Quaternion vector (a) displacement, (b) velocity and (c) acceleration profiles of *lateral* and *power* grasps made on a bottle at a depth of 30 cm and angle of 0° at table height from a single amputee subject. The grasp profiles have been extracted from the 3 second trials, and have been aligned using cross-correlation. *Power* grasps made have very little overall displacement, with UAz providing most of the motion during grasp. *Lateral* grasps have a much greater range of motion, mostly provided by forearm vector components FAx and FAz.

---

to grasps made by healthy subjects. In comparison to healthy subjects, the difference between the two grasps in the average maximum magnitude of FAz (in red) is 0.3390, which is still a substantial difference. Amputee grasp motion has a much lower velocity compared to those of healthy subjects, with for example, a difference in maximum FAz velocity of  $3.50 \times 10^{-4}$  for *lateral* grasps, given by the comparison of figures 5.12 and 5.13. The weight of the prosthesis bearing down on the residual limb as well as the lack of tactile feedback would force the subject to slow down reaching motion in order to improve the control and positioning of the prosthetic hand as it reaches the object's PoG.

#### **5.3.1.i Displacement: Healthy**

Example healthy subject data showing the effect of object location on Max(+) displacement when grasping a bottle is given in figure 5.14, which displays a series of box plots comparing the forearm and upper arm features across all 18 elevation, depth and angular positions for the Bottle object. The forearm X, Y and Z components are designated FAx, FAy and FAz respectively, and likewise the upper arm X,Y and Z components are represented by UAx, UAy and UAz.

PoG displacement shows a strong overall separation between *lateral* and *power* grasps across all forearm and upper arm components, with the discrimination of the forearm's orientation being more prominent. The overall range of displacement is very similar between grasps made at table height and those ascending, where as those made descending show a much lower range of motion. A change in object depth for descending grasps appears not to have much effect on the PoG displacement, and those made at table height and ascending also causes minimal variation in hand position apart from FAy, which shows a decrease in discriminatory power between the two grasps when the object is closer to the subject. Variance in angular position during descending grasps have marginal effect, however those made at table height and ascending result in reduced negative displacement for FAx and increased negative displacement for FAy. FAz shows the most invariance to change in depth and angular position for grasps made at table height and ascending.

Substantial discrimination is evident between the two grasps at Max(+):FAz displace-

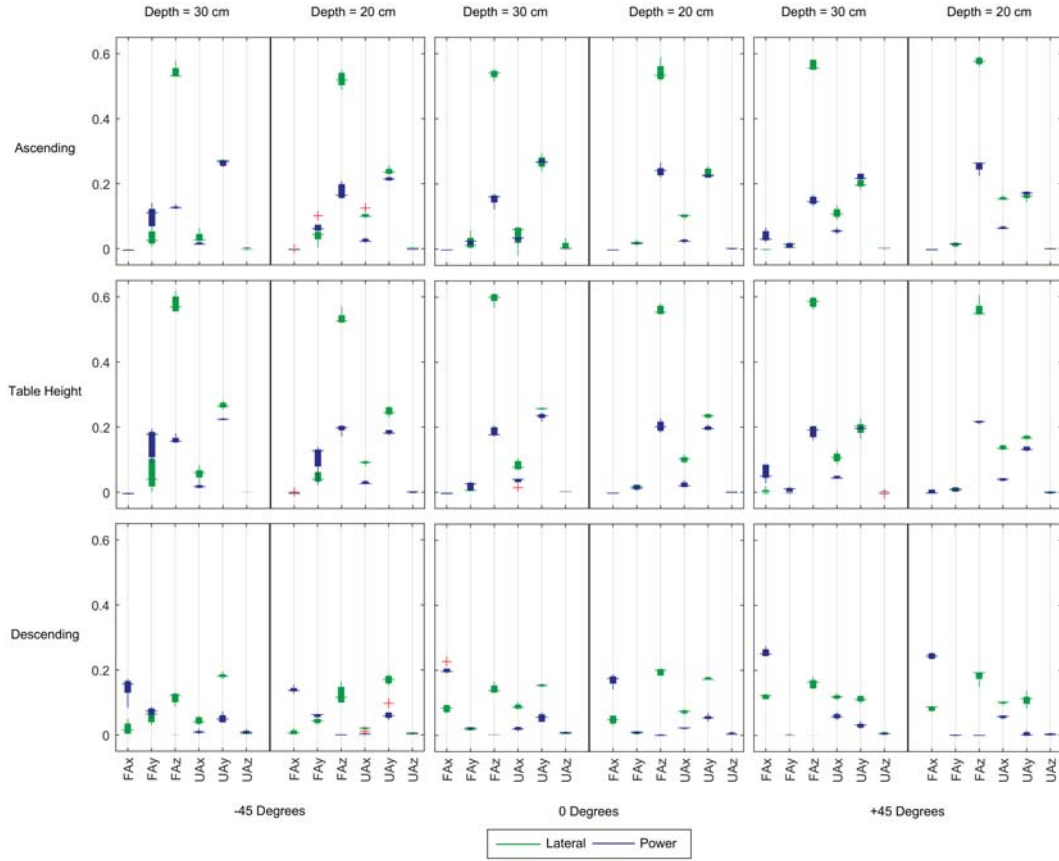


Figure 5.14: Example data from a single healthy subject comparing Max(+) displacement features across all elevation, depth and angular positions for *lateral* and *power* grasps made on a bottle. The forearm and upper arm X, Y and Z components are represented by the terms FAx, FAy, FAz, UAx, UAy and UAz respectively. Substantial discrimination is evident between the two grasps at Max(+):FAz displacement at table height and ascending elevation, however at descending, the *power* grasp reduces to zero. FAx shows positive Max(+):FAx displacement only at a descending elevation. A change in depth doesn't cause much variation in Max(+), however a change of angular position from negative to positive shows a small increase in Max(+):FAx displacement from zero, as well as a decrease in Max(+):FAy towards zero. Upper arm Max(+) features have lower separation across all elevation locations, but have much lower variance.

ment at table height and ascending elevation, however at descending, the *power* grasp reduces to zero. FAx shows positive Max(+):FAx displacement only at a descending elevation. A change in depth doesn't cause much variation in Max(+), however a change of angular position from negative to positive shows a small increase in Max(+):FAx displacement from zero, as well as a decrease in Max(+):FAy towards zero. Upper arm Max(+) features have lower separation across all elevation locations, but have much lower variance.

---

Max(-) forearm features show much stronger discrimination than the upper arm features, with Max(-):FAx and Max(-):FAy being the most prominent at table height and ascending elevation, however Max(-):FAz stays at zero. From  $-45^\circ$  to  $+45^\circ$ , Max(-):FAx displacement shows a decrease towards zero, whereas Max(-):FAy shows an increase. At a shorter depth of 20 cm, Max(-):FAy decreases with *lateral* grasps, but has negligible effect on *power* grasps. At a descending elevation, Max(-):FAz and Max(-):FAy have consistent negative displacement across all angular locations with good discrimination, however Max(-):FAx is reduced to zero. The upper arm components Max(-):UAX and Max(-):UAY are approximately zero throughout all locations. Max(-):UAz does show high negative displacement at table height and ascending elevation that lowers considerably when descending, however has consistently low discrimination between the two grasps.

### 5.3.1.ii Displacement: Amputee

Example data from the amputee subject showing the effect of object location on Max(+) displacement when grasping a bottle is given in figure 5.15.

PoG displacement shows good grasp separation across all components, especially in forearm components FAx and FAz, with both having approximately equal discriminatory power. The *power* grasp PoG displacement is quite small across all vector components, however the substantially higher displacement from the forearm components during *lateral* grasps provide very strong discrimination between the two. PoG:FAx and PoG:FAz are also very consistent across all object locations, having low variance. PoG:FAy has the largest variance of the vector components which can be seen across changes in angular position and elevation. Upper arm components are less variant to changes in object location, but show overall less discrimination between the two grasps.

Similar to PoG displacement, Max(+) and Max(-) displacement show very high discrimination between the two grasps for FAz, and FAx components respectively, with the large separation providing plenty of room for any variance between object locations. Other components have much less discriminatory power.

In comparison to healthy subject data, it can be seen that the discrimination between

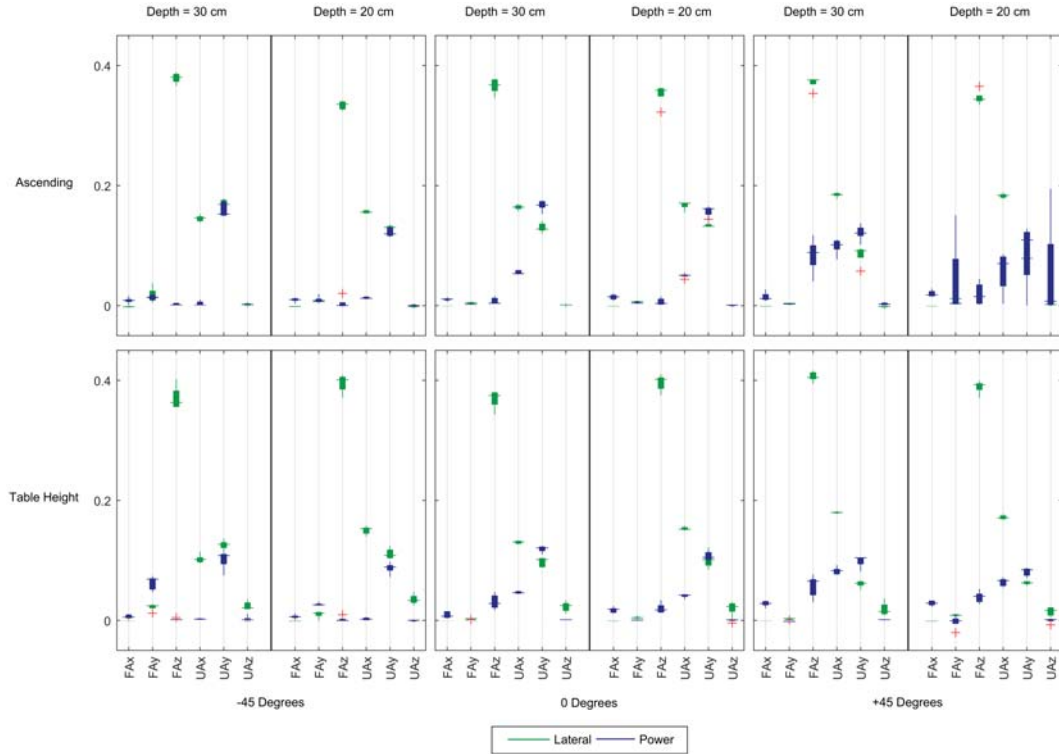


Figure 5.15: Example data from a single amputee subject comparing Max(+) displacement features across all depth and angular positions at table height and ascending for *lateral* and *power* grasps made on a bottle. The forearm and upper arm X, Y and Z components are represented by the terms Fx, Fy, Fz, Ux, Uy and Uz respectively. Max(+) displacement show very high discrimination between the two grasps for Fz, and Fx components respectively, with the large separation providing plenty of room for any variance between object locations. Other components have much less discriminatory power.

grasps is much greater in the amputee subject, mainly due to the large difference in the range of motion between the two. The much lower displacement during *power* grasp provides the largest discriminating factor between *lateral* grasps.

### 5.3.1.iii Velocity: Healthy

Example healthy subject data comparing the Max(+) velocity across all object locations when grasping a bottle is given in figure 5.16.

Max(+):FAz velocity has the greatest discrimination between the two grasps compared to the other vector components, showing reasonable invariance across all object locations with the exception of those made at a descent, which has a much lower magnitude. Max(+):FAx and Max(+):Fay have relatively poor separation across all object loca-



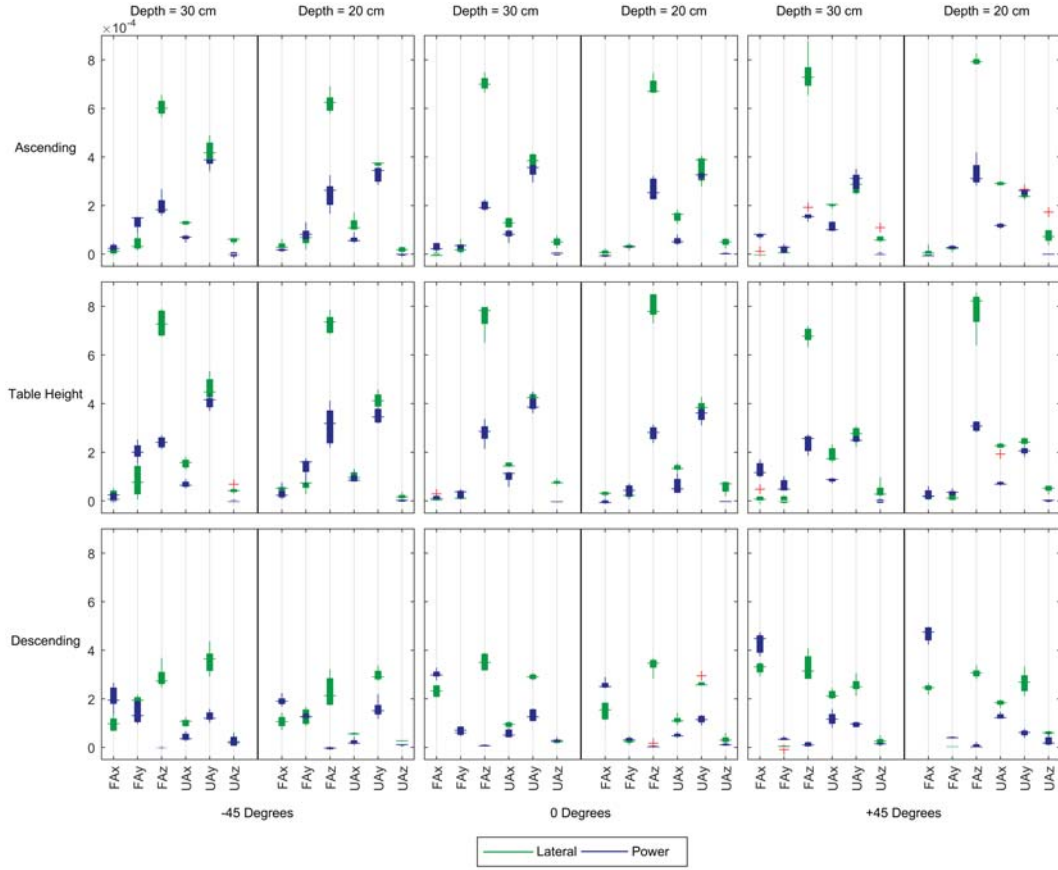


Figure 5.16: Example data from a single healthy subject comparing Max(+) velocity features across all elevation, depth and angular positions for *lateral* and *power* grasps made on a bottle. The forearm and upper arm X,Y and Z components are represented by the terms FAx, FAy, FAz, UAx, UAy and UAz respectively. Max(+):FAz velocity has the greatest discrimination between the two grasps compared to the other vector components, showing reasonable invariance across all object locations with the exception of those made at a descent, which has a much lower magnitude. Max(+):FAx and Max(+):FAy have relatively poor separation across all object locations. Max(+) upper arm components show reasonably good discrimination between the two grasps, and are also quite invariant across all object locations, including those made at descending.

tions. Max(+) upper arm components show reasonably good discrimination between the two grasps, and are also quite invariant across all object locations, including those made at descending.

Max(-):FAx velocity has the strongest overall discrimination with the least variance across all object locations, however those made at descending does decrease the magnitude. Max(-):FAy also shows good discrimination overall however has a strong increase in magnitude at +45°. Max(-):FAz remains at zero except at a descending elevation. The upper



---

arm components have negligible discrimination with the exception of Max(-):UAz which provides reasonably good grasp separation across all object locations.

Mean forearm features have strong discrimination and low variance across elevations at table height and ascending, however Mean:FAy has consistently reduced separation at a depth of 20 cm compared to 30 cm. At a descending elevation, there is a change in velocity direction of *power* grasps by Mean:FAx and Mean:FAz, however Mean:FAy stays relatively consistent. Upper arm components are a lot more invariant to changes in object location, however have lower discriminatory power in comparison to forearm vector components.

RMS:FAz has the highest discrimination at table height and ascending elevation, however is greatly reduced when descending. RMS:FAy is affected by a reduction in discrimination at a lower depth, and RMS:FAx velocity shows a reduction in magnitude for *lateral* and an increase in magnitude from *power* grasps, which will greatly reduce their overall discriminatory power. Upper arm features have relatively low overall discrimination in comparison to forearm features.

PK-RMS velocity features across both forearm and upper arm vector components have relatively high variance, and poor discrimination across all object locations.

#### **5.3.1.iv Velocity: Amputee**

Example data from the amputee subject comparing the Max(+) velocity across all object locations when grasping a bottle is given in figure 5.17.

Similarly to Max(+) and Max(-) displacement, Max(+) and Max(-) velocity show high discrimination between grasps in FAz and FAx respectively, with other vector components having much lower separability in comparison. Max(+) upper arm components UAx and UAz show some discrimination between the two grasps, however are subject to variance due to changes in angular position.

RMS:FAx and RMS:FAz show very high discrimination between grasps with minor variance. Other vector components show much lower separability in comparison. Mean velocity features show similar results, with Mean:FAx and Mean:FAz having the highest discriminatory power of all the vector components.

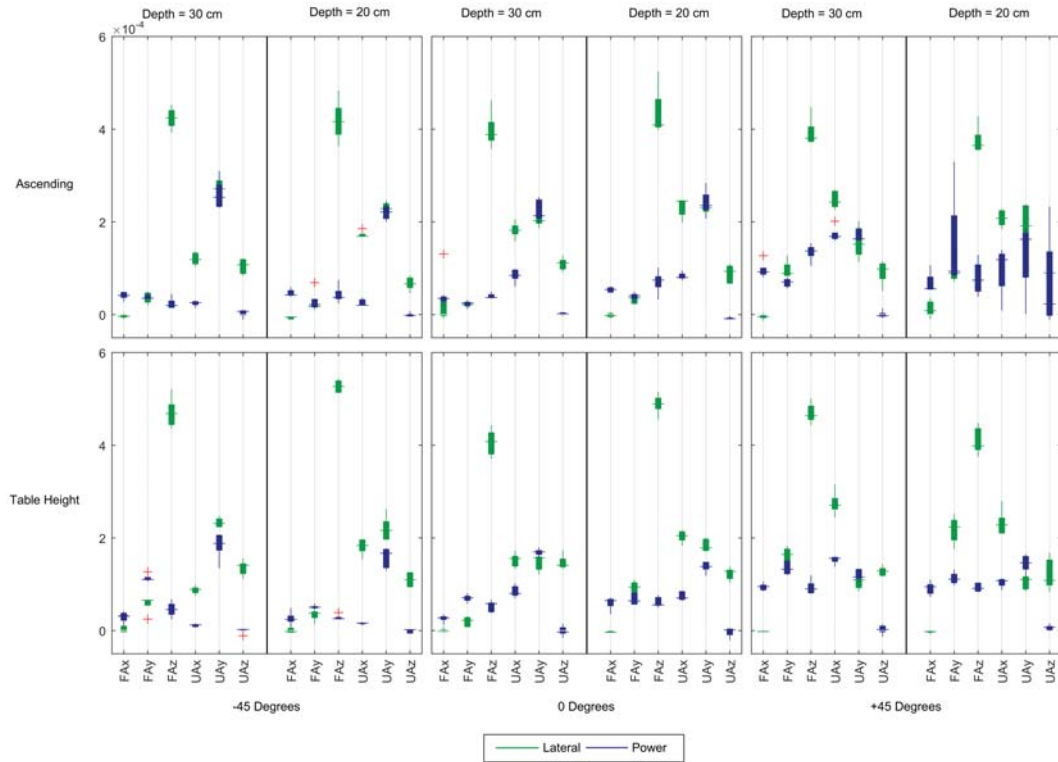


Figure 5.17: Example data from a single amputee subject comparing Max(+) velocity features across all elevation, depth and angular positions for *lateral* and *power* grasps made on a bottle. The forearm and upper arm X,Y and Z components are represented by the terms FAX, FAY, FAZ, UAX, UAY and UAZ respectively. Max(+) velocity show high discrimination between grasps in FAZ and FAX respectively, with other vector components having much lower separability in comparison. Max(+) upper arm components UAX and UAZ show some discrimination between the two grasps, however are subject to variance due to changes in angular position.

PK-RMS velocity features across both forearm and upper arm vector components have relatively high variance, and poor discrimination across all object locations, similar to that of healthy subjects.

### 5.3.1.v Acceleration: Healthy

Example healthy subject data comparing the Max(+) acceleration across all object locations when grasping a bottle is given in figure 5.18.

Max(+) forearm acceleration shows overall strong discrimination between the two grasps with Max(+):FAX and Max(+):FAZ being the most invariant to changes in object location with the exception of those made at a descent, which shows a reduction in mag-

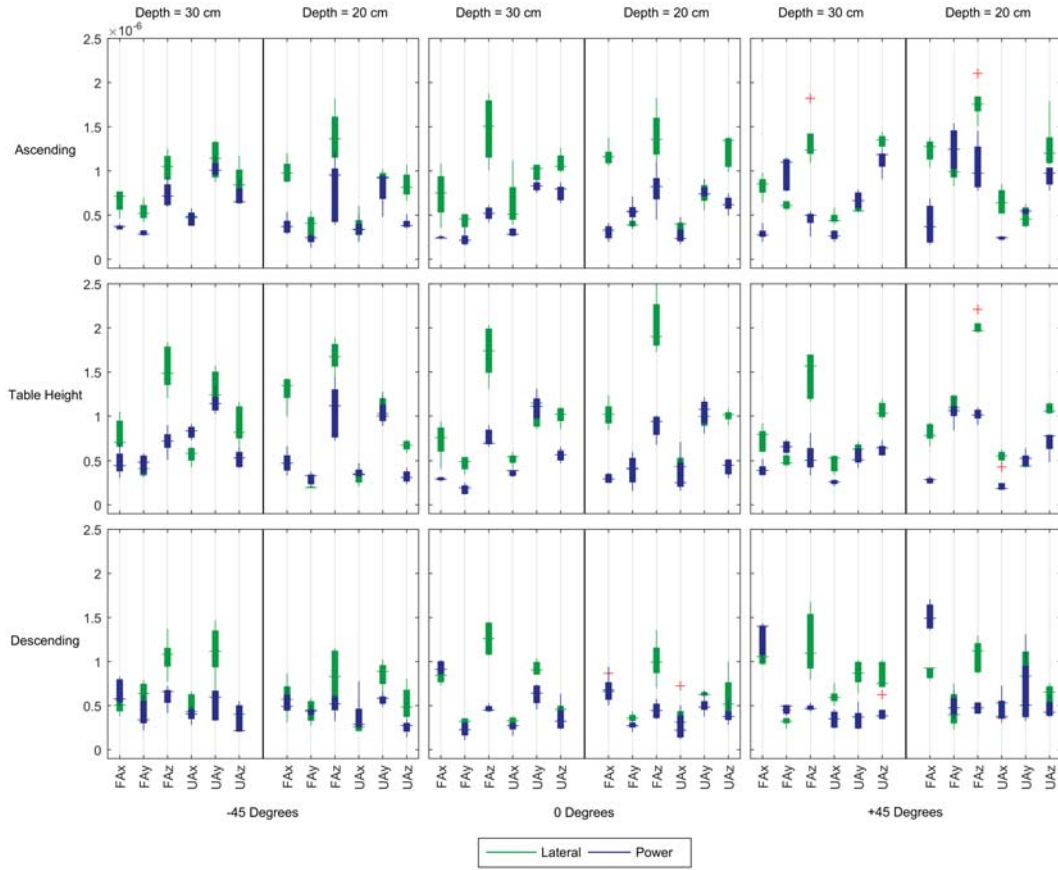


Figure 5.18: Example data from a single healthy subject comparing Max(+) acceleration features across all elevation, depth and angular positions for *lateral* and *power* grasps made on a bottle. The forearm and upper arm X,Y and Z components are represented by the terms FAx, FAy, FAz, UAx, UAy and UAz respectively. Max(+) forearm acceleration shows overall strong discrimination between the two grasps with Max(+):FAx and Max(+):FAz being the most invariant to changes in object location with the exception of those made at a descent, which shows a reduction in magnitude across all features. Max(+) has the poorest discrimination of the Max(+) forearm features and increases in variance due to changes in angular location. Max(+) upper arm acceleration shows lower discrimination in comparison with the exception of Max(+):UAz which shows good overall discrimination with low variance.

nitude across all features. Max(+) has the poorest discrimination of the Max(+) forearm features and increases in variance due to changes in angular location. Max(+) upper arm acceleration shows lower discrimination in comparison with the exception of Max(+):UAz which shows good overall discrimination with low variance.

Max(-) forearm acceleration shows overall high discrimination and reasonably good invariance to changes in object location, especially for Max(-):FAx and Max(-):FAz. Al-

---

though the discrimination of Max(-):FAz decreases at a descent, Max(-):FAx is more resilient. Max(-) upper arm acceleration shows higher variance due to changes in depth and angular location, as well as poorer discriminatory power.

RMS forearm acceleration provides strong discrimination and invariance with the exception of RMS:FAy which has a much higher variance in comparison. RMS upper arm acceleration shows lower overall discrimination with high variance. Grasps made at a descent provide a reduction in discriminatory power across all RMS features.

P2P forearm features show overall strong discrimination and good invariance between the two grasps across all object locations with the exception of P2P:FAy, which has lower discriminatory power. P2P upper arm features have poorer discrimination and higher variance in comparison.

PK-Dist and PK-RMS forearm and upper arm features show poor discrimination and relatively high variance across all object locations.

#### **5.3.1.vi Acceleration: Amputee**

Example data from the amputee subject comparing the Max(+) acceleration across all object locations when grasping a bottle is given in figure 5.19.

Max(+) acceleration features display good discrimination between the two grasps, with overall greater separation at table height compared to ascending. Max(+):FAx and Max(+):FAz show stronger discrimination with the least variance. Upper arm components show greater variance and lower discriminatory power compared to the forearm vector components. Max(-) features are subjected to very high variance with the exception of Max(-):FAx, which holds relatively good grasp separability across all object locations and much lower variance compared to other Max(-) vector components.

RMS:FAx and RMS:FAz acceleration features show good discrimination across all object locations with relatively low variance. RMS upper arm acceleration features have low separability between the two grasps across all object locations.

P2P acceleration features show overall low discrimination between the two grasps, with P2P:FAx and P2P:FAz being the most prominent.

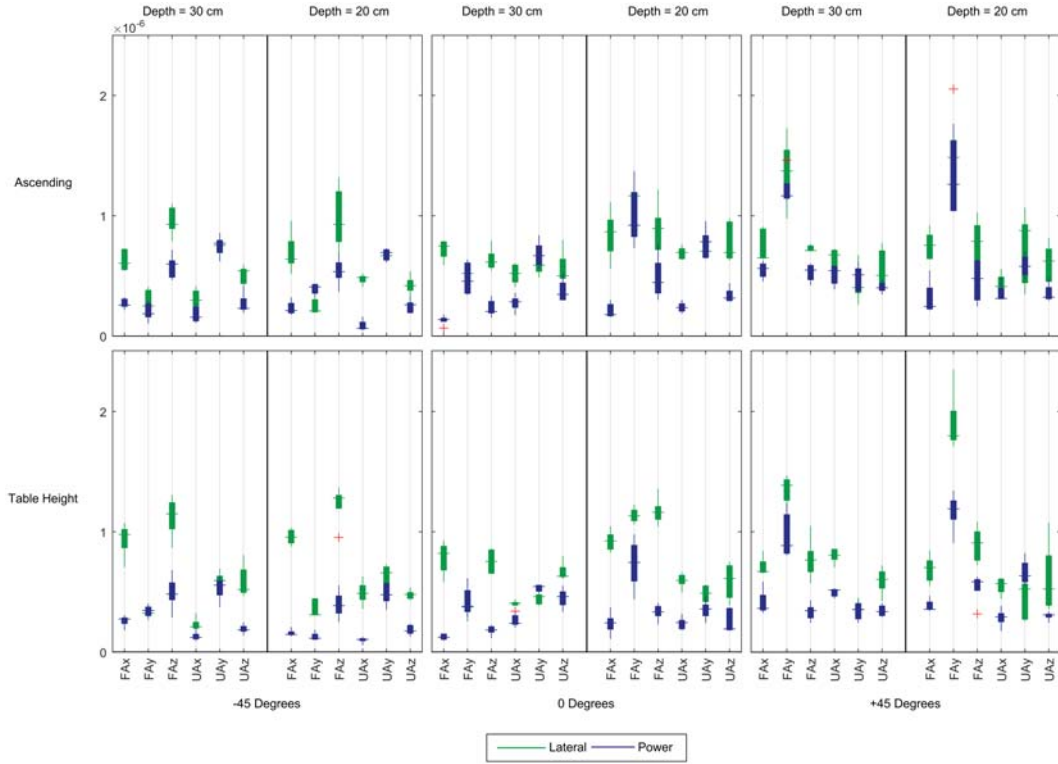


Figure 5.19: Example data from a single amputee subject comparing Max(+) acceleration features across all elevation, depth and angular positions for *lateral* and *power* grasps made on a bottle. The forearm and upper arm X,Y and Z components are represented by the terms FAx, FAy, FAz, UAx, UAy and UAy respectively. Max(+) acceleration features display good discrimination between the two grasps, with overall greater separation at table height compared to ascending. Max(+):FAx and Max(+):FAz show stronger discrimination with the least variance. Upper arm components show greater variance and lower discriminatory power compared to the forearm vector components.

PK-DIST features show high variance and mixed separability across all forearm and upper arm vector components, whereas PK-RMS shows very low separation between grasps across all object locations.

### 5.3.2 Object: Lid

Figure 5.20 shows the processed vector profiles of a single healthy subject for interacting with a lid with *lateral* and *precision* grasps at a depth of 30 cm and angle 0° at table height. The trajectories of these two grasps are much more similar in comparison to those of the bottle, with only minor visible differences. Velocity and acceleration profiles show greater potential, showing more obvious changes in magnitude between the two grasps. The

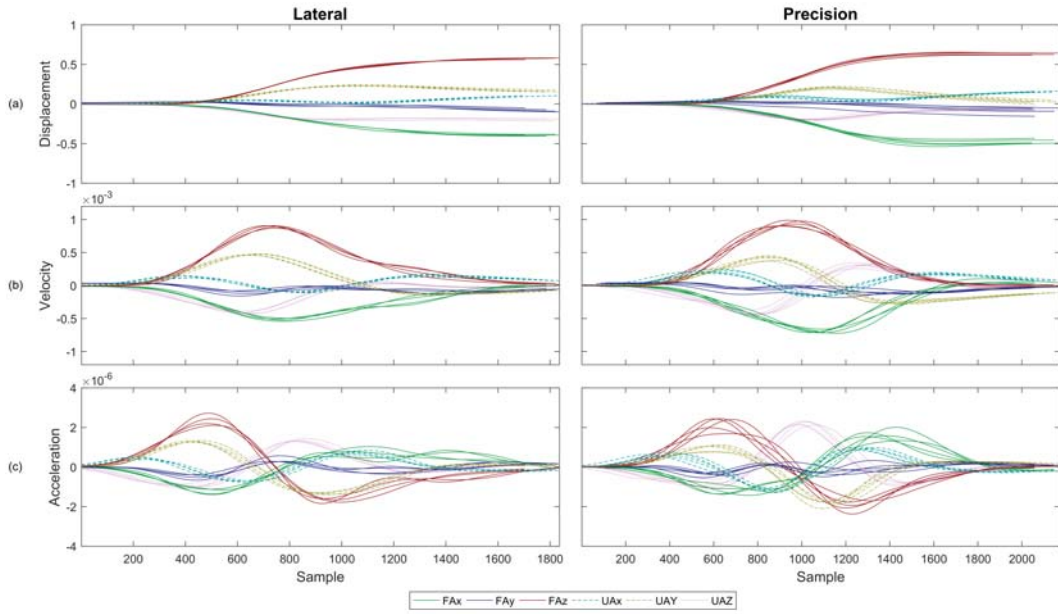


Figure 5.20: Quaternion vector (a) displacement, (b) velocity and (c) acceleration over time of *lateral* and *precision* grasps made on a lid at a depth of 30 cm and angle of  $0^\circ$  at table height from a single healthy subject. The grasp profiles have been extracted from the 3 second trials, and have been aligned using cross-correlation. The trajectories of these two grasps are much more similar, with only minor visible differences. Velocity and acceleration profiles show greater differences, however, the similarities in the two grasps leaves much less room for variance due to changes in object location.

similarities in the two grasps leaves much less room for variance due to changes in object location.

Amputee grasp profiles made on a lid in the same object location is given in figure 5.21. As with the grasps made by healthy subjects, the two grasps have much more similar motion, with the highest displacement coming from FAx and FAz. Amputee FAx displacement is greater than that of healthy subjects, showing the compensatory motion involved while using the prosthesis. The upper arm looks to have a larger role in determining grasp trajectory, especially UAY. It can be seen that amputee motion during grasp is much less smooth in comparison to healthy subjects, which is most likely due to micro adjustments made by the subject to improve control during reach.



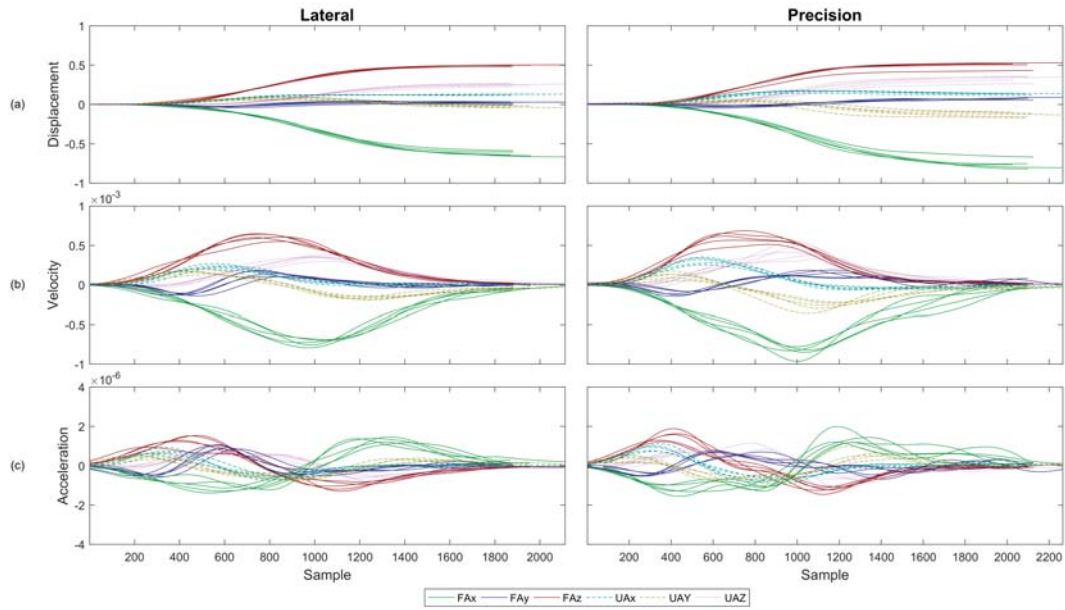


Figure 5.21: Quaternion vector (a) displacement, (b) velocity and (c) acceleration over time of *lateral* and *precision* grasps made on a lid at a depth of 30 cm and angle of  $0^\circ$  at table height from a single amputee subject. The grasp profiles have been extracted from the 3 second trials, and have been aligned using cross-correlation. The two grasps have much more similar motion, with the highest displacement coming from Fx and Fz. The upper arm looks to have a larger role in determining grasp trajectory, especially Uy.

### 5.3.2.i Displacement: Healthy

Example healthy subject data showing the effect of Max(-) displacement features when grasping a lid across all object locations is given in figure 5.22.

The discrimination between the two grasps at the PoG at each individual object location is much smaller in terms of forearm orientation, especially at PoG:Fy and PoG:Fz. PoG:Fx provides greater and more consistent discrimination between the two grasps across all object locations at table height and ascending elevation. As with the Bottle object, grasps made descending have considerably lower displacement compared to those made at table height and ascending. At a depth of 30 cm, upper arm displacement at the PoG shows much better separation in comparison to the forearm across object locations at table height and ascending, however at a depth of 20 cm, the difference in upper arm displacement reduces.

Max(+):Fz shows invariance in displacement across table height and ascending elevation locations with minor separation between grasps, being the most prominent Max(+) displacement feature. Max(+):Fy displacement tends towards zero from  $-45^\circ$  to  $+45^\circ$ ,

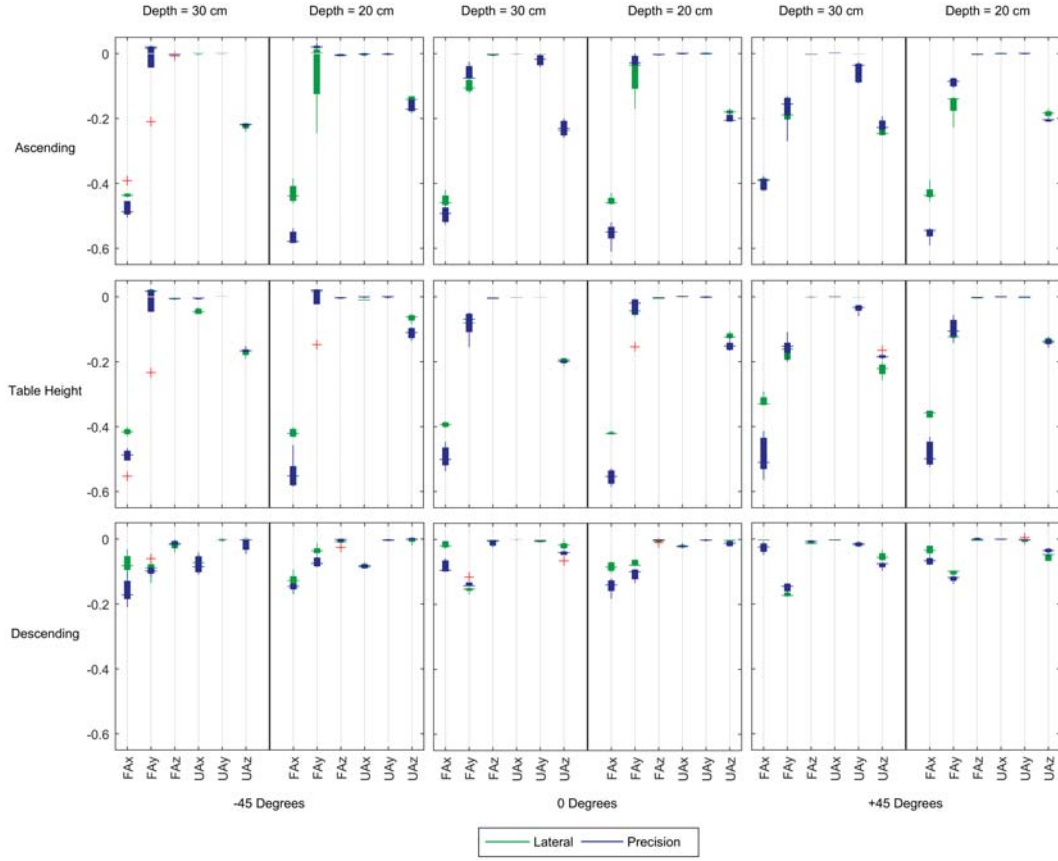


Figure 5.22: Example data from a single healthy subject comparing Max(-) displacement features across all elevation, depth and angular positions for *lateral* and *precision* grasps made on a lid. The forearm and upper arm X,Y and Z components are represented by the terms FAX, FAY, FAZ, UAX, UAY and UAZ respectively. Max(-):FAX shows strong discrimination between grasps and invariance in displacement at table height and ascending elevation, with a decrease in negative displacement at descending, however still shows strong discrimination between grasps. The remaining forearm and upper arm components have overall poor separation, with Max(-):FAZ, Max(-):UAX and Max(-):UAY approximated to zero across all object locations.

and Max(+):FAX remains at zero throughout all object locations with exception of those made at a descent, where there is a minor rise from  $-45^{\circ}$  to  $+45^{\circ}$ . Upper arm components Max(+):UAX and Max(+):UAY have relatively good discrimination, but with high variance across object locations. Max(+):UAZ remains at approximately zero across all object locations.

Max(-):FAX shows strong discrimination between grasps and invariance in displacement at table height and ascending elevation, with a decrease in negative displacement at descending, however still shows strong discrimination between grasps. The remaining fore-



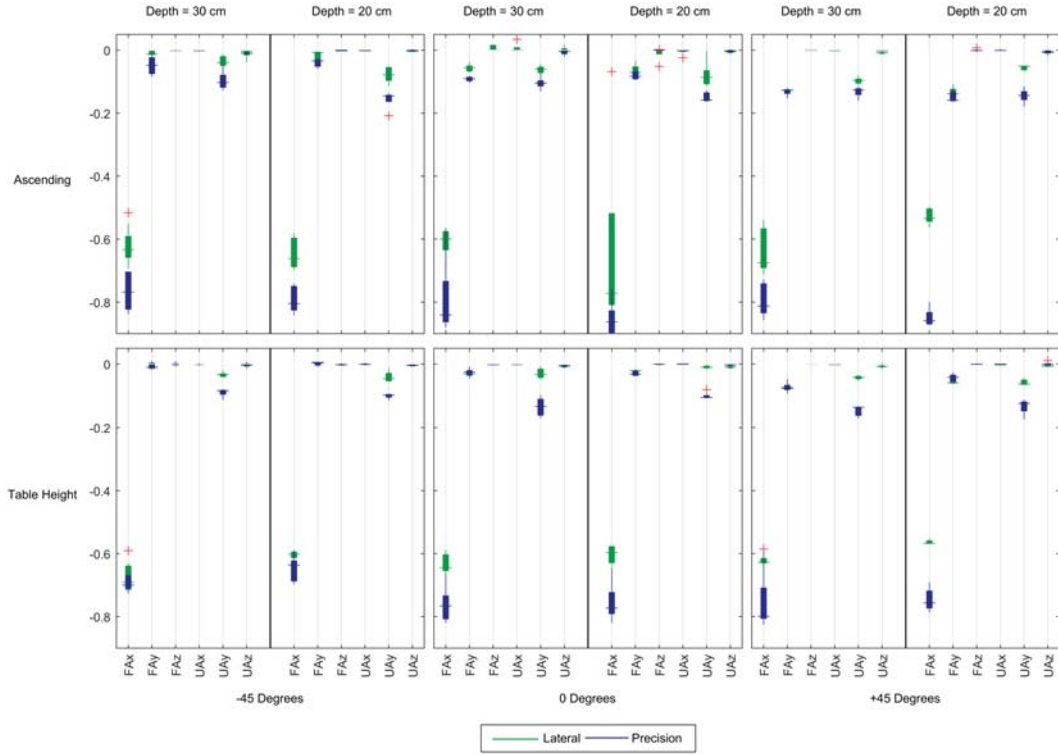


Figure 5.23: Example data from a single amputee subject comparing Max(-) displacement features across all elevation, depth and angular positions for *lateral* and *precision* grasps made on a lid. The forearm and upper arm X,Y and Z components are represented by the terms Fx, Fy, Fz, Ux, Uy and Uz respectively. Max(-) features has higher consistency of discrimination between grasps from components Fx and Uy, both being fairly invariant to changes in object location. All other Max(-) vector features show negligible discrimination between the two grasps.

arm and upper arm components have overall poor separation, with Max(-):Fz, Max(-):Ux and Max(-):Uy approximated to zero across all object locations.

### 5.3.2.ii Displacement: Amputee

Example data from the amputee subject comparing the Max(-) displacement across all object locations when grasping a lid is given in figure 5.23.

PoG features provide better discrimination at table height, but generally have low separability overall. The only vector components showing consistently good discrimination across all object locations are PoG:Fx and PoG:Uy. All PoG vector components show relatively high invariance except for Ux and Uz which are both affected by changes in elevation.

---

Max(+) forearm features show low discrimination between the two grasps with Max(+):FAx remaining at approximately zero across all object locations. Max(+):UAx and Mac(+):UAz upper arm components have overall stronger discriminatory power, however their magnitudes are affected by changes in elevation, resulting in greater variance.

Max(-) features has higher consistency of discrimination between grasps from components FAx and UAy, both being fairly invariant to changes in object location. All other Max(-) vector features show negligible discrimination between the two grasps.

### 5.3.2.iii Velocity: Healthy

Example healthy subject data comparing the RMS velocity across all object locations when grasping a lid is given in figure 5.24.

Max(+) forearm component features has overall poor discrimination with the exception of Max(+):FAz, however a reduction in depth greatly reduces its discriminatory power. The upper arm components show comparably stronger discrimination, however are subject to high variance across object locations with the exception of Max(+):UAz. Grasps made at a descent gives a reduction in overall magnitude and discriminatory power across all Max(+) velocity features.

Max(-):FAx velocity shows the strongest discrimination compared to other Max(-) vector component features, however is subject to minor variance due to changes in depth. Max(-):FAy has relatively lower discriminatory power, and higher variability due to changes in angular location, whereas Max(-):FAz can be considered negligible. Max(-) Upper arm features show better separation of grasps, however can be subject to higher variance due to changes in elevation. Grasps at a descent have reduced discrimination across all features with the exception of Max(-):FAx.

Mean forearm velocity has fairly low discriminatory power with the exception of Mean:FAx, which shows higher discrimination with a reduction in object depth location. Mean upper arm velocity features show fairly strong discrimination at a depth of 30 cm, however its strength is reduced significantly at a depth of 20 cm.

RMS:FAx shows relatively good discrimination and invariance in comparison to the

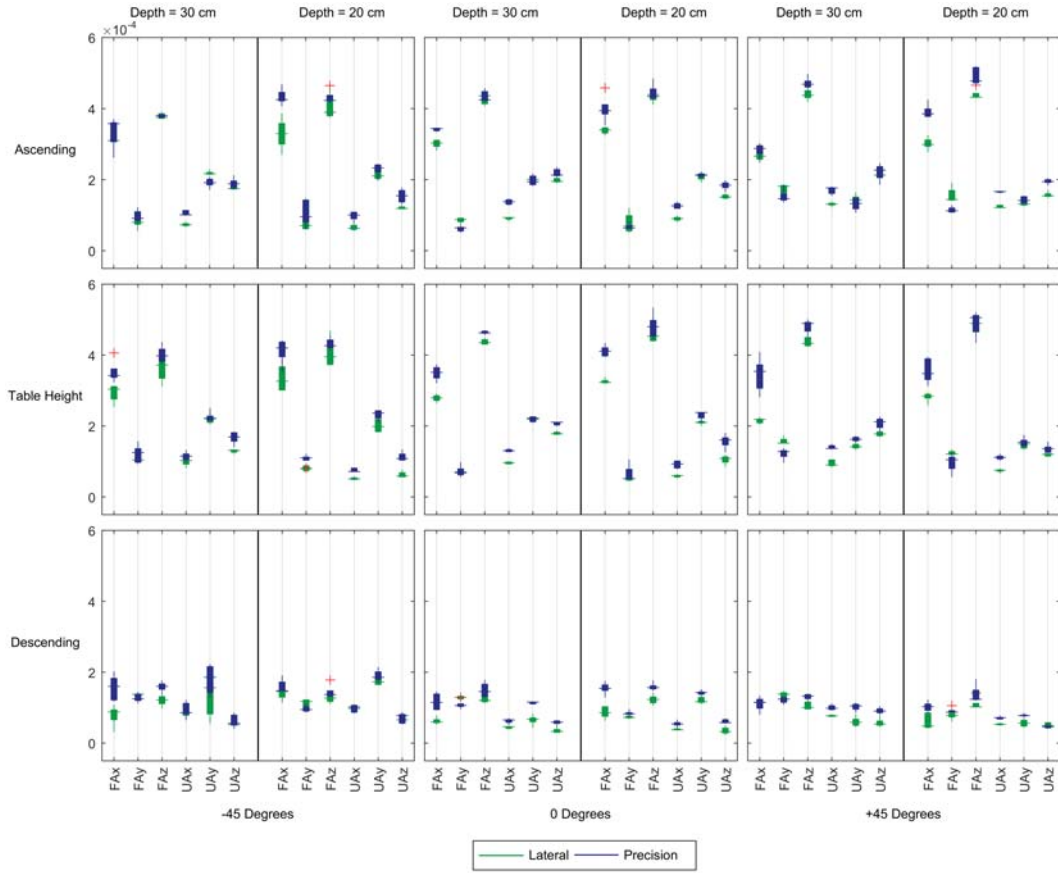


Figure 5.24: Example data from a single healthy subject comparing RMS velocity features across all elevation, depth and angular positions for *lateral* and *precision* grasps made on a Lid. The forearm and upper arm X,Y and Z components are represented by the terms FAX, FAY, FAZ, UAX, UAY and UAZ respectively. RMS:FAX shows relatively good discrimination and invariance in comparison to the other forearm components across all object locations, with the exception of those at descending elevation. Upper arm RMS velocity features have stronger invariance but lower discriminatory power, with RMS:UAX being the most prominent.

other forearm components across all object locations, with the exception of those at descending elevation. Upper arm RMS velocity features have stronger invariance but lower discriminatory power, with RMS:UAX being the most prominent.

PK-RMS forearm and upper arm velocity features show poor discrimination and relatively high variance across all object locations.

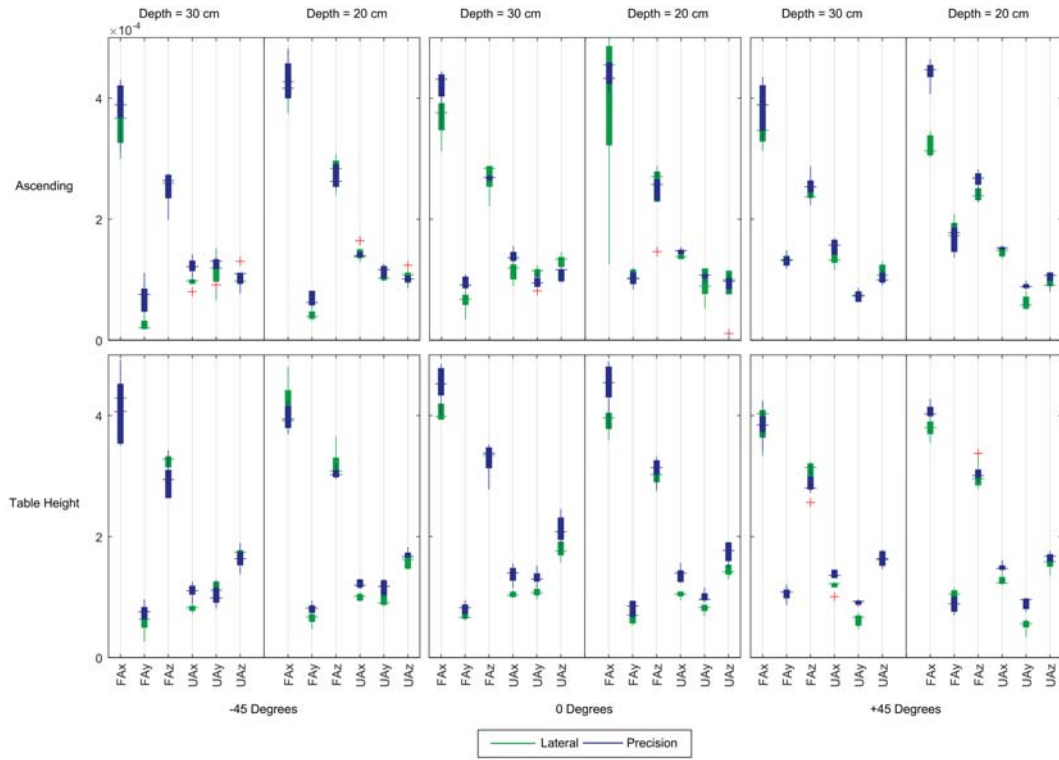


Figure 5.25: Example data from a single amputee subject comparing RMS velocity features across all elevation, depth and angular positions for *lateral* and *precision* grasps made on a lid. The forearm and upper arm X,Y and Z components are represented by the terms FAX, FAY, FAZ, UAX, UAY and UAZ respectively. RMS velocity shows fairly weak separation between grasps, with upper arm features performing better overall. Discrimination appears to be stronger at table height.

#### 5.3.2.iv Velocity: Amputee

Example data from the amputee subject comparing the RMS velocity across all object locations when grasping a lid is given in figure 5.25.

Max(+) velocity features show overall low discrimination between the two grasps at all object locations. Max(+) upper arm features show stronger separation, in particular UAX, however is subject to some variance on ascending grasps due to changes in angular location. Max(+):FAX has a magnitude of approximately zero for both grasps. All Max(-) velocity features show very little discrimination between grasps, with Max(-):FAX having the largest magnitude, but with minimal discriminatory power. Max(-):UAY shows better discrimination than the other Max(-) velocity vector components, however still isn't that strong overall.

---

RMS velocity also shows fairly weak separation between grasps, with upper arm features performing better overall. Discrimination appears to be stronger at table height. Mean velocity features show stronger and more consistent discrimination between the two grasps across all object locations than the RMS velocity, with FAX and UAY being the most prominent. Mean:FAY has stronger discriminatory power for grasps made at table height than ascending, however the discriminatory power of the remaining components is minimal.

PK-RMS forearm and upper arm velocity features show poor discrimination and relatively high variance across all object locations.

### **5.3.2.v Acceleration: Healthy**

Example healthy subject data comparing the RMS acceleration across all object locations when grasping a lid is given in figure 5.26.

Max(+) forearm acceleration shows relatively poor discrimination and high variance overall with the exception of Max(+):FAX. Max(+):FAX shows greater discrimination and invariance apart from at an angle of  $-45^\circ$  where its discriminatory power is reduced. Max(+) upper arm features are subject to high variance and relatively poor discrimination across all object locations. Grasps made at a descent shows a reduction in magnitude and discriminatory power.

RMS forearm acceleration features have overall poor discrimination and high variance. RMS:FAX has stronger discriminatory power however is subject to variance due to changes in depth location. RMS upper arm features show higher discrimination in comparison, with RMS:UAX and RMS:UAZ being more invariant to changes in object location. Grasps made at a descent show a reduction in magnitude and discriminatory power.

P2P forearm and upper arm acceleration features shows generally poor discrimination with the exception of P2P:FAX and P2P:UAX, however are both affected by relatively high variance. Grasps made at a descent show a large reduction in magnitude and discriminatory power.

Max(-), PK-Dist, PK-RMS forearm and upper arm acceleration features shows poor discrimination and relatively high variance across all object locations.

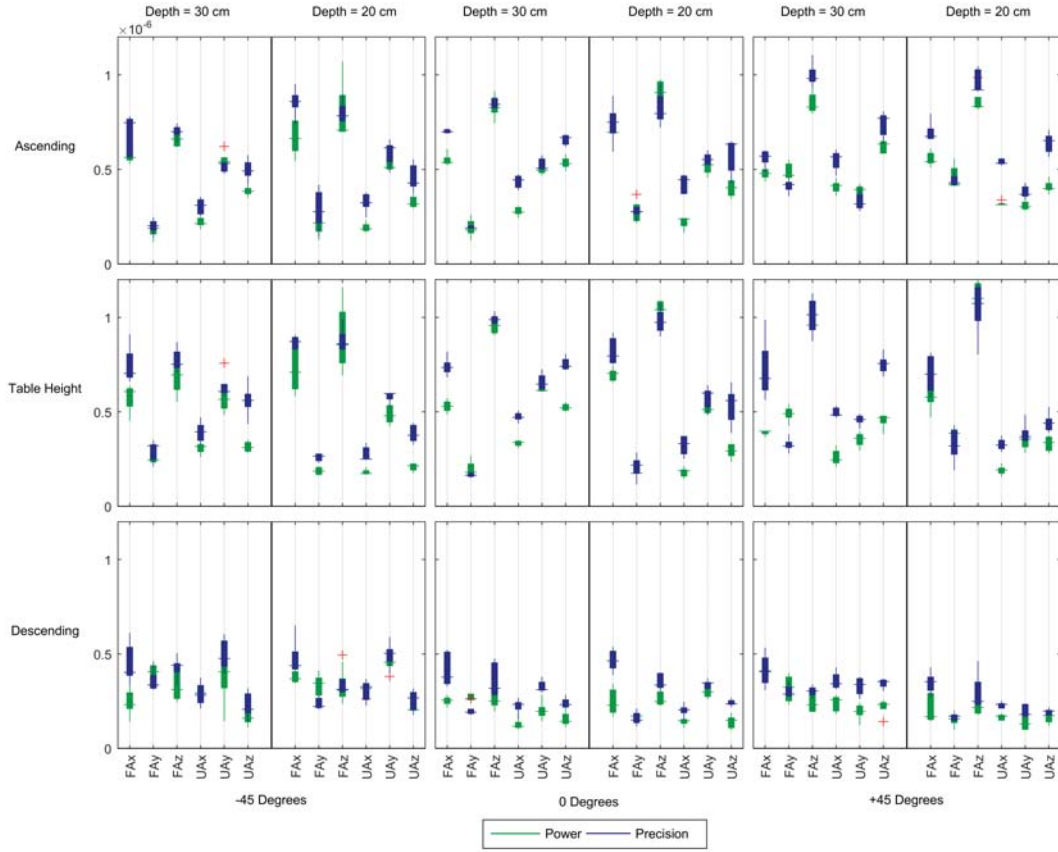


Figure 5.26: Example data from a single healthy subject comparing RMS acceleration features across all elevation, depth and angular positions for *lateral* and *precision* grasps made on a lid. The forearm and upper arm X,Y and Z components are represented by the terms FAX, FAY, FAZ, UAX, UAY and UAZ respectively. RMS forearm acceleration features have overall poor discrimination and high variance. RMS:FAX has stronger discriminatory power however is subject to variance due to changes in depth location. RMS upper arm features show higher discrimination in comparison, with RMS:UAX and RMS:UAZ being more invariant to changes in object location. Grasps made at a descent show a reduction in magnitude and discriminatory power.

### 5.3.2.vi Acceleration: Amputee

Example data from the amputee subject comparing the RMS acceleration across all object locations when grasping a lid is given in figure 5.27.

All acceleration features show very little separation between grasps and high variance across all object locations. The similarity of grasp trajectory between the two grasps produce even smaller differences in the acceleration features compared to those of velocity and displacement. This may be attributed to finer and slower control when positioning the

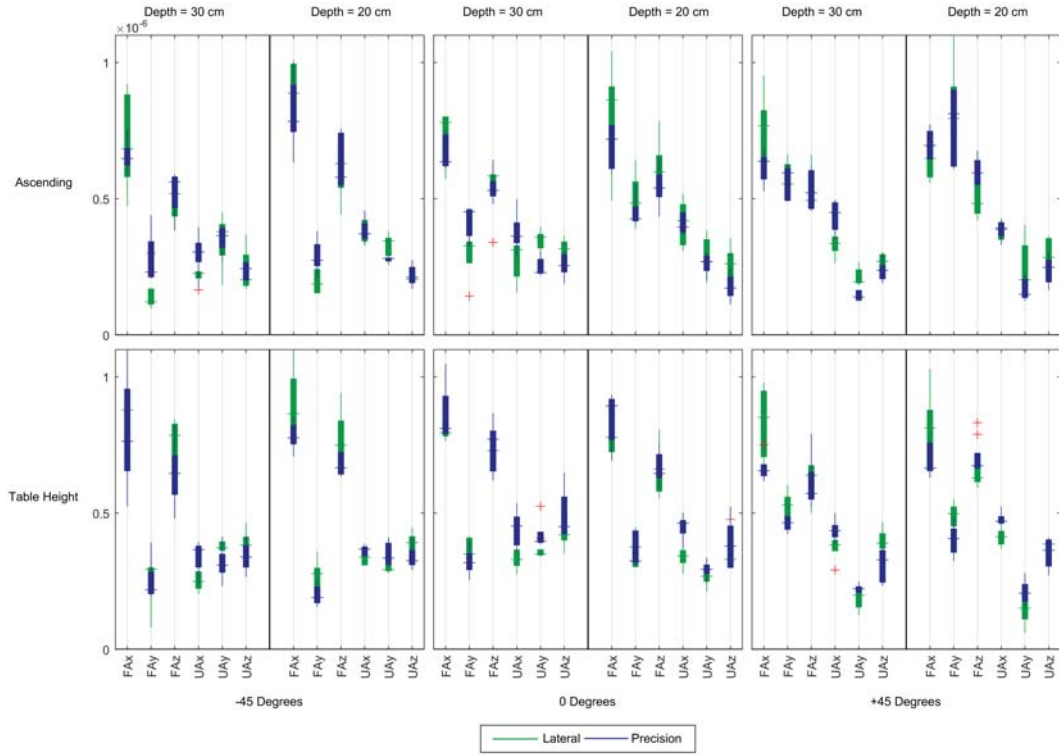


Figure 5.27: Example data from a single amputee subject comparing RMS acceleration features across all elevation, depth and angular positions for *lateral* and *precision* grasps made on a lid. The forearm and upper arm X,Y and Z components are represented by the terms FAx, FAy, FAz, UAx, UAy and UAz respectively. RMS acceleration features show very little separation between grasps and high variance across all object locations.

prosthesis at the lid's PoG.

### 5.3.3 Object: Box

Figure 5.28 shows the processed vector displacement-time profile of a single healthy subject for interacting with a box with *lateral*, *power* and *precision* grasps at a depth of 30 cm and angle  $0^\circ$  at table height. Visibly, *lateral* and *precision* grasps show a similar behavior to those made on the lid. Due to the orientation of the *power* grasp made on the box, it also shows similarities to the other two grasps, making it more difficult to differentiate between them.

Amputee grasp profiles on a box at the same location is given in figure 5.29. Amputee grasp profiles for the different grasps patterns are very similar, with FAx and FAz providing the largest change in motion. *Precision* grasps show slightly greater displacement in the



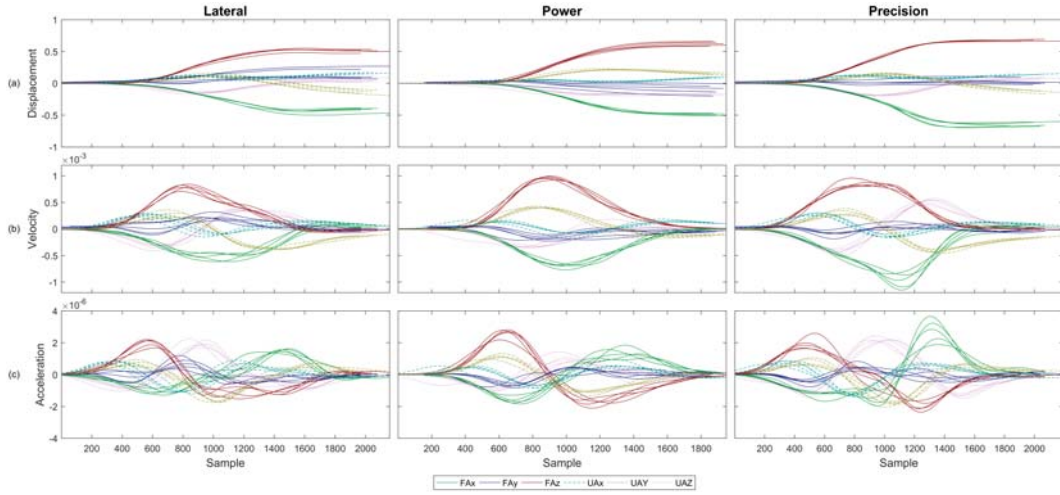


Figure 5.28: Quaternion vector (a) displacement, (b) velocity and (c) acceleration over time of *lateral*, *power* and *precision* grasps made on a box at a depth of 30 cm and angle of  $0^\circ$  at table height from a single healthy subject. The grasp profiles have been extracted from the 3 second trials, and have been aligned using cross-correlation. All three grasps have very similar reach trajectories, making it more difficult to differentiate between them.

negative direction, but upper arm motion looks to be very similar across all grasps. This may be attributed to the prosthesis restricting the free motion of the upper arm by compensating for the lack of available forearm rotation.

### 5.3.3.i Displacement: Healthy

Example healthy subject data comparing the PoG displacement across all object locations when grasping a box is given in figure 5.30.

Similarly with the lid, the main discrimination emphasis between the *lateral* and *precision* grasps are from forearm IMU components PoG:FAx and PoG:FAz, with PoG:FAy also showing reasonable discrimination across object locations. As with the lid, a reduction in object depth is found to reduce the distinction between the grasps. Forearm features show greater separation between the three grasps at both depths in comparison to the upper arm features. Grasps made at a descending elevation continue to show greatly reduced displacement. Although the grasps show separation at individual positions, especially among forearm IMU features, the high proximity between the PoG displacement of each grasp will make them less distinguishable.



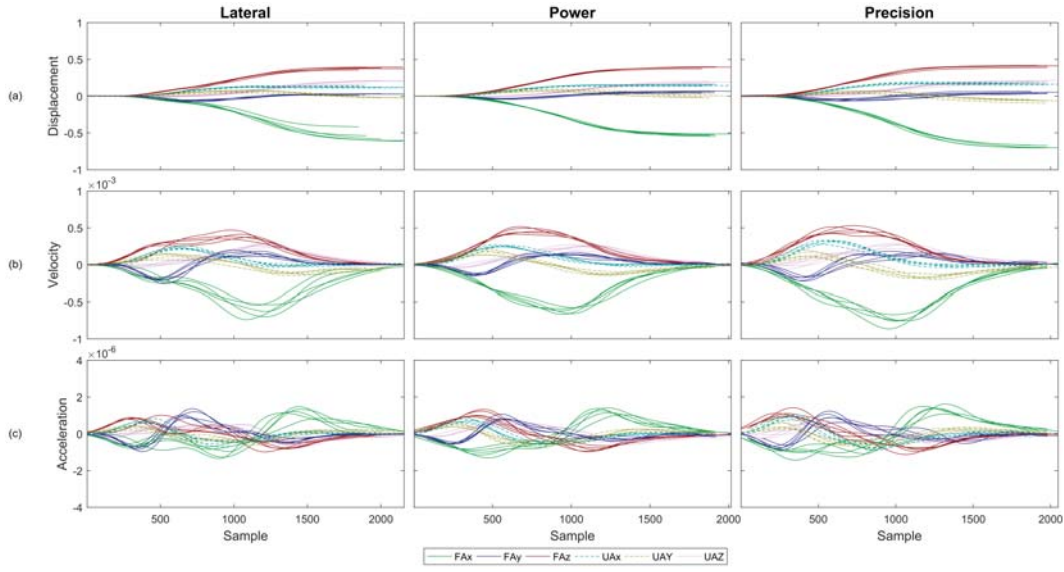


Figure 5.29: Quaternion vector (a) displacement, (b) velocity and (c) acceleration over time of *lateral*, *power* and *precision* grasps made on a box at a depth of 30 cm and angle of  $0^\circ$  at table height from a single amputee subject. The grasp profiles have been extracted from the 3 second trials, and have been aligned using cross-correlation. All three grasps have very similar reach trajectories, with Fx and Fz providing the largest change in motion. *Precision* grasps show slightly greater displacement in the negative direction, but upper arm motion looks to be very similar across all grasps.

Max(+):Fy and Max(+):Fz displacement has good discrimination between the *lateral* grasp and the other two grasps, however Max(+):Fy tends towards zero from  $-45^\circ$  to  $+45^\circ$ , having considerable overall variance across object locations. Max(+):Fz on the other hand remains reasonably invariant to changes in angular position and elevation, with the exception of grasps made at a descent. Max(+):Fx remains at approximately zero throughout all object locations, and only shows a marginal increase at a descent. Max(+) upper arm components have quite low discrimination overall.

Max(-):Fx shows good discrimination between all 3 grasps, having moderate invariance to change in angular position and elevation, with the exception of grasps made at a descent, with the separation between *precision* and the other two grasps being the most prominent. Max(-):Fy continues to have high variance with changes to angular position, and Max(-):Fz remains at approximately zero throughout. Max(-) upper arm components are affected strongly by a reduction in depth, and continue to have overall poor discrimination.

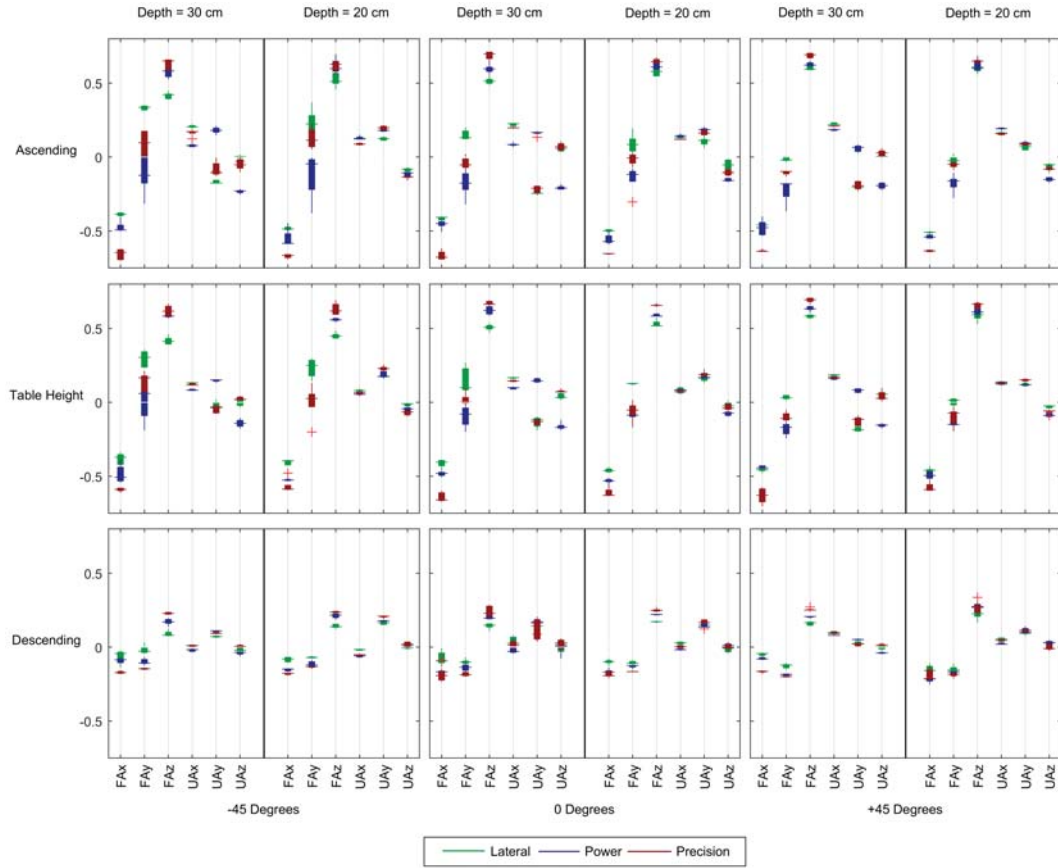


Figure 5.30: Example data from a single healthy subject comparing PoG displacement features across all elevation, depth and angular positions for *lateral*, *power* and *precision* grasps made on a box. The forearm and upper arm X,Y and Z components are represented by the terms FAx, FAy, FAz, UAx, UAy and UAz respectively. The main discrimination emphasis between the *lateral* and *precision* grasps are from forearm IMU components PoG:FAx and PoG:FAz, with PoG:FAy also showing reasonable discrimination across object locations. A reduction in object depth shows a reduction in the distinction between the grasps. Forearm features show greater separation between the three grasps at both depth positions in comparison to the upper arm features. Grasps made at a descending elevation shows greatly reduced displacement.

### 5.3.3.ii Displacement: Amputee

Example data from the amputee subject comparing the PoG displacement across all object locations when grasping a box is given in figure 5.31.

PoG:FAx shows good discrimination between *precision* and the other two grasps, having stronger individual discrimination at ascent in comparison to table height. Despite having low separation, the upper arm components do show some consistency between the three

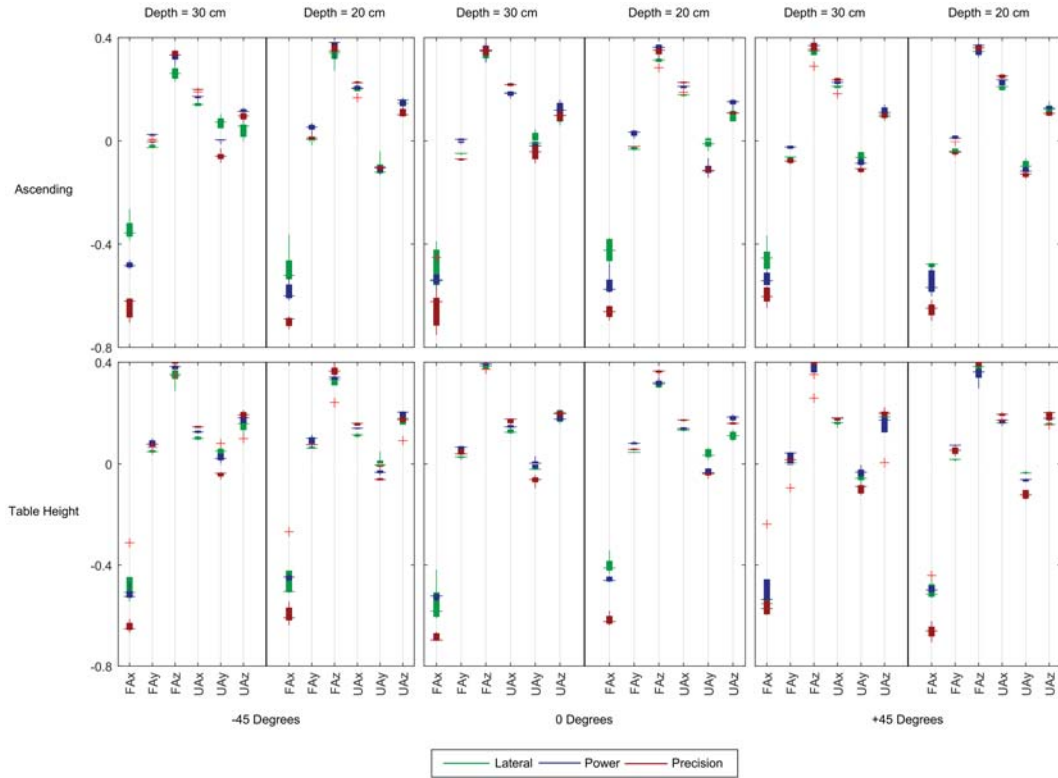


Figure 5.31: Example data from a single amputee subject comparing PoG displacement features across all elevation, depth and angular positions for *lateral*, *power* and *precision* grasps made on a box. The forearm and upper arm X,Y and Z components are represented by the terms FAx, FAy, FAz, UAx, UAy and UAz respectively. PoG:FAx shows good discrimination between *precision* and the other two grasps, having stronger individual discrimination at ascent in comparison to table height. Despite having low separation, the upper arm components do show some consistency between the three grasps.

grasps, however due to the proximity of the PoG displacement magnitudes between them, even minor variance across object locations can have a large effect on their overall discrimination.

Some individual grasp discrimination can be seen from Max(+):UAx however is affected by high variance due to changes in elevation. Other components also suffer from high variance across object locations relative to the poor discrimination between grasps. Max(-):FAx shows good discrimination between grasps, especially *precision* across all object locations. *Lateral* and *power* Max(-) displacement magnitude tend to merge at table height, greatly lowering their discriminatory power overall.

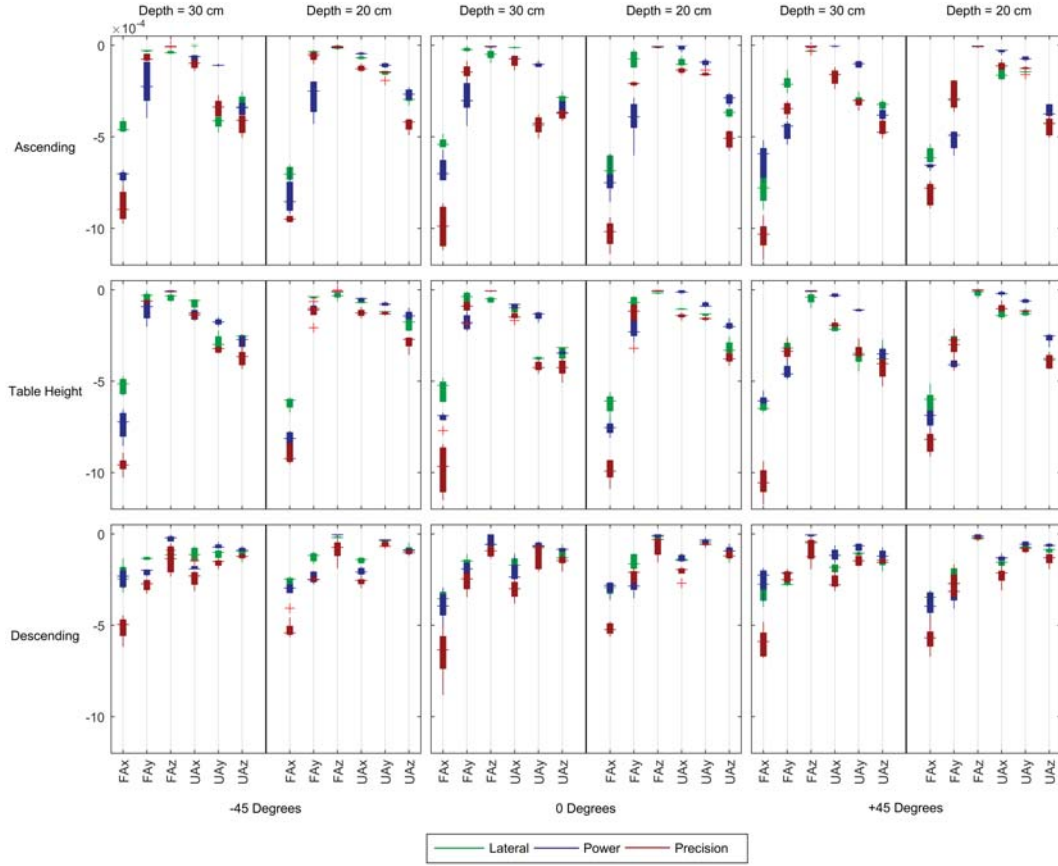


Figure 5.32: Example data from a single healthy subject comparing Max(-) velocity features across all elevation, depth and angular positions for *lateral*, *power* and *precision* grasps made on a box. The forearm and upper arm X,Y and Z components are represented by the terms FAX, FAY, FAZ, UAX, UAY and UAZ respectively. Max(-):FAY provides the largest discrimination and the least variance between the 3 grasps of the forearm components, with the separation of *precision* grasp being the most prominent. Max(-):FAY has higher variation from  $-45^\circ$  to  $+45^\circ$ , whereas Max(-):FAZ shows overall very poor discrimination. Upper arm components show lower discrimination between the grasps, but show stronger separation between the *power* grasp and the other two, with Max(-):UAY being the strongest component.

### 5.3.3.iii Velocity: Healthy

Example healthy subject data comparing Max(-) velocity across all object locations when grasping a box is given in figure 5.32.

Max(+):FAX provides overall poor discrimination between all three grasps, however Max(+):FAY and Max(+):FAZ velocity displays much stronger discrimination between *lateral* grasp and the other two, but has higher variance from  $-45^\circ$  to  $+45^\circ$ . Upper arm components have overall weak discrimination with the exception of Max(+):UAZ which shows

---

a stronger separation between *power* and the other two grasps. Grasps made at a descent have overall poor separation.

Max(-):FAy provides the largest discrimination and the least variance between the 3 grasps of the forearm components, with the separation of *precision* grasp being the most prominent. Max(-):FAy has higher variation from  $-45^{\circ}$  to  $+45^{\circ}$ , whereas Max(-):FAz shows overall very poor discrimination. Upper arm components show lower discrimination between the grasps, but show stronger separation between the *power* grasp and the other two, with Max(-):Uay being the strongest component. Grasps made at a descent continue to show low discrimination across all Max(-) features with the exception of Max(-):FAx which separates *precision* grasps more effectively, however their lower magnitude will clash with features from other grasps with changes in elevation.

Mean velocity forearm components show good discrimination at individual locations, with Mean:FAx having the least variance across multiple locations. Upper arm features provide poorer discrimination between grasps. *Power* grasps at a depth of 30 cm have good separation for Mean:Uay and Mean:UAz features, however it is greatly reduced at a depth of 20 cm. Grasps made at a descent show a decrease in overall magnitude and discrimination across all Mean features.

RMS velocity features provides relatively good discrimination at some locations however it varies greatly between grasps. RMS:FAx has the most consistent separation between the three grasps with *precision* having the highest discrimination. Upper arm features have much lower discrimination in comparison, with *power* grasps having the highest separation, and RMS:Uax having the least variance. RMS:Uay has a high variance due to changes in angular location, and RMS:UAz is subject to higher variance with changes in object depth. Grasps made at a descent have lower RMS velocity magnitude across all features, and have a reduction in discrimination with the exception of FAX, which still retains a good separation between *precision* and the other two grasps.

PK-RMS velocity features across both forearm and upper arm vector components have relatively high variance, and poor discrimination across all object locations.

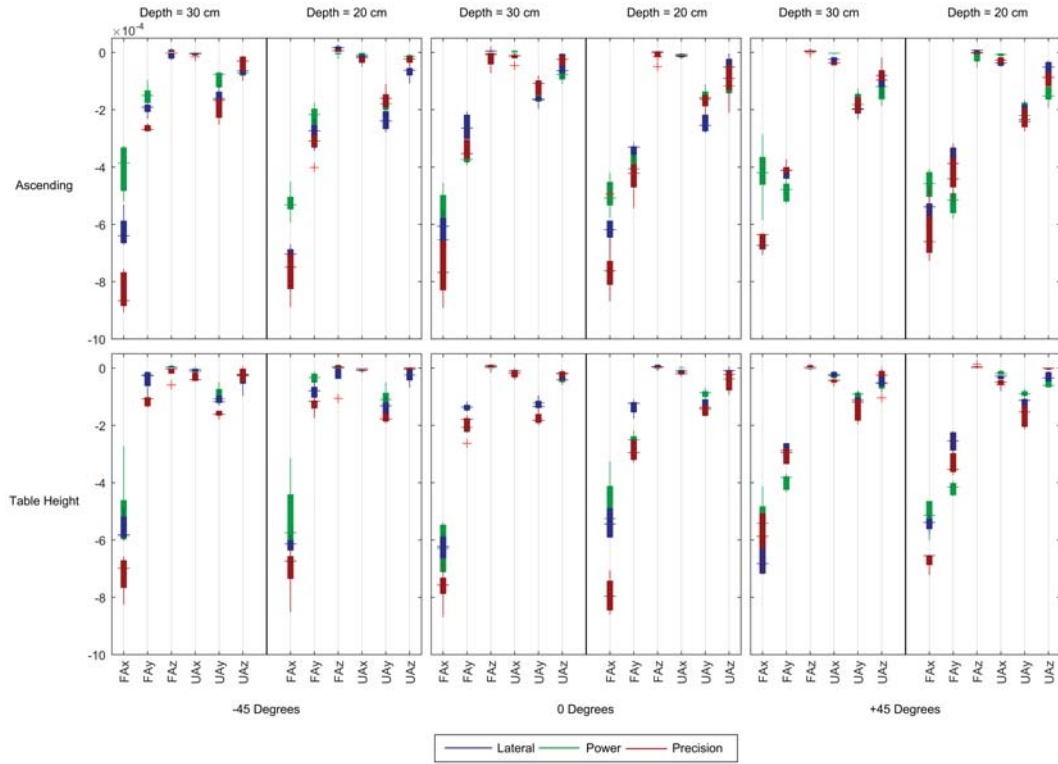


Figure 5.33: Example data from a single amputee subject comparing Max(-) velocity features across all elevation, depth and angular positions for *lateral*, *power* and *precision* grasps made on a box. The forearm and upper arm X,Y and Z components are represented by the terms FAx, FAy, FAz, UAx, UAy and UAz respectively. Max(-) upper arm vector features have poor separability, and forearm features Max(-):FAy has high variance across changes in depth and angular position, while Max(-):FAz remains at approximately zero throughout.

#### 5.3.3.iv Velocity: Amputee

Example data from the amputee subject comparing the Max(-) velocity across all object locations when grasping a box is given in figure 5.33.

Max(+) velocity features show some individual grasp discrimination at some object locations, however all vector components are subject to high variance, with the majority of object locations providing poor discrimination between grasps. Max(-) upper arm vector features have poor separability, and forearm features Max(-):FAy has high variance across changes in depth and angular position, while Max(-):FAz remains at approximately zero throughout. Max(-):FAx velocity, like its displacement features, has better discriminatory power than the other vector components, however is subject to some variance across changes in elevation.

---

RMS:FAx shows better grasp separation overall, with better discrimination between *lateral* grasps at ascent, and *precision* grasps at table height. The other forearm vector components show weaker discrimination and higher variance, along with the upper arm RMS velocity features. Mean:FAx shows a similar pattern, having stronger discriminatory power than the other mean velocity vector components. Minimal discrimination can be seen in upper arm mean velocity features however due to the proximity between their magnitudes, they are easily affected by variance.

PK-RMS shows poor discrimination and high variance between grasps across all object locations.

### 5.3.3.v Acceleration: Healthy

Example healthy subject data comparing the P2P acceleration across all object locations when grasping a box is given in figure 5.34.

Max(+) forearm and upper arm acceleration features have very high variance, making the grasps very difficult to discriminate. Max(+):FAx has better separation of *precision* grasps, and Max(+):FAz and Max(+):UAz has better separation of *power* grasps at individual object locations. Grasps made at a descent have poor discrimination across all features.

Max(-):FAx and Max(-):FAz show better separation of *lateral* grasps and Max(-) upper arm features show better separation of *power* grasps with relatively low variance. Grasps made at a descent decreases discrimination across all features.

RMS:FAx shows good discrimination between all three grasps, however is subject to variance with changes in object depth. RMS upper arm acceleration features generally shows better separation between *power* grasps despite having lower overall discrimination. Grasps made at a descent enhances the separation of *precision* grasps, however the overall discrimination across all features is still low.

P2P:FAx shows overall better discrimination between all three grasps than the other features, with the separation of *precision* grasps being the most prominent, however is subjected to higher variance with changes in object depth. P2P upper arm features show better separation of *power* grasps, however the overall grasp discrimination is still fairly low, not



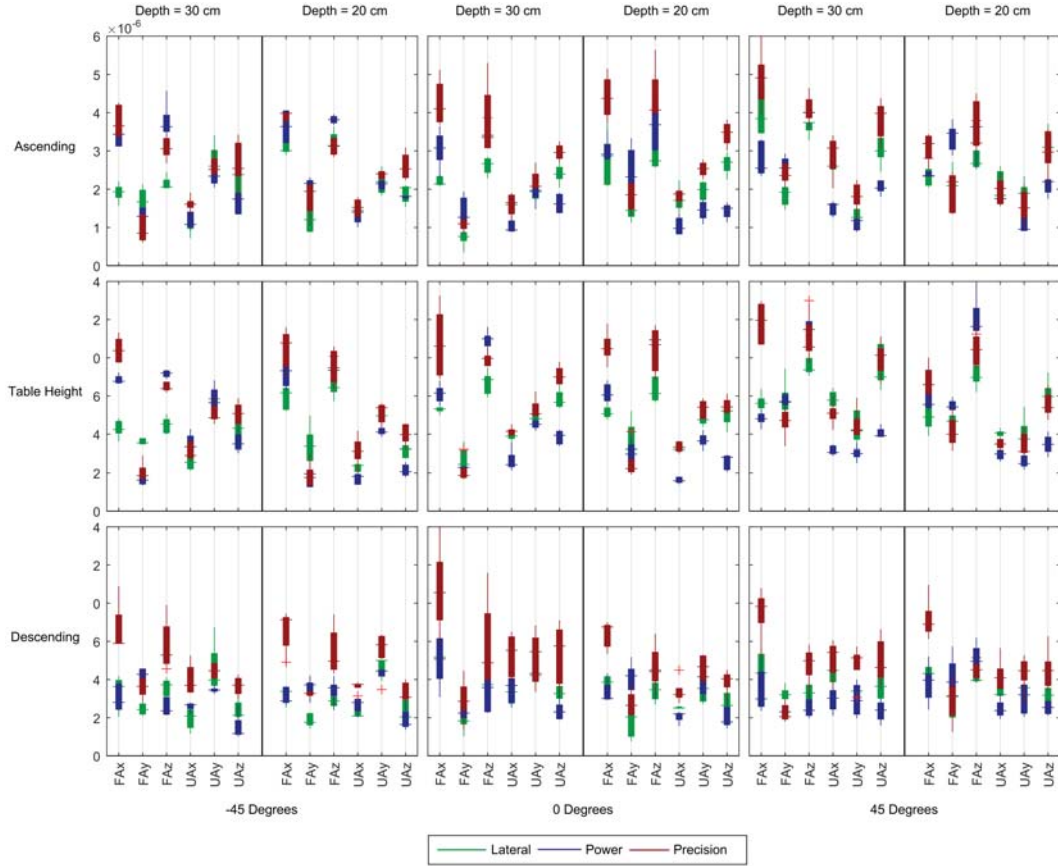


Figure 5.34: Example data from a single healthy subject comparing P2P acceleration features across all elevation, depth and angular positions for *lateral*, *power* and *precision* grasps made on a box. The forearm and upper arm X,Y and Z components are represented by the terms Fx, Fy, Fz, Ux, Uy and Uz respectively. P2P:Fx shows overall better discrimination between all three grasps than the other features, with the separation of *precision* grasps being the most prominent, however is subjected to higher variance with changes in object depth. P2P upper arm features show better separation of *power* grasps, however the overall grasp discrimination is still fairly low, not giving much room for variance due to changes in object location. Grasps made at a descent show overall better separation between *precision* grasps, however show overall lower discriminatory power.

giving much room for variance due to changes in object location. Grasps made at a descent show overall better separation between *precision* grasps, however show overall lower discriminatory power.

PK-Dist and PK-RMS velocity features across both forearm and upper arm vector components have relatively high variance, and poor discrimination across all object locations.



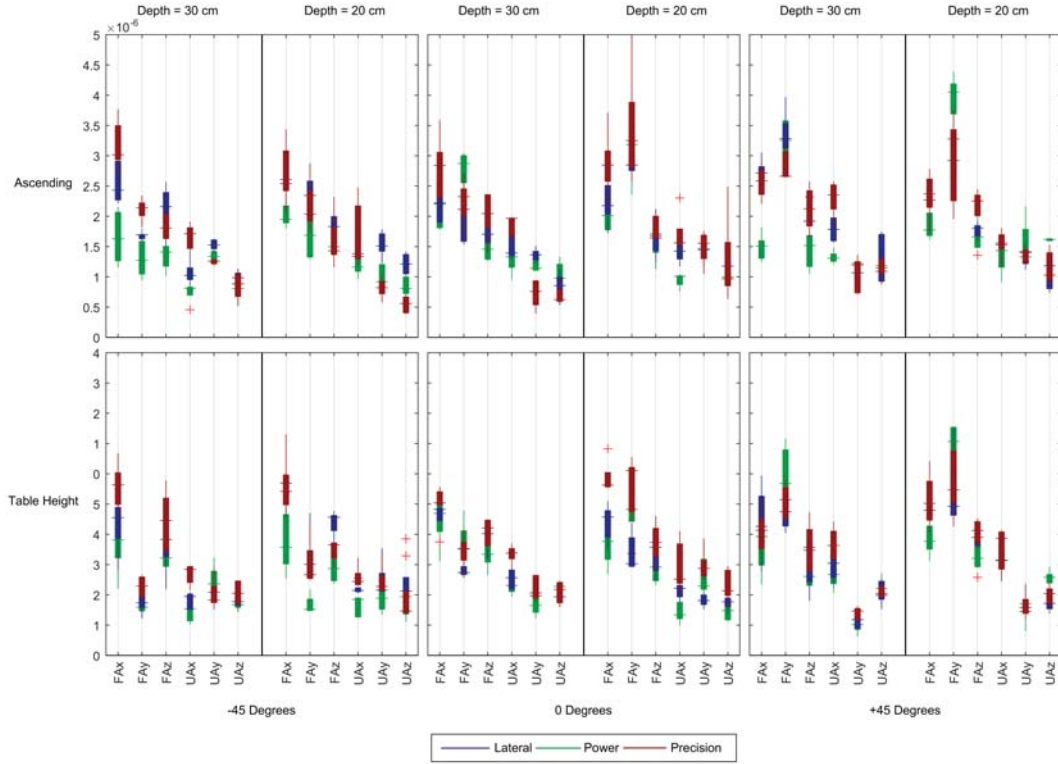


Figure 5.35: Example data from a single amputee subject comparing P2P acceleration features across all elevation, depth and angular positions for *lateral*, *power* and *precision* grasps made on a box. The forearm and upper arm X,Y and Z components are represented by the terms FAX, FAY, FAZ, UAX, UAY and UAZ respectively. P2P acceleration features show poor discrimination between grasps and high variance across all object locations.

### 5.3.3.vi Acceleration: Amputee

Example data from the amputee subject comparing the P2P acceleration across all object locations when grasping a box is given in figure 5.35.

All acceleration features shows poor discrimination between grasps and high variance across all object locations, showing similar results to grasps made on the lid. Like grasping the lid, lower overall acceleration minimises the difference in feature magnitude between the grasps. This increases the effect that variance has, greatly decreasing discriminatory power.

---

## 5.4 Feature Selection

The total of all displacement, velocity and acceleration features studied amount to 84, and it is evident that some features are more useful than others in terms of their overall discrimination between grasps for that particular object as well as their invariance across different object locations. With such a high number of features, it is essential to reduce the dimensionality to improve the efficiency and effectiveness of classification algorithms.

In order to find the minimum number of required features for classification, a sequential feature selection method is used. This involves the creation of candidate feature subsets by sequentially adding each feature in turn, and performing leave-one-out cross-validation using a criterion defined by a KNN classifier, which uses a Euclidean distance metric to measure feature performance. A KNN classifier is chosen as it allows better classification of subgroups within the data set such as grasps made at a descent, where feature values are generally much lower in magnitude compared to those made at other elevations. The data is first partitioned into different training subsets using leave-one-out, which is a special case of k-fold, where the number of folds is equal to the number of observations. A leave-one-out approach was used due to the possibility of multiple clusters of features forming as a result of differences in object location within the workspace. This method ensures that there is enough training data within each of the possible feature clusters. The criterion returned by the classifier is summed and divided by the number of observations, which is used to evaluate each candidate feature subset by adding features one by one based on the minimisation of the mean criterion value, in this case the error rate. The error rate is estimated as the average error rate of all the folded partitions according to equation 5.26, where  $E$  is the true error rate,  $K = N$  is the number of folds (where  $N$  is the total number of samples), and  $E_i$  is the error rate for fold  $i$ .

$$E = \frac{1}{N} \sum_{i=1}^N E_i \quad (5.26)$$

A total of 10 features are selected, and ordered in ascending error rate. These are taken and scored according to the order they are selected through forward sequential feature selection. The feature selected is issued a score given by equation 5.27, where  $R$  is its position in

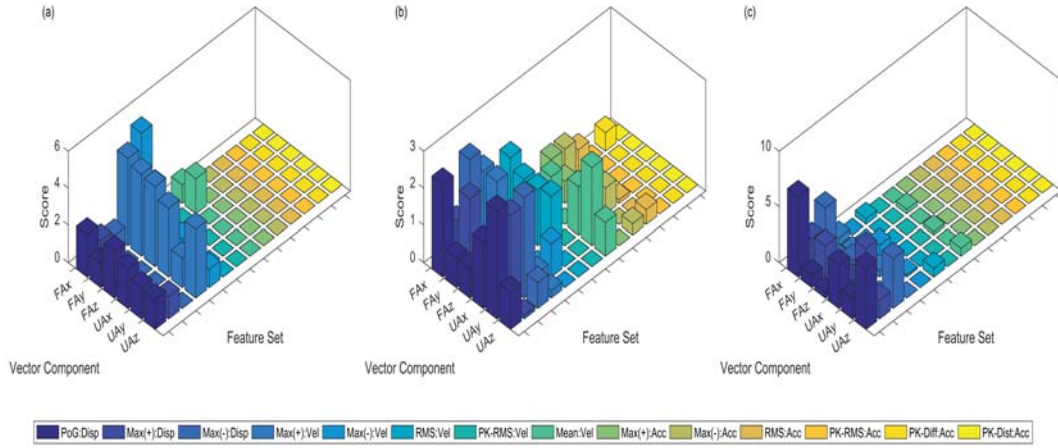


Figure 5.36: Cumulative feature scores of all subjects for grasping a (a) bottle with *lateral* and *power* grasps, where Max(+) velocity features performed the best across all forearm and upper arm vector components, however Max(-):FAx Velocity had the highest score overall; (b) lid with *lateral* and *precision* grasps, where forearm and upper arm vector components are spread more evenly, with the strongest performing feature being PoG:UAY displacement, closely followed by Max(-):UAY displacement; and (c) box with *lateral*, *power* and *precision* grasps across all object locations, where the displacement profile had the strongest scores all round, with PoG:FAx being the strongest, while velocity profile features show overall poor performance, and acceleration profile features scored zero across all feature sets.

the ordered selection, and  $S_c = 1$  is the maximum initial score. The mean scores are then calculated across all subjects.

$$S = S_c - 0.1(R - 1) \quad (5.27)$$

Feature scores for healthy subjects interacting with a bottle are shown in figure 5.36 (a). Max(+) velocity features performed the best across all forearm and upper arm vector components, however Max(-):FAx Velocity had the highest score overall of 5.5. Forearm features performed better overall than upper arm features when comparing the scores across the strongest features: Max(+):VEL, Max(-):VEL, PoG:DISP and Max(+):DISP. Velocity features performed the best out of all 3 motion profiles, whereby acceleration features didn't have any scoring features across all subjects. The rounded average number of features selected before reaching the minimum misclassification rate is 3. Feature scores for the amputee subject interacting with a bottle are shown in figure 5.37 (a). Grasp classification between *lateral* and *power* grasps on the bottle were so strong that it only required a

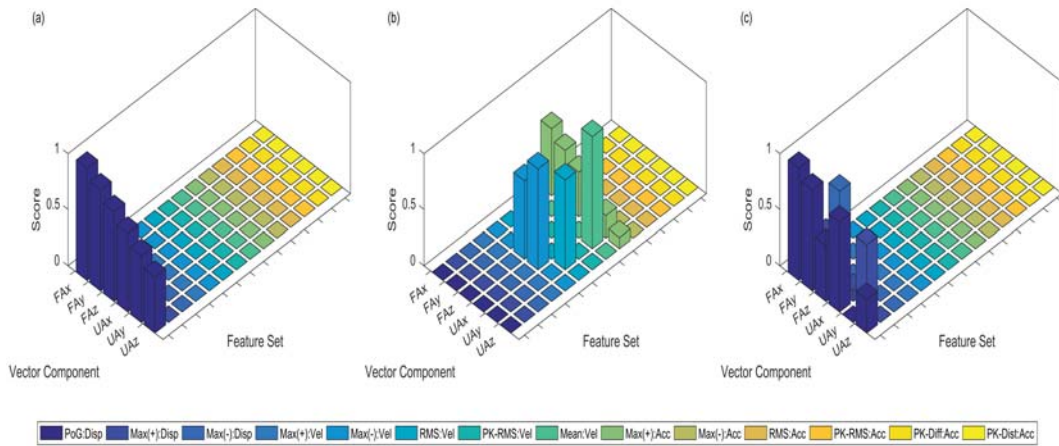


Figure 5.37: Feature scores of a single amputee subject for grasping a (a) bottle with *lateral* and *power* grasps, where discrimination was so strong that it only required a single displacement feature, PoG:FAx, to distinguish between the two grasp patterns; (b) lid with *lateral* and *precision* grasps, where upper arm velocity features appeared to provide the strongest separation; and (c) box with *lateral*, *power* and *precision* grasps across all object locations, where displacement features were the best performing, with PoG:FAx providing the best discrimination.

single displacement feature, PoG:FAx, to distinguish between the two. Moreover, multiple features have very high discriminatory power between the bottle's two grasps.

Feature scores for healthy subjects interacting with a lid are shown in figure 5.36 (b). It is evident from the larger spread of scoring features that grasp discrimination is much more subject-specific. Forearm and upper arm vector components are spread more evenly, with the strongest performing feature being PoG:UAY displacement, closely followed by Max(-):UAY displacement with scores of 2.9 and 2.7 respectively. Upper arm vector component UAY performed the best, having high scores in all displacement profile features, but is closely followed by PoG:FAx displacement. Displacement features provide the strongest overall performance compared to those of velocity and acceleration profiles. The rounded average number of features selected before reaching the minimum misclassification rate is 6. Feature scores for the amputee subject interacting with a lid are shown in figure 5.37 (b). Upper arm velocity features appeared to provide the strongest separation between *lateral* and *precision* grasps, only requiring a total of 3 features to reach the minimum misclassification rate, despite the similarity in trajectory between the two. Surprisingly, Max(+) acceleration vector component features showed some value in discriminating between the

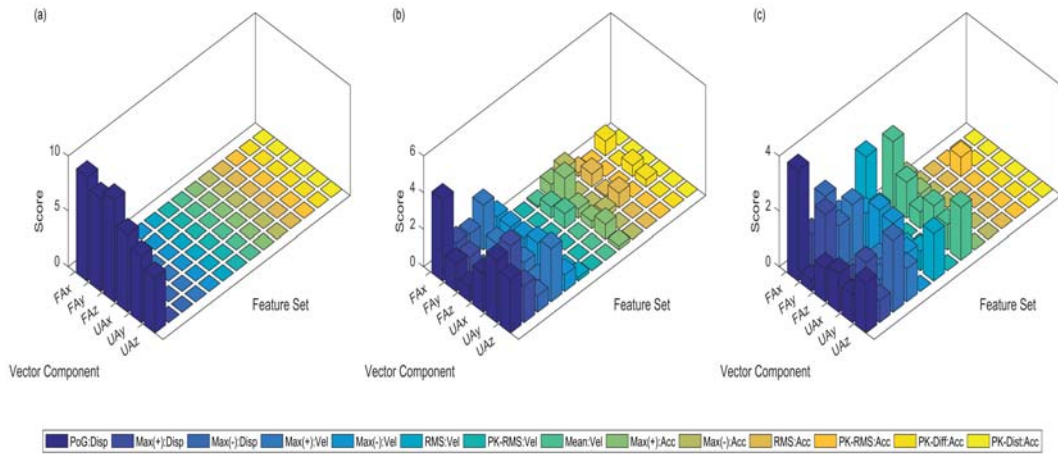


Figure 5.38: Cumulative feature scores of all healthy subjects at table height and ascending elevation for grasping a (a) bottle with *lateral* and *power* grasps, where PoG displacement providing the largest discrimination between the two; (b) lid with *lateral* and *precision* grasps, where displacement features show stronger discrimination, with velocity features still playing an important role in classification; and (c) box with *lateral*, *power* and *precision* grasps, where displacement features are the most prominent, with velocity features also playing a large role in grasp discrimination.

two grasps, however it must be noted that the minimum misclassification rate had already been reached before they were added through sequential feature selection.

Feature scores for healthy subjects interacting with a box are shown in figure 5.36 (c). The displacement profile had the strongest scores all round, with a top score of 7.2 for PoG:FAX. Velocity profile features show overall poor performance, and acceleration profile features scored zero across all feature sets. Despite the top score being taken by a forearm vector component, upper arm vector components scored higher overall. The rounded average number of features selected before reaching the minimum misclassification rate is 9. Feature scores for the amputee subject interacting with a box are shown in figure 5.37 (c). Displacement features were the best performing, with the PoG:FAX providing the best discrimination between *lateral*, *power* and *precision* grasps. Feature scores showed similarities to those of healthy subjects where displacement features were also more dominant, and both having the same top performing feature, PoG:FAX. Sequential feature selection required 7 features overall to reach the minimum misclassification rate.

As observed in the feature data, grasping objects at a descent has a much different grasp trajectory in comparison to grasps made at table height or ascending. Restricting object

---

interaction to above the waist produces a different set of features during forward sequential feature selection, as shown in figure 5.38. These features can be directly compared to those of amputee subjects as they cover the same object locations. Comparing feature selection for the bottle, (a) in both figures, it can be seen that the results are very similar, with both healthy and amputee feature data having PoG displacement providing the largest discrimination between the two grasps, and the forearm features being the most informative. PoG features from healthy subjects require between one and two features before reaching the minimum misclassification rate. Comparing the most prominent features for grasping a lid in (b), the healthy subject data shows stronger displacement features, however velocity features still play an important role in classification. Healthy subject data also contains scores for some acceleration features, in particular Max(+):ACC, which also scores in amputee data. Comparing grasp features on the box in (c) for healthy and amputee subject data, it can be seen that in both cases, displacement features are the most prominent, with velocity features also playing a large role in grasp discrimination in healthy subjects. It must be noted that data from only one amputee subject is available, and that a greater number of subjects would be more ideal to compare both demographics.

## 5.5 Grasp Classification

In order to evaluate and test the performance of motion features for grasp prediction, a few well known classifiers will be compared, using the minimum number of features that provide the least misclassification rate according to the forward sequential feature selection method described previously. Features used for classification are selected based on the individual's highest scoring features. Subject data is leave-one-out cross-validated, where the cross-validation loss is compared across different classifiers. K-nearest neighbors (KNN), linear discriminant analysis (LDA), quadratic discriminant analysis (QDA), decision trees (DT) and support vector machines (SVM) classifiers are compared, and are firstly introduced in the following sections.

---

## 5.5.1 Background: Classifiers

### 5.5.1.i K-Nearest Neighbours (KNN)

One of the simplest classifiers is the *nearest neighbour* classifier, which uses the minimum distance between points in Euclidean space. Assuming the signals to be made up of feature points in N-dimensional Euclidean space, the straight line distance between points can be defined as the Euclidean Distance. The Euclidean distance between unknown vector  $\bar{a}$  and template vector  $\bar{b}_m$ , where  $m = 1, 2, \dots, M$  can be calculated by equation 5.28.

$$d(\bar{a}, \bar{b}_m) = \|\bar{a} - \bar{b}_m\|^2 \quad (5.28)$$

The *nearest neighbour* classifier finds the neighbour with the shortest Euclidean distance away from the unknown vector  $\bar{a}$  from the template vector set  $\bar{b}_m$  of length  $M$ .  $\bar{a}$  is classified according to the class label of that neighbour from the template. Depending on the application, it can be useful to use more than a single neighbour to find an appropriate class label, up to  $k$  nearest neighbours. Although very simplistic in approach, it is also very effective, especially where classes can be split into multiple groups.

### 5.5.1.ii Discriminant Analysis

Discriminant analysis is a type of classifier derived from the approximation of the Bayes' rule, given by equation 5.29, which estimates the posterior probability,  $P(k | x)$ , that an observation  $x$  is of class  $k$ . The class conditional distribution of the data is denoted  $P(x | k)$ , and  $P(k)$  is the prior probability for each class  $k$ , where  $P(x)$  is a normalisation constant.

$$P(k | x) = \frac{P(x | k) P(k)}{P(x)} = \frac{P(x | k) P(k)}{\sum_l P(x | l) P(l)} \quad (5.29)$$

Linear and quadratic discriminant analysis, denoted by LDA and QDA respectively, makes the assumption that each class generates data based on a multivariate normal distribution,



---

where the density function can be described by equation 5.30.

$$P(x | k) = \frac{1}{(2\pi |\Sigma_k|)^{1/2}} \exp \left( -\frac{1}{2} (x - \mu_k)^T \Sigma_k^{-1} (x - \mu_k) \right) \quad (5.30)$$

For LDA, each class  $k$  has its own mean  $\mu_k$ , but shares a common covariance  $\Sigma_k$  at a point  $x$ , which leads to linear decision boundaries. QDA on the other hand makes no assumptions about the covariance matrices, so that each class can have its own mean and covariance matrix, which leads to quadratic decision boundaries.  $|\Sigma_k|$  denotes the determinant of  $\Sigma_k$ , and  $\Sigma_k^{-1}$  is the inverse matrix. An unknown observation  $x$  is classified as  $\hat{y}$  so as to minimise the expected classification cost according to equation 5.31, where  $K$  is the number of classes,  $C(y | k)$  is the cost of classifying an observation incorrectly, and  $\hat{P}(k | x)$  is the posterior probability of class  $k$  for observation  $x$ .

$$\hat{y} = \arg \min_{y=1, \dots, K} \sum_{k=1}^K P(x | k) C(y | k) \quad (5.31)$$

### 5.5.1.iii Decision Trees

Decision trees (DT), also known as regression or classification trees is a very simple method for classifying grasps based on individual feature values. Each tree consists of a series of *branches*, starting at the *root* node, and moving down towards a *leaf* node, which contains the classification response. Each intermediary node acts as a binary separator, checking the value of a single feature variable against a value based on template data. Depending on the feature value, the observation moves down one of two branches, reaching another node further down the tree. This process repeats until the observation reaches a leaf node, which results in an output class decision.

The DT is created using the standard CART algorithm [189], which examines all possible binary splits for every feature, selecting a split with the best optimisation criterion, in this case, the mean-squared error (MSE). This is repeated recursively for the two branch nodes until the node contains only observations of one class, resulting in a leaf node, and therefore a classification result. Figure 5.39 shows an example decision tree using the data an amputee subject when grasping a lid with *lateral* and *precision* grasps.



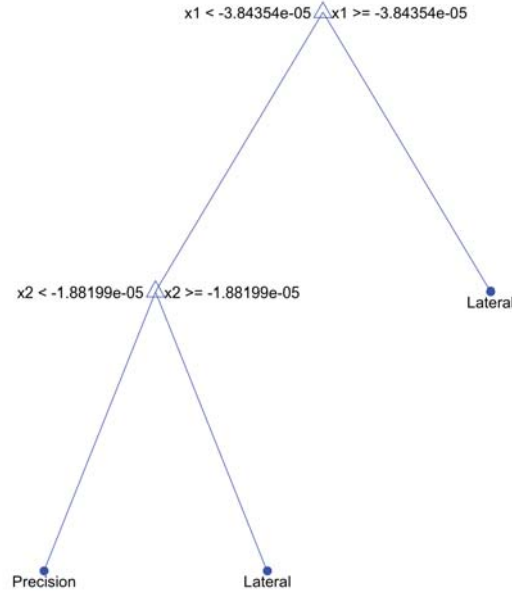


Figure 5.39: Example decision tree for an amputee subject when grasping a lid, where  $x_1$  and  $x_2$  represent different features. Triangular nodes represent a *branch*, and a circular node represents a *leaf*.

#### 5.5.1.iv Support Vector Machine

Support Vector Machine (SVM) is a supervised machine learning algorithm, which classifies an observation using a hyperplane that segregates two different classes. The hyperplane can be described as the boundary that leaves the greatest margin between the two classes, where the margin can be defined as the sum of distances to the hyperplane of the closest points (known as support vectors) between the two classes [190]. Considering just a simple case of a linearly separable binary classification problem, the hyperplane can be described by a straight line using equation 5.32, where  $w$  is the normal to the hyperplane, and  $\frac{b}{||w||}$ .

$$wx + b = 0 \quad (5.32)$$

A training data set  $x_i, y_i$  of length  $L$ , which is of one of two classes  $y_i \in -1, 1$  can be defined. The training set can be used to find  $w$ , given by equation 5.33, where  $\alpha_i \geq 0 \forall_i$  represents a Lagrange multiplier, which can be found by performing quadratic programming

---

optimisation.

$$w = \sum_{i=1}^L \alpha_i y_i x_i \quad (5.33)$$

The set of support vector indices denoted by  $S$  can be determined by finding the indices  $i$  where  $\alpha_i > 0$ . Taking the average over all support vectors in  $S$ ,  $b$  can be calculated by equation 5.34 [191].

$$b = \frac{1}{N_s} \sum_{s \in S} \left( y_s - \sum_{m \in S} \alpha_m y_m x_m x_s \right) \quad (5.34)$$

Although SVM is traditionally used for only binary classification, there are methods available that use the same approach when confronted with a multi-class classification problem. Error-Correcting Output Coding (ECOC) converts the  $F$  class problem into  $N$  number of 2-class problems, where each class is assigned a unique code word. The coding design determines which classes the binary learners train on, whereby each unknown observation is assigned the class  $\hat{k}$ , which minimises the aggregation of the losses for the  $N$  binary learners, given by equation 5.35.

$$\hat{k} = \arg \min_k \frac{\sum_{n=1}^N |m_{kn}| g(m_{kn}, s_n)}{\sum_{n=1}^N |m_{kn}|} \quad (5.35)$$

Where  $M$  is the coding design matrix of elements  $m_{kn}$ , and  $S_n$  is the predicted classification score for the positive class of learner  $n$ , where the decoding scheme uses a loss of  $g$ . The coding scheme used for comparison uses a one-versus-one design, whereby for each binary learner, one class is positive, one class is negative, and the rest are ignored, and uses a number of learners equal to  $N = K(k-1)/2$ .

### 5.5.2 Classifier Comparison

The mean misclassification rate across all 10 healthy subjects is given in figure 5.40 (a), which compares KNN, LDA, QDA, DT and SVM classifiers for grasps made across all object locations. Overall, the KNN classifier performed the best across all objects, while SVM performed the worst. The mean misclassification rate for classifying grasps for a bottle, lid and box are 3.83%, 23.03% and 13.59% respectively. Although the KNN classifier produces relatively low misclassification rates for classifying grasps on objects, they are

still high enough to cause an impact in real-time implementation. *Lateral* and *power* grasps made on a bottle have a much different forearm orientation and grasping trajectory, so a misclassification rate of 0% was expected. The high variance of observation features due to changes in object location greatly affects the misclassification rate. In particular, through previous observations, grasps made at descent causes difficulties in grasp classification due to the greatly reduced magnitude in trajectory features, forming multiple clusters for each grasp pattern. The classification accuracy of the KNN approach can be improved by increasing the number of feature points within the classifier template, as well as the number of object locations tested, however there is a high risk of different grasp clusters merging, as in the case of grasps made at a descent. This is evident from the presence of a misclassification rate greater than 0% from Bottle data, as the two grasp patterns are very different in terms of orientation.

With the descending object locations removed in 5.40 (b), it can be seen that the classification accuracy improves across all classifiers, with the misclassification rate for grasps made on the bottle being reduce to 0% using the KNN classifier. Mean misclassification rates for the lid and box objects are also reduced to 18.35% and 11.51% respectively.

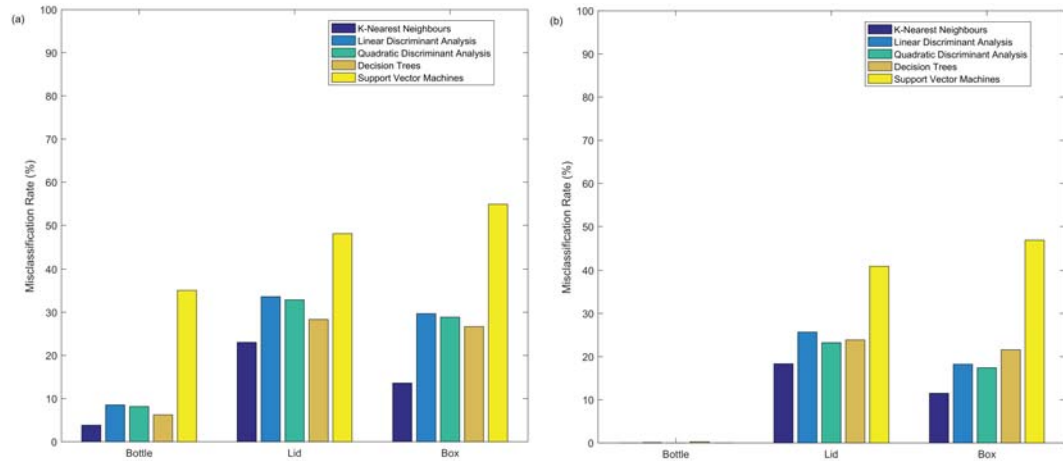


Figure 5.40: Comparison of mean misclassification rates for 10 healthy subjects for bottle, lid and box objects across (a) all object locations and (b) all object locations at ascending and table height only. The KNN classifier performed the best across all objects, with a mean misclassification rate of 3.83%, 23.03% and 13.59% at all object locations, and 0%, 18.35% and 11.51% at just table height and ascending elevations for the bottle, lid and box respectively, while SVM performed the worst.

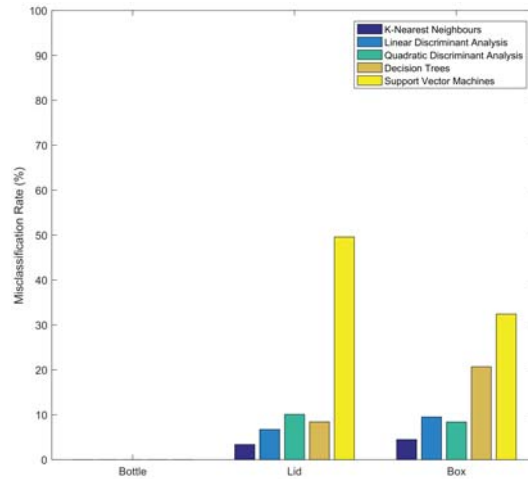


Figure 5.41: Comparison of misclassification rates for a single amputee subject for bottle, lid and box objects for grasps made at all object locations at ascending and table height. The KNN classifier performed the best across all objects, with a mean misclassification rate of 0%, 3.36% and 4.47%, while SVM performed the worst.

Comparing the misclassification rates to those taken from the amputee subject given in figure 5.41, it can be seen that amputee grasp classification performs better than the average healthy subject, with lid and box misclassification rates being considerably lower at 3.36% and 4.47% respectively. Combining the results across both demographics yields an average classification accuracy rate of 100%, 82.46% and 88.88% for bottle, lid and box objects respectively.

## 5.6 Discussion

To summarise, forearm and upper arm trajectories for grasping three different objects with various grasp patterns were studied: *lateral* and *power* grasps on the bottle, *lateral* and *precision* grasps on the lid, and *lateral*, *power* and *precision* grasps on the box. The objects were chosen to emulate common day-to-day object interactions, with each object focusing on testing different combinations of motion. Each object was grasped at a variety of locations within a subject's immediate reaching workspace, looking at how changes in an object's angular position, depth and elevation affect the arm's trajectory when interacting with an object in different ways. By studying various underlying features within the motion of the arm during grasp, it has been found that the grasp intention on an object can be

---

predicted.

The bottle considered two very different grasps patterns, which are approached very differently in terms of arm orientation for two very different purposes; a *power* grasp for a stable and strong grasp around the bottle's centre for transportation, and a *lateral* grasp for lid removal. The aim was to measure the separability of two very different grasps to look for any factors which could still affect discrimination. Results showed very strong grasp separation resulting in 0% or near 0% grasp misclassification, however it was found that a reduction of accuracy was caused by the discrepancy among grasps made below the waist. Grasps made on objects below the waist (at descent) for healthy subjects show a large reduction in displacement magnitude, and therefore motion specific features. This reduction in displacement led to the formation of multiple clusters of features within the overall data. Comparing grasps made at ascent and at table height, the changes in trajectory were much less noticeable. Removing feature data from grasps made at descent reduced the misclassification rate between grasps across all 3 objects. Changes in angular position and depth produced much less variance overall, with some vector components being affected more than others.

The lid looked at two fundamentally different grasps, both of which can have a much more similar approach. Both grasps had a more generalised purpose behind them, for pick-and-place applications. Although a healthy subject has no problem with grasping objects for pick-and-place intention in numerous ways, an amputee subject using a myoelectric prosthesis has much fewer options available. The aim for this object was to look at the consistency of grasp; whether two grasps that are similar in approach but different in contact can still be distinguishable from each other. Overall, grasp discrimination showed good results with the amputee subject, however healthy subjects showed much lower classification accuracy. Although restrictions were made in terms of the grasp pattern, and a wrist splint being used to reduce wrist flexion/extension, it is evident that the freer range of motion gives leeway for much greater variance in arm trajectory. The amputee subject using a transradial prosthesis has much greater restriction of movement. With no rotation in the forearm, and the incapability of fine adjustments in hand position on object contact means much less

flexibility on the point of grasp. This results in lower variance among grasp trajectory from changes in object location, improving overall grasp discrimination.

The box tested the capability of discriminating between three different grasps, all of which are fairly similar in terms of motion. Two of the grasps, *lateral* and *power* are used for interacting with the box itself, and the *precision* grasp is used for interacting with any objects inside the box. The aim was to see if more than three grasps can be differentiated between in comparison to only two, like with the bottle and lid objects. The similarity of the grasp trajectories made them difficult to differentiate, especially from healthy subjects. The restrictions imposed on the amputee subject made the grasps easier to distinguish, as grasping the object with the prosthesis requires the arm's motion and position to be much more precise. Surprisingly, the average misclassification rate for the box is lower than that of the lid for healthy subjects. Thus, the classification success rate isn't dependent on the number of grasps available for each object, but depends mostly on the dissimilarity between the available grasps.

### 5.6.1 Subject-specific physiological motion

As hypothesised in the introduction of this chapter, arm motion may not only be influenced on different anatomical features, but may also be heavily dependent on an individual's neural motor control. Although the spread in the variety of features across subjects does suggest that the arm motion during reach of each subject is different, it is important to clarify this by identifying the statistical significance of the hypothesis. By also comparing healthy and amputee subject data together, the extent of which the two demographics differ in terms of arm motion can indicate whether either or both require subject specific template calibration.

	Bottle		Lid		Box		
	Lateral	Power	Lateral	Precision	Lateral	Power	Precision
<b>P-value</b>	$2.11e^{-10}$	$1.07e^{-5}$	$4.06e^{-9}$	$1.81e^{-10}$	$9.47e^{-14}$	$1.88e^{-9}$	$3.96e^{-10}$

Table 5.2: Summary of the average p-values yielded across all features for each object and grasp from a Kruskal-Wallis test. Each grasp for each object class rejects the null hypothesis that each set of subject samples come from the same distribution at a  $< 1\%$  significance level.

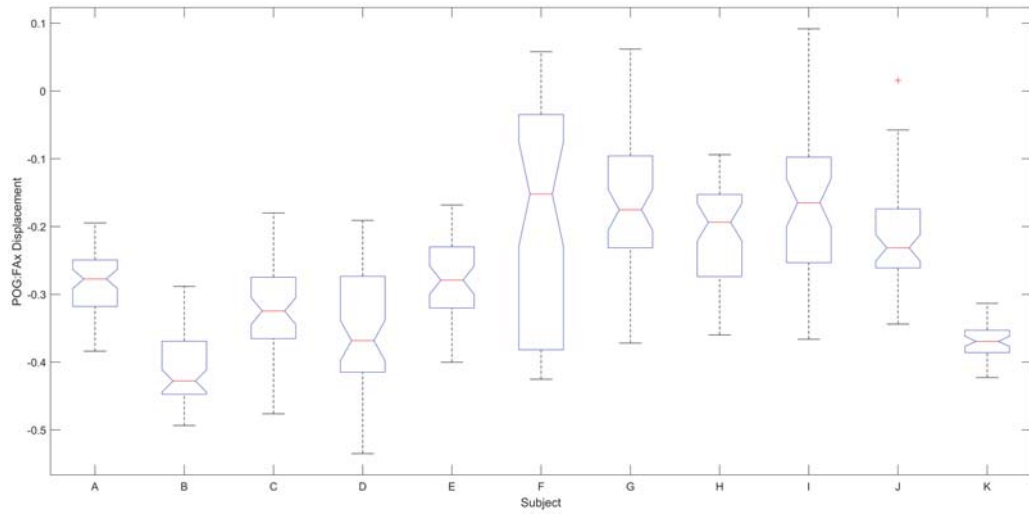


Figure 5.42: Comparison of individual subject POG:FAX displacement distributions for *lateral* grasps made on a bottle at table height and ascending elevation. The median and variance of the feature is considerably varied between subjects, provides evidence to suggest that the features are subject-specific.

Figure 5.42 displays the subject distribution of PoG:FAX displacement magnitude following a Kruskal-Wallis test for *lateral* grasps made on the bottle across all subjects, for all trials taken at table height and ascending elevation (for comparison between healthy and amputee demographics). It can be seen that the median and variance of the feature is considerably varied between subjects. The spread of medians of the POG:FAX magnitude range from -0.15 to -0.43, which is a considerable margin. The amputee subject (Subject K) shows a median magnitude of -0.37, at neither end of the spectrum. The distribution of values provides evidence to suggest that the features are subject-specific. This conclusion is reinforced by the resulting p-value of  $1.14 \times 10^{-54}$ , showing that the Kruskal-Wallis test rejects the null hypothesis that each set of subject samples come from the same distribution. Conducting the test on each individual feature yield similar results across each grasp and object. The average p-values from the Kruskal-Wallis test across all features for each grasp and object is given in table 5.2. Overall, each grasp for each object class rejects the null hypothesis at a  $< 1\%$  significance level. A complete table of individual feature p-values can be found in Appendix B. From the results of these tests, it is clear that identifying features for use across multiple subjects is a very difficult problem, as arm motion features between subjects are clearly from different distributions. This identifies the necessity for

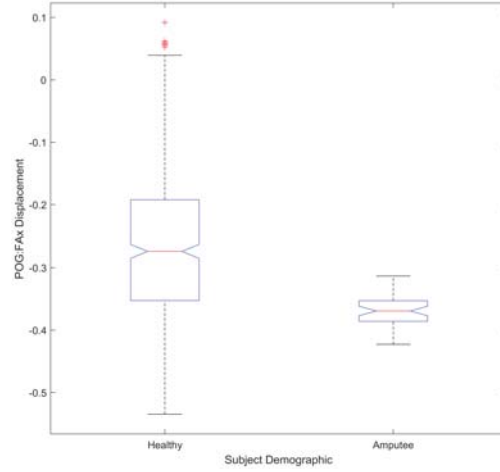


Figure 5.43: Comparison of healthy and amputee POG:FAX displacement distributions for *lateral* grasps made on a bottle at table height and ascending elevation. The Kruskal-Wallis test rejected the null hypothesis that POG:FAX displacement from both subject populations come from the same distribution. This suggests that subjects can be grouped according to these two demographics, however it must be noted that only a single amputee subject took part in the study.

subject-specific templates.

By splitting the data in terms of subject demographic (healthy and amputee populations), the null hypothesis that both subject populations come from the same distribution can be tested. Figure 5.43 shows the distribution of POG:FAX displacement between healthy and amputee demographics. The Kruskal-Wallis test yielded a p-value of  $4.96 \times 10^{-11}$ , rejecting the null hypothesis that POG:FAX displacement from both subject populations come from the same distribution. This suggests that subjects can be grouped according to these two demographics, however it must be noted that only a single amputee subject took part in the study. A greater number of amputee subjects are required to identify variance between individuals within that population. Conducting the test across all 84 features, for

	Bottle		Lid		Box		
	Lateral	Power	Lateral	Precision	Lateral	Power	Precision
P-value	$4.14e^{-2}$	$5.71e^{-2}$	$3.72e^{-2}$	$3.96e^{-2}$	$3.71e^{-2}$	$1.47e^{-2}$	$2.89e^{-2}$

Table 5.3: Summary of the average p-values yielded across all features for each object and grasp from a Kruskal-Wallis test. The Kruskal-Wallis test rejects the null hypothesis that healthy and amputee population feature values come from the same distribution at the  $< 5\%$  significance level on average. It must be noted that only a single amputee subject took part in the study.



each object and grasp yields the average p-values given in table 5.3. It can be seen that on average, the null hypothesis is rejected at the  $< 5\%$  significance level. Individual feature comparison across both demographics is provided in Appendix C. Although tests suggest that subject distributions can be grouped according to healthy and amputee demographics, only a single amputee subject took part in the study. The variance between subjects within the amputee demographic is still unclear, and would require additional subjects to provide a better indication of the differences between both populations.

### 5.6.2 Anthropomorphic Correlation

As the majority of subjects taking part in the study were from a healthy demographic, it is clear that the variance between arm motion amongst subjects, as discussed in the previous section, may be attributed to either or both anthropomorphic or neural factors. To discern between the two, anthropomorphic measurements of the height, arm span and hand span were taken from healthy subjects to see if there is any correlation between features. To first assess the relationship between the three measurements, scatter plots were created to find any correlation between them, given in figure 5.44. Although seemingly obvious, there

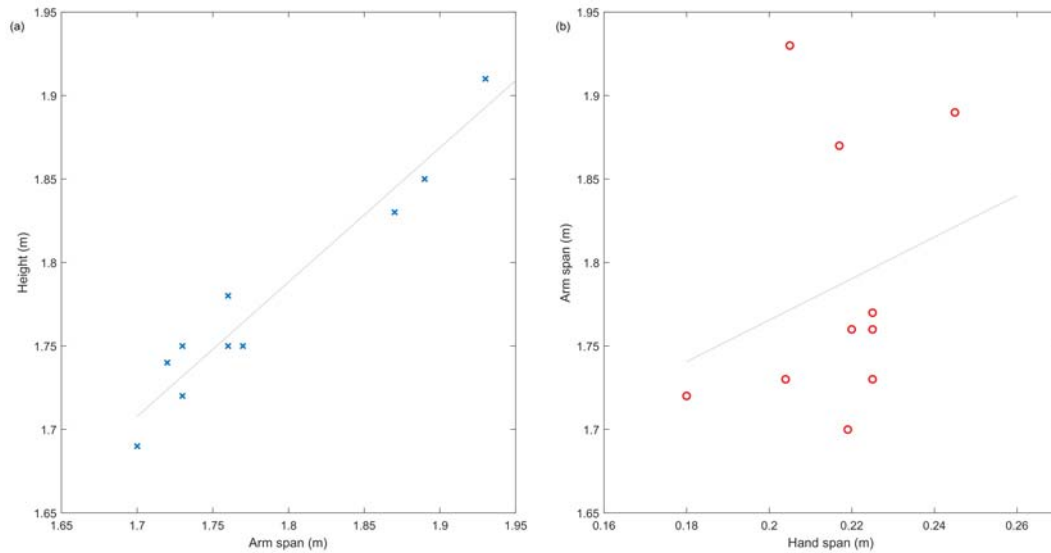


Figure 5.44: Correlation across healthy subjects of (a) height and arm span, showing a strong positive correlation, whereby taller subjects have a wider arm span; and (b) arm span and hand span, showing a weak positive correlation, indicating that taller subjects tend to have slightly larger hands.

---

is a strong positive correlation between height and arm span shown in (a), whereby taller subjects have a wider arm span. Comparing arm span and hand span, given in (b), shows a weak positive correlation, indicating that taller subjects tend to have slightly larger hands.

By looking at the relationship between feature magnitude and subject arm span and hand span, any correlation between physiological motion during grasp and relevant anthropomorphic factors can be identified. Finding the median magnitude of each feature across all subjects, and by calculating the Pearson correlation coefficients given by equation 5.36, the resulting p-values of whether or not there is a statistically significant relationship between anthropomorphic factors and physiological motion features are obtained.

$$\rho(A, B) = \frac{\text{cov}(A, B)}{\rho_A \rho_B} \quad (5.36)$$

The average p-value of all features over all object, locations and grasps against hand span is 0.4156, and arm span is 0.5373. This suggests that there is no statistically significant correlations overall, however, on an object-to-object, per grasp basis, some individual features do show statistically significant correlations, and are provided in Appendix D. These features differ between grasps and objects, but aren't related to its discriminatory power. Correlation inconsistency among objects and grasps is also a testimony to its overall statistical insignificance. Thus it can be said that anthropomorphic factors do not have a statistical significant relationship with physiological motion, and that it is more reliant on neural control factors.

### 5.6.3 Influence of displacement, velocity and acceleration

In addition to the importance of the discrimination rate between grasps for different objects, it is also important to look at the distribution of important features. A comparison of the distribution of the most of important features is given in figure 5.45. When considering the distribution of displacement, velocity and acceleration features, it can be seen that acceleration features provide the poorest discrimination overall. Displacement features were the strongest on average with two out of three objects for the amputee subject only using displacement features for maximum grasp separation. Velocity features are found to still have a reasonable impact on grasp discrimination, being the strongest set of features for

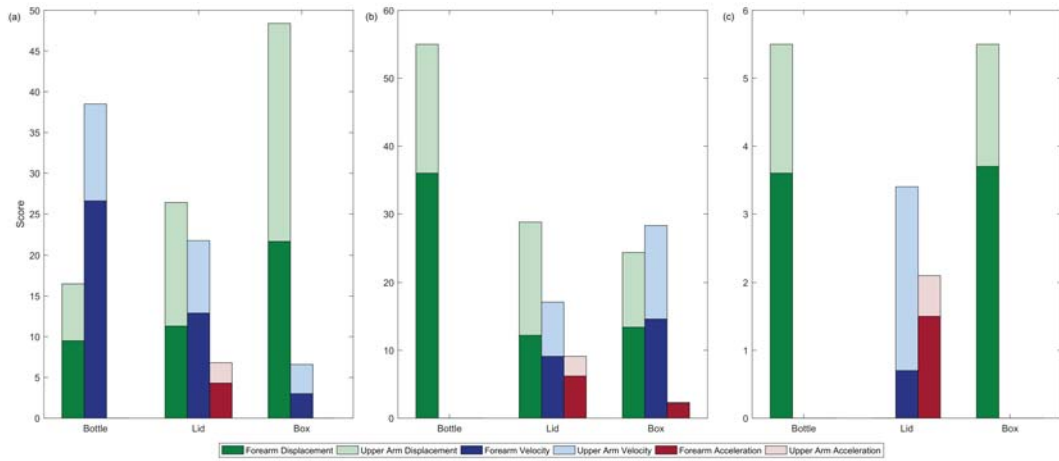


Figure 5.45: Displacement, velocity and acceleration feature score distribution across forearm and upper arm for (a) healthy subjects for all object locations, (b) healthy subjects for all objects locations at table height and ascending, and (c) amputee subjects for all object locations at table height and ascending. Displacement features provided the greatest discrimination between grasps, with velocity features also showing strong importance. Acceleration features on the other hand have very low discriminatory power. Both forearm and upper arm motion shows a relatively even distribution between scoring features, with forearm features performing slightly better. This suggests that upper arm motion is just as important as forearm motion when determining grasp.

the bottle in (a), the box in (b) and the lid in (c). In summary, the overall distribution of displacement, velocity and acceleration features across all objects and subject comparisons gave an average of 60.75%, 33.39% and 5.86% respectively. It is evident that acceleration features play a very minor role in determining grasp, and that displacement features are the most important group of features within grasp trajectory. Looking at the forearm and upper arm split, overall forearm features perform only slightly better than the upper arm, with 56.16% to 43.84% respectively. This suggests that the upper arm motion is just as important as the forearm motion when determining grasp.

## 5.7 Chapter Summary

This chapter presented a detailed analysis of displacement, velocity and acceleration features inherent in the arm's motion when reaching to grasp three different objects. A study was conducted on 10 healthy subjects and 1 amputee subject, involving reaching to grasp a bottle, lid and box with different grasp patterns. The reaching trajectories were recorded

---

and analysed, extracting a total of 84 features from both forearm and upper arm displacement, velocity and acceleration profiles. The objects were varied in location within the subject's workspace to identify the most useful features independent of changes to reaching elevation, angular and depth position. The methods used were discussed, and the resulting features extracted were described. The effect of object location on variance and discriminatory power of each feature was detailed for both subject demographics. It was found that grasps made at a descent provided feature values with a reduced magnitude in comparison to grasps made at table height or ascent, creating difficulties in grasp discrimination in the entire workspace. Reducing the analysis to locations only at table height and ascent showed an improvement in grasp classification accuracy. A KNN classifier provided the greatest grasp classification accuracy in comparison to LDA, QDA, DT and SVM classifiers. Although a very simple classifier, the KNN approach works very well with the formation of multiple clusters for each grasp pattern in feature space as a result of varying object position. The formation of multiple clusters in feature space makes boundary or region-based classifiers such as SVM, less effective.

Statistical analysis using the Kruskal-Wallis non-parametric test on each feature rejected the null hypothesis that all subjects came from the same distribution. The high variance between subjects shows that finding global features for predicting grasp is a very difficult problem, and provides evidence for the necessity of subject-specific calibration templates. Analysis between healthy and amputee demographics suggest that both populations come from different distributions, however a greater number of amputee subjects are required for a more concrete analysis.

Correlating anthropomorphic factors such as hand span and arm span with physiological features found that there was no statistical significance overall, and that motion is more reliant on neural control.

Overall, displacement features were found to be the most useful in providing the greatest discrimination between grasps, with velocity features also showing strong importance. Acceleration features on the other hand have very little discriminatory power. A comparison of both forearm and upper arm motion show relatively equal importance for determining

---

grasp, with forearm features being only slightly more dominant. Classification results are relatively strong, and suggest excellent potential for assistive HMI applications.



## **Chapter 6**

# **A Low-Cost Heterogeneous Sensor Suite for Automated Grasp Switching of a Myoelectric Hand Prosthesis**

As discussed in Chapter 2, the state of the art in myoelectric hand control in regular patient use is currently limited to proportional control of a set of pre-programmed grasp patterns. Although individual control of digits has been achieved using EMG gesture analysis, the technology is still immature. Despite having the lower flexibility of a single DOF, conventional EMG control using grasp patterns offers a relatively effective and simple method for carrying out a variety of different functions. However, with many amputees discontinuing the use of their prosthesis, it is essential to improve existing control strategies to make them more effective and easier to use.

This chapter focuses on applying the conceptual system design described in Chapter 3, to automate grasp control of a myoelectric hand prosthesis, the Bebionic V2, and is the culmination of the studies conducted on MMG and computer vision in Chapter 4 and inertial-based grasp prediction in Chapter 5. The sensor suite developed is used in a selection of real-time experiments to validate the performance of the proposed system, comparing against conventional control using MMG (instead of EMG) sensors.

---

## 6.1 Sensor Suite

### 6.1.1 Sensors

As described in Chapter 3, the sensor suite is split into different subsystems, the muscle activation subsystem (MASS), computer vision subsystem (CVSS), and grasp prediction subsystem (GPSS), all of which utilise different sensors. Figure 6.1 shows the various sensors used in the sensor suite. The MASS uses a single MMG sensor to detect the activation of the extensor digitorum in the forearm. This sensor is sewn into an arm compression sleeve, and connected directly into the upper arm IMU, shown in (a), which transmits the data to the computer via BT. The microphone-based MMG sensor is described in detail in Chapter 4. The GPSS consists of a pair of IMU sensors to measure the arm's motion during reach. The forearm IMU sensor sewn on to a wrist splint, shown in (b), fitting over the prosthetic hand and the adapter described in Chapter 3. The upper arm IMU sensor is sewn on to a compression arm sleeve, which is fitted over the outside of the bicep, given in (a). The CVSS, shown in (c), consists of a Logitech C525 HD web camera fixed to a pair of



Figure 6.1: Various sensors built into the sensor suite, including: (a) the MMG sensor sewn into the compression sleeve, (b) the forearm IMU sewn into the wrist split over the Bebionic hand and adapter, (c) the computer vision system consisting of a pair of safety goggles, web camera and fish eye lens, and (d) the audio headset used to prompt user actions.



---

safety goggles using adhesive Velcro. A clip-on 180° fish-eye lens by Mpow [192] is fitted to the web camera to increase the field of vision of the camera, which is used to record video with a 640x480 pixel resolution. The fish eye lens at 640x480 resolution provides a wide viewing angle for the workspace. Using the camera at a higher internal resolution would create a video image that interferes with the edge of the fish eye lens. The camera's tilt and rotation angle are adjustable for positioning the object in the centre of the image when the subject focuses on it. The camera setup does not occlude the user's vision. An audio headset, displayed in (d), is also placed on the head to prompt subject actions during template data collection and to indicate when the sensor suite begins to record reaching motion. Data previously collected in the study described in Chapter 5 used visual cues in the software interface to prompt the user to reach, however when using the sensor suite, the eyes are required to look at the objects, so instead, audio cues were used. Although the provision of audio cues require the use of an additional piece of hardware, the choice was made for testing purposes only. These Cues can be given by vibrations, or flashing LED lights for a less obtrusive feedback system in mobile environments.

#### **6.1.1.i Setup**

The compression sleeve embedded with the IMU and MMG sensor is pulled over the subject's right arm, with the IMU positioned over the bicep to measure the motion of the upper arm, and the MMG sensor over the extensor digitorum in the forearm. The edge of the compression sleeve is pulled over the shirt sleeve if required, to make sure it doesn't fit loosely. Additional rubber bands and straps are used to ensure a tight fit if it appears loose on the subject. The Bebionic hand is connected to the adapter, which houses the battery and controller that is used to receive the grasp selection output commands from the computer via BT. The wrist splint (with the metal support removed) embedded with a second IMU to measure the motion of the forearm is fitted over the adapter. The subject (healthy) holds the Bebionic hand between the thumb and fingers as shown in figure 6.2, which is kept in place close to the forearm using a Velcro strap, preventing flexion and extension of the wrist. For the amputee subject, the compression sleeve was fitted higher up on the upper arm, with



Figure 6.2: Healthy subject fitted with the sensor suite and Bebionic V2 Hand.

the MMG sensor positioned on the bicep instead of the forearm. Ideally the sensor would be positioned on the remaining muscle on the forearm, however, the subject's own forearm prosthesis was being used, leaving no room for the sensor. The vision system is fitted on the subject's head, along with the audio headset, and the straps are adjusted if necessary. The camera's tilt and angular position on the goggles is adjusted so that when the user looks directly at an object, the object is approximately positioned in the centre of the image. The complete setup of the sensor suite on a subject is given in figure 6.2.

### 6.1.2 Control Flow

Reiterating from Chapter 3, the control architecture is split between the *sensor control system (SCS)* and the *local control system (LCS)*. The SCS is the HMI which directly receives input from the user, converting those signals to classify the appropriate grasp and send the appropriate commands to the LCS, which controls the Bebionic hand. Figure 6.3 shows the complete control architecture of the system.

When a user intends to interact with an object, he or she turns their head towards it, centering its position in the camera's image. The user activates the extensor digitorum in the forearm, creating vibrations on the skin's surface. These vibrations are measured by the MMG sensor, where the signal is transmitted to the computer for further processing. The MMG signal processing steps are explained in detail in Chapter 4.1.2. Gyroscope informa-

---

tion from the IMU sensors are used to detect motion, where if the gyroscope measurement  $g(t) \geq g_{thres}$ , the MMG response is considered to be a result from arm motion rather than intentional muscle activation, resulting in no further output from the system. If the response is considered to be from an intentional muscle activation, and the signal output  $h(t) \geq OC_{thres}$ , the system will send a command to the Bebionic hand to changes its current state. If the hand is already in a closed position, then a *grasp open* command is sent, opening the hand. If the hand is in the open position, then the system proceeds to predict whether a grasp change is required before closing the hand.

The CVSS is then used to take a snapshot of the target object, which is currently centered on the camera's viewpoint. Once the image is taken, it follows a series of image processing steps described in Chapter 4.2.2.i. Image processing results in a binary image, highlighting the edges within the captured scene. Connected regions, known as blobs, are found within the resulting image, and go through an iterative process to remove those that are most unlikely to be the focused object. This removal step compares each blob's intrinsic properties to various thresholds, where if the  $area < A_{min}$ ,  $area > A_{max}$ ,  $height \geq H_{cam}$ ,  $width \geq W_{cam}$  and the Euclidean distance from the camera's centre,  $E_{dist} \geq E_{cen}$ , the blob will be removed. Those that meet the requirements are given a score based on their pixel area,  $A$ , and its Euclidean distance from the centre of the image,  $E_{dist}$  with the relationship  $B_{score} = \frac{A}{E_{dist}}$ . The blob with the highest score is considered to be the focused object, and is classified according to a template using a KNN classifier.

Once the object has been classified, physiological information begins recording from the forearm and upper arm IMU sensors, and the user is prompted by an audio cue to reach towards the object with the desired grasp in mind, holding the arm's position at the point of grasp (PoG). After three seconds of motion data has been collected, grasp features are then extracted and compared against a user-specific grasp template for that object class, predicting the desired grasp pattern according to a KNN classifier. Once a grasp pattern has been determined, the system considers the currently selected grasp pattern and determines whether a *grasp change* command is required. When the correct grasp has been selected on the Bebionic hand, a *grasp close* command is sent to close the hand around the object. The

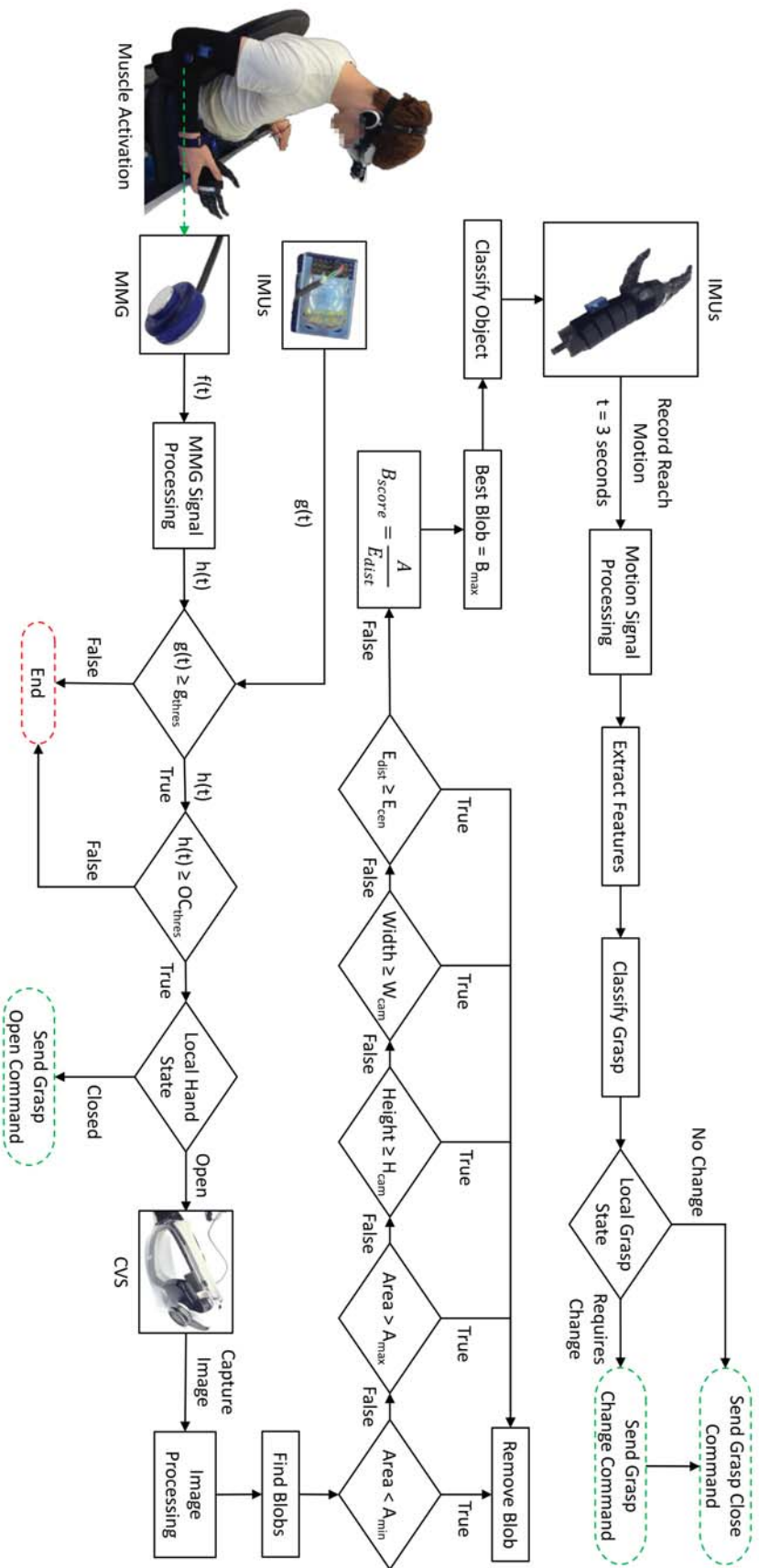


Figure 6.3: Complete sensor suite control architecture for controlling a Bebionic V2 hand. When a user intends to interact with an object, he or she turns their head towards it, centering its position in the camera's image. The user activates the extensor digitorum in the forearm, and the muscular response is measured with a MMG sensor. If the muscle response goes beyond a certain threshold, and arm motion is not detected by the IMU gyroscopes, then the response is considered an intentional muscle activation. If the hand is already in a closed position, then a *grasp open* command is sent, opening the hand. If the hand is in the open position, then the system proceeds to predict whether a grasp change is required before closing the hand. The camera is used to take a snapshot of the user's point of view, where the image follows a series of image processing and blob filtering steps to classify the target object of interest. Once classified, arm motion is recorded for 3 seconds as the user reaches towards the object. Grasp features are then extracted and compared against a user-specific grasp template for that object class, predicting the desired grasp pattern according to a KNN classifier. The classified grasp pattern is then selected using a *grasp change* command if required, followed by a *grasp close* command, closing the hand around the object.

---

system is reset to measure MMG recordings again, where the next successful intentional muscle activation will result in a *grasp open* command being sent to open the hand again. It must be noted that the sensor suite does apply some additional cognitive load to both healthy and amputee subjects in terms of sensor usage and localisation, even if relatively minimal.

### **6.1.3 Software Environment**

The software used is split between the sensor control system (SCS) and the local control system (LCS). The SCS software is used to connect the sensors, record and analyse the data, and act as the test interface when conducting experiments. The LCS software is the interface for the internal configuration settings in the Bebionic Hand, and also used to configure the EMG electrodes.

#### **6.1.3.i Bebalance+**

The Bebalance+ software, shown in figure 6.4, is the latest version of configuration software for the Bebionic Hand, developed by RSL Steeper. The software is capable of programming all the respective versions of the Bebionic hand, which use either radio frequency (RF) or Bluetooth (BT) for wireless programming and changing of settings. Bebalance+ allows the user to select which active grasps are installed on the hand, and whether they are selected as the *default* or *alternate* positions or on the *primary* or *secondary* switch position. This allows the user to customise the hand to their preferences. Different modes are also selectable, such as for use with single or dual-site electrodes, proportional or discrete control, or activations using simple muscle flexing, or co-contraction. It also enables the prothesist to look at the EMG response from the muscles to make adjustments to the activation thresholds.

#### **6.1.3.ii Sensor Control Interface**

The software developed for the sensor suite is used as an interfacing tool to connect and record data from the various sensors simultaneously in real-time. It is also used as the

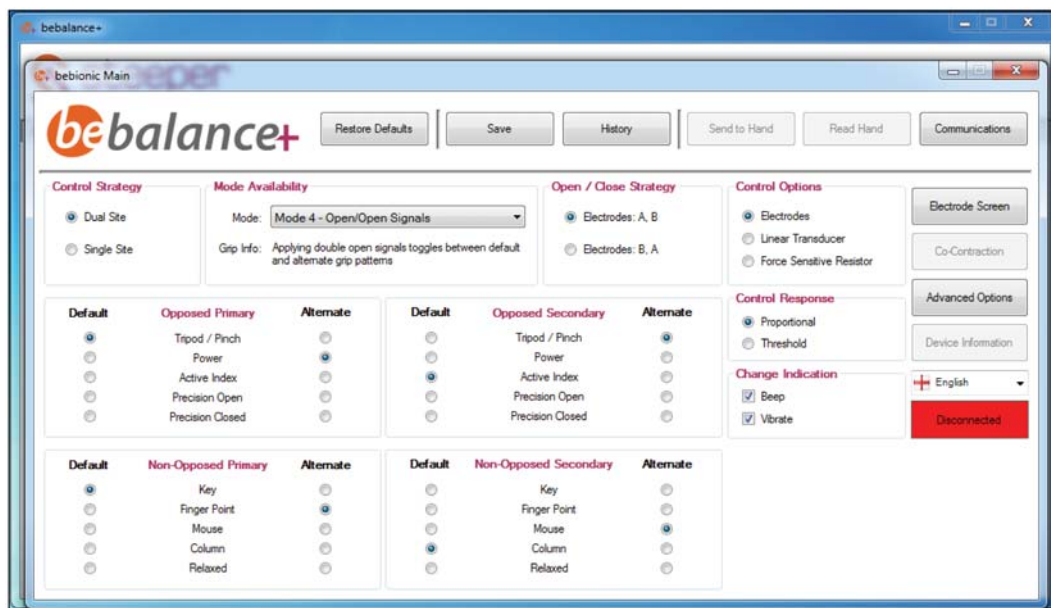


Figure 6.4: Bebalance+ software to adjust the configuration of the Bebionic hand, how it is controlled and the selection of pre-installed grasp patterns.

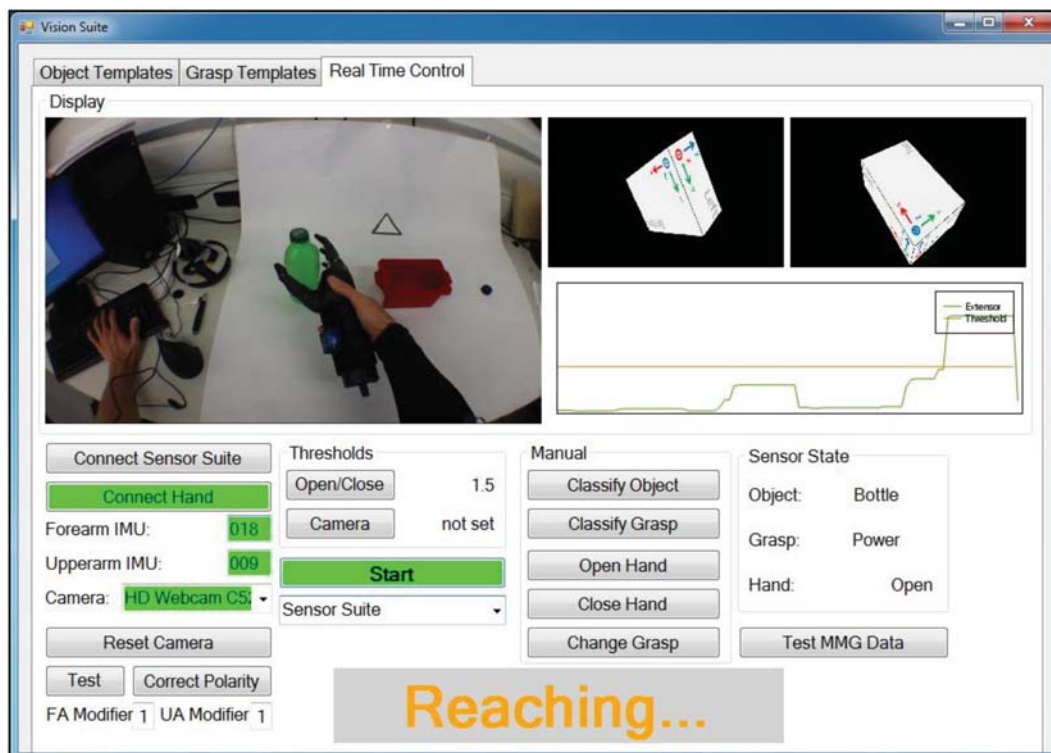


Figure 6.5: The sensor control interface output when carrying out a grasp task using the sensor suite. The interface displays the live video input to the camera, orientation of the IMU sensors, and processed MMG signal, as well as calibration and manual control options.



---

testing environment for recording and saving data to a database for offline analysis, and for the creation of subject-specific grasp templates. The same interface was used to collect the physiological data during grasp analysed in Chapter 5. The object template is also created by saving processed image properties to a database.

During real time control using the sensor suite, the interface displays the live video input to the camera, orientation of the IMU sensors, and processed MMG signal. The MMG threshold can be set by recording 10 seconds worth of MMG data while the subject activates the appropriate muscle several times. The average of the peaks is taken as the new activation threshold. For most subjects however, the default threshold was sufficient. Options allow switching the control method between the sensor suite, and traditional MMG control for the task performance assessment. Manual control is available using buttons in the interface to test the hand or to select the grasp. The object and grasp classifiers can also be manually run for testing purposes. The current estimated state of the system is also shown, which keeps track of the object and grasp selected and whether the hand is open or closed. A visual display is also provided to indicate the current activity taking place. Figure 6.5 shows the real-time control interface during the reach phase of a grasp using the sensor suite.

## **6.2 Participants**

In total, 10 healthy subjects (8 male, and 2 female) participated in both classification performance Assessment (CPA) and task performance assessment (TPA) experiments following the collection of a partial template in a single session. It must be noted that most participants came from an engineering background. The time taken for the session varied between 1.5 hours to 2.5 hours depending on the performance of the subject. A few of the subjects had previously taken part in the collection of physiological data, described in Chapter 5. This may have been beneficial, as these subject would have prior knowledge of the grasp template collection procedure and the grasping patterns to be tested, potentially resulting in marginally more consistent reaching trajectories. The majority of participants had no prior experience using a myoelectric hand. The sleeve was adjusted in position depending on

---

Subject ID	Type	Sex	Age /yr	Height /m	Arm-span /m	Hand-span /m
A	Healthy	M	27	1.83	1.87	0.217
B	Healthy	M	27	1.67	1.67	0.20
C	Healthy	M	27	1.78	1.76	0.225
D	Healthy	M	25	1.91	1.93	0.205
E	Healthy	M	23	1.85	1.89	0.245
F	Healthy	M	29	1.75	1.73	0.225
G	Healthy	M	37	1.75	1.76	0.22
H	Healthy	F	24	1.55	1.575	0.201
I	Healthy	M	33	1.69	1.70	0.219
J	Healthy	F	58	1.55	1.52	0.18
K	Amputee	M	36	-	-	-

Table 6.1: Participant information for physiological data collection experiment consisting of 10 healthy subjects, and 1 amputee subject.

the participant’s arm-span, where extra straps were used to tighten the sleeve on the arm if necessary. Any new participants were required to sign a consent form before participating, and details on age, sex, height, arm-span and hand-span were recorded (see table 6.1).

A single amputee subject took part in the CPA, however did not complete the TPA following observations made during the CPA, which is discussed in section 6.4. The experiment took approximately 4 hours to complete. The same subject had previously taken part in the collection of physiological data. The subject required some additional time to practice grasping objects with the myoelectric hand using the MMG sensors, having no prior experience with the sensors before hand.

### 6.3 Pre-assessment Training

With the exception of the amputee subject who had a few minutes to practice using the prosthetic hand during the study on physiological motion in Chapter 5, none of the other subjects (healthy) have had any experience with grasping objects with a prosthetic hand before. Proficient control of a myo-electric limb typically requires a lot of training, for basic reproduction of EMG signals for intentional proportional or threshold control from muscle activity as well as prosthesis positional awareness when grasping different objects for different purposes, due to the lack of haptic feedback. It is understandable that prosthesis control with a high degree of accuracy takes time, and that some people are faster learners



---

than others. For healthy subjects, accurate control will come easier due to the human hand being positioned along side the prosthetic hand. Although this doesn't provide the subject with haptic feedback from the prosthesis, it does ease positional control, while also being at a similar distance from the elbow. For the amputee subject however, this will not be the case, as the length of the entire prosthesis is held by the residual limb, connecting to the prosthesis at the elbow. The length of the prosthetic forearm is abnormally long in comparison to a normal forearm, which is due to the custom interfacing between a mechanical based forearm prosthesis and a myo-electric hand. This causes the high weight of the hand to provide a large moment across the residual limb, resulting in less stability and control.

Before the study is conducted, all subjects are given some time to learn to use the prosthetic hand. Healthy subjects are given up to 10 minutes, and the amputee subject is given up to 30 minutes. Although not ideal in terms of training time, it will provide subjects with some positional awareness when interacting with the objects with their designated grasps. Subjects are required to spend the training time practicing the different grasps on each object as directed by the investigator.

After the prosthesis training period, a new feature template for the subject is required to calibrate the grasp prediction system. Although a number of the healthy participants involved took part in the study detailed in Chapter 5, a new template is still required. This is due to the difference in motion of the arm when wielding the prosthetic hand. Not only will the hand provide a reduction in arm maneuverability, but will also provide some resistance due to its weight. In addition, with the lack of haptic feedback, the subject is more likely to decrease arm speed to improve positional control of the hand. As observed in the analysis of amputee physiological activity in Chapter 5, the Bebionic V2 hand doesn't have much flexibility when it comes to its predefined grasp patterns, limiting the variability in the object's point of grasp, which can have the effect of reducing the variance in displacement features, potentially resulting in improved classification accuracy. The template consists of column vectors of the most discriminatory feature values from each grasp trial for each object, using the same feature selection method described in Chapter 5.

Collecting a full set of physiological data across all object locations to be used in the

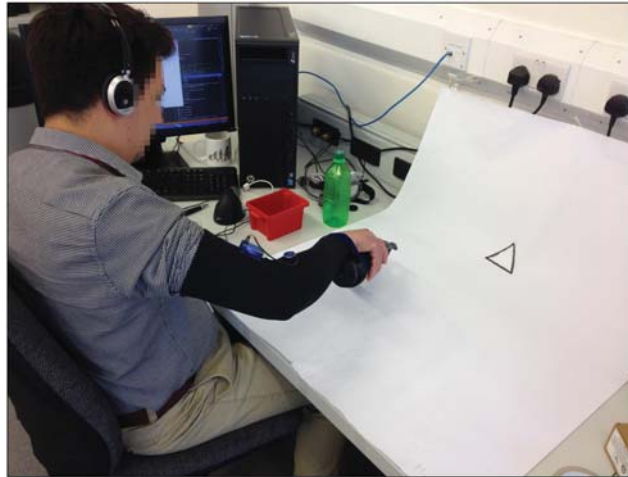


Figure 6.6: A healthy subject collecting partial template data using the sensor sleeve and BeBionic V2 hand.

CPA and TPA would be infeasible, as the total template collection time would take up to two hours. Wielding the prosthesis for a long period of time would result in increased fatigue due to the weight of the hand and battery, which is housed inside the adapter to power it. This would affect the results of the study by affecting physiological activity in terms of a reduction in arm speed and an increase in lazy movements which would affect the grasp prediction rate. Fatigue can also have a large effect on using the MMG sensors for muscle activation over extended periods of time, which would result in having to lower activation thresholds to cater for the reduction in arm motion when performing weaker contractions. This may result in a higher number of accidental activations due to noise artifacts from arm movement. Instead, only a partial template was collected specifically for interacting with objects on the table while seated. This will involve the collection of physiological data for all three objects at table height at  $-45^\circ$ ,  $0^\circ$  and  $+45^\circ$ . Physiological activity is not required for using a *finger point* grasp on the dummy timer object, as there is only a single grasp designated to it. The *finger point* grasp will be selected directly from the detection of the object, skipping the physiological data recording process. Figure 6.6 shows a subject using the sensor sleeve and BeBionic hand to collect a partial template prior to the CPA and TPA.

Although only a partial template is used for the following real-time assessments due to fatigue constraints, the system's performance can still be effectively evaluated for desk-

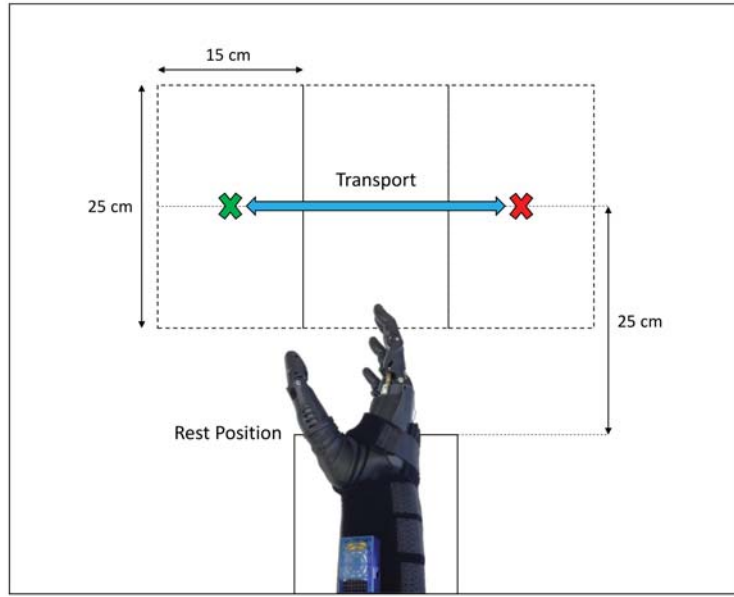


Figure 6.7: Classification performance assessment workspace. The object is located in the center of the left cordon, and is transported towards the right cordon using a specific grasp pattern, and vice versa. The hand starts and ends at the *rest* position.

based tasks, which typically do not require standing up. The system can also be compared to different methods of control to validate its effectiveness as an assisstive HMI.

## 6.4 Classification Performance Assessment

In order to test the grasp classification performance of the system, a simple pick-and-place experiment is implemented. The aim of the study is to measure the grasp classification success rate of the sensor suite in an uncluttered environment across all designated grasps for bottle, lid and box objects. Although theoretical grasp classification rates for arm motion have been estimated in Chapter 5, practical verification is necessary. By recording the success rate of each of the subsystems, the usability of the sensor fusion control architecture between MMG, computer vision and IMU as a whole can be evaluated.

### 6.4.1 Experimental Protocol

The subject workspace consists of a tabletop divided into three sections, each 15 x 25 cm as shown in figure 6.7. Each object and grasp pattern is tested in the following order: bottle

---

(*power* and *lateral*), lid (*lateral* and *precision*) and box (*power*, *lateral* and *precision*). The first object (bottle) is positioned in the center of the left cordon, and the hand is placed in the *rest* position. The subject moves his or her head so that the object is approximately in the centre of vision. The grasp prediction system is then initiated by the subject's muscle activation using the MMG sensors. When prompted, the subject reaches towards the object to make the first grasp (*power*). When the grasp has been predicted, the hand will close around the object. Once grasped, the subject transports the object between the left and right cordons, using muscle activation to open the hand prosthesis, releasing the object from the grasp. The subject returns their hand to the rest position. Once a total of 5 grasps have been made, the experiment is repeated using the next grasp (*lateral*). Once all the designated grasps for that object have been made, the object is replaced by the next one in line (lid) and the experiment is repeated. During this experiment, object and grasp classification rate are recorded by the investigator for each grasp carried out. Figure 6.8 shows the steps taken in the assessment by a single subject using a *power* grasp on a bottle. Figure 6.9 shows the amputee subject performing the CPA on a bottle.

## **6.4.2 Results**

### **6.4.2.i Computer Vision**

Combining the object recognition performance of the CVSS for both amputee and healthy subjects, it can be seen from the confusion matrix in table 6.10 that overall the classification accuracy was relatively high at 86.7%. The diagonals represent the classification rate where the object was correctly identified, while conversely the off-diagonals represent the classification rates where the object was incorrectly identified. The lid had the best average classification rate of 99.1%, while the bottle and box performed reasonable well with a rate of 84.6% and 76.4% respectively. The box and the bottle had the largest difficulty being distinguished from one another, represented by their associated misclassification rate.

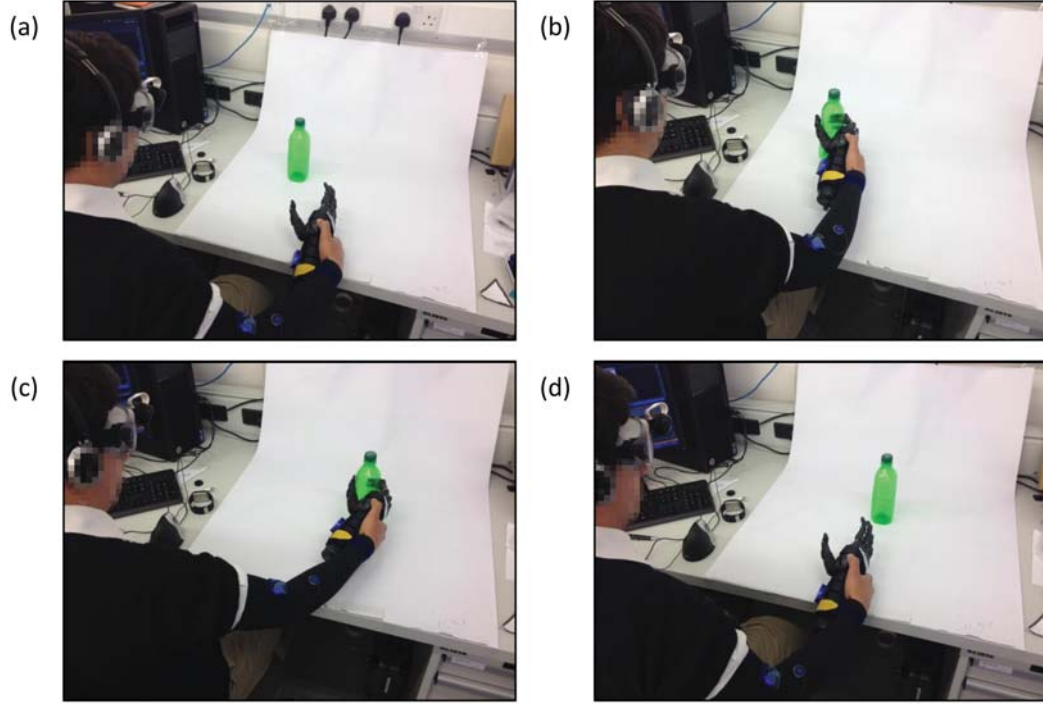


Figure 6.8: A healthy subject carrying out the classification performance experiment on a bottle using a *power* grasp, starting with the hand in the (a) *rest* position, (b) grasping the bottle in the left cordon, (c) transporting the bottle towards the right cordon, and (d) returning to the *rest* position.

#### 6.4.2.ii Grasp Prediction

Due to the nature of the proposed control architecture, if the object is wrongly classified, the system will be using a wrong set of grasp templates during the reaching phase. This will usually result in a misclassified grasp, due to the comparison of arm motion to the wrong template. However, this is not always the case, as some grasp patterns on the different objects may be quite similar, and still classify correctly, for example the *lateral* grasps on both the bottle and lid objects are very similar. Due to the manual switching of the thumb position to gain access to the different grasps, if the wrong object and/or grasp is classified, and results in a grasp with the incorrect thumb position, then the software interface will lose track of which grasp pattern the hand is in, and will have to be corrected manually in the software interface to match that of the hand. However, it does mean that if the grasp is wrongly classified to a pattern requiring a change in thumb position, the correct grasp may still be selected by the hand. A myoelectric hand with a motorised thumb will not have this

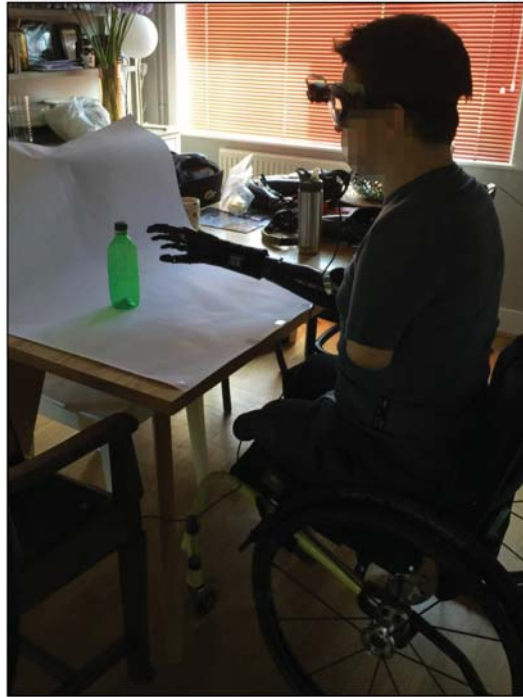


Figure 6.9: An amputee subject carrying out the classification performance assessment on a bottle using a *power* grasp.

issue. To assess the overall classification performance of the system, confusion matrices are used to describe the following parameters:

**True Positive** The proportion of correct grasps made that were correctly classified in both object and grasp pattern.

**False Positive** The proportion of correct grasps made where the object or the grasp has been classified falsely.

		Predicted Object		
		Bottle	Box	Lid
Actual Object	Bottle	84.6% (93)	15.5% (17)	0.0% (0)
	Box	23.6% (39)	76.4% (126)	0.0% (0)
	Lid	0.9% (1)	0.0% (0)	99.1% (109)
Accuracy		86.7%		

Figure 6.10: Confusion matrix for the average classification performance of the CVSS across both healthy and amputee participants.

(a)		Predicted	
		Positive	Negative
Actual	Positive	85.7% (84)	87.5% (14)
	Negative	0.0% (0)	12.5% (2)
Accuracy		98.0%	

(b)		Predicted	
		Positive	Negative
Actual	Positive	100.0% (71)	0.0% (0)
	Negative	0.0% (0)	100.0% (29)
Accuracy		71.0%	

(c)		Predicted	
		Positive	Negative
Actual	Positive	55.9% (62)	52.7% (49)
	Negative	0.0% (0)	47.3% (44)
Accuracy		71.6%	

(d)		Predicted	
		Positive	Negative
Actual	Positive	90.0% (9)	100.0% (1)
	Negative	0.0% (0)	0.0% (0)
Accuracy		100.0%	

(e)		Predicted	
		Positive	Negative
Actual	Positive	87.5% (7)	33.3% (1)
	Negative	0.0% (0)	66.7% (2)
Accuracy		80.0%	

(f)		Predicted	
		Positive	Negative
Actual	Positive	40.0% (4)	54.6% (6)
	Negative	0.0% (0)	45.5% (5)
Accuracy		66.7%	

Figure 6.11: Confusion matrix for the overall classification performance of the system for (a) bottle, (b) lid and (c) box for all healthy subjects, and (d) bottle, (e) lid and (f) box for amputee subjects.

**False Negative** The proportion of incorrect grasps made due to the grasp being classified correctly.

**True Negative** The proportion of incorrect grasps made due to the object and grasp being classified falsely.

Figure 6.11 describes the overall system performance, where (a), (b) and (c) represents all 10 healthy subjects, and (d), (e) and (f) represents the amputee subject for the bottle, lid and box objects respectively. It must be noted that a greater number of amputee subjects are required in order to have a better representation of system performance for that particular demographic. Healthy subjects that took part in the experiment emulate its use by an amputee. Although not ideal, the data presented from healthy subjects can still be useful in determining the system's performance. For indication of the classification success rate of individual grasps for the correctly identified objects, 3-class confusion matrices were calculated for all 10 healthy subjects in (a), (b) and (c), and the amputee subject in (d), (e) and (f)



(a)		Predicted Grasp	
		Power	Lateral
Actual Grasp	Power	100.0% (44)	0.0% (0)
	Lateral	0.0% (0)	100.0% (40)
Accuracy		100.0%	

(b)		Predicted Grasp	
		Lateral	Precision
Actual Grasp	Lateral	60.0% (30)	40.0% (20)
	Precision	16.3% (8)	83.7% (41)
Accuracy		71.7%	

(c)		Predicted Grasp		
		Power	Lateral	Precision
Actual Grasp	Power	56.4% (22)	41.0% (16)	2.6% (1)
	Lateral	30.8% (12)	53.9% (21)	15.4% (6)
	Precision	22.5% (9)	35.0% (14)	42.5% (17)
Accuracy		50.9%		

(d)		Predicted Grasp	
		Power	Lateral
Actual Grasp	Power	100.0% (5)	0.0% (0)
	Lateral	0.0% (0)	100.0% (4)
Accuracy		100.0%	

(e)		Predicted Grasp	
		Lateral	Precision
Actual Grasp	Lateral	100.0% (5)	0.0% (0)
	Precision	60.0% (3)	40.0% (2)
Accuracy		70.0%	

(f)		Predicted Grasp		
		Power	Lateral	Precision
Actual Grasp	Power	40.0% (2)	60.0% (3)	0.0% (0)
	Lateral	60.0% (3)	40.0% (2)	0.0% (0)
	Precision	33.3% (1)	66.7% (2)	0.0% (0)
Accuracy		26.7%		

Figure 6.12: 3-Class confusion matrices for individual grasp classification performance across correctly identified objects for (a) bottle, (b) lid and (c) box for all healthy subjects, and (d) bottle, (e) lid and (f) box for the amputee subject.

for the bottle, lid and box respectively (see figure 6.12). The diagonals represent the classification rate where the grasp was correctly identified, while conversely, the off-diagonals represent the classification rate where the grasp was incorrectly identified. On an individual basis, both subject demographics performed very similarly to each other, with no significant differences in classification results.

Overall success rate for the bottle across both healthy and amputee subjects was very high, with an accuracy of 98% and 100% respectively. Although the bottle did incur some misclassifications across healthy subject data, 87.5% of them still provided the correct grasp. 85.7% of the correctly selected grasps were classified as intended. Classification performance for the amputee subject showed similar results, with 90% of grasps having a *true positive* outcome. Following a correct bottle identification, both *power* and *lateral* grasps for healthy and amputee subjects had a 100% classification rate, showing that all misclassifications occurred during object identification.



---

Grasp selection of the lid was also reasonably successful, providing an average accuracy rate of 71% and 80% for healthy and amputee subjects respectively. All misclassifications present in healthy subject data incurred a *true negative* outcome. Individual grasp classification rate can vary a lot on the subject, but resulted in an average accuracy of 71.7% and 70% between the two grasps for healthy and amputee subjects respectively. Healthy subjects found *precision* grasps easier to classify than *lateral* grasps, with an 83.7% against a 60% success rate. Conversely, the amputee subject found a 100% classification rate for *lateral* grasp compared to just 40% for *precision*.

Both healthy and amputee subjects found it much more difficult to select the correct grasp for the box. With the box being designated three grasps instead of two for both the bottle and lid, it was expected that the classification performance would be lower in comparison, especially when the grasp patterns are so similar in approach. This still resulted in a relatively good grasp selection accuracy of 71.6% and 66.7% for healthy and amputee subjects respectively, however the success rate was an approximately even split between *true positive* and *false positive* outcomes. Only 55.9% and 40% of successful grasps for healthy and amputee subjects were made as the system intended. Misclassifications were split relatively evenly between having a positive and a negative outcome across both subject categories. Overall, the *precision* grasp was the hardest to classify correctly, with a success rate of 42.5% and 0% for healthy and amputee subjects respectively, although the other grasps didn't fair that much better either, resulting in an overall grasp classification accuracy of just 50.9% and 26.7%. *Power* and *lateral* grasps shared the most similarities in terms of trajectory features, having both being misclassified for one another the most.

### **6.4.3 Discussion**

#### **6.4.3.i Computer Vision**

As previously mentioned, object recognition is not the main focus of this research, however its integration still provides an important role in the determination of grasp. According to figure 6.13, it can be seen that incorrectly classifying the object does lead to a greater risk of misclassifying the grasp, especially when grasping the box with a misclassification rate

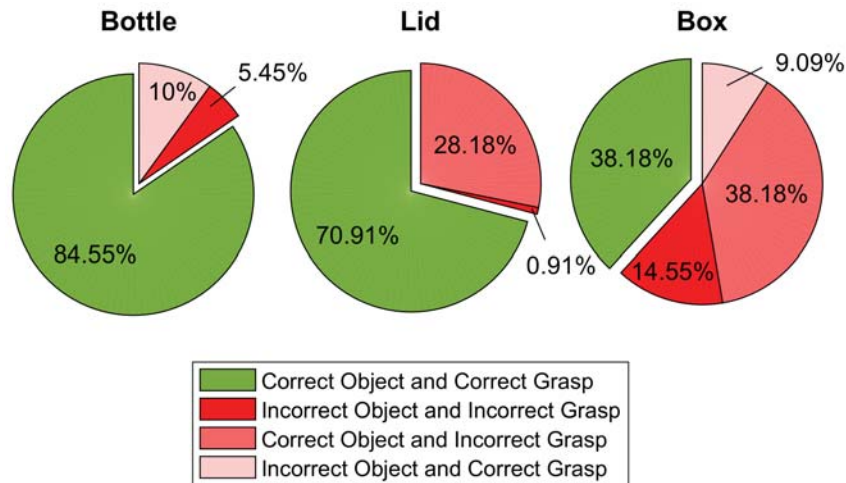


Figure 6.13: Pie charts displaying the average classification outcomes for each object across both healthy and amputee subjects.

of 14.55%. If a greater number of objects were studied, classifying the object incorrectly may lead to a larger percentage of incorrect grasps being selected due to the larger amount of possible combinations, however this would require further investigation.

Although showing relatively good classification rates, the object recognition algorithm has still plenty of room for improvement, and with the application of a very strong classifier, the CVSS can be greatly improved, reducing the overall grasp selection error rate. The current algorithm only classifies between 4 different objects, a bottle, lid, box and timer object, however a much larger range of objects can be added. The robustness of the algorithm is very dependent on the extensiveness of the template, and using a KNN classifier means that generally, the higher the number of images used for the template, the higher the accuracy of the classifier. The images used would also have to be from a much wider range of viewing angles in order to account for different object orientations.

The bottle and the box objects had the most difficulty distinguishing from each other, despite being dissimilar in shape. Depending on the camera's view, the objects can appear different in size. The distance between the camera on the subject's viewpoint and the object in the workspace can vary the property values of the object, which greatly affects the classification, especially between the bottle and box, where their sizes are similar. Therefore it is important that the subject is sitting correctly at an ideal distance from the table for

---

classification. Although some ratio measurements were used from the object's properties, these can be distorted due to the camera picking up visual artifacts within the image, such as shadows caused by poorly distributed lighting on the object as well as on uneven surfaces. If the artifact blobs are close by to the object's blob in the image, they can merge during Gaussian filtering, forming a single blob with a slightly distorted shape. The distorted shape can lead to property ratios that do not align with those from its template, giving it a higher chance for misclassification.

Although partially represented in the evaluation of the CVSS, the main disadvantage of the algorithm combined with the hardware used, is its inability to distinguish objects from the environment itself, which results in a high sensitivity to visual artifacts, despite using a white background to improve the classification rate. It is evident that the current state of this particular CVSS is not currently suited for real-life applications, however implementing a state of the art object recognition system will make it much more compatible with the sensor suite. The CVSS has plenty of room for improvement, and many of its shortcomings can be overcome in future work.

#### **6.4.3.ii Muscle Activation with MMG Sensing**

The response of the MMG sensor during muscle activation was not recorded during experimentation, as it only provided a means for initiating the grasp selection algorithm, however there were some important observations made in regards to them that can potentially have an overall detrimental effect on the system's usability. Although the MMG sensors responded reasonably well in the majority of trials when conducting the experiment with regards to intentional muscle activation, there was a tendency for unintentional activation, especially during arm movement. Despite the methods used to restrict unintentional muscle activation during arm motion by monitoring the gyroscopic values in both IMU sensors, there were still a large number of cases of unintentional activation when still. The quantity of cases during the study was not recorded however, but was observed to be a problem. This was not consistent across all subjects, as some had much fewer unintentional MMG activations than others. This was apparent in both healthy and amputee subjects, and it is important to find

---

the reason behind the issue in order to make further improvements to the MMG subsystem. This is beyond the scope of this research, however it is definitely worth improving.

Healthy subjects had the MMG sensor located on the extensor digitorum of the right forearm, and could have suffered from interference from the partially activated muscle due to holding the Bebionic hand. With the forearm already partially contracted, some subjects found it harder to raise the signal above the threshold to activate the system. As a result, the threshold had to be lowered, increasing the chance of unintentional activations due to motion artifacts. Generally, the higher the threshold is kept, the lower the risk of unintentional activations, however this can lead to greater muscle fatigue. It was also noticed that a few of the subjects performed an unnecessarily hard clench when trying to activate the muscle, which would result in the hand itself jolting. This action sets the gyroscopic values over the threshold, so the system detects a motion, preventing intentional muscle activation from firing. Lowering the gyroscopic threshold to counter this would result in a greater number of unintentional activations due to arm motion. Some subjects performed much better than others, having little trouble in activating the system intentionally, as well as having a reduction in the number of misfires.

The amputee subject on the other hand had the MMG sensor located on the bicep, as the subject's forearm prosthesis was unable to accommodate the MMG sensor. Unfortunately, with the high weight of the entire prosthesis on the elbow joint, the bicep was constantly being activated just trying to move the arm, or even just holding it place. The position of the sensor made the system very difficult to use for the subject due to the high frequency of unintentional activations. In comparison, healthy subjects hold the prosthesis in their reaching arm, partially supported by a strap. The sensor positioning on the forearm allows reach with much fewer motion artefacts. Although the weight of the prosthesis held along the forearm still has an effect on the measured MMG signal, it is to a much lesser extent due to the static nature of contracting the extensor digitorum. Although the CPA was completed by the amputee subject, it was clear that it would be too difficult to use during the TPA that followed. A subject specific prosthesis designed to fit with the MMG sensors is necessary for real-time implementation of this system for amputees, as positioning the sensor on the

---

upper arm results in too much muscle interference. TPA with the amputee subject would not be good indication of system performance for grasp selection, as a lot of the time spent would be on correcting the grasp due to unintentional activations. Integration using an EMG prosthesis can easily be implemented instead, as it would provide the same control functions as the MMG system. With the Bebionic hand, the current grasp needs to be tracked effectively in order to switch to the correct grasp after classification. Due to the requirement of the manual changing of the thumb position to access different grasp patterns, the current grasp tracking can easily be lost due to an incorrect classification, as the system assumes that the user has selected the correct thumb position before initiating the grasp selection system. A fully automated prosthesis would be more adept in this application, as grasp tracking wouldn't be necessary.

It is unclear if using EMG sensors would present similar effects if positioned on the bicep to be used for activation of the prosthetic hand, as the sensor would also detect the signal, in this case electrical, generated from lifting and holding the prosthesis as well when moving the arm. It must be noted that activating the MMG sensors to control the arm does improve with practice, and given more time, participants may improve intentional activation control of the muscle, lowering susceptibility to motion artifacts.

#### **6.4.3.iii Grasp Prediction**

Although overall accuracy for predicting grasp for both healthy and amputee subjects was very high for the bottle and lid objects, the box provided mixed results. Although the bottle and lid performed well, false positives provided quite a high percentage of the overall accuracy. Ideally the accuracy would be formed out of *true positive* outcomes, with both object and grasp identified correctly as intended.

All the misclassified grasps present when interacting with the bottle was a result of object misclassification, with the bottle being incorrectly classified as a box. The object misclassification had little effect on the outcome of the correct grasp, as often, either a *lateral* or *power* grasp was still classified. The correct grasp was selected due to both grasp patterns being set as the default grasp following a thumb position change. Considering that

---

both *power* and *lateral* grasps are very different in terms of arm orientation, a grasp misclassification would only occur if the wrong object was identified and sent a *grasp change* command, such as switching to a *precision* grasp in the case of the bottle being classified as a box.

Predicting between the *lateral* and *precision* grasp for the lid object proved a bit more challenging, however a relatively high accuracy was still obtained. Although the majority of correct grasp classifications were made up of *true positives*, any misclassifications incurred would produce a *true negative* outcome, except in the rare case of the hand controller not receiving the *grasp change* command via BT, as in the case of the amputee subject, which resulted in a *false positive*. With the object classification rate for the lid at 99.09%, it is clear that the loss in performance is due to poor grasp prediction. It was seen in Chapter 5 that both grasps are much more similar to one another, leaving much less room for error in terms of approach and arm position at the point of grasp. Healthy subject data suggests that the *precision* grasp is much more likely to be predicted correctly, having a classification success rate of 83.67%, potentially due to the arm approaching the object higher at the elbow to interact with the lid from directly above to improve the success rate of picking it up. It was evident that all the subjects found difficulty in interacting with the lid using a *lateral* grasp, with only a handful of successful pickups made. Although designed to be consistent with the interaction of the bottle with a *lateral* grasp, it was found that due to its difficulty (partially due to the lack of a gripping surface on the edge of the fingers), the grasp would be much less likely used in a real-life scenario, despite given the option.

The three grasps designated to the box found a much greater difficulty in distinguishing between them, presenting relatively poor grasp classification performance. Despite this, the overall accuracy of the system was still relatively good, however the even split between *true positive* and *false positive* outcomes is disconcerting. The large quantity of *false positive* outcomes occurred as the result of a *power* or *lateral* grasp being classified as one another. With both being set as the default grasp for each thumb position, a misclassification would not result in a *grasp change* command being sent to the hand. The *true negative* outcomes would occur as the result of the *precision* grasp being classified incorrectly, or being incor-

---

rectly classified during an intentional *power* or *lateral* grasp. Using a different prosthetic device such as the Michelangelo Hand, which has a motorised thumb, would turn a lot of those *false positive* outcomes into *true negative* outcomes, as the hand would always be able to select the correctly identified grasp, greatly reducing the overall accuracy. It was apparent however that having three grasps designated to the box may not have been necessary, as just two grasps, *lateral* and *precision* would have easily sufficed.

Considering the overall classification performance of the sensor suite concept, the system provided positive results for identifying the correct grasp when interacting with a bottle or a lid, obtaining a classification success rate (*true positive*) of 84.55% and 70.91% respectively, but performed much poorer with the box with just 38.18% of grasps classified as intended. Although the results do show plenty of promise, extending the system beyond the three objects considered would require rethinking the way objects are modeled in terms of their interaction. It is evident that the system relies heavily on predicting the correct grasp during reach for each object. It is important to note however, that the available grasp patterns from the hand are very simplistic in nature, and the patterns available do not interact with objects in the same way that the human hand does. So although implementing more grasp patterns may increase the number of interaction options available for different objects, often just one or two patterns are sufficient to provide the desired control. Limiting the number of grasp patterns per object would increase the overall grasp classification rate, however would also increase the burden on the object recognition system, especially when increasing the number of object classes available. Evening out the classification workload between computer vision and grasp prediction would result in overall better performance of the sensor suite, and would be a major consideration for further system development.

## 6.5 Task Performance Assessment

Having analysed the system's classification performance in terms of object recognition, grasp prediction and muscle activation intention, the system is ready to test real-time task-oriented performance. A 'Tray' test is implemented to record the time taken to carry out simple pick-and-place tasks on a table, similar to the tests conducted by M. Mace [121] and

---

R. Woodward [193]. The protocol carried out by R. Woodward, is the most similar to the one carried out in this study. The same grasp patterns were used when interacting with each of the objects. On the other hand, the experiments carried out by M. Mace used different grasp selections for the objects. The subjects in both experiments were standing, as opposed to this study, where the subjects will be seated in order to standardise the position across all subjects, taking into account amputee subjects who may not be able to stand. These are only minor difference however, and the performance results can still be compared. Although a direct comparison with the results obtained by R. Woodward and M. Mace may not provide an accurate comparison due to their subjects having prior training, repeating the experiment with these control strategies under the same conditions as this study will enable a direct comparison of a large range of HMIs, and highlight the benefits of cognitive prosthesis control.

The aim of this study is to compare the overall system performance with that of conventional MMG control in order to demonstrate the potential of a sensor fusion system for automated grasp selection. The chosen test is ideal, not only due to the availability of comparable results for different control strategies, but also because of the ability to test the system for use in cluttered environments, and the automated switching between grasps made with the thumb in the opposed and non-opposed position. The amputee subject who participated in previous studies did not take part in this experiment due to the reasons discussed previously.

### **6.5.1 Experimental Protocol**

This study involves completing the experiment with three different control strategies:

<b>Natural</b>	The task is performed using a normal human hand, used as a benchmark. This control strategy does not apply to amputee subjects.
<b>MMG</b>	The task is performed using only the MMG sensors, similar to conventional EMG control of the Bebionic hand. Sending two consecutive muscle activation signals will prompt a grasp switch to and from the default and alternate grasp patterns.



**Sensor Suite** The task is performed using the developed sensor fusion system consisting of computer vision, IMU and MMG sensors.

The subject workspace consists of a tabletop divided into three sections, each 15 x 25 cm as shown in figure 6.14. The bottle, box and lid are positioned in the centre of the left, centre and right cordons respectively. The centre of the cordon is 25 cm from the rest position. The dummy timer object is positioned above the centre cordon. The hand prosthesis starts in the *rest* position with the thumb non-opposed. The subject selects a *finger point* grasp, and presses the dummy timer object. When the dummy timer object has been pressed, the investigator begins recording the time using a hand held timer. The subject returns the hand to the rest position, and then manually opposes the thumb. If using the sensor fusion system, the subject looks at the next object while the thumb is being manually changed, in case the MMG sensors are unintentionally triggered during this process, however this rarely occurred. The subject then proceeds to select a *power* grasp and picks up the bottle from the left cordon, and place it into the box, located in the centre cordon

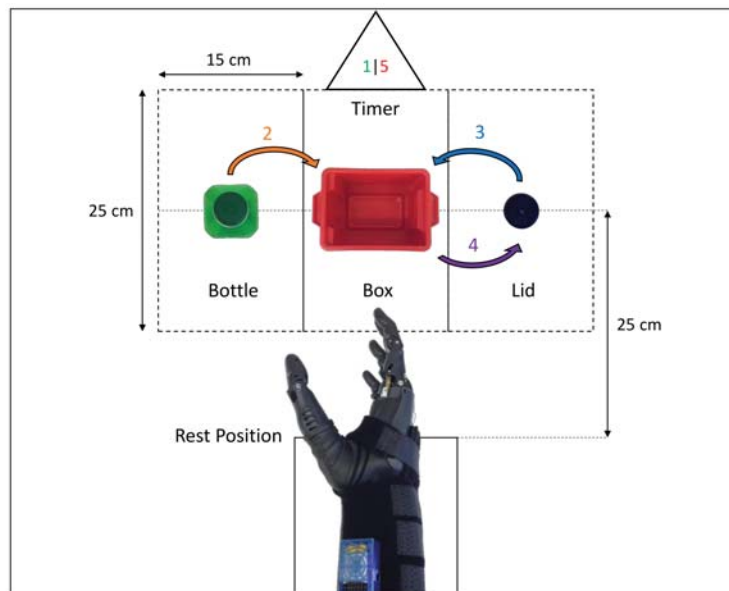


Figure 6.14: Task assessment workspace. 1) The timer is started using a *finger point* grasp. 2) The bottle is transported from the left cordon into the box in the centre cordon using a *power* grasp. 3) The lid is transported from the right cordon into the box in the centre cordon using a *precision* grasp. 4) The box is transported from the centre cordon to the right cordon using a *lateral* grasp. 5) The timer is stopped using a *finger point* grasp. The hand starts at the *rest* position whenever a grasp is initiated.

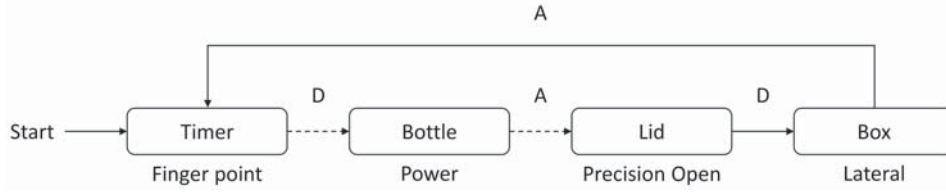


Figure 6.15: Flow diagram highlighting the change in grasp during the task, where D and A represent the default and alternate grasp patterns respectively. A dashed line represents a grasp made with the thumb in the opposed position, and a solid line represents a grasp made with the thumb in the non-opposed position.

cordon. The hand is returned to the *rest* position. The subject selects a precision grasp (doesn't require a change in thumb position) and proceeds to pick up the lid located in the right cordon, and place it into the box in the centre cordon. The hand is returned to the *rest* position, and the thumb is manually changed from opposed to non-opposed. The subject then selects a *lateral* grasp and picks up the box from the centre cordon, and transport it to the right cordon. The hand is returned to the *rest* position and the subject selects a *finger point* grasp (doesn't require a change in thumb position). The dummy timer object is then pressed to prompt the investigator to stop recording the time. The task is repeated 5 times for each control strategy.

With the thumb in the opposed position, the default grasp is set to *power*, and the alternate grasp is *precision*. With the thumb non-opposed, the default grasp is *lateral*, and the alternate is the *finger point*. A flow diagram of the different grasp states of the task is given in figure 6.15. Figure 6.16 shows each step taken in the assessment by a single subject.

### 6.5.2 Results

Table 6.2 shows the median timings for the task for each subject, with the mean and standard deviation (STD) taken across all subjects for each of the three control strategies. A visually summary can be seen in figure 6.17, which shows (a) the raw timings for each trial and (b) a boxplot summary for each control strategy for each subject. It can be seen that overall, the sensor suite provided a faster medium to carry out the task, having a mean time of 110.03 seconds in comparison to 119.42 seconds for conventional control, which is a 8.53%

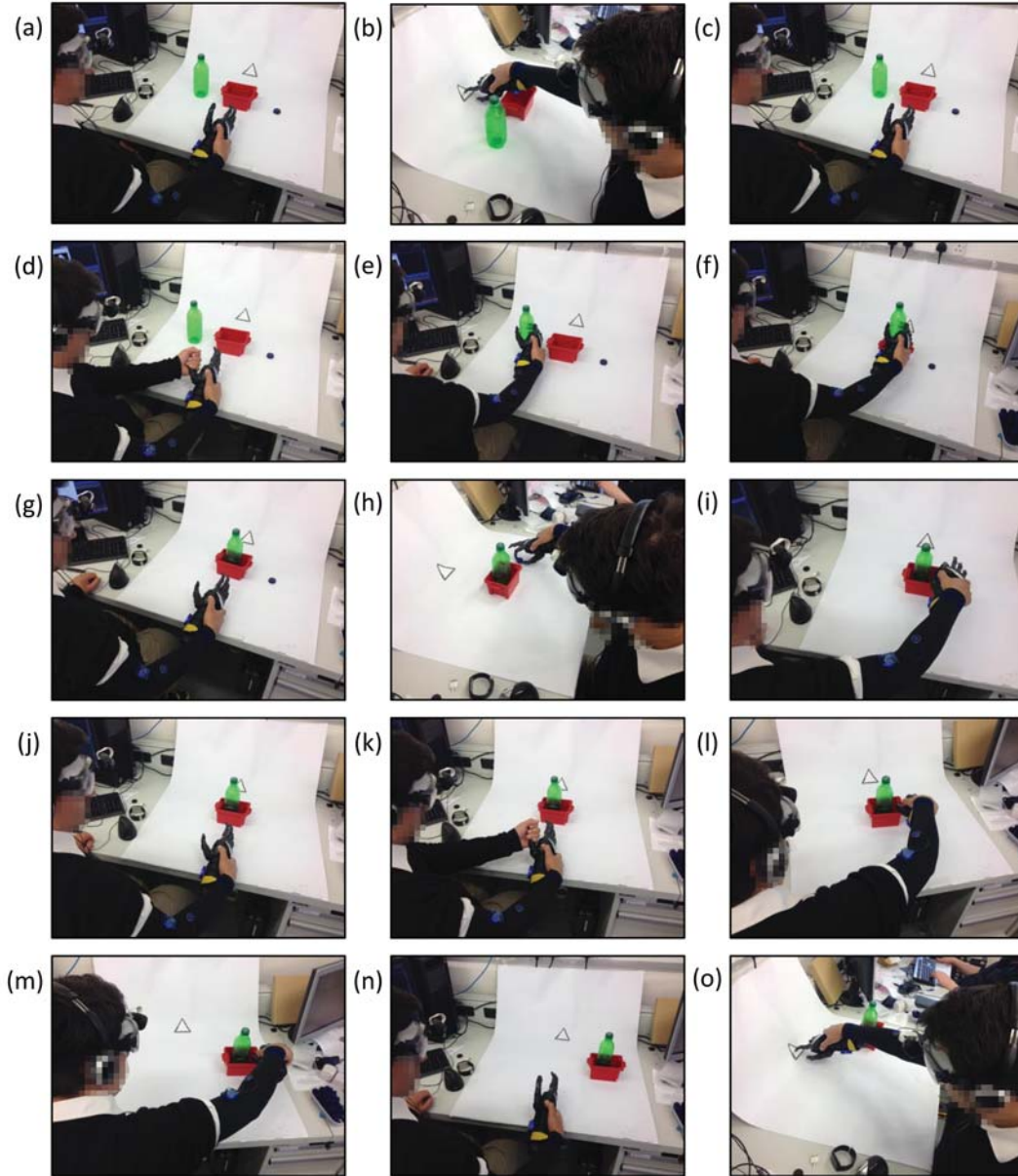


Figure 6.16: A subject carrying out the task performance experiment. Starting with the hand in the (a) *rest* position, the subject uses the sensor suite to (b) press the triangle with a *finger point* grasp to start the timer, (c) return the hand to the *rest* position, (d) manually change the thumb position, (e) pick up the bottle using a *power* grasp, (f) place the bottle in the box, (g) return the hand to the *rest* position, (h) pick up the lid using a *precision* grasp, (i) place the lid into the box, (j) return the hand to the *rest* position, (k) manually change the thumb position, (l) use a *lateral* grasp on the box, (m) move the box to the right cordon, (n) return the hand to the *rest* position, and (o) touch the triangle using a *finger point* grasp to stop the timer.

---

Subject	Sensor Suite	MMG	Natural
A	89.84	120.51	3.29
B	141.25	81.83	3.29
C	69.53	86.08	5.47
D	92.79	108.76	4.20
E	169.93	166.20	4.20
F	137.16	83.87	7.16
G	110.42	135.00	4.12
H	68.63	90.05	3.57
I	100.05	136.34	3.74
J	120.74	185.58	4.74
<b>Mean</b>	110.03	119.42	4.38
<b>STD</b>	32.61	36.30	1.18

Table 6.2: Table displaying the median timings for each subject carrying out the task performance assessment experiment for sensor suite, MMG and natural control strategies. The sensor suite provided a faster medium to carry out the task, with an 8.53% time improvement over conventional control.

reduction in the time taken. However, the time taken for either control strategy is still much longer than that of a human hand. Task performance was fairly evenly spread, with some subjects performing better or worse than others. The standard deviation between sensor suite control and conventional control with MMG sensors were relatively similar. For subjects without any prior experience using the MMG sensors, sensor suite or Bebionic hand, overall performance was consistently good with only the occasional outlier.

### 6.5.3 Discussion

The task completion timings between the sensor suite and conventional MMG control strategies were not statistically significant, however the sensor suite did perform better on the whole. Observationally however, prosthesis control using the sensor suite did have some large advantages over conventional MMG-based control.

It was evident during the trials, that the subjects did suffer from greater muscle fatigue using conventional MMG control, as the subject was required to activate the muscle many times to provide any kind of response from the hand. In comparison, only a single muscle activation is required when using the sensor suite to switch grasps and close the hand. The subject was required to monitor the MMG response and its relation to the threshold during

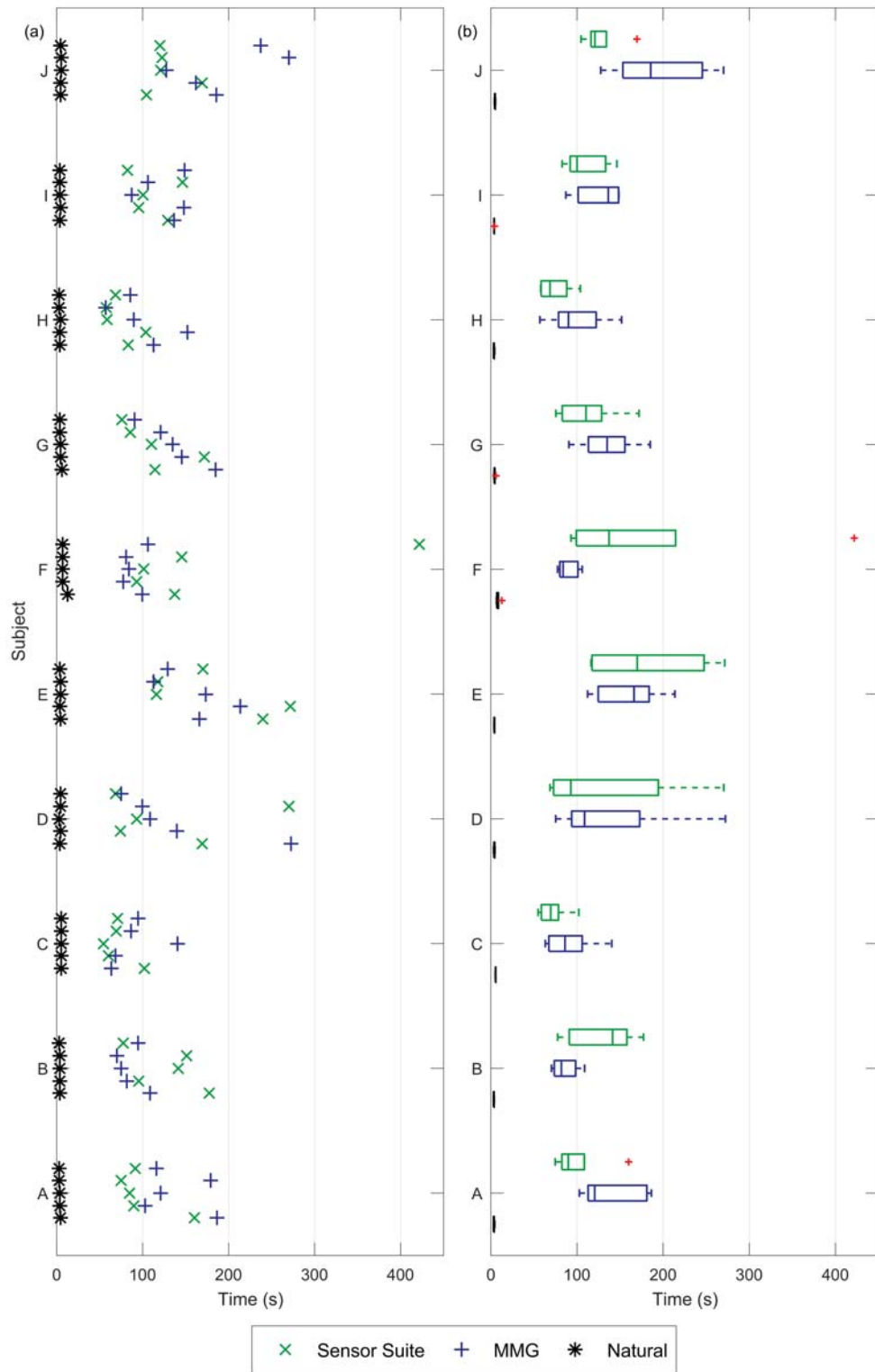


Figure 6.17: Timing results of the task performance assessment showing (a) raw results, and (b) boxplots for each subject performing five trials for each of the three control strategies. The sensor suite provided a faster medium to carry out the task, with an 8.53% time improvement over conventional control.

---

conventional control in order to prevent unnecessary activations. Motion artifacts were also an issue, and would sometimes open, close and switch grasps unintentionally, forcing the subject to activate the muscle additional times in order to switch them back. Unintentional activations were not the only problem, as a slight movement while intentionally trying to either open or close the hand would result in prolonging the signal above the threshold, causing a grasp change to be sent instead. This in turn would result in the subject having to send a double muscle activation in order to switch the grasp pattern back, causing additional fatigue.

During conventional MMG control, occasionally the subject would forget what grasp is currently selected, forcing them to close and reopen the hand to check, or cause an incorrect grasp to be made accidentally. This highlights the benefit of reducing the cognitive load on the user. When using the sensor suite, the subject did not need to remember what grasp the hand was currently in, as the system would just select the appropriate grasp based on current tracking information. Therefore a decrease in cognitive load can lead to a reduction in the time taken to complete tasks.

Subjects carrying out the task using the sensor suite, did however have to be wary of their distance from the target object in order to get a correct object classification. This was most relevant when targeting the timer object to initiate a *finger point* grasp. Sitting too far away could classify the timer as a lid, initiating motion recording, instead of switching to the grasp immediately. Selecting the correct object in the cluttered environment generally performed well, provided that the camera was correctly positioned to point at the center of the subject's vision. Targeting the box after the bottle and lid had been placed inside normally resulted in an incorrect object classification, and in most cases identifying it as a lid. The incorrect lid classification was a result of the lid on the bottle itself being classified rather than the box, due to its contrast in colors. The wrong classification still led to a *false positive* outcome, as a *lateral* grasp was still classified to carry out the task as intended.

Generally, longer trials when using the sensor suite occurred due to incorrect grasp classification when reaching to pick up the lid using a *precision* grasp. Despite subjects showing relatively good separation between both designated grasps, reaching consistency

---

during timed conditions appeared much different than when carrying out the more repetitive and controlled template collection stage. Although the majority of subjects had no problem with classifying a *precision* grasp, it must be made aware that certain grasp features may change when facing certain conditions. A subject whose main grasp template features rely on the velocity or acceleration profiles would find it more difficult to classify the grasp correctly when rushing to complete a timed task. Therefore in terms of adaptability, displacement template features may be more desirable as they are less vulnerable to changes in external pressure conditions on the subject.

#### 6.5.4 HMI Comparison

As mentioned earlier, the 'tray' test was an experiment previously conducted by R. Woodward [193] and M. Mace [22] who compared the time taken to complete the task using a variety of different HMI control strategies.

The test carried out by R. Woodward was the most similar to the TPA, with the only difference being, that the task was carried out with the subject standing. 5 healthy subjects (trained) carried out the experiment using 5 different strategies over 3 trials. *Natural* control consisted of carrying out the task using the subject's own hand, *MMG with visual* and *EMG with visual* was using gesture switch control with a single MMG and EMG sensor respectively, with visual feedback of the signal, *MMG without visual* and *EMG without visual* was using gesture switch control with the MMG and EMG sensor respectively without visual feedback. Gesture switch control involved activating the muscle with the hand positioned by the opposite shoulder in order send a *grasp change* command. The tests produced mean completion times of 10, 48, 45, 40 and 39 seconds for *Natural*, *MMG with visual*, *EMG with visual*, *MMG without visual* and *EMG without visual* respectively.

The test carried out by M. Mace was more different than the TPA, where different grasp selections were used for the objects. Grasping the bottle, lid and tray were all carried out with the thumb in the opposed position. The non-opposed position was only used for a *finger point* grasp used to start and stop the timer. 3 subjects carried out the test using 4 different control strategies over 10 trials. *Natural* control consisted of carrying out the task using



---

the subject's own hand, *FSR* was using conventional control using force sensitive resistors (FSRs) with the opposite hand, *FSR + tongue* was using the FSRs for proportional control of the hand, and tongue control for grasp switching, and *tongue* control was using complete discrete control of the hand. The tests found mean task completion times of 9.9, 28.03, 28.7 and 43.93 seconds for *natural*, *FSR*, *FSR + tongue* and *tongue* control respectively.

By comparison, the TPA conducted in this chapter yielded much slower completion times to that of R. Woodward and M. Mace. The sensor suite appears to perform poorer in comparison to that of MMG and EMG gesture switch control, with the average time taken being over double. However, it must be noted that tests were carried out by R. Woodward with subjects who had prior experience with the Bebionic hand and MMG control. The MMG sensor was also placed on the opposite hand to the one carrying the Bebionic hand, using only isometric contractions, which are significantly cleaner than when using the MMG sensor on the same arm holding the prosthetic hand. The *tongue* control strategy proposed by M. Mace also yielded much faster task completion times, also less than half that of the sensor suite. However, it must also be noted that subjects were thoroughly trained beforehand, and the experiment was much more different. The subjects in both studies were also carrying out the experiment without any movement constraints. Subjects carrying out the TPA had wrist flexion and extension constrained to mimic the anthropomorphic constraints imposed on amputees.

As mentioned previously, the results of R. Woodward and M. Mace cannot be directly compared due to the differences in setup and protocol, however they do provide a number of useful strategies that could potentially be compared with repeated experiments using the same procedures as the TPA in future work. Repeating the TPA using these strategies under the same constraints would provide a much more balanced and useful comparison.

## 6.6 Chapter Summary

This chapter presented and analysed the real-time classification assessment of the sensor suite concept for prosthetic hand control, looking at the performance of the CVSS for object recognition, MMG for muscle activation and inertial motion for grasp prediction. The



---

performance of the sensor suite was actively compared against conventional prosthetic hand control using MMG sensors in a task-oriented experiment. The sensor suite provided overall good results, showing a reduction in the time taken to complete the designated task compared to conventional control with MMG sensors. Although a reduction in cognitive load can be presumed due to the automation of grasp selection, further experiments are required to quantify the extent of this reduction and its impact on task completion time. The effect on cognitive workload can be measured with the use of a secondary task, comparing subject reaction times and completion accuracy, while using various control strategies to complete the primary task with the prosthetic hand. Similarly, the automation of some cognitive processes while using the prosthetic hand would also reduce the physical processes required from the user, potentially resulting in a reduction in muscle fatigue. This would require further evaluation to quantify changes in muscle fatigue during the primary grasping task by monitoring changes in the muscle's EMG response.

The work presented proves the viability of the sensor suite concept, and how the technology, with some refining, can lead towards improving conventional control strategies for upper limb myoelectric prosthesis.



## Chapter 7

# Conclusion and Future Work

### 7.1 Thesis Summary

The goal of this research was developing a sensor fusion concept capable of utilising the natural motion of the upper limb in order to provide more natural robotic arm control without the cognitive burden imposed on the operator. Decoding physiological features in upper arm motion has been highlighted as a novel method for the prediction of grasp, offering significant advantages over conventional methods of control. Using the natural motion of the arm when reaching to interact with objects in the environment can help reduce the cognitive burden of control, while also reducing overall muscle fatigue. With technology rapidly improving, especially towards the development of compact and minimalist wearable sensors, the proposed sensor fusion concept, described in Chapter 3, can provide a low-cost, non-invasive solution for upper limb robotic control with a reduction in the physical and cognitive burden inherent in conventional control strategies. Although not perfect, the potential of the conceptual system has been proved, and with some further refinement in terms of both hardware and software processing, an ideal solution to cognitive-free robotic arm control can be obtained.

The fusion of alternative sensor technologies for conventional control has provided new insights and solutions for tackling well known upper limb prosthesis control problems by attacking it at a different angle. Replacing traditional EMG sensors with MMG sensors

---

for the control of myoelectric hands can provide a number of advantages within constrained scenarios. Although the EMG sensors have the benefit of greater accuracy and consistency, being generally more widely accepted in literature and clinical studies, MMG sensors do provide an alternative for use in environments, situations and applications where conventional sensors are unsuitable. Computer vision enables an additional layer of useful feedback, which can provide an active role in determining grasp by itself, as shown in Chapter 4, and the combination with MMG sensing can provide a complete integrated control system.

Physiological decoding deals with interpreting user intention expressed through natural motion, without the cognitive burden of traditional gesture-based human machine interfaces. Based on this idea, the main focus has been on the analysis of physiological information during the reaching phase leading up to a grasp or interaction. The incorporated concepts of feature extraction, feature selection and class-specific classification for different objects achieved overall effective decoding of different grasp patterns. Improvements to preliminary work, discussed in Appendix A, formed the collation of reach trajectory analysis in Chapter 5.

The proposed sensor suite combined work carried out on MMG, computer vision and physiological information according to the conceptual control architecture described in Chapter 3. The integrated system was implemented for the real-time control of a myoelectric hand prosthesis in a pair of experiments designed to assess the system's classification performance and viability for completing simple tasks in Chapter 6. The sensor suite performed better than conventional control with MMG sensors in task-oriented experimentation, demonstrating the potential of sensor fusion, and more specifically, physiological information, for assistive HMI applications.

## **7.2 Conclusions**

Although controlling individual DOF of robotic arms using multiple gestures does have the benefits of greater flexibility in user actions, precise control is still far from perfect, and users are faced with extensive periods of training, high cognitive load, and increased muscle fatigue. On the other hand, conventional control using pre-programmed grasp patterns

---

generally works very well, however is still let down by the same debilitating factors.

The proposed sensor suite aimed to solve these common problems associated with myoelectric hand control, with results demonstrating good overall grasp classification and selection. The sensor suite shows potential to reduce cognitive load and muscle fatigue on the user due to the automation of grasp prediction and selection processes, although this has yet to be quantitatively evaluated. The use of physiological information as a novel grasp classification strategy proved to be a useful tool in interpreting user intention. The ability to apply control commands to a robotic system without requiring the need to make any additional and potentially fatiguing gestures can vastly improve the usability of modern robotics devices for prolonged periods of time. The strategy's potential is not just limited to applications in prosthetics within the medical field, but can also be adapted to rehabilitation for stroke and other neurological disorders using exoskeletons to help patients relearn motor functions.

Although erroneous behaviour cannot be fully eliminated, and the accuracy of the system is still not up to a suitable standard required for regular patient use, the sensor suite concept shows plenty of potential with some refinement to all aspects of the system, as well as in terms of improved hardware development for a more integrated, minimalist and aesthetic appeal. Greater in-depth signal processing for motion segmentation and feature construction is required to improve grasp prediction using inertial motion, as well as stronger integration with the MMG sensor to reduce susceptibility to motion artifacts and unintentional activation. Improved object recognition in cluttered, everyday environments, and the formation of simpler but more functional object categories and their associated selection of grasp patterns would provide a reduction in object, and therefore grasp misclassification rate and would extend the system for a wider range of activities.

### **7.2.1 Summary of Contributions**

The summary of contributions, highlighted in Chapter 1 are reiterated below.

#### **1. Decoding Grasp Intention**

- Analysis of displacement, velocity and acceleration features inherent in arm

---

motion during grasp established a novel method for predicting grasp intention when grasping different objects with various grasp patterns (Chapter 5).

## **2. Human-machine Interfaces**

- Development of an unobtrusive eye-in-hand vision system for automated grasp pattern selection of a myoelectric hand prosthesis to grasp objects of different sizes (Chapter 4). This preliminary work combined both computer vision and mechanomyogram sensors, and formed the base of which the complete sensor suite was designed.
- Development of a wearable heterogeneous sensor fusion control architecture combining mechanomyogram sensors, computer vision and inertial motion for upper limb robotic control, offering solutions to major problems inherent in conventional strategies (Chapter 3).
- Real-time implementation of the proposed heterogeneous sensor suite to provide improved natural control over myoelectric hand prosthesis using predictive grasp selection, while potentially reducing the cognitive burden imposed on amputees (Chapter 6).

### **7.2.2 Suggested Future Directions**

While the ability to discriminate between different grasp patterns through physiological activity has been demonstrated, there are a number of modifications that can be made to improve functional use. The results obtained leave plenty of room for improvement, and given additional time and resources, grasp selection accuracy can be increased by comparing and integrating a wider variety of classification strategies, which can lead to enhanced performance and wider applicability of the framework to a broader range of operations. Further development of the object recognition and grasp classification algorithms are the most obvious solutions, however even state of the art classifiers do not provide 100% accuracy, especially if the underlying control structure has some flaws.

The sensor suite concept has the potential to continually grow with the integration of additional sensors to further improve environmental awareness of the system, leading to

---

improved grasp selection accuracy, and the reduction of false positives. A balance between classification accuracy, user control, and cognitive load must be found, all while keeping the number of required sensors minimal and unobtrusive. Many of the improvements discussed can potentially be studied in enough depth to become research topics themselves, so it is important to note how much the scope of this research can grow, given the time, energy and resources. This section aims to address a number of limitations of the proposed system in terms of both hardware, signal analysis and control architecture.

#### **7.2.2.i Correctional Feedback**

Although the sensor fusion concept proposed resulted in the reduction of cognitive load and muscle fatigue on the user, it is essential to provide some form of correctional control to reduce systematic errors. It was evident during task-oriented experimentation that if the object was wrongly classified, there was a risk that the grasp would be classified incorrectly too. The user has no method of correcting the wrong object classification, or even knowing of it before inertial motion recording began. Even the state of the art in object recognition is far from perfect, so a means of class correction at the initial stage would go a long way in the reduction of errors further down the line.

Restructuring the control architecture to provide an additional layer of sensory input would give a degree of control back to the user, but would potentially increase the cognitive and physical burden if requiring too much additional input from them. Providing the user with a method of correcting false object classification if necessary would also require providing them with a form of feedback. Although not currently widely available, the development of augmented reality technology products such as the *Google Glass* could enable real-time monitoring of the camera's point of view, potentially aiding in the manual targetting of objects, which would be an exceptionally useful feature for use in cluttered environments. This could decrease the number of indirect grasp misclassifications associated with poor object targetting. An integrated miniature RGB-D camera or even stereo camera pair for calculating depth can also vastly improve object targetting, while also aiding in the removal of the background clutter in the image for improved object classification.

---

It was found during experimentation, that subjects benefited from being able to view the MMG signal response as it provided them with visual feedback to tell them when the muscle signal would or would not be detected, reducing the number of ignored intentional muscle activations. An augmented reality display would also be able to provide the user with this feedback, enabling complete monitoring of the entire sensor suite.

Additional input from the user could be in the form of a secondary MMG sensor, located on the brow if connected to the glasses, or on the flexor digitorum of the active arm. One sensor could be used to activate the object recognition system, and the other for grasp prediction. Augmented reality would be able to give the user feedback on the predicted object and grasp, giving them a chance to interrupt and correct the classification if necessary.

#### **7.2.2.ii Sensor Design**

In terms of hardware, a lot can be done to improve the sensor technology used in the sensor suite, with the most important being the redesign of the MMG sensor. The current design described in Chapter 4 suffers significantly from motion artifacts, with misinterpretation of arm motion and muscle activation being the main issues. Although methods were used to reduce it by monitoring gyroscopic data, it would also result in intentional muscle activations being ignored, thus increasing muscle fatigue. The method would still not prevent 100% of unintentional activations through dynamic arm motion from being detected. Any external interference on the skin or MMG sensor itself such as tapping, brushing of material or anything that perturbs the skin in some way, would induce large spikes in the signal, potentially causing unintentional activations. This is a major flaw of the sensor, however, research into sensor design and experimenting with different materials could help to reduce external interference and motion artifacts, which would increase its overall viability in a wider number of applications.

Inertial sensing can also benefit from improvements, not only in terms of the algorithms used for the estimation of orientation, but also in the reduction of drift. With many grasp patterns having very similar reaching trajectories, reducing drift is very important in the correct prediction of grasp. Using inertial measurements to differentiate between dif-



---

ferent elevation and angular positions to use multiple position-specific templates for each subject could greatly improve the accuracy of the system. Position-specific templates would greatly reduce the variance in grasp motion data between grasps, however, would add another level for potential misclassification.

#### **7.2.2.iii Further Studies**

Extending the current study to test on additional amputee participants will be beneficial in terms of evaluating the system for end users. Incorporating a secondary task in the experimental protocol would provide quantitative analysis of the reduction in cognitive load that the sensor suite provides. The addition of EMG sensors to measure muscle fatigue would also aid in evaluating the reduction in physical load.

By providing a wider range of grasp patterns across a larger number of object categories, further assessment of the system's viability for a wider range of activities of daily living (ADL) can be conducted. Although, some changes would be required in the modeling of object categories and their associated grasp patterns, to make sure that only the most common, relevant and useful patterns are assigned. This in turn would help split the workload of grasp prediction between the CVSS and GPSS, which would improve overall grasp classification performance for each object. This would mean improvements to the CVSS would be a necessary step in order to increase the object classification accuracy to make sure the correct grasp templates are being used. Some form of object correctional feedback described previously would be a useful option to reduce misclassification errors.

#### **7.2.2.iv Applications in Rehabilitation**

Although the sensor suite's application in prosthesis control has validated its effectiveness, applying the system to a variety of applications within the medical field would highlight its generality as an assistive HMI. Adapting the system for exoskeleton control as a rehabilitation device for stroke patients and other neurological disorders can potentially improve motor learning as well as provide a performance measurement tool for assessment. A pair of IMU sensors can be used to monitor the grasp trajectory of impaired individuals for dif-

---

ferent objects and grasps, and quantitatively measure improvement over time by comparing motion against that of a healthy individual. An exoskeleton could use this information for an adaptive controller to help impaired individuals relearn natural reaching motion for various grasps depending on the object and desired interaction.

### **7.3 Final Comments**

This work has investigated combining MMG sensors for muscle activation, computer vision for object recognition, and inertial motion for grasp prediction to provide automated command input for assistive HMIs for robotic arm control. The predominant focus was the extraction of features within physiological information during the reaching phase of grasp, in order to predict user intention. The use of physiological activity enables a natural, gesture-free and non-invasive HMI system to predict user intention without further increasing cognitive and physical load. The proposed heterogeneous sensor suite was validated through the real-time control of a myoelectric hand prosthesis, demonstrating comparable results to conventional control strategies while potentially reducing cognitive load and muscle fatigue.

# Bibliography

- [1] D. G. Evans, R. Drew, and P. Blenkhorn, “Controlling mouse pointer position using an infrared head-operated joystick,” *IEEE Transactions on rehabilitation engineering*, vol. 8, no. 1, pp. 107–117, 2000.
- [2] J. Musić, M. Cecić, and M. Bonković, “Experimental measurement of information transfer rate of the inertial sensor based human-computer interface for the disabled,” *Transactions on systems (WSEAS)*, vol. 8, no. 9, pp. 1072–1082, 2009.
- [3] K. Toya, T. Miyagawa, and Y. Kubota, “Power-assist glove operated by predicting the grasping mode,” *Journal of System Design and Dynamics*, vol. 5, no. 1, pp. 94–108, 2011.
- [4] M. Takagi, K. Iwata, Y. Takahashi, S.-i. Yamamoto, H. Koyama, and T. Komeda, “Development of a grip aid system using air cylinders,” in *Proceedings of the IEEE International Conference on Robotics and Automation (ICRA)*, pp. 2312–2317, 2009.
- [5] R. Woodward, S. Shefelbine, and R. Vaidyanathan, “Integrated grip switching and grasp control for prosthetic hands using fused inertial and mechanomyography measurement,” in *Swarm/Human Blended Intelligence Workshop (SHBI), 2015*, pp. 1–8, IEEE, 2015.
- [6] “Ossur: Symbiotic leg 3.” <http://www.ossur.com/symbionicleg/>. Accessed: 26-08-2016.

- 
- [7] W. W. Abbott and A. A. Faisal, "Ultra-low-cost 3d gaze estimation: an intuitive high information throughput compliment to direct brain-machine interfaces," *Journal of neural engineering*, vol. 9, no. 4, p. 046016, 2012.
- [8] A. Bulling, D. Roggen, and G. Tröster, *Wearable EOG goggles: eye-based interaction in everyday environments*. ACM, 2009.
- [9] X. Huo, J. Wang, and M. Ghovanloo, "Wireless control of powered wheelchairs with tongue motion using tongue drive assistive technology," in *Proceedings of the 30th Annual International Conference of the IEEE Engineering in Medicine and Biology Society*, pp. 4199–4202, 2008.
- [10] "Touch Bionics: i-limb." <http://www.touchbionics.com/products>. Accessed: 03-08-2016.
- [11] C. Cipriani, C. Antfolk, M. Controzzi, G. Lundborg, B. Rosén, M. C. Carrozza, and F. Sebelius, "Online myoelectric control of a dexterous hand prosthesis by transradial amputees," *IEEE Transactions on Neural Systems and Rehabilitation Engineering*, vol. 19, no. 3, pp. 260–270, 2011.
- [12] C. Orizio, "Muscle sound: bases for the introduction of a mechanomyographic signal in muscle studies.," *Critical reviews in biomedical engineering*, vol. 21, no. 3, p. 201, 1993.
- [13] S. Došen, C. Cipriani, M. Kostić, M. Controzzi, M. C. Carrozza, and D. B. Popović, "Cognitive vision system for control of dexterous prosthetic hands: experimental evaluation," *Journal of neuroengineering and rehabilitation*, vol. 7, no. 1, p. 1, 2010.
- [14] M. Marković, S. Došen, C. Cipriani, D. Popović, and D. Farina, "Stereovision and augmented reality for closed-loop control of grasping in hand prostheses," *Journal of neural engineering*, vol. 11, no. 4, p. 046001, 2014.
- [15] M. Marković, S. Došen, D. Popović, B. Graimann, and D. Farina, "Sensor fusion and computer vision for context-aware control of a multi degree-of-freedom prosthesis," *Journal of neural engineering*, vol. 12, no. 6, p. 066022, 2015.

- 
- [16] R. Woodward, S. Shefelbine, and R. Vaidyanathan, "Pervasive motion tracking and muscle activity monitor," in *Proceedings of the 27th IEEE International Symposium on Computer-Based Medical Systems*, CBMS '14, (Washington, DC, USA), pp. 421–426, IEEE Computer Society, 2014.
- [17] S. O. H. Madgwick, A. J. L. Harrison, and R. Vaidyanathan, "Estimation of imu and marg orientation using a gradient descent algorithm," in *Proceedings of the IEEE International Conference on Rehabilitation Robotics (ICORR)*, pp. 1–7, June 2011.
- [18] J. Belter and A. Dollar, "Performance characteristics of anthropomorphic prosthetic hands," in *Proceedings of the IEEE International Conference on Rehabilitation Robotics (ICORR)*, pp. 1–7, 2011.
- [19] R. Weir, "The great divide - the human-machine interface. issues in the control of prostheses, manipulators, and other human machine systems," in *Proceedings of the 29th IEEE Annual Bioengineering Conference*, pp. 275–276, 2003.
- [20] A. Fougner, . Staudahl, P. Kyberd, Y. Losier, and P. Parker, "Control of upper limb prostheses: Terminology and proportional myoelectric control—a review," *IEEE Transactions on Neural Systems and Rehabilitation Engineering*, vol. 20, no. 5, pp. 663–677, 2012.
- [21] C. Castellini and P. v. d. Smagt, "Surface emg in advanced hand prosthetics," *Biological Cybernetics*, vol. 100, pp. 35–47, Jan. 2009.
- [22] M. Mace, S. Subbich, A. A. Naeem, and R. Vaidyanathan, "Augmenting neuroprosthetic hand control through evaluation of a bioacoustic interface," in *Proceedings of the IEEE/RSJ International Conference on Intelligent Robots and Systems(IROS)*, pp. 1499–1505, 2013.
- [23] "RSL Steeper: The bebionic hand." <http://bebionic.com/>. Accessed: 27-08-2013.
- [24] W. H. Organization *et al.*, *World report on disability*. World Health Organization, 2011.

- 
- [25] S. H. Kozin, "Upper-extremity congenital anomalies," *Journal of Bone Joint Surg Am*, vol. 85, no. 8, pp. 1564–1576, 2003.
- [26] K. Ziegler-Graham, E. J. MacKenzie, P. L. Ephraim, T. G. Trivison, and R. Brookmeyer, "Estimating the prevalence of limb loss in the united states: 2005 to 2050," *Archives of physical medicine and rehabilitation*, vol. 89, no. 3, pp. 422–429, 2008.
- [27] F. M. Maynard, M. B. Bracken, G. Creasey, J. Ditunno, W. H. Donovan, T. B. Ducker, S. L. Garber, R. J. Marino, S. L. Stover, C. H. Tator, *et al.*, "International standards for neurological and functional classification of spinal cord injury," *Spinal cord*, vol. 35, no. 5, pp. 266–274, 1997.
- [28] C. M. Gibson, M. D. Donnelly, and T. Turner, "One degree of separation: Paralysis and spinal cord injury in the united states," tech. rep., Christopher and Dana Reeve Foundation, 2003.
- [29] P. Langhorne, F. Coupar, and A. Pollock, "Motor recovery after stroke: a systematic review," *The Lancet Neurology*, vol. 8, no. 8, pp. 741–754, 2009.
- [30] A. Compston and A. Coles, "Multiple sclerosis," *The Lancet*, vol. 372, no. 9648, pp. 1502–1517, 2008.
- [31] G. Bauer, F. Gerstenbrand, and E. Ruml, "Varieties of the locked-in syndrome," *Journal of neurology*, vol. 221, no. 2, pp. 77–91, 1979.
- [32] B. A. Myers, "A brief history of human-computer interaction technology," *Interactions*, vol. 5, no. 2, pp. 44–54, 1998.
- [33] S. Guo, R. Cooper, M. Boninger, A. Kwarcia, and B. Ammer, "Development of power wheelchair chin-operated force-sensing joystick," in *Proceedings of the 2nd Joint IEEE Conference on Engineering in Medicine and Biology (EMBS) and the Annual Fall Meeting of the Biomedical Engineering Society (BMES)*, vol. 3, pp. 2373–2374, 2002.

- 
- [34] C. A. M. Pereira, R. Bolliger Neto, A. C. Reynaldo, M. C. d. M. Luzo, and R. P. Oliveira, "Development and evaluation of a head-controlled human-computer interface with mouse-like functions for physically disabled users," *Clinics*, vol. 64, no. 10, pp. 975–981, 2009.
- [35] M. Nunoshita and Y. Ebisawa, "Head pointer based on ultrasonic position measurement," in *Proceedings of the 24th IEEE Annual Conference on Engineering in Medicine and Biology*, vol. 2, pp. 1732–1733, 2002.
- [36] Y.-L. Chen, "Application of tilt sensors in human-computer mouse interface for people with disabilities," *IEEE Transactions on neural systems and rehabilitation engineering*, vol. 9, no. 3, pp. 289–294, 2001.
- [37] M. Betke, J. Gips, and P. Fleming, "The camera mouse: visual tracking of body features to provide computer access for people with severe disabilities," *IEEE Transactions on neural systems and Rehabilitation Engineering*, vol. 10, no. 1, pp. 1–10, 2002.
- [38] H. Kim and D. Ryu, "Computer control by tracking head movements for the disabled," in *International Conference on Computers for Handicapped Persons*, pp. 709–715, 2006.
- [39] J. Gray, P. Jia, H. H. Hu, T. Lu, and K. Yuan, "Head gesture recognition for hands-free control of an intelligent wheelchair," *Industrial Robot: An International Journal*, vol. 34, no. 1, pp. 60–68, 2007.
- [40] Z.-f. Hu, L. Li, Y. Luo, Y. Zhang, and X. Wei, "A novel intelligent wheelchair control approach based on head gesture recognition," in *IEEE International Conference on Computer Application and System Modeling (ICCASM)*, vol. 6, pp. V6–159, 2010.
- [41] T. Starner, J. Auxier, D. Ashbrook, and M. Gandy, "The gesture pendant: A self-illuminating, wearable, infrared computer vision system for home automation control and medical monitoring," in *International Symposium on Wearable Computers*, pp. 87–94, 2000.

- 
- [42] T. Takahashi and F. Kishino, "Hand gesture coding based on experiments using a hand gesture interface device," *ACM SIGCHI Bulletin*, vol. 23, no. 2, pp. 67–74, 1991.
- [43] W. Kadous *et al.*, "Grasp: Recognition of australian sign language using instrumented gloves," Master's thesis, University of New South Wales, 1995.
- [44] C. Lee and Y. Xu, "Online, interactive learning of gestures for human/robot interfaces," in *Proceedings of the IEEE International Conference on Robotics and Automation (ICRA)*, vol. 4, pp. 2982–2987, 1996.
- [45] C. Vogler and D. Metaxas, "Adapting hidden markov models for asl recognition by using three-dimensional computer vision methods," in *IEEE International Conference on Systems, Man, and Cybernetics (SMC)*, vol. 1, pp. 156–161, 1997.
- [46] H. Brashear, T. Starner, P. Lukowicz, and H. Junker, "Using multiple sensors for mobile sign language recognition," in *IEEE International Symposium on Wearable Computers*, 2003.
- [47] J. L. Patton and F. A. Mussa-Ivaldi, "Robot-assisted adaptive training: custom force fields for teaching movement patterns," *IEEE Transactions on Biomedical Engineering*, vol. 51, no. 4, pp. 636–646, 2004.
- [48] P. Heo, G. M. Gu, S.-j. Lee, K. Rhee, and J. Kim, "Current hand exoskeleton technologies for rehabilitation and assistive engineering," *International Journal of Precision Engineering and Manufacturing*, vol. 13, no. 5, pp. 807–824, 2012.
- [49] Y. Kadowaki, T. Noritsugu, M. Takaiwa, D. Sasaki, and M. Kato, "Development of soft power-assist glove and control based on human intent," *Journal of Robotics and Mechatronics*, vol. 23, no. 2, p. 281, 2011.
- [50] L. Martinez, O. Olaloye, M. Talarico, S. Shah, R. Arends, and B. BuSha, "A power-assisted exoskeleton optimized for pinching and grasping motions," in *Proceedings of the 36th IEEE Annual Northeast Bioengineering Conference (NEBEC)*, pp. 1–2, 2010.



- 
- [51] M. F. Rotella, K. E. Reuther, C. L. Hofmann, E. B. Hage, and B. F. BuSha, "An orthotic hand-assistive exoskeleton for actuated pinch and grasp," in *Proceedings of the 35th IEEE Annual Northeast Bioengineering Conference (NEBEC)*, pp. 1–2, 2009.
- [52] M. Baker, M. McDonough, E. McMullin, M. Swift, and B. BuSha, "Orthotic hand-assistive exoskeleton," in *IEEE 37th Annual Northeast Bioengineering Conference (NEBEC)*, pp. 1–2, 2011.
- [53] D. Kotiadis, H. Hermens, and P. Veltink, "Inertial gait phase detection for control of a drop foot stimulator: Inertial sensing for gait phase detection," *Medical engineering & physics*, vol. 32, no. 4, pp. 287–297, 2010.
- [54] N. Miura, T. Watanabe, K. Akasaka, and T. Suzuki, "A clinical trial of a prototype of wireless surface fes rehabilitation system in foot drop correction," in *2011 Annual International Conference of the IEEE Engineering in Medicine and Biology Society*, pp. 5461–5464, 2011.
- [55] B. G. Lambrecht and H. Kazerooni, "Design of a semi-active knee prosthesis," in *Proceedings of the IEEE International Conference on Robotics and Automation (ICRA)*, pp. 639–645, 2009.
- [56] H. M. Herr and A. M. Grabowski, "Bionic ankle–foot prosthesis normalizes walking gait for persons with leg amputation," in *Proceedings of the Biological Science / Royal Society*, vol. 279, pp. 457–464, 2012.
- [57] D. W. Hansen and Q. Ji, "In the eye of the beholder: A survey of models for eyes and gaze," *IEEE Transactions on pattern analysis and machine intelligence*, vol. 32, no. 3, pp. 478–500, 2010.
- [58] F. Corno, L. Farinetti, and I. Signorile, "A cost-effective solution for eye-gaze assistive technology," in *Proceedings of the IEEE International Conference on Multimedia and Expo (ICME)*, vol. 2, pp. 433–436, 2002.

- 
- [59] G. Edwards, "New software makes eye tracking viable: You can control computers with your eyes," in *Proceedings of CSUN Technology and Persons with Disabilities Conference*, 1998.
- [60] L. E. Sibert and R. J. Jacob, "Evaluation of eye gaze interaction," in *Proceedings of the ACM SIGCHI conference on Human Factors in Computing Systems*, pp. 281–288, 2000.
- [61] A. E. Kaufman, A. Bandopadhyay, and B. D. Shaviv, "An eye tracking computer user interface," in *Proceedings of the IEEE Symposium on Research Frontiers in Virtual Reality*, pp. 120–121, 1993.
- [62] C.-S. Lin, C. Ho, W. Chen, C. Chiu, and M. Yeh, "Powered wheelchair controlled by eye-tracking system," *Optica Applicata*, vol. 36, no. 2/3, p. 401, 2006.
- [63] K. Arai and R. Mardiyanto, "Eyes based eletric wheel chair control system," *International Journal of Advanced Computer Science and Applications (IJACSA)*, vol. 2, no. 12, 2011.
- [64] Q. Nguyen and S. Jo, "Electric wheelchair control using head pose free eye-gaze tracker," *Electronics letters*, vol. 48, no. 13, p. 1, 2012.
- [65] S. Yathunanthan, L. Chandrasena, A. Umakanthan, V. Vasuki, and S. Munasinghe, "Controlling a wheelchair by use of eog signal," in *Proceedings of the 4th IEEE International Conference on Information and Automation for Sustainability*, pp. 283–288, 2008.
- [66] R. Barea, L. Boquete, M. Mazo, E. López, and L. M. Bergasa, "Eog guidance of a wheelchair using neural networks," in *Proceedings of the 15th IEEE International Conference on Pattern Recognition*, vol. 4, pp. 668–671, 2000.
- [67] A. Al-Haddad, R. Sudirman, and C. Omar, "Guiding wheelchair motion based on eog signals using tangent bug algorithm," in *Proceedings of the 3rd IEEE International Conference on Computational Intelligence, Modelling & Simulation*, pp. 40–45, 2011.

- 
- [68] R. Barea, L. Boquete, M. Mazo, and E. López, “System for assisted mobility using eye movements based on electrooculography,” *IEEE transactions on neural systems and rehabilitation engineering*, vol. 10, no. 4, pp. 209–218, 2002.
- [69] R. Bates and H. O. Istance, “Why are eye mice unpopular? a detailed comparison of head and eye controlled assistive technology pointing devices,” *Universal Access in the Information Society*, vol. 2, no. 3, pp. 280–290, 2003.
- [70] A. Pérez, M. L. Córdoba, A. Garcia, R. Méndez, M. Munoz, J. L. Pedraza, and F. Sanchez, “A precise eye-gaze detection and tracking system,” in *International Conference in Central Europe on Computer Graphics, Visualization and Computer Vision*, 2003.
- [71] R. Valenti and T. Gevers, “Accurate eye center location and tracking using isophote curvature,” in *IEEE Conference on Computer Vision and Pattern Recognition (CVPR)*, pp. 1–8, 2008.
- [72] K.-N. Kim and R. Ramakrishna, “Vision-based eye-gaze tracking for human computer interface,” in *Proceedings of the IEEE International Conference on Systems, Man, and Cybernetics (SMC)*, vol. 2, pp. 324–329, 1999.
- [73] J. Daugman, “The importance of being random: statistical principles of iris recognition,” *Pattern recognition*, vol. 36, no. 2, pp. 279–291, 2003.
- [74] D. W. Hansen and A. E. Pece, “Eye tracking in the wild,” *Computer Vision and Image Understanding*, vol. 98, no. 1, pp. 155–181, 2005.
- [75] D. Li, D. Winfield, and D. J. Parkhurst, “Starburst: A hybrid algorithm for video-based eye tracking combining feature-based and model-based approaches,” in *IEEE Computer Society Conference on Computer Vision and Pattern Recognition (CVPR)*, pp. 79–79, 2005.
- [76] A. L. Yuille, P. W. Hallinan, and D. S. Cohen, “Feature extraction from faces using deformable templates,” *International journal of computer vision*, vol. 8, no. 2, pp. 99–111, 1992.

- 
- [77] J. P. Ivins and J. Porrill, "A deformable model of the human iris for measuring small three-dimensional eye movements," *Machine Vision and Applications*, vol. 11, no. 1, pp. 42–51, 1998.
- [78] J.-Y. Deng and F. Lai, "Region-based template deformation and masking for eye-feature extraction and description," *Pattern recognition*, vol. 30, no. 3, pp. 403–419, 1997.
- [79] J. Bala, K. DeJong, J. Huang, H. Vafaie, and H. Wechsler, "Visual routine for eye detection using hybrid genetic architectures," in *Proceedings of the 13th IEEE International Conference on Pattern Recognition*, vol. 3, pp. 606–610, 1996.
- [80] R. Herpers, M. Michaelis, K.-H. Lichtenauer, and G. Sommer, "Edge and keypoint detection in facial regions," in *Proceedings of the 2nd IEEE International Conference on Automatic Face and Gesture Recognition*, pp. 212–217, 1996.
- [81] S. Sirohey, A. Rosenfeld, and Z. Duric, "A method of detecting and tracking irises and eyelids in video," *Pattern Recognition*, vol. 35, no. 6, pp. 1389–1401, 2002.
- [82] T. D’Orazio, M. Leo, G. Cicirelli, and A. Distanto, "An algorithm for real time eye detection in face images," in *Proceedings of the 17th IEEE International Conference on Pattern Recognition (ICPR)*, vol. 3, pp. 278–281, 2004.
- [83] Y.-I. Tian, T. Kanade, and J. F. Cohn, "Dual-state parametric eye tracking," in *Proceedings of the 4th IEEE International Conference on Automatic Face and Gesture Recognition*, pp. 110–115, 2000.
- [84] J. Yang, R. Stiefelhagen, U. Meier, and A. Waibel, "Real-time face and facial feature tracking and applications," in *International Conference on Auditory-Visual Speech Processing (AVSP)*, 1998.
- [85] K. Grauman, M. Betke, J. Gips, and G. R. Bradski, "Communication via eye blinks-detection and duration analysis in real time," in *Proceedings of the 2001 IEEE Computer Society Conference on Computer Vision and Pattern Recognition (CVPR)*, vol. 1, pp. I–1010, 2001.

- 
- [86] W. Huang and R. Mariani, "Face detection and precise eyes location," in *Proceedings of the 15th IEEE International Conference on Pattern Recognition*, vol. 4, pp. 722–727, 2000.
- [87] J. Huang and H. Wechsler, "Eye detection using optimal wavelet packets and radial basis functions (rbfs)," *International Journal of Pattern Recognition and Artificial Intelligence*, vol. 13, no. 07, pp. 1009–1025, 1999.
- [88] P. Viola and M. J. Jones, "Robust real-time face detection," *International journal of computer vision*, vol. 57, no. 2, pp. 137–154, 2004.
- [89] T. Ishikawa, "Passive driver gaze tracking with active appearance models," tech. rep., Carnegie Mellon University, 2004.
- [90] D. W. Hansen, J. P. Hansen, M. Nielsen, A. S. Johansen, and M. B. Stegmann, "Eye typing using markov and active appearance models," in *Proceedings of the 6th IEEE Workshop on Applications of Computer Vision (WACV)*, pp. 132–136, 2002.
- [91] A. Duchowski, *Eye tracking methodology: Theory and practice*, vol. 373. Springer Science & Business Media, 2007.
- [92] X. L. Brolly and J. B. Mulligan, "Implicit calibration of a remote gaze tracker," in *IEEE Computer Vision and Pattern Recognition Workshop (CVPRW)*, pp. 134–134, 2004.
- [93] C. H. Morimoto and M. R. Mimica, "Eye gaze tracking techniques for interactive applications," *Computer Vision and Image Understanding*, vol. 98, no. 1, pp. 4–24, 2005.
- [94] Q. Ji and X. Yang, "Real-time eye, gaze, and face pose tracking for monitoring driver vigilance," *Real-Time Imaging*, vol. 8, no. 5, pp. 357–377, 2002.
- [95] J.-G. Wang, E. Sung, and R. Venkateswarlu, "Estimating the eye gaze from one eye," *Computer Vision and Image Understanding*, vol. 98, no. 1, pp. 83–103, 2005.

- 
- [96] D. Beymer and M. Flickner, "Eye gaze tracking using an active stereo head," in *Proceedings of the IEEE Computer Society Conference on Computer Vision and Pattern Recognition*, vol. 2, pp. II-451, 2003.
- [97] R. J. Jacob, "Eye movement-based human-computer interaction techniques: Toward non-command interfaces," *Advances in human-computer interaction*, vol. 4, pp. 151-190, 1993.
- [98] F. A. Glenn, H. P. Iavecchia, L. V. Ross, J. M. Stokes, W. J. Weiland, D. Weiss, and A. L. Zaklad, "Eye-voice-controlled interface," in *Proceedings of the Human Factors and Ergonomics Society Annual Meeting*, vol. 30, pp. 322-326, 1986.
- [99] A. J. Glenstrup and T. Engell-Nielsen, "Eye controlled media: Present and future state," *University of Copenhagen, DK-2100*, 1995.
- [100] S. Zhai, C. Morimoto, and S. Ihde, "Manual and gaze input cascaded (magic) pointing," in *Proceedings of the ACM SIGCHI conference on Human Factors in Computing Systems*, pp. 246-253, 1999.
- [101] X. A. Zhao, E. D. Guestrin, D. Sayenko, T. Simpson, M. Gauthier, and M. R. Popovic, "Typing with eye-gaze and tooth-clicks," in *Proceedings of the ACM Symposium on Eye Tracking Research and Applications*, pp. 341-344, 2012.
- [102] A. B. Usakli, S. Gurkan, F. Aloise, G. Vecchiato, and F. Babiloni, "On the use of electrooculogram for efficient human computer interfaces," *Computational intelligence and neuroscience*, vol. 2010, p. 1, 2010.
- [103] Z. Lv, X. Wu, M. Li, and C. Zhang, "Implementation of the eog-based human computer interface system," in *Proceedings of the 2nd IEEE International Conference on Bioinformatics and Biomedical Engineering*, pp. 2188-2191, 2008.
- [104] P. Majaranta and A. Bulling, "Eye tracking and eye-based human-computer interaction," in *Advances in physiological computing*, pp. 39-65, Springer, 2014.

- 
- [105] J. Kim, S. Mastnik, and E. André, “Emg-based hand gesture recognition for real-time biosignal interfacing,” in *Proceedings of the 13th international conference on Intelligent user interfaces*, pp. 30–39, 2008.
- [106] M. R. Ahsan, M. I. Ibrahimy, O. O. Khalifa, *et al.*, “Emg signal classification for human computer interaction: a review,” *European Journal of Scientific Research*, vol. 33, no. 3, pp. 480–501, 2009.
- [107] Y. Kuno, T. Yagi, and Y. Uchikawa, “Development of eye pointer with free head-motion [eog-based system],” in *Proceedings of the 20th Annual International Conference of the IEEE Engineering in Medicine and Biology Society*, vol. 4, pp. 1750–1752, 1998.
- [108] I. Mougharbel, R. El-Hajj, H. Ghamlouch, and E. Monacelli, “Comparative study on different adaptation approaches concerning a sip and puff controller for a powered wheelchair,” in *Proceedings of the IEEE Science and Information Conference (SAI)*, pp. 597–603, 2013.
- [109] M. Ghovanloo, “Tongue operated assistive technologies,” *IEEE engineering in medicine and biology magazine*, vol. 1, p. 4376, 2007.
- [110] C. Gerdtnan and M. Lindén, “Six-button click interface for a disabled user by an adjustable multi-level sip-and-puff switch,” in *Proceedings of SIGRAD 2010: Content aggregation and visualization*, pp. 59–63, 2010.
- [111] S. Furui, “50 years of progress in speech and speaker recognition,” *International Conference on Speech and Computer (SPECOM)*, pp. 1–9, 2005.
- [112] M. Nishimori, T. Saitoh, and R. Konishi, “Voice controlled intelligent wheelchair,” in *Proceedings of the Annual conference of the IEEE Society of Instrument and Control Engineers (SICE)*, pp. 336–340, 2007.
- [113] K. Komiya, K. Morita, K. Kagekawa, and K. Kurosu, “Guidance of a wheelchair by voice,” in *Proceedings of the 26th Annual Conference of the IEEE Industrial Electronics Society (IECON)*, vol. 1, pp. 102–107, 2000.

- 
- [114] G. Pires and U. Nunes, "A wheelchair steered through voice commands and assisted by a reactive fuzzy-logic controller," *Journal of Intelligent and Robotic Systems*, vol. 34, no. 3, pp. 301–314, 2002.
- [115] E. Mainardi and A. Davalli, "Controlling a prosthetic arm with a throat microphone," in *Proceedings of the 29th Annual International Conference of the IEEE Engineering in Medicine and Biology Society*, pp. 3035–3039, 2007.
- [116] S. Harada, J. A. Landay, J. Malkin, X. Li, and J. A. Bilmes, "The vocal joystick: evaluation of voice-based cursor control techniques for assistive technology," *Disability and Rehabilitation: Assistive Technology*, vol. 3, no. 1-2, pp. 22–34, 2008.
- [117] T. Igarashi and J. F. Hughes, "Voice as sound: using non-verbal voice input for interactive control," in *Proceedings of the 14th annual ACM symposium on User interface software and technology*, pp. 155–156, 2001.
- [118] A. J. Sporka, S. H. Kurniawan, and P. Slavík, "Acoustic control of mouse pointer," *Universal Access in the Information Society*, vol. 4, no. 3, pp. 237–245, 2006.
- [119] W. Nutt, C. Arlanch, S. Nigg, and G. Staufert, "Tongue-mouse for quadriplegics," *Journal of Micromechanics and Microengineering*, vol. 8, no. 2, p. 155, 1998.
- [120] C. Salem and S. Zhai, "An isometric tongue pointing device," in *Proceedings of the ACM SIGCHI Conference on Human factors in computing systems*, pp. 538–539, 1997.
- [121] M. Mace, K. Abdullah-al Mamun, A. A. Naeem, L. Gupta, S. Wang, and R. Vaidyanathan, "A heterogeneous framework for real-time decoding of bioacoustic signals: Applications to assistive interfaces and prosthesis control," *Expert Systems with Applications*, vol. 40, pp. 5049–5060, Oct. 2013.
- [122] T. Simpson, C. Broughton, M. J. Gauthier, and A. Prochazka, "Tooth-click control of a hands-free computer interface," *IEEE Transactions on Biomedical Engineering*, vol. 55, no. 8, pp. 2050–2056, 2008.



- 
- [123] T. Mohamed and L. Zhong, “Teethclick: Input with teeth clacks,” tech. rep., Technical Report. Rice University, 2006.
- [124] A. Plotkin, L. Sela, A. Weissbrod, R. Kahana, L. Haviv, Y. Yeshurun, N. Soroker, and N. Sobel, “Sniffing enables communication and environmental control for the severely disabled,” *Proceedings of the National Academy of Sciences*, vol. 107, no. 32, pp. 14413–14418, 2010.
- [125] A. Kushki, A. J. Andrews, S. D. Power, G. King, and T. Chau, “Classification of activity engagement in individuals with severe physical disabilities using signals of the peripheral nervous system,” *PLOS ONE*, vol. 7, no. 2, p. e30373, 2012.
- [126] G. E. Loeb and C. Gans, *Electromyography for experimentalists*. University of Chicago Press, 1986.
- [127] P. Zipp, “Recommendations for the standardization of lead positions in surface electromyography,” *European Journal of Applied Physiology and Occupational Physiology*, vol. 50, no. 1, pp. 41–54, 1982.
- [128] G. R. Naik, D. K. Kumar, and M. Palaniswami, “Multi run ica and surface emg based signal processing system for recognising hand gestures,” in *Proceedings of the 8th IEEE International Conference on Computer and Information Technology (CIT)*, pp. 700–705, 2008.
- [129] D. Farina, N. Jiang, H. Rehbaum, A. Holobar, B. Graimann, H. Dietl, and O. C. Aszmann, “The extraction of neural information from the surface emg for the control of upper-limb prostheses: emerging avenues and challenges,” *IEEE Transactions on Neural Systems and Rehabilitation Engineering*, vol. 22, no. 4, pp. 797–809, 2014.
- [130] J.-S. Han, Z. Z. Bien, D.-J. Kim, H.-E. Lee, and J.-S. Kim, “Human-machine interface for wheelchair control with emg and its evaluation,” in *Proceedings of the 25th Annual International Conference of the IEEE Engineering in Medicine and Biology Society*, vol. 2, pp. 1602–1605, 2003.

- 
- [131] K. Choi, M. Sato, and Y. Koike, "A new, human-centered wheelchair system controlled by the emg signal," in *Proceedings of the IEEE International Joint Conference on Neural Network*, pp. 4664–4671, 2006.
- [132] M. DiCicco, L. Lucas, and Y. Matsuoka, "Comparison of control strategies for an emg controlled orthotic exoskeleton for the hand," in *Proceedings of the IEEE International Conference on Robotics and Automation (ICRA)*, vol. 2, pp. 1622–1627, 2004.
- [133] M. Mulas, M. Folgheraiter, and G. Gini, "An emg-controlled exoskeleton for hand rehabilitation," in *Proceedings of the 9th IEEE International Conference on Rehabilitation Robotics (ICORR)*, pp. 371–374, 2005.
- [134] D. P. Ferris, K. E. Gordon, G. S. Sawicki, and A. Peethambaran, "An improved powered ankle–foot orthosis using proportional myoelectric control," *Gait & posture*, vol. 23, no. 4, pp. 425–428, 2006.
- [135] "Ottobock: Michelangelo prosthetic hand." <http://www.ottobockus.com/prosthetics/upper-limb-prosthetics/solution-overview/michelangelo-prosthetic-hand/>. Accessed: 12-07-2016.
- [136] B. Hudgins, P. Parker, and R. N. Scott, "A new strategy for multifunction myoelectric control," *IEEE Transactions on Biomedical Engineering*, vol. 40, no. 1, pp. 82–94, 1993.
- [137] M. Zecca, S. Micera, M. Carrozza, and P. Dario, "Control of multifunctional prosthetic hands by processing the electromyographic signal," *Critical Reviews in Biomedical Engineering*, vol. 30, no. 4-6, 2002.
- [138] D. Nishikawa, W. Yu, H. Yokoi, and Y. Kakazu, "Emg prosthetic hand controller using real-time learning method," in *Proceedings of the IEEE International Conference on Systems, Man, and Cybernetics (SMC)*, vol. 1, pp. 153–158, 1999.

- 
- [139] D. Nishikawa, W. Yu, H. Yokoi, and Y. Kakazu, "On-line learning method for emg prosthetic hand control," *Electronics and Communications in Japan (Part III: Fundamental Electronic Science)*, vol. 84, no. 10, pp. 35–46, 2001.
- [140] F. Tenore, A. Ramos, A. Fahmy, S. Acharya, R. Etienne-Cummings, and N. V. Thakor, "Towards the control of individual fingers of a prosthetic hand using surface emg signals," in *Proceedings of the 29th Annual International Conference of the IEEE Engineering in Medicine and Biology Society*, pp. 6145–6148, 2007.
- [141] F. V. Tenore, A. Ramos, A. Fahmy, S. Acharya, R. Etienne-Cummings, and N. V. Thakor, "Decoding of individuated finger movements using surface electromyography," *IEEE Transactions on Biomedical Engineering*, vol. 56, no. 5, pp. 1427–1434, 2009.
- [142] M. Haris, P. Chakraborty, and B. V. Rao, "Emg signal based finger movement recognition for prosthetic hand control," in *Proceedings of the IEEE Communication, Control and Intelligent Systems (CCIS)*, pp. 194–198, 2015.
- [143] G. Gordon and A. Holbourn, "The sounds from single motor units in a contracting muscle," *The Journal of physiology*, vol. 107, no. 4, p. 456, 1948.
- [144] G. Oster and J. S. Jaffe, "Low frequency sounds from sustained contraction of human skeletal muscle," *Biophysical journal*, vol. 30, no. 1, p. 119, 1980.
- [145] D. T. Barry, "Acoustic signals from frog skeletal muscle.," *Biophysical journal*, vol. 51, no. 5, p. 769, 1987.
- [146] Y. Yoshitake, H. Ue, M. Miyazaki, and T. Moritani, "Assessment of lower-back muscle fatigue using electromyography, mechanomyography, and near-infrared spectroscopy," *European journal of applied physiology*, vol. 84, no. 3, pp. 174–179, 2001.
- [147] T. J. Herda, J. T. Cramer, E. D. Ryan, M. P. McHugh, and J. R. Stout, "Acute effects of static versus dynamic stretching on isometric peak torque, electromyography, and mechanomyography of the biceps femoris muscle," *The Journal of Strength & Conditioning Research*, vol. 22, no. 3, pp. 809–817, 2008.

- 
- [148] T. K. Evetovich, N. J. Nauman, D. S. Conley, and J. B. Todd, "Effect of static stretching of the biceps brachii on torque, electromyography, and mechanomyography during concentric isokinetic muscle actions.," *The Journal of Strength & Conditioning Research*, vol. 17, no. 3, pp. 484–488, 2003.
- [149] J. Marusiak, A. Jaskólska, K. Kisiel-Sajewicz, G. H. Yue, and A. Jaskólski, "Emg and mmg activities of agonist and antagonist muscles in parkinson's disease patients during absolute submaximal load holding," *Journal of Electromyography and Kinesiology*, vol. 19, no. 5, pp. 903–914, 2009.
- [150] X. Hu, K. Tong, and L. Li, "The mechanomyography of persons after stroke during isometric voluntary contractions," *Journal of Electromyography and Kinesiology*, vol. 17, no. 4, pp. 473–483, 2007.
- [151] M. G. Antonelli, P. Beomonte Zobel, and J. Giacomini, "Use of mmg signals for the control of powered orthotic devices: development of a rectus femoris measurement protocol," *Assistive Technology*, vol. 21, no. 1, pp. 1–12, 2009.
- [152] J. Silva, W. Heim, and T. Chau, "A self-contained, mechanomyography-driven externally powered prosthesis," *Archives of Physical Medicine and Rehabilitation*, vol. 86, pp. 2066–2070, Oct. 2005.
- [153] M. A. Islam, K. Sundaraj, R. B. Ahmad, N. U. Ahamed, and M. A. Ali, "Mechanomyography sensor development, related signal processing, and applications: a systematic review," *IEEE Sensors Journal*, vol. 13, no. 7, pp. 2499–2516, 2013.
- [154] E. Biddiss, D. Beaton, and T. Chau, "Consumer design priorities for upper limb prosthetics," *Disability and Rehabilitation: Assistive Technology*, vol. 2, pp. 346–357, Jan. 2007.
- [155] K. Ostlie, I. M. Lesjo, R. J. Franklin, B. Garfelt, O. H. Skjeldal, and P. Magnus, "Prosthesis rejection in acquired major upper-limb amputees: a population-based

- 
- survey,” *Disability and Rehabilitation: Assistive Technology*, vol. 7, pp. 294–303, Nov. 2011.
- [156] J. A. Piepmeier, B. Gumpert, and H. Lipkin, “Uncalibrated eye-in-hand visual servoing,” *The International Journal of Robotics Research*, vol. 22, no. 10-11, pp. 805–819, 2003.
- [157] G. Flandin, F. Chaumette, and E. Marchand, “Eye-in-hand/eye-to-hand cooperation for visual servoing,” in *Proceedings of the IEEE International Conference on Robotics and Automation (ICRA)*, vol. 3, pp. 2741–2746, 2000.
- [158] S. Došen and D. B. Popović, “Transradial prosthesis: artificial vision for control of prehension,” *Artificial organs*, vol. 35, no. 1, pp. 37–48, 2011.
- [159] M. C. Carrozza, G. Cappiello, S. Micera, B. B. Edin, L. Beccai, and C. Cipriani, “Design of a cybernetic hand for perception and action,” *Biological cybernetics*, vol. 95, no. 6, pp. 629–644, 2006.
- [160] C. Cipriani, M. Controzzi, and M. C. Carrozza, “The smarthand transradial prosthesis,” *Journal of neuroengineering and rehabilitation*, vol. 8, no. 1, p. 1, 2011.
- [161] RSL Steeper, Leeds, UK, *Bebionic V3 Technical Manual*, 2013. Document RSLIT317 Issue 3 2013.
- [162] A. Posatskiy and T. Chau, “Design and evaluation of a novel microphone-based mechanomyography sensor with cylindrical and conical acoustic chambers,” *Journal of Medical engineering and physics*, vol. 34, no. 8, pp. 1184–1190, 2012.
- [163] A. Posatskiy and T. Chau, “The effects of motion artifact on mechanomyography: A comparative study of microphones and accelerometers,” *Journal of Electromyography and Kinesiology*, vol. 22, no. 2, pp. 320–324, 2012.
- [164] “Homefly: Mylar membrane.” <https://www.homefly.com/>. Accessed: 01-08-2016.
- [165] M. Stokes and P. Dalton, “Acoustic myography for investigating human skeletal muscle fatigue,” *Journal of applied physiology*, vol. 71, no. 4, pp. 1422–1426, 1991.

- 
- [166] C. Orizio, R. Perini, B. Diemont, M. M. Figini, and A. Veicsteinas, “Spectral analysis of muscular sound during isometric contraction of biceps brachii,” *Journal of applied physiology*, vol. 68, no. 2, pp. 508–512, 1990.
- [167] P. Corke, *Robotics, vision and control: fundamental algorithms in MATLAB*. Springer, 2011.
- [168] M. Gardner, R. Woodward, E. Burdet, R. Vaidyanathan, and B. C. Khoo, “An unobtrusive vision system to reduce the cognitive burden of hand prosthesis control,” in *Proceedings of the IEEE International Conference on Automation, Robotics, Control and Vision (ICARCV)*, (Singapore), pp. 1279–1284, 2014.
- [169] S. Došen, C. Cipriani, M. Kostić, M. Controzzi, M. C. Carrozza, and D. B. Popović, “Cognitive vision system for control of dexterous prosthetic hands: Experimental evaluation,” *Journal of neuroengineering and rehabilitation*, vol. 7, no. 1, p. 42, 2010.
- [170] S. Došen and D. B. Popović, “Transradial prosthesis: Artificial vision for control of prehension,” *Artificial Organs*, vol. 35, no. 1, pp. 37–48, 2010.
- [171] “Alex Lewis Trust.” <http://www.alex-lewis.co.uk/>. Accessed: 06-07-2017.
- [172] J. Diebel, “Representing attitude: Euler angles, unit quaternions, and rotation vectors,” *Matrix*, vol. 58, no. 15-16, pp. 1–35, 2006.
- [173] W. R. Hamilton, *Elements of quaternions*. Longmans, Green, & Company, 1866.
- [174] M. J. Baker, “Euclidean space - quaternions.” <http://www.euclideanspace.com/maths/algebra/realNormedAlgebra/quaternions/>. Accessed: 28-04-2016.
- [175] J. B. Kuipers, *Quaternions and rotation sequences*, vol. 66. Princeton University Press, 1999.
- [176] R. E. Kalman, “A new approach to linear filtering and prediction problems,” *Journal of Basic Engineering*, vol. 82, pp. 35–45, Mar. 1960.

- 
- [177] P. Slycke, *MTi User Manual*. Xsens Technologies B.V, Enschede, The Netherlands, February 2015. Document MT0605P.F.
- [178] LORD MicroStrain Sensing Systems, Vermont, USA, *3DM-GX4-45 Inertial Navigation System User Manual*. Document 8500-0041 Revision E.
- [179] VectorNav Technologies, Texas, USA, *VN-300 User Manual*. Document UM005 v0.14.
- [180] Intersense Incorporated, Massachusetts, USA, *InertiaCube BT User Manual*. Document 072-ICBT0-0010 Rev. 1.0.
- [181] R. Brown and P. Hwang, *Introduction to random signals and applied Kalman filtering : with MATLAB exercises and solutions*. Wiley, 1997.
- [182] B. Barshan and H. F. Durrant-Whyte, “Inertial navigation systems for mobile robots,” *IEEE Transactions on Robotics and Automation*, vol. 11, no. 3, pp. 328–342, 1995.
- [183] E. Foxlin, “Inertial head-tracker sensor fusion by a complementary separate-bias kalman filter,” in *Proceedings of the IEEE Virtual Reality Annual International Symposium*, pp. 185–194, 1996.
- [184] J. L. Marins, X. Yun, E. R. Bachmann, R. B. McGhee, and M. J. Zyda, “An extended kalman filter for quaternion-based orientation estimation using marg sensors,” in *Proceedings of the IEEE/RSJ International Conference on Intelligent Robots and Systems*, vol. 4, pp. 2003–2011, 2001.
- [185] A. M. Sabatini, “Quaternion-based extended kalman filter for determining orientation by inertial and magnetic sensing,” *IEEE Transactions on Biomedical Engineering*, vol. 53, no. 7, pp. 1346–1356, 2006.
- [186] H. J. Luinge and P. H. Veltink, “Measuring orientation of human body segments using miniature gyroscopes and accelerometers,” *Medical and Biological Engineering and computing*, vol. 43, no. 2, pp. 273–282, 2005.
- [187] x-io Technologies Limited, UK, *x-IMU User Manual 5.2*, November 2013.

- 
- [188] A. K. Jain, R. P. Duin, and J. Mao, “Statistical pattern recognition: A review,” *IEEE Transactions on Pattern Analysis and Machine Intelligence*, vol. 22, no. 1, pp. 4–37, 2000.
- [189] L. Breiman, J. Friedman, C. J. Stone, and R. A. Olshen, *Classification and regression trees*. CRC press, 1984.
- [190] V. Vapnik, *The nature of statistical learning theory*. Springer Science & Business Media, 2013.
- [191] T. Fletcher, “Support vector machines explained,” 2009.
- [192] “Mpow: 180 degree supreme fisheye + 0.65x wide angle+ 10x macro lens.” <https://www.amazon.co.uk/Degree-Supreme-Fisheye-Samsung-Smartphone/dp/B00OPZENR2>. Accessed: 23-07-2016.
- [193] R. Woodward, *Pervasive Motion Tracking and Physiological Monitoring*. PhD thesis, Imperial College London, 2015.
- [194] M. Gardner, R. Vaidyanathan, E. Burdet, and B. C. Khoo, “Motion-based grasp selection: Improving traditional control strategies of myoelectric hand prosthesis,” in *Proceedings of the IEEE International Conference on Rehabilitation Robotics (ICORR)*, pp. 307–312, 2015.
- [195] “X-IO Technologies: x-imu.” <http://x-io.co.uk/x-imu/>. Accessed: 01-08-2016.



# Appendices



## Appendix A

# Preliminary validation of motion-based grasp prediction

Preliminary work (peer-reviewed and published in [194]) for validation was conducted using a pair of X-IMU sensors by X-IO Technologies [195] for interacting with objects with generalised sizes and shapes. Three object classes: very small (VS), small (S), medium (M) and cup (CP), were chosen to evaluate the discrimination capability of the most common grasps for that class. The M class was excluded from the study for simplicity, as it was assumed that all grasps made would be a *power* grasp, either from above or the front of the object. The grasps chosen for the VS class were *power*, *pinch* and *open palm*; S class were *power*, *pinch* and *tripod*; and C class were *power* and *tripod*, shown in figure A.1.

### A.1 Experimental Procedure

The pair of X-IMU inertial sensors were fitted with a Velcro strap and worn around the wrist and bicep as shown in A.2. A wrist strap was used to prevent wrist flexion and extension during grasp. Each IMU is equipped with on board attitude and heading reference system (AHRS) algorithms. The sensors are connected to a MATLAB interface via Bluetooth, and calibration is conducted using the provided software. The sensors are both configured to only provide quaternion data at a rate of 256Hz. The IMUs are initialised by sending a command to initialise and tare the AHRS algorithm, restarting it from initial conditions and

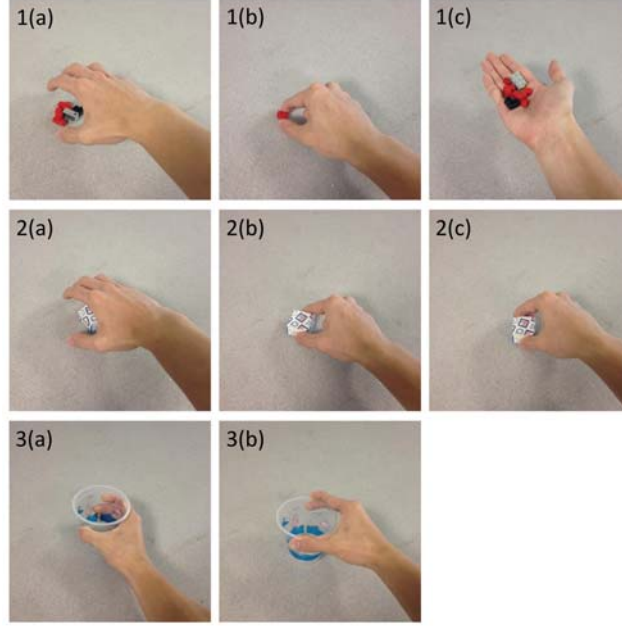


Figure A.1: 1: Very Small (VS) object class grasped using a) *power*, b) *pinch* and c) *open palm* grasp; 2: Small (S) object class grasped using a) *power*, b) *pinch*, and c) *tripod* grasp; 3: Cup (C) object class grasped using a) *power* and b) *tripod* grasp.

setting the current orientation as a reference vector. The reference vector is used by both sensors to compare the orientation transformations with respect to a single point. Initialisation was conducted with the subject seated upright and close to the desk in the rest position, with the dominant hand located at the edge of the table in line with their shoulder, with the elbow bent at  $90^\circ$ . Each grasp was recorded by key press, recording arm motion as the subject performed the grasp on the object from rest. The hand was returned to the rest position after each grasp. 25 trials were conducted per grasp, where each trial consisted of grasping the object positioned at a depth of 40 cm from the edge of the table, in line with the center of the subject's body. A total of 200 trials were made across all objects, with 4 participants taking part in the study.

## A.2 Data Processing

The raw data is decoded packet by packet and converted into a quaternion vector. The input quaternion vector  $q$  is converted to a unit quaternion  $q_u$  using equation A.1 and used as a rotation vector to transform the reference vector  $q_r$  to a new orientation  $q_o$  (See equation

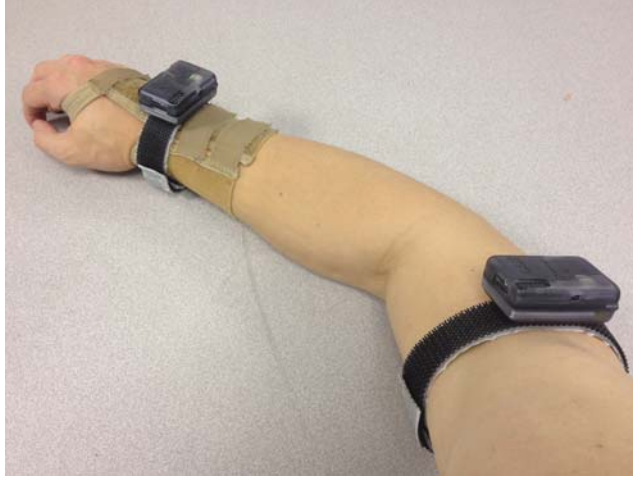


Figure A.2: A pair of x-IMU sensors fitted on the forearm and upper arm using a velcro strap. A wrist strap was used to prevent wrist flexion and extension during grasp.

A.2), which is subsequently stored into a data structure.

$$q_u = \frac{q}{\|q\|} \quad (\text{A.1})$$

$$q_o = q_u q_r q_u^{-1} \quad (\text{A.2})$$

A spike reduction algorithm (See equation A.3) is administered to the data to remove spikes caused by dropped IMU packets. The algorithm goes through each data point in sequence, comparing the size of neighbors to find spikes. In order to remove adjacent spikes, the next data point is set equivalent to the previous data point before checking. The data spikes are replaced by the previous point's data, giving a much smoother signal.

$$q_d = \begin{cases} q_{d-1}, & \text{if } |q_d - q_{d-1}| \geq S \\ q_d, & \text{otherwise} \end{cases} \quad (\text{A.3})$$

Where  $q_d$  is the quaternion vector after despiking and  $S = 0.3$  is the spike threshold. After the spikes have been removed from the data, a moving average filter is applied to smooth the signal. The X, Y and Z vector components of the despiked signal for each IMU are separated when calculating the mean, standard deviation, skewness and kurtosis features. Each component can be used to separate the data into classes according to grasp, giving

---

a total of 24 features. In order to reduce dimensionality, the most informative features must be found. The data was split into two sets, with 20% used for training, and 80% used for testing. The Anderson-Darling hypothesis test found a mixture of Gaussian and non-Gaussian feature distributions, therefore the Kruskal-Wallis test was selected to find the most informative features. A K-nearest neighbors classification algorithm was used ( $K = 1$ ) with an Euclidean distance metric to classify the data into different grasps.

### A.3 Results

Fig. A.3, A.4 and A.5 displays the orientation of the IMUs over time after the data has been despiked and smoothed for object classes VS, S and CP respectively. When comparing motion data between subjects, it can be seen that each subject's arm trajectory is slightly different, suggesting that each subject requires a tailored model to match their own motion patterns. Fig. A.6, A.7 and A.8 show the clusters of the top three most informative features for each subject. 86.1% of the top features were from the forearm IMU data, suggesting that the motion of the forearm is more important than the upper arm in determining grasp.

The VS class successfully classified between the three grasps with an accuracy of 96.7%, 83.3%, 88.3% and 95% for subjects A, B, C and D respectively. During the VS class trials, it was noticed that Subject B's forearm motion tended to gradually drift across the trials during the pinch grasp, with increased elbow flexion, displaying a greater spread in arm trajectory. This may be remedied by mixing all the grasp trials at random to make sure that the subject is focusing rather than just going through the grasping motions.

The S class showed very similar motion patterns when comparing pinch and tripod grasps. Using a tripod grasp with both fingers on the opposite side of the thumb, or with one finger on resting on top of the object seems to be a matter of preference. The expected similarities between pinch and tripod grasps meant that classification accuracy was much lower between the two, with the experiment yielding overall accuracies for the S object class of 81.6%, 58.3%, 56.7% and 80% for subjects A, B, C and D respectively.

Looking at the CP class, it can be seen that upper arm motion patterns for both grasps are very similar across all subjects. The power grasp forearm trajectory is quite similar to

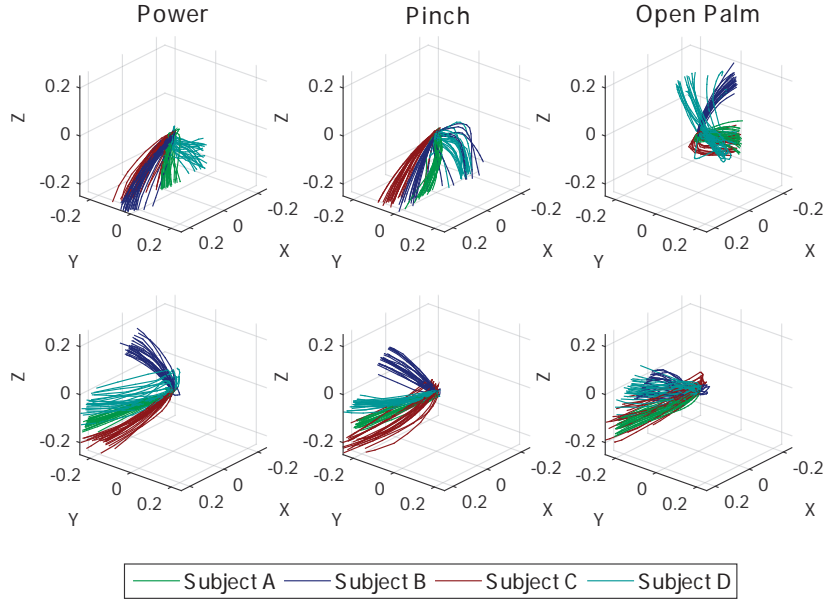


Figure A.3: Subject Forearm IMU (top) and Upper arm IMU (bottom) quaternion vectors over time for the very small object class

that of a pinch or tripod grasp on the S class object. The forearm's motion during a tripod grasp however is more of a mix between a power grasp from above and a pinch or tripod grasp on the VS and S object classes. The classifier successfully separated the two grasps with a 92.5%, 97.5%, 77.5% and 85% success rate for subjects A, B, C and D respectively.

## A.4 Discussion and Conclusion

Inertial data features in the forearm and upper arm proved to be an effective method of predicting the grasp intention during reach, with an overall success rate of 90.8%, 69.2% and 88.1% for VS, S and CP object classes respectively. Despite the study being relatively successful in terms of validating upper arm motion as a method for grasp prediction, there is still plenty of room for improvement. The classification success rate would have to be much higher to serve practical application for amputee use. This study has only tested the separability of the most common grasp patterns for three generic object classes based on size, however many objects have yet to be studied. In many cases, an object's application is not just dependent on size with the exception of some pick-and-place tasks, but are object-

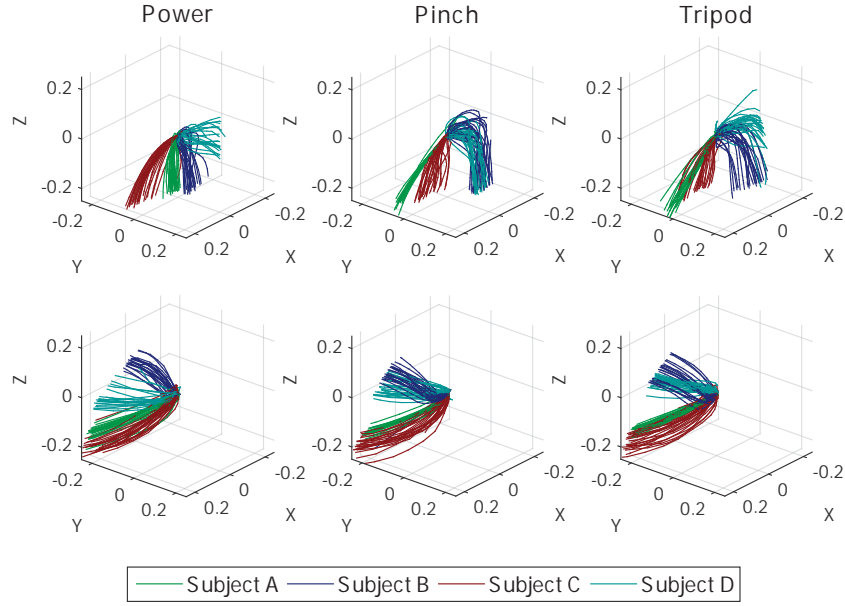


Figure A.4: Subject Forearm IMU (top) and Upper arm IMU (bottom) quaternion vectors over time for the small object class

specific, and require tailored grasp patterns for carrying them out. A greater number of unique object classes are required to increase the versatility of the system, making it capable of classifying more specialised tasks. Future work will build on the number of object classes and their respective grasp classes to develop a more thorough database for automated grasp selection in myoelectric hand prosthesis.

Object orientation is an important factor in the way it is grasped, and can account for a portion of the spread in trajectory displayed in the experiments. The system can be subject to very high variance when the position of the object is changed. In real-world applications, the target object can be located anywhere within the operator's immediate workspace. Further research is required into the classification of grasp patterns in different object locations, and studying how the arm's motion is affected. Further improvements require greater in-depth analysis of motion features to reduce the effect of variance between the grasp patterns at different locations in order to provide stronger classification rates. Although the study presented is at a validation stage, the experiments provided useful information on what aspects to improve on in further system development.



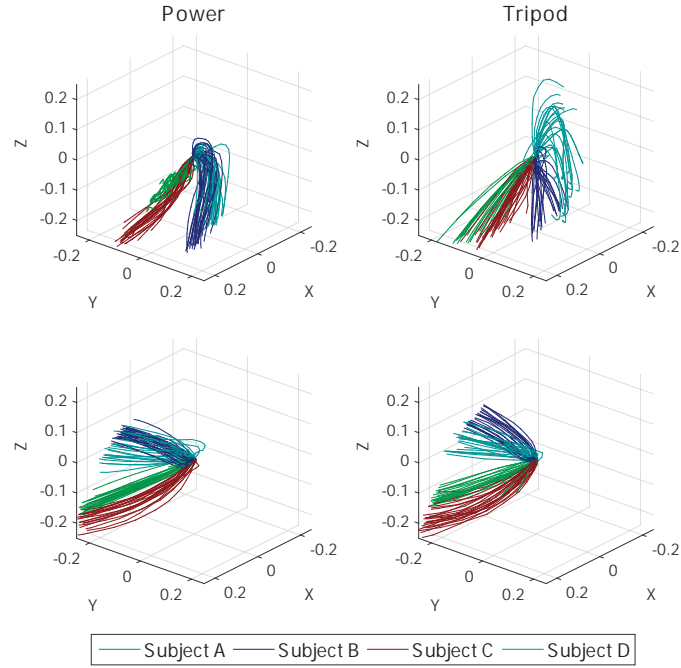


Figure A.5: Subject Forearm IMU (top) and Upper arm IMU (bottom) quaternion vectors over time for the cup object class

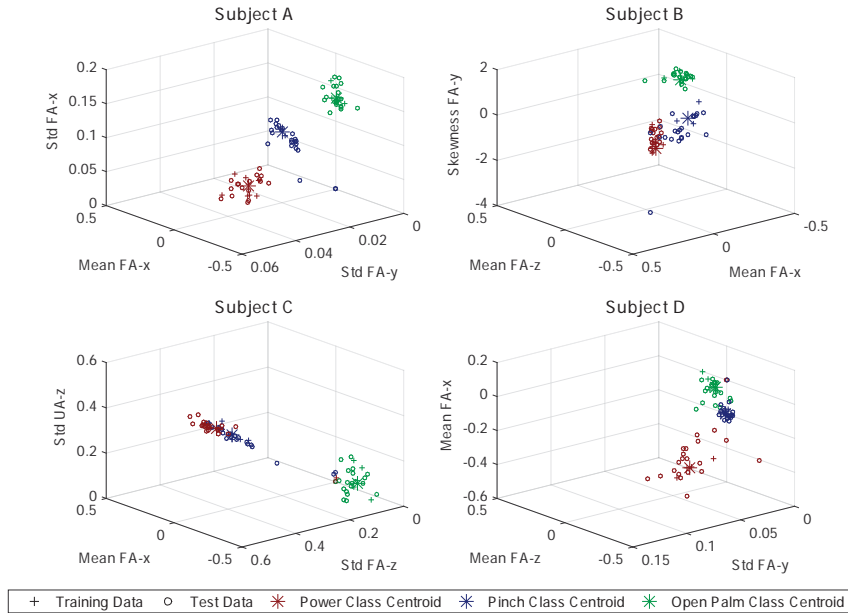


Figure A.6: Grasp class clusters using the top 3 most identifiable features for each subject for the very small object class

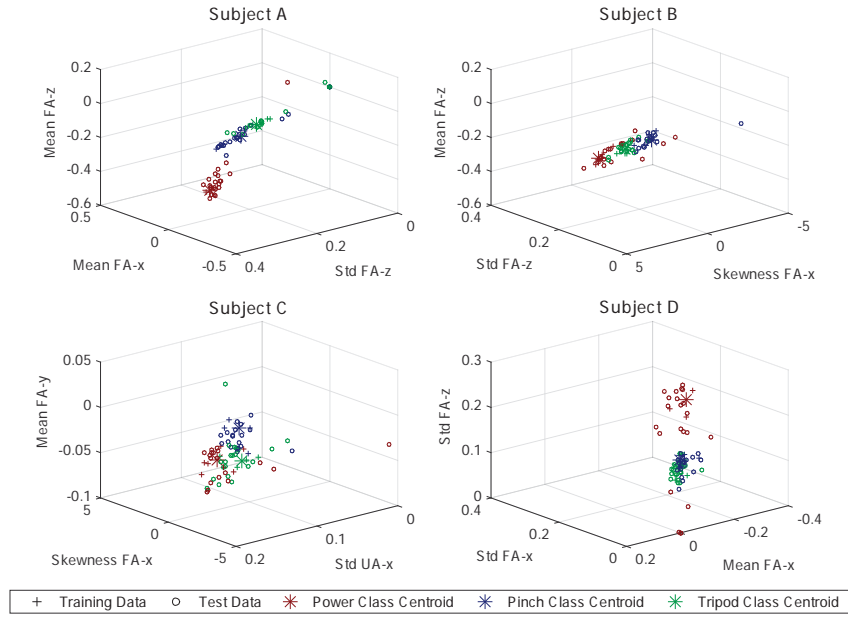


Figure A.7: Grasp class clusters using the top 3 most identifiable features for each subject for the small object class

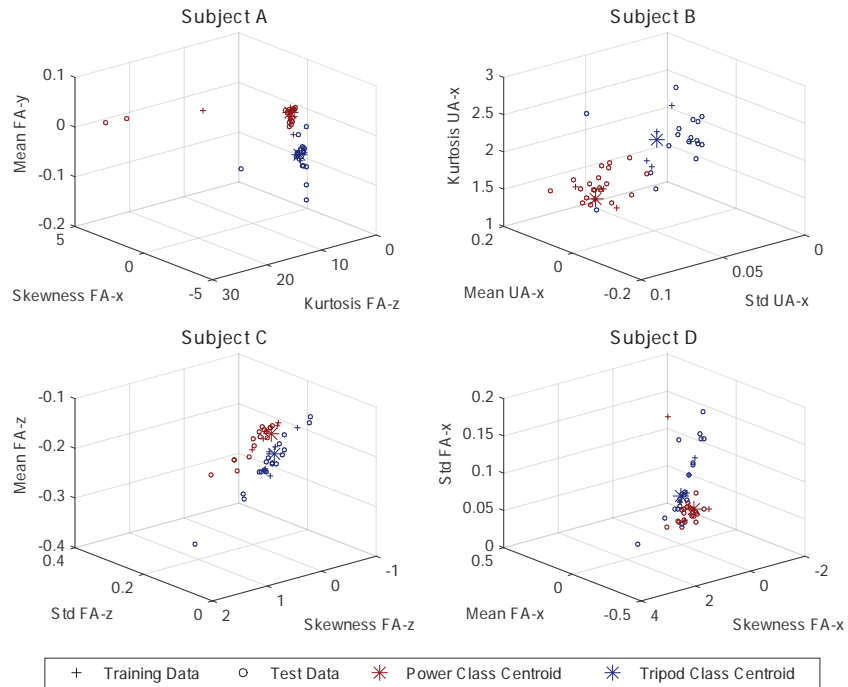


Figure A.8: Grasp class clusters using the top 3 most identifiable features for each subject for the cup object class

## Appendix B

# Inter-subject Kruskal-Wallis p-values for individual features

P-Value	Bottle		Lid		Box		
Feature	Lateral	Power	Lateral	Precision	Lateral	Power	Precision
'PoG:FAx'	1.135e-54	3.76e-16	1.574e-55	1.152e-81	2.866e-62	6.315e-67	9.507e-85
'PoG:FAy'	5.467e-37	2.128e-05	1.155e-28	5.778e-28	3.772e-35	1.288e-32	1.003e-28
'PoG:FAz'	1.163e-63	3.954e-55	7.616e-68	2.945e-66	8.759e-40	8.959e-49	1.427e-58
'PoG:UAx'	3.497e-40	1.364e-38	1.499e-46	1.096e-41	3.35e-43	1.345e-34	5.589e-51
'PoG:Uay'	4.98e-42	6.549e-39	2.589e-53	3.908e-53	3.508e-45	1.089e-60	3.711e-52
'PoG:UAz'	8.714e-39	1.846e-26	9.583e-59	4.264e-62	4.783e-63	4.472e-45	8.974e-54
'MaxDisp:FAx'	5.256e-16	7.686e-08	2.19e-44	2.682e-41	2.156e-49	1.55e-34	1.48e-44
'MaxDisp:FAy'	6.546e-11	7.255e-14	1.986e-20	1.007e-22	2.55e-26	1.028e-20	4.127e-21
'MaxDisp:FAz'	1.06e-62	2.844e-52	7.005e-68	1.828e-66	5.984e-42	5.051e-49	8.269e-59
'MaxDisp:UAx'	1.443e-39	4.37e-42	1.168e-46	2.296e-49	8.75e-43	1.138e-33	4.697e-48
'MaxDisp:Uay'	7.028e-39	3.734e-38	3.493e-45	1.031e-47	1.102e-41	1.746e-46	7.883e-51
'MaxDisp:UAz'	1.711e-08	0.0002119	2.112e-35	7.54e-27	6.889e-32	8.686e-35	8.513e-34
'MinDisp:FAx'	1.946e-51	1.869e-21	1.001e-50	6.614e-81	2.221e-60	9.031e-63	3.462e-84
'MinDisp:FAy'	8.939e-34	0.0005219	1.102e-18	9.192e-17	1.199e-19	4.266e-19	2.431e-17
'MinDisp:FAz'	2.637e-13	1.672e-15	1.381e-19	1.462e-17	2.817e-38	8.311e-29	1.794e-38
'MinDisp:UAx'	2.821e-12	2.873e-12	3.407e-07	1.536e-11	1.309e-21	5.836e-13	9.335e-24
'MinDisp:Uay'	1.33e-18	1.114e-09	1.374e-38	1.464e-37	1.897e-14	3.668e-35	4.452e-35
'MinDisp:UAz'	6.948e-38	1.988e-26	1.059e-48	1.141e-49	1.233e-41	1.418e-38	6.235e-39

Table B.1: Individual displacement feature p-values returned by a Kruskal-Wallis test for each object and grasp across all subjects grasping at table height and ascending elevation, with the null hypothesis that each set of subject samples comes from the same distribution.

P-Value	Bottle		Lid		Box		
Feature	Lateral	Power	Lateral	Precision	Lateral	Power	Precision
'MaxVel:FAx'	1.657e-45	9.644e-13	3.414e-31	6.929e-34	7.431e-37	9.655e-34	7.154e-25
'MaxVel:FAy'	5.663e-10	3.198e-23	4.827e-31	1.482e-17	6.031e-25	4.145e-34	8.101e-12
'MaxVel:FAz'	1.786e-69	7.134e-52	3.185e-68	1.729e-66	3.096e-69	1.025e-60	1.025e-71
'MaxVel:UAx'	1.13e-38	4.387e-47	2.413e-38	1.791e-33	4.491e-33	1.51e-26	2.25e-33
'MaxVel:Uay'	3.465e-39	3.155e-36	3.103e-42	2.865e-42	3.81e-47	4.014e-41	3.685e-54
'MaxVel:UAz'	6.054e-38	8.212e-19	6.285e-51	1.747e-66	8.73e-49	1.404e-60	9.92e-61
'MinVel:FAx'	2.254e-45	1.181e-19	1.049e-29	1.146e-59	1.552e-36	3.021e-42	2.585e-61
'MinVel:FAy'	1.414e-31	2.627e-05	7.007e-27	1.714e-24	1.003e-21	7.038e-22	2.043e-25
'MinVel:FAz'	3.255e-24	1.249e-41	1.87e-21	5.671e-13	2.466e-36	1.108e-28	4.955e-32
'MinVel:UAx'	4.028e-36	1.245e-23	3.627e-41	1.164e-39	1.306e-52	3.735e-38	3.978e-67
'MinVel:Uay'	9.811e-36	2.712e-09	1.738e-43	2.215e-47	1.086e-39	4.512e-50	1.053e-51
'MinVel:UAz'	1.625e-45	2.08e-39	9.19e-53	1.681e-48	1.267e-48	2.829e-40	1.947e-43
'RMSVel:FAx'	1.748e-45	3.164e-15	6.112e-36	2.996e-69	4.69e-43	2.301e-51	4.15e-68
'RMSVel:FAy'	4.233e-33	6.201e-07	1.123e-26	1.46e-25	7.191e-12	1.018e-17	4.83e-30
'RMSVel:FAz'	2.156e-66	9.861e-50	6.139e-70	4.528e-65	5.512e-61	2.743e-57	1.494e-68
'RMSVel:UAx'	1.98e-24	1.089e-36	1.322e-20	5.248e-20	3.119e-23	1.735e-19	4.579e-31
'RMSVel:Uay'	4.817e-41	2.534e-34	1.204e-40	5.471e-37	7.413e-51	6.471e-39	6.2e-57
'RMSVel:UAz'	6.809e-41	1.874e-28	5.479e-25	1.098e-30	1.346e-35	1.956e-18	1.221e-44
'PK-RMSVel:FAx'	2.985e-31	7.879e-19	1.92e-25	1.964e-38	6.713e-42	5.467e-42	1.551e-39
'PK-RMSVel:FAy'	3.751e-32	4.077e-32	3.834e-27	3.468e-21	1.724e-17	4.723e-21	2.356e-11
'PK-RMSVel:FAz'	3.856e-38	2.092e-33	2.618e-45	4.242e-50	9.665e-47	6.715e-40	7.891e-42
'PK-RMSVel:UAx'	6.927e-33	5.105e-30	1.217e-13	4.459e-19	8.113e-14	1.582e-18	1.347e-15
'PK-RMSVel:Uay'	3.579e-44	6.521e-62	3.216e-61	1.757e-60	2.296e-56	3.084e-41	2.157e-46
'PK-RMSVel:UAz'	2.716e-57	2.015e-66	1.644e-38	1.006e-53	6.164e-49	8.098e-37	7.233e-41
'MeanVel:FAx'	1.565e-49	2.83e-15	1.736e-50	4.286e-74	4.024e-53	3.067e-54	5.151e-71
'MeanVel:FAy'	2.07e-41	8.73e-05	6.801e-32	6.236e-31	2.383e-40	1.624e-34	1.743e-35
'MeanVel:FAz'	3.253e-59	7.489e-53	3.031e-63	2.245e-65	6.227e-46	3.134e-46	2.55e-59
'MeanVel:UAx'	2.25e-39	1.027e-37	2.35e-42	2.147e-36	9.907e-40	1.021e-29	2.499e-45
'MeanVel:Uay'	5.329e-43	1.113e-32	4.902e-53	1.578e-53	6.482e-46	7.816e-60	4.462e-53
'MeanVel:UAz'	7.048e-40	3.496e-24	9.599e-61	1.231e-64	1.361e-63	3.125e-44	3.479e-54

Table B.2: Individual velocity feature p-values returned by a Kruskal-Wallis test for each object and grasp across all subjects grasping at table height and ascending elevation, with the null hypothesis that each set of subject samples comes from the same distribution.

P-Value	Bottle		Lid		Box		
Feature	Lateral	Power	Lateral	Precision	Lateral	Power	Precision
'MaxAcc:FAx'	8.715e-53	1.277e-21	2.586e-41	2.491e-45	2.567e-44	3.058e-49	1.546e-56
'MaxAcc:FAy'	6.258e-35	4.444e-28	5.579e-37	2.884e-35	2.208e-23	9.928e-24	2.156e-30
'MaxAcc:FAz'	3.27e-69	2.389e-41	1.297e-64	2.387e-68	5.531e-65	2.846e-63	2.644e-68
'MaxAcc:UAX'	8.357e-38	8.834e-47	7.257e-30	3.748e-18	1.707e-35	4.847e-32	1.732e-35
'MaxAcc:UAY'	5.158e-42	6.193e-42	5.87e-48	2.118e-48	1.248e-59	3.214e-52	8.794e-66
'MaxAcc:UAz'	1.561e-62	1.36e-61	1.075e-49	1.959e-44	1.567e-49	8.126e-59	8.149e-67
'MinAcc:FAx'	4.723e-52	1.455e-14	2.861e-37	5.515e-49	5.029e-43	2.098e-52	1.46e-58
'MinAcc:FAy'	1.368e-41	1.172e-17	9.082e-37	4.952e-39	2.737e-28	2.061e-31	1.321e-39
'MinAcc:FAz'	1.327e-70	7.818e-53	6.373e-73	3.603e-71	5.966e-73	1.128e-69	3.518e-75
'MinAcc:UAX'	2.129e-50	1.083e-51	8.713e-45	2.893e-31	6.471e-46	4.397e-44	2.145e-48
'MinAcc:UAY'	6.802e-55	5.52e-50	1.784e-47	3.891e-39	3.687e-56	6.701e-39	1.06e-66
'MinAcc:UAz'	4.877e-58	2.926e-55	1.08e-51	7.045e-50	3.149e-55	5.342e-48	4.998e-58
'PK-DistAcc:FAx'	1.081e-37	9.253e-11	2.36e-19	1.93e-32	3.441e-33	3.369e-35	7.065e-32
'PK-DistAcc:FAy'	1.125e-34	1.465e-14	2.471e-10	1.518e-08	2.935e-19	2.784e-31	7.827e-25
'PK-DistAcc:FAz'	6.002e-37	1.733e-17	2.904e-47	3.411e-55	8.237e-43	1.17e-34	8.546e-45
'PK-DistAcc:UAX'	1.635e-31	7.015e-17	1.901e-42	2.769e-44	3.781e-36	6.029e-35	2.38e-32
'PK-DistAcc:UAY'	3.201e-65	1.091e-47	1.775e-45	8.433e-58	1.438e-49	1.003e-46	1.116e-46
'PK-DistAcc:UAz'	1.223e-56	2.996e-42	5.837e-56	9.951e-47	3.393e-35	3.371e-55	7.551e-39
'RMSAcc:FAx'	3.687e-56	5.997e-17	5.276e-38	6.094e-50	5.328e-47	1.478e-58	4.735e-65
'RMSAcc:FAy'	3.187e-38	1.387e-19	8.66e-37	3.601e-38	4.124e-23	6.086e-26	1.355e-36
'RMSAcc:FAz'	1.09e-77	8.757e-52	1.604e-73	3.834e-71	1.798e-74	3.683e-69	8.507e-78
'RMSAcc:UAX'	5.148e-40	8.347e-47	8.32e-37	5.6e-23	1.044e-42	4.735e-35	1.135e-43
'RMSAcc:UAY'	1.501e-48	1.241e-41	9.152e-46	1.292e-40	1.903e-56	9.401e-44	1.374e-66
'RMSAcc:UAz'	6.205e-60	8.897e-55	1.351e-47	1.383e-41	1.485e-51	7.782e-55	7.455e-66
'PK-RMSAcc:FAx'	1.049e-24	2.054e-15	1.228e-12	3.441e-13	7.429e-16	1.047e-15	8.422e-13
'PK-RMSAcc:FAy'	1.721e-17	1.165e-31	3.216e-10	2.144e-16	5.551e-21	1.575e-07	2.037e-10
'PK-RMSAcc:FAz'	1.549e-14	3.705e-05	1.54e-23	5.287e-23	6.61e-13	4.367e-20	3.3e-08
'PK-RMSAcc:UAX'	1.415e-25	4.572e-13	7.069e-17	8.316e-20	4.51e-18	2.306e-27	1.863e-25
'PK-RMSAcc:UAY'	3.565e-32	2.582e-20	5.004e-30	7.081e-27	2.859e-22	2.439e-34	2.102e-19
'PK-RMSAcc:UAz'	2.026e-36	2.892e-13	1.288e-20	4.237e-19	3.882e-26	2.208e-21	3.076e-23
'P2PAcc:FAx'	6.858e-60	1.458e-19	1.402e-42	1.037e-50	1.125e-49	1.891e-56	3.898e-63
'P2PAcc:FAy'	1.087e-39	1.635e-23	3.468e-36	2.966e-37	3.338e-25	1.197e-26	2.988e-35
'P2PAcc:FAz'	2.86e-77	7.249e-51	9.195e-72	3.765e-73	3.679e-74	1.252e-68	6.641e-76
'P2PAcc:UAX'	2.681e-45	3.153e-51	4.74e-39	3.015e-22	5.002e-43	1.313e-39	2.797e-41
'P2PAcc:UAY'	3.753e-49	1.06e-47	1.53e-49	9.537e-44	6.079e-61	6.762e-47	3.297e-68
'P2PAcc:UAz'	1.729e-64	5.373e-62	1.126e-53	9.095e-48	1.005e-54	6.157e-58	1.103e-67

Table B.3: Individual acceleration feature p-values returned by a Kruskal-Wallis test for each object and grasp across all subjects grasping at table height and ascending elevation, with the null hypothesis that each set of subject samples comes from the same distribution.



## Appendix C

# Inter-population Kruskal-Wallis p-values for individual features

P-Value	Bottle		Lid		Box		
Feature	Lateral	Power	Lateral	Precision	Lateral	Power	Precision
'PoG:FAx'	4.96e-11	5.525e-07	8.641e-33	6.769e-27	2.708e-18	2.807e-23	8.499e-21
'PoG:FAy'	4.445e-24	0.3569	6.46e-26	1.169e-20	6.158e-08	2.417e-29	3.471e-18
'PoG:FAz'	5.425e-29	1.083e-25	1.359e-27	2.199e-12	1.166e-27	5.759e-32	8.849e-30
'PoG:UAx'	0.004215	0.05207	1.222e-09	5.286e-10	3.191e-05	2.248e-17	7.596e-23
'PoG:Uay'	2.127e-08	1.665e-07	8.668e-29	2.724e-27	1.088e-14	5.754e-24	7.205e-22
'PoG:UAz'	4.749e-27	3.038e-08	5.589e-33	4.484e-27	2.264e-26	1.697e-31	1.047e-27
'MaxDisp:FAx'	3.229e-11	3.149e-07	3.061e-20	7.727e-17	8.26e-20	3.561e-17	6.987e-20
'MaxDisp:FAy'	4.299e-06	9.803e-10	0.8049	0.0002731	6.127e-05	8.799e-05	0.1021
'MaxDisp:FAz'	4.981e-29	2.796e-28	1.011e-27	1.995e-12	1.146e-28	2.547e-32	5.102e-30
'MaxDisp:UAx'	0.006618	0.001584	2.866e-10	5.743e-17	0.000188	7.277e-18	4.704e-23
'MaxDisp:Uay'	1.072e-08	1.288e-08	3.932e-22	3.461e-20	3.771e-14	7.603e-16	5.096e-23
'MaxDisp:UAz'	1.117e-05	0.5852	5.589e-33	4.484e-27	6.131e-25	2.815e-31	2.31e-27
'MinDisp:FAx'	3.671e-09	1.899e-18	9.343e-33	6.769e-27	1.443e-16	3.068e-22	2.601e-19
'MinDisp:FAy'	1.411e-20	0.7569	2.226e-14	7.137e-07	0.1675	4.014e-14	0.0002534
'MinDisp:FAz'	5.323e-12	1.787e-05	9.039e-17	9.602e-13	1.52e-22	2.911e-21	2.204e-21
'MinDisp:UAx'	0.2753	0.3621	0.1558	0.4119	0.06977	0.03997	0.005861
'MinDisp:Uay'	0.3595	0.6595	1.457e-26	2.724e-27	7.308e-05	1.153e-12	2.706e-21
'MinDisp:UAz'	3.815e-23	3.006e-08	1.836e-29	6.324e-25	9.326e-26	1.379e-27	2.387e-28

Table C.1: Individual displacement feature p-values returned by a Kruskal-Wallis test for each object and grasp across all subjects grasping at table height and ascending elevation, with the null hypothesis that healthy and amputee populations come from the same distribution.

P-Value	Bottle		Lid		Box		
Feature	Lateral	Power	Lateral	Precision	Lateral	Power	Precision
'MaxVel:FAx'	1.645e-22	0.1019	1.687e-16	1.14e-11	2.484e-15	1.892e-12	6.922e-17
'MaxVel:FAy'	5.404e-05	0.1328	8.079e-12	1.11e-11	0.3277	1.245e-16	3.345e-07
'MaxVel:FAz'	1.371e-29	1.324e-29	1.666e-32	1.369e-26	1.978e-30	1.207e-32	4.385e-31
'MaxVel:UAx'	0.03861	1.385e-07	1.29e-05	8.811e-10	0.32	8.834e-07	8.783e-10
'MaxVel:UAy'	1.797e-14	7.855e-19	1.12e-23	9.95e-22	3.728e-18	1.21e-18	7.293e-25
'MaxVel:UAz'	7.578e-14	0.003421	5.424e-23	8.011e-16	0.0007285	2.158e-15	0.4683
'MinVel:FAx'	0.0451	1.102e-15	2.188e-06	3.239e-08	0.001097	1.406e-07	0.0001508
'MinVel:FAy'	5.353e-14	0.01101	1.324e-13	2.963e-06	0.006301	8.229e-12	0.0004695
'MinVel:FAz'	5.335e-13	0.006877	3.382e-16	0.005566	2.32e-25	1.128e-21	1.171e-22
'MinVel:UAx'	3.446e-09	0.0002041	1.659e-07	0.7093	6.915e-17	2.073e-05	1.499e-16
'MinVel:UAy'	0.03618	2.152e-07	5.911e-22	3.218e-20	0.01023	1.555e-19	6.581e-08
'MinVel:UAz'	1.399e-27	6.801e-21	1.319e-32	1.182e-26	1.345e-27	7.878e-29	7.673e-30
'RMSVel:FAx'	0.6697	2.779e-18	4.004e-16	1.824e-15	0.5371	0.3179	0.7776
'RMSVel:FAy'	1.064e-19	0.01181	7.64e-15	6.272e-09	0.0003395	1.075e-09	0.0001874
'RMSVel:FAz'	1.271e-29	9.185e-30	1.508e-32	9.783e-27	1.957e-30	1.313e-32	3.415e-31
'RMSVel:UAx'	0.0005224	1.893e-14	0.005436	1.415e-07	0.007029	1.81e-07	4.238e-08
'RMSVel:UAy'	4.21e-15	4.586e-14	3.335e-18	8.136e-10	6.194e-19	1.285e-12	4.19e-23
'RMSVel:UAz'	5.413e-25	1.563e-12	0.7068	0.6855	2.672e-19	0.0005795	1.325e-22
'PK-RMSVel:FAx'	1.281e-07	0.007107	7.232e-11	3.891e-17	1.088e-14	9.04e-22	1.116e-15
'PK-RMSVel:FAy'	0.01044	7.754e-09	0.2498	0.4242	0.009406	5.358e-09	1.504e-06
'PK-RMSVel:FAz'	1.746e-09	2.942e-07	3.709e-18	1.341e-09	3.52e-18	5.068e-18	2.841e-14
'PK-RMSVel:UAx'	4.678e-10	5.76e-10	0.05023	0.0001457	0.04508	0.002327	0.1438
'PK-RMSVel:UAy'	0.000216	1.058e-20	9.336e-25	1.775e-17	2.331e-14	1.251e-19	2.214e-17
'PK-RMSVel:UAz'	7.28e-24	4.283e-27	5.457e-20	3.112e-16	1.99e-17	5.48e-23	3.009e-19
'MeanVel:FAx'	0.001708	5.849e-06	6.338e-29	6.79e-23	2.721e-10	6.754e-09	2.227e-10
'MeanVel:FAy'	1.325e-26	0.1389	1.032e-27	5.697e-22	8.249e-10	3.078e-30	1.103e-20
'MeanVel:FAz'	2.066e-29	1.534e-25	6.487e-32	1.568e-24	1.333e-29	5.64e-32	7.518e-30
'MeanVel:UAx'	0.4852	0.06671	0.0007573	0.163	0.04284	2.024e-11	4.861e-18
'MeanVel:UAy'	7.393e-10	0.0003292	1.832e-28	1.741e-26	8.997e-15	1.47e-23	2.076e-21
'MeanVel:UAz'	1.911e-27	1.557e-06	5.589e-33	6.221e-27	1.48e-25	2.753e-30	5.693e-27

Table C.2: Individual velocity feature p-values returned by a Kruskal-Wallis test for each object and grasp across all subjects grasping at table height and ascending elevation, with the null hypothesis that healthy and amputee populations come from the same distribution.



P-Value	Bottle		Lid		Box		
Feature	Lateral	Power	Lateral	Precision	Lateral	Power	Precision
'MaxAcc:FAx'	2.264e-16	1.026e-09	0.001128	1.699e-06	1.006e-19	8.637e-14	3.632e-13
'MaxAcc:FAY'	7.088e-06	8.324e-06	0.03859	0.06176	0.0008792	0.0003774	0.000361
'MaxAcc:FAz'	1.844e-28	1.998e-24	1.161e-31	1.113e-23	5.582e-30	7.396e-32	6.519e-30
'MaxAcc:UAX'	1.534e-09	4.809e-18	0.5616	0.001447	2.512e-09	0.5212	0.2113
'MaxAcc:UAY'	4.928e-16	5.467e-18	1.847e-25	5.382e-22	3.273e-21	3.562e-21	3.501e-25
'MaxAcc:UAz'	2.02e-24	2.129e-25	1.039e-20	2.05e-21	1.007e-26	5.652e-24	1.512e-28
'MinAcc:FAx'	7.078e-11	6.801e-12	6.574e-05	0.01958	1.951e-12	4.343e-18	1.269e-13
'MinAcc:FAY'	1.398e-11	0.0001166	3.166e-14	5.422e-09	7.239e-06	6.476e-14	1.008e-06
'MinAcc:FAz'	2.914e-29	3.687e-18	8.353e-32	1.818e-27	4.053e-30	1.49e-32	3.951e-31
'MinAcc:UAX'	1.224e-23	1.915e-25	7.012e-11	2.133e-07	1.534e-21	2.407e-09	8.633e-12
'MinAcc:UAY'	8.913e-24	1.906e-24	9.944e-20	5.074e-18	8.433e-25	1.746e-13	1.583e-24
'MinAcc:UAz'	5.072e-28	2.609e-20	1.825e-17	2.669e-18	4.402e-28	1.922e-25	2.294e-30
'PK-DistAcc:FAx'	4.903e-05	2.885e-07	9.833e-06	1.251e-12	7.573e-08	1.273e-18	5.033e-14
'PK-DistAcc:FAY'	0.6614	0.00272	0.3773	6.053e-06	2.291e-07	2.555e-06	8.411e-13
'PK-DistAcc:FAz'	1.248e-07	6.52e-12	2.923e-22	7.208e-21	1.336e-11	4.417e-16	2.784e-19
'PK-DistAcc:UAX'	3.952e-21	3.775e-06	4.416e-20	1.748e-19	8.091e-21	1.6e-26	1.39e-24
'PK-DistAcc:UAY'	1.512e-08	0.06044	0.02814	9.183e-05	0.0002948	0.2021	0.0005644
'PK-DistAcc:UAz'	2.218e-10	5.646e-11	1.079e-31	4.975e-26	3.444e-15	1.63e-28	3.514e-16
'RMSAcc:FAx'	8.937e-12	1.555e-11	0.001588	0.002154	4.078e-18	2.925e-18	5.911e-14
'RMSAcc:FAY'	3.227e-10	0.0002349	1.5e-07	3.304e-06	8.179e-05	5.339e-08	1.979e-05
'RMSAcc:FAz'	1.463e-29	3.109e-24	1.021e-32	2.334e-28	1.957e-30	1.207e-32	1.713e-31
'RMSAcc:UAX'	1.526e-17	2.829e-22	8.05e-05	0.043	2.261e-17	0.02249	0.001826
'RMSAcc:UAY'	7.245e-20	1.406e-20	2.216e-22	8.373e-20	8.998e-23	1.145e-15	5.55e-26
'RMSAcc:UAz'	1.247e-27	2.812e-23	5.353e-18	1.067e-20	2.742e-27	5.806e-24	2.817e-30
'PK-RMSAcc:FAx'	4.672e-13	0.07119	0.0002785	9.914e-05	1.483e-09	4.206e-06	0.002505
'PK-RMSAcc:FAY'	0.1817	1.363e-06	0.0002128	0.2082	0.5519	0.02187	0.1006
'PK-RMSAcc:FAz'	0.00264	6.545e-06	3.908e-05	0.0154	0.2711	0.1096	0.4788
'PK-RMSAcc:UAX'	1.746e-08	6.462e-08	0.008229	2.403e-06	0.7478	1.968e-06	0.06971
'PK-RMSAcc:UAY'	0.4816	0.7639	0.1363	0.4565	4.192e-07	0.0001167	0.0587
'PK-RMSAcc:UAz'	0.2168	0.6463	6.35e-11	0.001299	1.103e-15	2.866e-12	0.006289
'P2PAcc:FAx'	2.67e-15	7.78e-12	2.756e-05	8.102e-05	3.646e-20	4.959e-20	3.573e-15
'P2PAcc:FAY'	1.346e-08	2.634e-05	2.376e-06	0.0001066	8.116e-05	5.835e-08	1.639e-05
'P2PAcc:FAz'	2.326e-29	4.524e-24	2.403e-32	1.469e-27	2.374e-30	1.246e-32	2.321e-31
'P2PAcc:UAX'	6.01e-18	1.588e-23	6.81e-05	0.1168	1.209e-17	0.000291	0.0003248
'P2PAcc:UAY'	3.713e-20	4.122e-22	9.189e-24	2.05e-21	1.418e-24	2.836e-18	1.594e-26
'P2PAcc:UAz'	9.914e-28	1.086e-23	2.24e-20	2.314e-21	2.884e-28	2.508e-26	1.792e-30

Table C.3: Individual acceleration feature p-values returned by a Kruskal-Wallis test for each object and grasp across all subjects grasping at table height and ascending elevation, with the null hypothesis that healthy and amputee populations come from the same distribution.



## **Appendix D**

# **Correlation between anthropomorphic and physiological features**

Object	Grasp	Feature	Pearson's Coefficient	P-value
Bottle	Lateral	MaxDisp:UAz	-0.6458	0.0437
		MaxVel:UAx	-0.6555	0.0396
		MinAcc:UAy	-0.7030	0.0233
	Power	MaxVel:FAx	-0.6462	0.0435
		PK-RMSVel:FAx	-0.6916	0.0267
		PK-DistAcc:UAz	-0.8583	0.0015
Lid	Lateral	MaxDisp:UAz	-0.7408	0.0142
		MinDisp:FAz	-0.7829	0.0074
		MinDisp:UAz	-0.6400	0.0462
		MinVel:UAz	-0.6932	0.0262
		PK-DistAcc:UAz	0.7182	0.0193
	Precision	MinDisp:FAz	-0.6380	0.0471
		MinDisp:UAz	-0.7068	0.0223
		MinVel:FAx	-0.7777	0.0081
		RMSVel:FAx	0.7622	0.0104
Box	Lateral	PK-DistAcc:UAz	0.6726	0.0331
		MaxDisp:UAz	-0.6564	0.0393
		MaxAcc:UAy	0.6898	0.0273
		PK-DistAcc:UAz	0.7304	0.0164
		RMSAcc:UAy	0.6356	0.0483
	Power	MaxDisp:FAx	-0.6747	0.0393
		MaxDisp:UAz	-0.6695	0.0342
		MinDisp:FAz	-0.7907	0.0065
		MinVel:FAy	-0.7435	0.0137
		MinVel:FAz	-0.6721	0.0333
		PK-DistAcc:UAz	0.7338	0.0157
	Precision	PoG:FAx	-0.6956	0.0255
		MaxVel:UAy	0.6684	0.0346
		PK-RMSVel:FAz	0.6705	0.0338
		MaxAcc:UAy	0.7517	0.0122
		MinAcc:UAy	-0.8742	0.0009
		PK-distAcc:UAy	-0.8574	0.0015
		RMSAcc:UAy	0.9162	0.0002
		RMSAcc:UAz	0.7387	0.0147
		PK-RMSAcc:FAy	0.6389	0.0467
		PK-RMSAcc:FAz	0.8201	0.0037
		PK-RMSAcc:UAx	0.6403	0.0461
		P2PAcc:UAy	0.8162	0.0040

Table D.1: Individual physiological feature Pearson's coefficients and p-values for a statistically significant correlation with the hand span of healthy subjects across all object locations.

Object	Grasp	Feature	Pearson's Coefficient	P-value
Bottle	Lateral	MinDisp:FAz	-0.7599	0.0108
		MinVel:FAy	-0.7532	0.0119
		MinVel:FAz	-0.6370	0.0476
	Power	PoG:FAz	-0.6665	0.0353
		MaxDisp:FAz	-0.6485	0.0425
		MaxVel:FAz	-0.7824	0.0075
		MaxAcc:FAz	-0.7038	0.0231
Lid	Lateral	MinDisp:FAz	-0.6530	0.0407
		MinDisp:Uay	-0.8917	0.0005
		MinVel:Uay	-0.6685	0.0346
		MaxAcc:FAy	0.6753	0.0321
	Precision	MinDisp:Uay	-0.7972	0.0057
		MinVel:FAy	-0.6338	0.0491
		MaxAcc:FAy	0.6608	0.0375
		MinAcc:FAy	-0.6483	0.0426
		MinAcc:FAz	0.7718	0.0089
		PK-DistAcc:FAz	0.8213	0.0036
Box	Lateral	PoG:FAx	-0.6850	0.0288
		RMSVel:FAy	0.7002	0.0242
		MaxAcc:FAy	0.6353	0.0484
		MinAcc:Uay	0.6351	0.0485
	Power	PoG:FAy	-0.7695	0.0092
		MinDisp:FAy	-0.6902	0.0272
		MeanVel:FAx	-0.6671	0.0351
		MeanVel:FAy	-0.6939	0.0260
		MaxAcc:FAy	0.6786	0.0310
		MinAcc:Uax	0.6944	0.0259
	Precision	MaxDisp:FAy	0.6387	0.0469
		MaxVel:FAy	0.8638	0.0013
		MaxAcc:FAy	0.7434	0.0137
		PK-DistAcc:FAy	0.6554	0.0397

Table D.2: Individual physiological feature Pearson's coefficients and p-values for a statistically significant correlation with the arm span of healthy subjects across all object locations.